

# MONTE CARLO SIMULATIONS FOR COMPLEX OPTION PRICING

A THESIS SUBMITTED TO THE UNIVERSITY OF MANCHESTER  
FOR THE DEGREE OF DOCTOR OF PHILOSOPHY  
IN THE FACULTY OF ENGINEERING AND PHYSICAL SCIENCES

2010

**Dong-Mei Wang**

School of Mathematics

# Contents

<b>Abstract</b>	<b>17</b>
<b>Declaration</b>	<b>18</b>
<b>Copyright Statement</b>	<b>19</b>
<b>Acknowledgements</b>	<b>20</b>
<b>Dedication</b>	<b>21</b>
<b>1 Introduction</b>	<b>22</b>
<b>2 Preliminaries</b>	<b>27</b>
2.1 Principles of derivatives pricing . . . . .	28
2.1.1 Arbitrage pricing . . . . .	28
2.1.2 Risk-neutral probabilities . . . . .	29
2.2 Principles of Monte Carlo . . . . .	30
2.2.1 Law of large numbers . . . . .	30
2.2.2 Central limit theorem . . . . .	32
2.3 Generating random numbers . . . . .	34
2.4 Variance reduction techniques . . . . .	35
2.4.1 Control variates . . . . .	35
2.4.2 Antithetic variates . . . . .	36
2.4.3 Importance sampling . . . . .	37
2.5 Discretization methods . . . . .	39

2.5.1	The Euler method . . . . .	39
2.5.2	The Milstein method . . . . .	40
2.5.3	The second-order Milstein method . . . . .	41
2.5.4	The extrapolation method . . . . .	43
2.6	Efficient Monte Carlo methods . . . . .	44
2.7	Quasi-Monte Carlo method . . . . .	45
2.8	Monte Carlo for Greeks . . . . .	49
2.8.1	Finite-difference approximation . . . . .	49
2.8.2	Finite difference methods for Greeks . . . . .	50
2.8.3	Pathwise method and the likelihood ratio method . . . . .	50
2.9	American options . . . . .	51
2.9.1	Duality simulation . . . . .	52
2.9.2	Regression simulation . . . . .	53
<b>3</b>	<b>Option Pricing with Jump Processes</b>	<b>56</b>
3.1	Background to the Merton jump diffusion (MJD) model . . . . .	58
3.2	Generating sample paths in the MJD model . . . . .	62
3.3	Pricing 1D Bermudan put options using the MJD model . . . . .	64
3.3.1	Implementation . . . . .	65
3.3.2	Sensitivity of option price to the choice of the parameters . . .	67
3.3.3	$\lambda$ impact on pricing option . . . . .	71
3.4	Pricing multi-dimensional Bermudan put option using the MJD model	72
3.4.1	Implementation . . . . .	74
3.4.2	Numerical results . . . . .	76
3.5	Pricing 1D Bermudan put option using the double-jump stochastic volatility (SVJJ) model . . . . .	77
3.5.1	Implementation . . . . .	79
3.5.2	Pricing European options . . . . .	80
3.5.3	Exercise opportunities $N$ impact on pricing Bermudan options	81

3.5.4	Sensitivity of Bermudan options to the choice of numerical parameters . . . . .	82
3.6	Pricing multi-dimensional Bermudan put option using the SVJJ model	85
3.6.1	Implementation . . . . .	86
3.6.2	Numerical results . . . . .	87
3.7	Comparison of jump diffusion models . . . . .	89
<b>4</b>	<b>Feedback Models with Illiquidity</b>	<b>93</b>
4.1	Background . . . . .	93
4.2	Modelling framework . . . . .	96
<b>5</b>	<b>First-Order Feedback - Constant Illiquidity</b>	<b>100</b>
5.1	Implementation . . . . .	101
5.2	Numerical results . . . . .	104
5.2.1	Denominator of the volatility term . . . . .	104
5.2.2	Put-call parity . . . . .	111
5.2.3	Illiquidity $\lambda$ impact on pricing option . . . . .	118
5.3	Comparison with Glover (2008) model . . . . .	123
<b>6</b>	<b>First-Order Feedback - Stochastic Illiquidity</b>	<b>129</b>
6.1	Implementation . . . . .	132
6.2	Comparison between constant and stochastic illiquidity parameter . . . . .	133
6.2.1	Denominator of the volatility term . . . . .	134
6.2.2	Sensitivity of option price to the choice of parameters . . . . .	141
6.2.3	Illiquidity $\theta$ impact on pricing option . . . . .	147
6.3	First-order feedback wrap-up . . . . .	150
<b>7</b>	<b>Full Feedback Model - Constant Illiquidity</b>	<b>151</b>
7.1	Implementation . . . . .	152
7.2	Smoothed payoffs . . . . .	156
7.2.1	A problem with using standard payoff functions . . . . .	156
7.2.2	Resolution . . . . .	158

7.3	Problems arising from smoothed function - failure paths . . . . .	161
7.3.1	Abandoned paths . . . . .	161
7.3.2	Extreme values of Gamma . . . . .	166
7.4	Illiquidity $\lambda$ impact on pricing option . . . . .	170
7.4.1	Option pricing with standard payoffs . . . . .	170
7.4.2	Option pricing with smoothed payoffs . . . . .	173
7.5	Summary . . . . .	181
<b>8</b>	<b>Full Feedback Model - Stochastic Illiquidity</b>	<b>182</b>
8.1	Implementation . . . . .	182
8.2	Standard payoffs $\omega = 0$ . . . . .	186
8.2.1	Illiquidity $\lambda$ impact on option pricing . . . . .	186
8.2.2	Maturity $T$ impact on option pricing . . . . .	189
8.2.3	A comparison of full feedback model and first-order feedback model with constant and stochastic illiquidity . . . . .	190
8.3	Smoothing payoffs $\omega \neq 0$ . . . . .	191
8.3.1	Illiquidity $\lambda$ impact on pricing option . . . . .	191
8.3.2	Implied volatility in illiquidity models . . . . .	193
<b>9</b>	<b>Conclusions</b>	<b>198</b>
9.1	Summaries . . . . .	198
9.2	Further research . . . . .	201
<b>A</b>	<b>Basic Notation and Abbreviation</b>	<b>203</b>
<b>B</b>	<b>Computational Time for 1D-MJD Models</b>	<b>205</b>
<b>References</b>		<b>206</b>

# List of Tables

2.1	Illustration of radical inverse function $\psi_2(k)$ and $\psi_3(k)$ . . . . .	46
3.1	FTSE100 Data information . . . . .	60
3.2	Parameter estimators . . . . .	61
3.3	1D-MJD: Impact of $\lambda$ on pricing Bermudan and European options under the following parameter setting: $S = K = 100, T = 1, r = 0.05, \sigma = 0.15, \mu = -0.9, \delta = 0.45, M = 2000$ and $M_{run} = 5000$ . The results for European options are calculated by Eq (3.2). . . . .	72
3.4	This set of parameters is used to demonstrate the numerical approach of pricing a Bermudan put under two assets with jump diffusion. . . . .	77
3.5	This set of parameters is used to demonstrate the numerical approach for pricing a Bermudan put on 1D SVJJ model, which is from Duffie, Pan and Singleton (2000) . . . . .	80
3.6	The optimal parameter setting is used in pricing a Bermudan put with the extrapolation procedure. . . . .	84
3.7	This set of parameters is used to demonstrate the numerical approach of pricing a Bermudan put on 2D SVJJ model . . . . .	88
3.8	Parameter setting for different jump models and Black-Scholes models, which are one-dimensional Black-Scholes model (1D-BS), one-dimensional Merton jump diffusion model (1D-MJD) and one-dimensional stochastic volatility jump diffusion model (1D-SVJJ), and their two-dimensional versions: 2D-BS, 2D-MJD, and 2D-SVJJ. . . . .	90

3.9	comparison of put prices in different jump models. The results shown in the column $M^{ext}$ are given by the simulation with the extrapolation scheme for $M = 2000, 4000$ and $8000$ . All the results are obtained after $M_{run} = 5000$ runs.	91
5.1	European option pricing and Deviation of PCP with respect to the number of time-steps $N$ for (a) $\bar{S} = 7$ & (b) $\bar{S} = 10$ , assumed parameters: $\lambda = 1, S_0 = K = 1, r = 0.04, \sigma = 0.2, T = 10$ and $M = 10^6$ . The numbers in the parentheses of the first column are the discretization bias estimated by $1/\sqrt{N} - 1/\sqrt{N_{2000}}$ where $N_{2000} = 2000$ and others are the value differences from the one given by $N = 2000$ .	115
6.1	The number of abandoned paths with negative prices in $10^6$ sample paths.	136
6.2	Comparison of reference value $\theta^*$ calculated by Eq (6.18) with the approximate value by simulation with $10^6$ sample paths.	149
7.1	Smoothing payoff function for different derivatives used in Glover (2008) $f_2(S, T)$ and our model $f_1(S, T)$ . The standard payoff function is defined as $f_0(S, T)$ .	158
7.2	The impact of $\omega$ on the price of European options under the parameter setting: $\lambda = 0.1, S(t_0) = K = 1, r = 0.04, \sigma = 0.2, T = 10, N = 2000$ . The results is given by $10^6$ simulated paths and the last column data are given by $Dev = C + Ke^{-rT} - P - S(t_0)$ .	160
7.3	Three Causes & Four Causes Contribution to Abandonment Paths (%) for pricing a European put with $S(t_0) = K = 1, r = 0.04, \sigma = 0.2, T = 10, \lambda = \omega = 1$ and $N = 2000, 5000, 10000$ . The results are given by $10^6$ simulations based on 64-bit machines	162
7.4	Abandonment rate of paths with different $h$ & $\epsilon$ when pricing a European put with $S = K = 1, r = 0.04, \sigma = 0.2, T = 10, N = 2000$ and $\lambda = \omega = 1$	166

7.5	The number of the abandoned paths in the full feedback model with constant $\lambda$ . The data in parentheses stand for put options and others for call options. . . . .	173
7.6	The number of the abandoned paths for European options in $10^6$ sample paths. The data in parentheses stand for put options and others for call options. . . . .	175
8.1	Default parameter setting for constant illiquidity model and stochastic illiquidity model. $\lambda^c$ stands for the default value of constant illiquidity. . . . .	185
8.2	The number of the abandoned paths in the full feedback model with stochastic $\lambda$ . The data in parentheses stand for put options and others for call options. . . . .	188
8.3	The number of the abandoned paths for European options in $10^6$ sample paths. The data in parentheses stand for put options and others for call options. . . . .	194
A.1	Mathematical Symbols . . . . .	203
A.2	Elements of options . . . . .	204
A.3	Abbreviations . . . . .	204
B.1	The total computational time (minutes) required for 1D-MJD models. The parameters employed are the same as those in Fig 3.5 . . . . .	205

# List of Figures

2.1	Monte Carlo approximation to $\mathbb{E}(e^Z)$ , where $Z \sim N(0, 1)$ . Vertical lines give computed 95% confidence intervals, middle points on the vertical lines are the approximations. Horizontal dashed line is at height $\mathbb{E}(e^Z) = \sqrt{e}$ .	33
2.2	Monte Carlo approximation to delta of European call option, $S = 0.9, X = 1.0, T = 1, r = 0.04, \sigma = 0.1$ , dashed line gives approximation by finite difference method, horizontal line is exact value from Black-Scholes formula	51
3.1	Pricing European call options by Merton and Black-Scholes models under different parameter sets (shown on the top of each graph). The other parameters applied here are $S = 50, r = 0.05, \sigma = 0.2$ and $T = 0.25$ .	59
3.2	European Option Price from Merton Model against FTSE100 Index Option Price	62
3.3	Pricing European options by Merton and Monte Carlo methods, $S = K = 100, r = 0.05, \sigma = 0.2, T = 1, \lambda = 0.1, \delta = 0.8, \mu = -\delta^2/2$ .	64
3.4	1D-MJD: Bermudan put option respect to different sample sizes in the least squares calculation under the parameter setting: $S = 100, K = 100, T = 0.25, r = 0.05, \sigma = 0.15, N^* = 900, \lambda = 0.1, \mu = -0.9, \delta = 0.45, M_{run} = 5000, \bar{J} = 6$ . The left panel shows the results for $5 \leq N \leq 100$ and the right panel is for $100 \leq N \leq 900$	68

3.5	1D-MJD: Pricing Bermudan put option with different sample sizes $M$ and different runs $M_{run}$ , $S = 100, K = 100, T = 0.25, r = 0.05, \sigma = 0.15, N = 900, \lambda = 0.1, \mu = -0.9, \delta = 0.45$ . . . . .	70
3.6	1D-MJD: Pricing Bermudan put option with different sizes of timesteps $\Delta t$ with the parameter setting: $S = 100, K = 100, T = 1.0, r = 0.05, \sigma = 0.15, \lambda = 0.1, \mu = -0.9, \delta = 0.45, N = 12$ and $M_{run} = 10000$	71
3.7	2D-MJD: Bermudan put option prices depend on the highest order of Chebyshev polynomials $\bar{J}$ and the sample size $M$ . Every knot is obtained from 1000 runs. . . . .	78
3.8	1D-SVJJ: European call and put options pricing by Monte Carlo simulation using the parameters shown in Table 3.5. The x-axis refers to the number of paths which is determined by $N^*$ in Section 3.3.1. . . . .	81
3.9	1D-SVJJ: Bermudan put options pricing by Monte Carlo using the parameters shown in Table 3.5 and $M = 2000, \bar{J} = 6$ . . . . .	81
3.10	1D-SVJJ: Bermudan put options pricing by Monte Carlo simulation using the parameters shown in Table 3.5 and $N = 100, \bar{J} = 6, \Delta t = T/N$ . . . . .	83
3.11	1D-SVJJ: Bermudan put options pricing by Monte Carlo simulation using the parameters shown in Table 3.5 and $N = 100$ , [a] using $J = 6, M = 2000, 4000, 8000$ and [b] using $\Delta t = T/N, M = 4000, 8000, 16000$ . . . . .	84
3.12	2D-SVJJ: Pricing Bermudan put options on the two underlyings with respect to the number of exercise opportunities $N$ using parameter list showed in Table 3.7, $\bar{J} = 6, \Delta t = 0.01$ and $M = 2000$ . . . . .	89
3.13	2D-SVJJ: Bermudan put options pricing by Monte Carlo using parameter list showed in Table 3.7, $J = 6$ , exercise opportunities $N = 100$ and $\Delta t = 0.01$ . . . . .	90
5.1	Value of $SV_{SS}^{BS}$ with respect to $S & t$ , assuming $K = 1, r = 0.04, \sigma = 0.2, T = 10$ and $\Delta t = 0.2$ . . . . .	104
5.2	Location of $(S, \tau)$ for Eq (5.5) to vanish the denominator with different $\lambda$ , assuming $K = 1, r = 0.04, \sigma = 0.2$ . . . . .	106

5.3	The cumulative number of abandoned paths caused by negative price with respect to time-to-expiry $\tau$ & the corresponding location of negative prices, assuming $S_0 = K = 1, r = 0.04, \sigma = 0.2, T = 10, N = 2000, dt = 0.005, M = 10^6$	110
5.4	Pricing European options and examining the violation of PCP under the identical underlying price process with the following parameters: $\lambda = 1, S_0 = K = 1, r = 0.04, \sigma = 0.2, T = 10$ and $N = 2000$ after $M = 10^6$	112
5.5	European option pricing depends on the number of samples paths with varying caps $\bar{S}$ assumed parameters: $\lambda = 1, S_0 = K = 1, r = 0.04, \sigma = 0.2, T = 10$ and $N = 2000$ after $M = 10^6$ runs. The left panel for a European call option and the right one for a European put option.	113
5.6	The violation of PCP depends on the number of samples paths with varying caps $\bar{S}$ assumed parameters: $\lambda = 1, S_0 = K = 1, r = 0.04, \sigma = 0.2, T = 10$ and $N = 2000$ after $M = 10^6$ runs.	114
5.7	The number of abandoned paths with respect to time-to-expiry $\tau$ , assuming $S_0 = K = 1, r = 0.04, \sigma = 0.2, T = 10, N = 2000, dt = 0.005, M = 10^6$	117
5.8	Option prices with respect to the illiquidity $\lambda$ for the parameter setting: $\bar{S} = 10, S = K = 1, r = 0.04, \sigma = 0.2, T = 10$ and $N = 2000$ after $M = 10^6$ . The green lines presents the results for the Black-Schole model to compare with the first-order feedback model	120
5.9	Average volatility & deviation of PCP with respect to the illiquidity $\lambda$ using the same parameter setting as the previous Fig 5.8. The green lines presents the results for the Black-Schole model to compare with the first-order feedback model	121
5.10	Random paths with illiquidity $\lambda = 1.0, \lambda = 2.5$ and $\lambda = 0.0$ . The red paths stand for 1st order feedback model and the green paths for standard Black-Scholes model (i.e. $\lambda = 0.0$ ). Use the same parameter setting as the previous Fig 5.8.	122

5.11	Error of put-call parity changes with respect to illiquidity $\lambda$ in the cases of different caps $\bar{S}$ with parameters: $S = K = 1$ , $r = 0.04$ , $\sigma = 0.2$ , $T = 10$ and $N = 2000$ after $M = 10^5$	123
5.12	Comparison of Glover (2008) model (left hand) and our model (right hand): vanishing regions with respect to varying $\lambda$ under the parameters: $S = K = 1$ , $r = 0.04$ , $\sigma = 0.2$ , $T = 10$ and $N = 2000$ after $M = 10^6$	125
5.13	Comparison of Glover (2008) model (left hand) and our model (right hand): put prices for $T = 1$ (a) and $T = 10$ (b) with respect to varying $\lambda$ under the parameters: $S = K = 1$ , $r = 0.04$ , $\sigma = 0.2$ , $T = 10$ and $N = 2000$ after $M = 10^6$	126
5.14	Comparison of Glover (2008) model (left hand) and our model (right hand): call prices (a) and deviation of PCP (b) with respect to varying $\lambda$ under the parameters: $S = K = 1$ , $r = 0.04$ , $\sigma = 0.2$ , $T = 10$ and $N = 2000$ after $M = 10^6$	128
6.1	The cumulative number of abandoned paths caused by negative price with respect to time-to-expiry $\tau$ & the corresponding location of negative prices. The results are given by $10^6$ simulated paths	135
6.2	The location of $\lambda$ for negative prices with varying maturity $T$ . The scattered points is given by the results of $M = 10^6$ runs.	137
6.3	Pricing European options and examining the violation of PCP under the identical underlying price process. The thicker lines are for the stochastic illiquidity model and the thinner lines for the constant illiquidity model.	140
6.4	The difference of put prices with stochastic $\lambda$ and constant $\lambda$ depends on varying maturity $T$ under the parameters: $\kappa = 0.35$ , $\zeta = 0.2$ , $\rho = 0$ and others shown in the section. The standard Black-Scholes prices are evaluated for the following parameters: $S_0 = K = 1$ , $r = 0.04$ , $\sigma = 0.2$ . The scattered points is given by the results of $M = 10^6$ runs.	142

6.5 Put prices with stochastic $\lambda$ and constant $\lambda$ depends on varying moneyness under the parameters: $K = 1$ , $T = 1$ , $\kappa = 0.35$ , $\zeta = 0.2$ , $\rho = 0$ and others shown in the section. The scattered points is given by the results of $M = 10^6$ runs . . . . .	143
6.6 The difference of put prices with stochastic $\lambda$ and constant $\lambda$ depends on varying moneyness using the results from Fig 6.5. The scattered points is given by the results of $M = 10^6$ runs; the smoothed curve line is produced by least-squares fitting & the fitting function is assumed as $f(x) = \frac{a}{b+(x-1)^2}$ . . . . .	144
6.7 The prices of put option with respect to the correlation $\rho$ under the parameters: $S_0 = K = 1$ , $T = 10$ , $\kappa = 0.35$ , $\zeta = 0.2$ and others shown in the section. . . . .	145
6.8 The prices of put option with respect to the adjustment speed $\kappa$ and the volatility $\zeta$ under the parameters: $T = 10$ , $\rho = 0$ ( $\zeta = 0.2$ , $\kappa = 0.35$ ) and others shown in the section. . . . .	146
6.9 Pricing a European put option depends on long-term illiquidity $\theta$ (or $\lambda^c$ ) with different maturity $T = 0.1$ , $1.0$ and $10$ in the left panel. The corresponding differences in the put prices between two models are given in the right panel, which is calculated by the formula $P_{stoch} - P_{const}$ . The thicker line indicates the stochastic illiquidity model and the thinner line for the constant illiquidity model. $\theta$ is taken as $0.1, 0.2, 0.3, \dots, 9.9, 1.0$ . . . . .	148
6.10 Abandonment rate of paths depends on long-term illiquidity $\theta$ (or $\lambda^c$ ) with different maturity $T = 0.1$ , $1.0$ and $10$ in the left panel. The thicker line indicates the stochastic illiquidity model and the thinner line for the constant illiquidity model. $\theta$ is taken as $0.1, 0.2, 0.3, \dots, 9.9, 1.0$ . These results are as result of $10^6$ sample paths. . . . .	149

7.1	Estimate of $V_{SS}(t_0)$ for a European call option in a perfect liquid market, i.e. $\lambda = 0$ with a standard payoff function $f_0(S, T) = \max(S(T) - K, 0)$ in the left panel and with a smoothing payoff function $f_1(S, T) = \frac{K(S(T)-K+\sqrt{(S(T)-K)^2+\omega^2})}{K+\sqrt{K^2+\omega^2}}$ in the right panel under the same parameter setting: $S(t_0) = K = 1, r = 0.04, \sigma = 0.2, T = 10, N = 2000$ . . . . .	157
7.2	Different smoothing payoff functions depend on the illiquidity $\omega$ , which are the standard payoff function $f_0(S, T)$ , Glover's smoothed payoff $f_2(S, T)$ and the modified smoothed payoff $f_1(S, T)$ . . . . .	159
7.3	Abandonment rate of paths in pricing a European put with $S(t_0) = K = 1, r = 0.04, \sigma = 0.2, T = 10, \lambda = \omega = 1$ and $N = 2000$ . . . . .	162
7.4	The number of abandoned (living) paths with the changes of the sign of the denominator pricing a European put with $S(t_0) = K = 1, r = 0.04, \sigma = 0.2, T = 10, \lambda = \omega = 1$ and $N = 2000$ . Each sample is given by $10^6$ paths. . . . .	163
7.5	Contour figures of abandonment rate in the $\omega$ versus $\lambda$ plane for pricing a European put with $S = K = 1, r = 0.04, \sigma = 0.2, T = 10, N = 2000$ and $\bar{S} = 10$ . The red dash lines $\alpha$ stand for the condition line $\alpha : \lambda = 2\omega$ while the black curve $\beta$ stands for the condition line $\beta : \lambda = \omega(1 + \sqrt{1 + (\omega/K)^2})/\bar{S}$ . The data is given by $10^5$ sample paths.	164
7.6	Abandonment rate of paths with different $S$ when pricing a European put with $K = 1, r = 0.04, \sigma = 0.2, T = 10, N = 2000$ and $\lambda = \omega = 1$ .	166
7.7	A particular path with extreme values of Gamma in pricing a European put with $S = K = 1, r = 0.04, \sigma = 0.2, T = 10, \lambda = \rho = 1$ and $N = 2000$	167
7.8	A particular path with extreme values of Gamma in pricing a European put with $S = K = 1, r = 0.04, \sigma = 0.2, T = 10, \lambda = \rho = 1$ and $N = 2000$	167
7.9	A particular path with extreme values of Gamma in pricing a European put with $S = K = 1, r = 0.04, \sigma = 0.2, T = 10, \lambda = \rho = 1$ and $N = 2000$	168
7.10	A test by $10^5$ sample paths with $S = K = 1, r = 0.04, \sigma = 0.2, T = 10, \lambda = \rho = 1$ and $N = 2000$ . . . . .	169

7.11 The number of abandoned (living) paths with extreme values of Gamma in pricing a European put with $S(t_0) = K = 1$ , $r = 0.04$ , $\sigma = 0.2$ , $T = 10$ , $\lambda = \omega = 1$ and $N = 2000$ . Each sample is given by $10^6$ paths.	170
7.12 European option prices depend on the illiquidity $\lambda$ . Note the green line with $\lambda = 0.5$ is close to the red line with $\lambda = 0.0$ in the case of call & the three lines: blue ( $\lambda = 1$ ), green ( $\lambda = 0.5$ ) and red ( $\lambda = 0.0$ ) are close in the case of put.	171
7.13 European option price depends on the illiquidity $\lambda$ : 0, 0.1, 0.3, 0.5, 0.7, 1, 3 and 5 and the corresponding violation of put-call parity. We use the same parameter setting as Fig 7.12. All points are produced by $10^6$ sample paths.	172
7.14 Pricing a European Call Option in various moneyness: DITM ( $S = 1.5$ ), ITM ( $S = 1.2$ ), ATM ( $S = 1.0$ ), OTM ( $S = 0.8$ ) and DOTM ( $S = 0.5$ ) in a liquid market (thicker lines) or an illiquid market (thinner lines). The following parameters are used: $K = 1.0$ , $\rho = 1.0$ , $T = 10$ , $r = 0.04$ and $\sigma = 0.2$	174
7.15 European option prices depend on the illiquidity $\lambda$ and the deviation from put-call parity.	176
7.16 Comparison of European option prices and the corresponding deviation of the put-call parity between full feedback model with a cap $\bar{S} = 10$ and without any caps. The other parameters are the same values as Fig 7.15.	177
7.17 Histogram for $\ln(S_T/S_0)$ from $10^5$ sample paths, with lognormal density function for perfect liquid assets, i.e. $\lambda = \omega = 0$ . Top: $\omega = 0$ , middle: $\omega = 0.1$ and bottom: $\omega = 1$ .	178
7.18 European option prices and the corresponding deviation of the put-call parity when the same values of $V_{SS}$ are used in the full feedback model. We assume $\lambda = 1$ , $\omega = 0.1$ and cap $\bar{S} = 10$ ; the other parameters are the same values as Fig 7.17.	180

8.1	Option price depends on illiquidity using the standard payoffs in the stochastic (constant) illiquidity full feedback model. We assume $\theta = \lambda_0 = \lambda^c$ .	186
8.2	Probability density estimate of log return over ten-year horizon for pricing call options (left side) and put options (right side) under the stochastic (constant) illiquidity full feedback model with $N((r - \frac{1}{2}\sigma^2)T, \sigma^2T)$ density superimposed for Black-Scholes model.	187
8.3	Call prices depends on maturity $T$ in full feedback models with constant illiquidity (thinner lines) and stochastic illiquidity (thicker lines). The error percent is calculated by $(C_{stoch} - C_{const})/C_{const}$ .	189
8.4	Option pricing in different feedback models: first-order feedback model with constant illiquidity (1st-ci) and with stochastic illiquidity (1st-si), full feedback model with constant illiquidity (full-ci) and with stochastic illiquidity (full-si), compared with Black-Scholes prices (bs).	190
8.5	Option price depends on illiquidity in the stochastic (constant) illiquidity full feedback model under smoothing payoffs. We also give the corresponding error from put call parity assuming $\theta = \lambda_0 = \lambda^c$ . The left panel is for $\omega = 0.1$ and the right panel for $\omega = 1.0$ .	192
8.6	Probability density estimate of log return over a ten-year horizon for pricing call options (left side) and put options (right side) under the stochastic (constant) illiquidity full feedback model for $\lambda^c = 1$ with $N((r - \frac{1}{2}\sigma^2)T, \sigma^2T)$ density superimposed for Black-Scholes model. Top: $\omega = 0$ , middle: $\omega = 0.1$ and bottom: $\omega = 1$ .	195
8.7	Pricing European put options (left) and the Black-Scholes implied volatilities (right) with respect to varying strike prices in different feedback models: first-order feedback model with constant illiquidity (1st-ci) and with stochastic illiquidity (1st-si), full feedback model with constant illiquidity (full-ci) and with stochastic illiquidity (full-si), compared with Black-Scholes prices (bs).	196

# The University of Manchester

Dong-Mei Wang

Doctor of Philosophy

monte carlo simulations for complex option pricing

December 14, 2010

The thesis focuses on pricing complex options using Monte Carlo simulations. Due to the versatility of the Monte Carlo method, we are able to evaluate option prices with various underlying asset models: jump diffusion models, illiquidity models, stochastic volatility and so on. Both European options and Bermudan options are studied in this thesis.

For the jump diffusion model in Merton (1973), we demonstrate European and Bermudan option pricing by the Monte Carlo scheme and extend this to multiple underlying assets; furthermore, we analyse the effect of stochastic volatility.

For the illiquidity model in the spirit of Glover (2008), we model the illiquidity impact on option pricing in the simulation study. The four models considered are: the first order feedback model with constant illiquidity and stochastic illiquidity; the full feedback model with constant illiquidity and stochastic illiquidity. We provide detailed explanations for the present of path failures when simulating the underlying asset price movement and suggest some measures to overcome these difficulties.

# **Declaration**

No portion of the work referred to in this thesis has been submitted in support of an application for another degree or qualification of this or any other university or other institute of learning.

# Copyright Statement

- i. The author of this thesis (including any appendices and/or schedules to this thesis) owns any copyright in it (the “Copyright”) and s/he has given The University of Manchester the right to use such Copyright for any administrative, promotional, educational and/or teaching purposes.
- ii. Copies of this thesis, either in full or in extracts, may be made **only** in accordance with the regulations of the John Rylands University Library of Manchester. Details of these regulations may be obtained from the Librarian. This page must form part of any such copies made.
- iii. The ownership of any patents, designs, trade marks and any and all other intellectual property rights except for the Copyright (the “Intellectual Property Rights”) and any reproductions of copyright works, for example graphs and tables (“Reproductions”), which may be described in this thesis, may not be owned by the author and may be owned by third parties. Such Intellectual Property Rights and Reproductions cannot and must not be made available for use without the prior written permission of the owner(s) of the relevant Intellectual Property Rights and/or Reproductions.
- iv. Further information on the conditions under which disclosure, publication and exploitation of this thesis, the Copyright and any Intellectual Property Rights and/or Reproductions described in it may take place is available from the Head of the School of Mathematics.

# Acknowledgements

I would like to express my sincere appreciation and gratitude to my supervisors Professor Peter W. Duck and Professor David P. Newton for their helpful suggestions and discussions throughout of my research. Without their support, collaboration and guidance, I would not come to this stage along the way.

Also I would gratefully acknowledge the colleagues in Financial Mathematics Group in University of Manchester for their generous help and advice. A special thanks to Sebastian Law and Edwin Broni-Mensah in particular for their unwavering enthusiasm and encouragement.

Last, but by no means least, I am deeply indebted to my parents. Their love and endless support gave me the energy to attain the study. This thesis is dedicated to them.

# **Dedication**

*To Dad and Mom...*

# Chapter 1

## Introduction

*What is the last thing you do before you climb on a ladder? You shake it, and that is Monte Carlo simulation.*

– Sam Savage

*Business Week, 22 January 2001*

The enormous growth of derivatives markets since the 1970s has made option-pricing theory one of the most dynamic areas in finance. It has become more important than before because many corporate liabilities can be expressed in terms of options or combinations of options. In the absence of closed-form analytical solutions of derivatives' prices, numerical solution is required. For example, the pricing of American, path-dependent and multi-asset options features, generally involves the use of numerical methods. Aside from these relatively more complicated options, it is also difficult to provide analytic solutions to European style options based on underlying asset price models incorporating jumps in returns, jumps in volatility and stochastic interest rates. Thus, pricing problems ultimately very often require a numerical procedure, and the choice of methods involves the best combination of speed, accuracy, simplicity and generality.

In a frictionless market, the arbitrage price of options can be expressed as the expectation of the corresponding payoff, which is usually defined as a function of the underlying asset price process. The founding papers in option pricing are Black and

Scholes (1973) and Merton (1973). Black and Scholes assume that the underlying asset price follows a geometric Brownian motion and set up a replicating portfolio which consists of an option and short a number of units of the underlying. A no arbitrage argument leads to a second-order-linear partial differential equation (PDE) determining the option values (the Black-Scholes-Merton PDE). Boundary conditions are then applied, according to the option type and option pricing is achieved by solving the PDE. The Black-Scholes formula can be viewed in terms of a risk-neutral world, given that there is continuous hedging. This means that in such a world, expected returns on the portfolio are equal to the risk-free rate of interest.

The present thesis focuses on Monte Carlo simulation to obtain numerical solutions to option pricing problems. Monte Carlo simulation is a widely used tool within finance for computing the price of financial instruments. Boyle (1977) first proposed the application of Monte Carlo the technique to evaluate the value of European options. Other pioneering works include Bossaerts (1989) and Tilley (1993). The basic principle behind option pricing by the Monte Carlo method is to calculate the expected value of a quantity which is a function of the solution to a stochastic differential equation (SDE). Recent research focuses on: (1) path simulation methods, especially when there are nonlinearities in the financial SDEs such as full feedback models studied by Frey and Patie (2002); (2) computational improvements through variance reduction techniques discussed in detail in Glasserman (2003); (3) extending the Monte Carlo method to price complex financial derivatives, such as American options proposed in Longstaff and Schwartz (2001) and foreign exchange derivatives in Xiao (2007). Extensive discussions on the development of Monte Carlo simulation for option pricing are given by Boyle, Broadie and Glasserman (1997) and Glasserman (2003). For a more comprehensive reference on analysis of numerical methods for solving SDEs, see Kloeden and Platen (1999).

The Monte Carlo method has distinct advantages in dealing with a wide range of option types because it is simple and flexible. The method is based on the distribution of terminal asset prices, determined by the process governing the future price movements. The calculation generates a series of asset price trajectories and

the terminal asset prices from the series are used to estimate the option price and compute the confidence limits at the same time. The standard error of the estimate scales as  $1/\sqrt{n}$ , where  $n$  denotes the number of the trajectories. Since this is independent of the number of dimensions, the Monte Carlo method does not suffer from the “curse of dimensionality” that affects other numerical techniques in finance. As for the improvement of the efficiency, much attention has been put on quasi-Monte Carlo and low-discrepancy methods (see Niederreiter, 1992; Birge, 1995; Paskov and Traub, 1995; Joy, Boyle and Tan, 1996; Owen, 1997).

This thesis will focus on Monte Carlo simulations to solve option pricing problems on particular underlying (complex) asset models, including jump diffusion models and feedback models. The main contributions made in this thesis are stated as follows:

In the jump diffusion models, we calibrate the Merton (1976) model using an analytical solution and compare the result with that of the Black-Scholes option pricing formula. We also introduce another kind of jump diffusion model in this thesis, which is called double-jump stochastic volatility model. Both models are extended into multiple dimensional case to price basket options. The key contribution made here is to illustrate a least square regression method of pricing Bermudan options under these jump diffusion models. Numerical results show how the parameters of specific models impact on pricing options. In addition, the simulation is accompanied by an extrapolation technique to improve the accuracy.

The another main contribution of the thesis is to provide a numerical solution to pricing options in feedback models, which are developed from Glover (2008), using Monte Carlo simulation. We derive two kinds of the feedback models: the first-order feedback and the full feedback models. The implementation of the first-order feedback model is straightforward. However, there still exist a small amount of invalid sample paths that have to be discarded. We give the reason to explain the phenomenon and suggest to discard these paths from the simulation, under the assumption that the law of large number holds. For the full feedback model, the implementation is more complicate than that of the first-order feedback model. We use a three-point finite difference method to compute the second partial derivatives of option prices

with respect to asset prices (i.e. Gamma). The Gammas are calculated at each time step from the current simulated path, then we reproduce the same path using these Gammas. The procedure continues iterating until a convergent option price is obtained from the path. As the first-order feedback model, there are invalid sample paths observed during the simulation. We propose several methods to reduce the abandonment rate of the sample paths. One of them is that we price a call option by the corresponding put option value with the put-call parity. This is because the abandoned paths occur less frequently when pricing a put option than pricing a call option. To obtain a convergent option price, we suggest to use a smoothed payoff function instead of a standard payoff. But there exists a restriction of the smoothing parameter. If the restriction did not satisfies, there would be a number of abandoned paths during the simulation. The feedback models have been extended to include a stochastic illiquidity process. An option price comparison of these four feedback models is made in this thesis. For a long-term option,<sup>1</sup> the model with the stochastic illiquidity leads to a modest lower option price, compared with the constant illiquidity model. The option price in the full feedback model is lower than that of the first-order feedback model. A discussion of the corresponding implied volatilities are included in this thesis.

In sum, we provide numerical solutions to pricing Bermudan options in the Merton jump diffusion model and the double-jump stochastic volatility model using Monte Carlo simulation. With an extrapolation method, a desirable estimate can be achieved. In feedback models, we concentrate on solving the difficulties in the model implementation using Monte Carlo simulation. The thesis also presents numerical results of parameter sensitivity in all models.

Chapter 2 provides a brief introduction to the fundamental principles underlying Monte Carlo simulation and theorems of derivative pricing. A short review of various techniques to improve the accuracy of the simulation pricing is presented, which includes variance reduction methods, discretization methods and Quasi Monte Carlo methods. Calculation of Greeks and American option pricing through simulation

---

<sup>1</sup>Normally, its maturity is longer than two years.

methods are discussed in this chapter.

In Chapter 3, we investigate the underlying asset process involving unpredictable jump events. The basic jump diffusion model has been extended in two ways: turning single asset cases into multiple asset cases and replacing a constant volatility with a stochastic volatility. The correlations between asset returns and their volatilities are also discussed. The examples covered in this chapter are arranged in increasing order of complexity. We start with pricing one-dimensional Bermudan options with constant volatility in Section 3.3, then consider pricing multi-dimensional options in Section 3.4. In Section 3.5 and Section 3.6, we study underlying asset price processes with jumps and stochastic volatility in one-dimensional and multi-dimensional cases, respectively.

From Chapter 4 to Chapter 8, we focus on another kind of asset model, referred to *feedback* models, which include the price impact of trade volume in an illiquid market for the underlying. Chapter 4 gives an introduction to the model types and derives two generalized forms of feedback model: first-order feedback and full-order feedback. The former are discussed in Chapter 5 where the illiquidity is assumed to be constant and Chapter 6 where stochastic illiquidity is employed; the latter are addressed in the next two chapters: Chapter 7 focuses on the full feedback model with constant illiquidity and Chapter 8 considers stochastic illiquidity.

Chapter 9 gives a summary of the thesis and several suggestions for further studies.

# Chapter 2

## Preliminaries

*Anyone who considers arithmetical methods of producing random digits  
is, of course, in a state of sin.*

– John von Neumann

*Various techniques used in connection with random digits, 1951*

This chapter is arranged as follows. We address principles underlying derivative pricing in Section 2.1 and Monte Carlo methods in Section 2.2. The core algorithm of Monte Carlo methods is based on a uniform random number generator, which is introduced in Section 2.3. To improve the Monte Carlo simulation, Section 2.4 discusses various variance reduction techniques and analyzes the advantages and disadvantages of the application of such methods. Section 2.5 presents several basic discretization schemes to reduce the bias in Monte Carlo estimates. Section 2.6 develops an optimal strategy for allocation of computing time to reduce sampling error and discretization error in the simulation. The implementation of Monte Carlo methods for the evaluation of the Greeks is introduced in Section 2.8 and a numerical example is illustrated to show that Monte Carlo estimates converge towards the corresponding exact values calculated by the Black-Scholes formula (the exact solution of the Black-Scholes-Merton PDE for plain European options). Section 2.9 presents several modified Monte Carlo simulations to deal with pricing American options.

## 2.1 Principles of derivatives pricing

Kwok (2008, p. 35) states that “The concepts of *replicable contingent claims*, *absence of arbitrage* and *risk neutrality* form the cornerstones of modern option pricing theory.” In this section, basic mathematical concepts underlying derivative pricing are presented, with important applications of Monte Carlo methodology.

### 2.1.1 Arbitrage pricing

One of the basic requirements of (financial) derivatives pricing is the no-arbitrage principle. The absence of arbitrage opportunities brings to mind the common expression “there’s no such thing as a free lunch”. More formally, an arbitrage can arise in either of the following scenarios (see Glasserman, 2003):

1.  $\theta(0)^\top S(0) < 0$  and  $\mathbb{P}(\theta(t)^\top S(t) \geq 0) = 1$ ;
2.  $\theta(0)^\top S(0) = 0$  and  $\mathbb{P}(\theta(t)^\top S(t) \geq 0) = 1$ , and  $\mathbb{P}(\theta(t)^\top S(t) > 0) \geq 0$ ;

where  $\mathbb{P}$  represents the true (objective) probability measure in the real world;  $S(t)$  represents the current state of  $d$  assets at time  $t$ , i.e.  $S(t) = (S_1(t), \dots, S_d(t))^\top$ ;  $\theta(t) = (\theta_1(t), \dots, \theta_d(t))$  is the number of units of each asset held at time  $t$ , which is a self-financing trading strategy<sup>1</sup>. The first statement (1) describes that one can follow the trading strategy with a negative current net commitment that yet produces a positive profit in the future. The second trading strategy (2) without net investment today can guarantee a nonnegative final wealth. Both strategies lead to arbitrage opportunities to create an excess profit that contradicts the existence of economic equilibrium. In practice, arbitrage opportunities may exist during short intervals; however these mispricings will be corrected by the pressure of supply and demand in the market. The no-arbitrage argument is one of the fundamental assumptions in deriving the celebrated Black-Scholes-Merton partial differential equation (see for example Wilmott, Howison and Dewynne, 1995).

---

<sup>1</sup>A trading strategy is *self-financing* if it satisfies  $\theta(t)^\top S(t) - \theta(0)^\top S(0) = \int_0^t \theta(u)^\top dS(u)$ .

### 2.1.2 Risk-neutral probabilities

A risk-neutral probability, which we denote by  $\mathbb{Q}$ , is a synthetic probability corresponding to  $\mathbb{P}$ , meaning that they have the same set of zero probability. The fundamental theorem of asset pricing states that in the absence of arbitrage opportunities in a complete market implies that there exists a unique equivalent risk-neutral measure (e.g. Kwok, 2008). Hence, under the risk-neutral measure, the valuation of an option is given by the expected payoff of the option discounted by a risk-free rate rather than the real (time varying) rate for the underlying asset. For example, consider the price of the  $i$ -th of  $d$  assets following a system of SDEs:

$$\frac{dS_i(t)}{S_i(t)} = \mu_i dt + \sigma_i^\top dW^{\mathbb{P}}(t) ,$$

where  $\mu_i$  is the drift parameter reflecting investor attitudes towards risk: she may expect to riskier assets to win a higher return;  $\sigma_i$  is the diffusion parameter and  $W^{\mathbb{P}}$  is a Brownian motion under the objective measure  $\mathbb{P}$ . The relative risk-neutral dynamics of the asset prices can be described as:

$$\frac{dS_i(t)}{S_i(t)} = r dt + \sigma_i^\top dW^{\mathbb{Q}}(t) ,$$

with a riskless growth rate  $r$  and a different Brownian motion  $W^{\mathbb{Q}}$  under the risk-neutral measure  $\mathbb{Q}$ . Comparing the two systems of SDEs, we find the relation between  $W^{\mathbb{P}}$  and  $W^{\mathbb{Q}}$ , which is:

$$dW^{\mathbb{Q}}(t) = dW^{\mathbb{P}}(t) + \nu(t)dt ,$$

for some  $\nu(t)$  satisfying

$$\mu_i = r + \sigma_i^\top \nu , \quad i = 1, \dots, d .$$

This presentation suggests that  $\nu(t)$  can be interpreted as a risk premium, which is an additional return from the risky asset over that from a risk-free asset.  $\nu$  is also called the market price of risk. There are advantages in using  $\mathbb{Q}$  measure over the  $\mathbb{P}$  measure for Monte Carlo simulation:

- It is easier to produce sample paths with a risk-free rate  $r$  under risk-neutral measure. Because under the real probability measure  $\mathbb{P}$ , the drift parameter  $\mu_i$  associated with varying risk preferences of investors is much harder to estimate, while  $r$  can be estimated as a riskless interest rate.
- The option price can be estimated as the expected payoff at expiry discounted at a risk-free rate, namely,

$$V(t) = e^{-r(T-t)} \mathbb{E}^{\mathbb{Q}}(V(T)), \quad t < T,$$

where  $\mathbb{E}^{\mathbb{Q}}$  is the expectation under the risk-neutral measure  $\mathbb{Q}$ . This also implies that the price process  $V(t)$  is a  $\mathbb{Q}$ -martingale as the expected discounted value of  $e^{-r(T-t)}V(T)$  does not change with time and is equal to the current value  $V(t)$ .

## 2.2 Principles of Monte Carlo

In this section, some fundamental theorems of probability and statistics applied to the Monte Carlo techniques will be introduced. The definition and results reviewed in this section can help readers understand what principles support the numerical method.

When we analyse a method, there are three particularly important considerations: bias, variance and computing time.

### 2.2.1 Law of large numbers

Consider the case of a general random variable  $X$ , whose expected value  $\mathbb{E}(X) = \mu$  and variance  $Var(X) = \sigma^2$  are not known. If we let  $X_1, X_2, \dots, X_n$  denote independent random variables with the same distribution as  $X$ , then we might expect the estimator  $\hat{\mu}$

$$\hat{\mu} := \frac{1}{n} \sum_{i=1}^n X_i \tag{2.1}$$

$$\begin{aligned}
 \mathbb{E}(\hat{\mu}) &= \frac{1}{n}\{\mathbb{E}(X_1) + \mathbb{E}(X_2) + \cdots + \mathbb{E}(X_n)\} \\
 &= \frac{1}{n}\{\mu + \mu + \cdots + \mu\} \\
 &= \mu
 \end{aligned}$$

to be a good approximation to  $\mu$ . This is a unbiased estimator, that is, its expected value is the same as  $\mu$ . The detailed definition is given as follows.

**Theorem 2.1 (Law of Large Numbers).** *Let  $X_1, X_2, \dots, X_n$  be an independent trials process, with finite expected value  $\mu = \mathbb{E}(X_i)$  and finite variance  $\sigma^2 = \text{Var}(X_i)$ . Let  $S_n = X_1 + X_2 + \dots + X_n$ , then for any  $\epsilon > 0$ ,*

$$P\left(\left|\frac{S_n}{n} - \mu\right| \leq \epsilon\right) \rightarrow 0 \quad \text{as } n \rightarrow \infty.$$

Equivalently,

$$P\left(\left|\frac{S_n}{n} - \mu\right| < \epsilon\right) \rightarrow 1 \quad \text{as } n \rightarrow \infty.$$

In fact, the law of large numbers ensures that this estimate  $\hat{\mu}$  converges to the correct value,  $\mu$ , as the number of random variables increases. This idea leads us to the basic Monte Carlo method for approximating the expectation of a function of a random variable. We take a long run average of the function as its expectation. Using a similar method, one can estimate the variance  $\sigma^2$  using the sample variance  $\hat{\sigma}^2$  as follows (Miller and Miller, 2004):

$$\begin{aligned}
 \hat{\sigma}^2 &:= \frac{1}{n-1} \sum_{i=1}^n (X_i - \hat{\mu})^2. \tag{2.2} \\
 \mathbb{E}(\hat{\sigma}^2) &= \mathbb{E}\left(\frac{1}{n-1} \sum_{i=1}^n (X_i - \hat{\mu})^2\right) \\
 &= \frac{1}{n-1} \mathbb{E}\left(\sum_{i=1}^n (X_i^2 - 2\hat{\mu}X_i + \hat{\mu}^2)\right) \\
 &= \frac{1}{n-1} \{\mathbb{E}(\sum_{i=1}^n X_i^2) - \mathbb{E}(\sum_{i=1}^n 2\hat{\mu}X_i) + \mathbb{E}(\sum_{i=1}^n \hat{\mu}^2)\} \\
 &= \frac{1}{n-1} (\mathbb{E}(\sum_{i=1}^n X_i^2) - \mathbb{E}(n\hat{\mu}^2)) \\
 &= \frac{1}{n-1} (n\mathbb{E}(X_i^2) - n\mathbb{E}(\hat{\mu}^2)),
 \end{aligned}$$

$$\begin{aligned} \text{since } \mathbb{E}(\hat{\mu}^2) &= Var(\hat{\mu}) + \mathbb{E}^2(\hat{\mu}) \\ &= \frac{\sigma^2}{n} + \mu^2, \\ \text{thus } \mathbb{E}(\hat{\sigma}^2) &= \frac{1}{n-1} [n(\sigma^2 + \mu^2) - n(\frac{\sigma^2}{n} + \mu^2)] \\ &= \sigma^2, \end{aligned}$$

which shows that  $\hat{\sigma}^2$  is an appropriate unbiased estimate of  $\sigma^2$ .

### 2.2.2 Central limit theorem

Now we are interested in the difference between  $\hat{\mu}$  and  $\mu$ , that is  $\hat{\mu} - \mu$ . First we introduce the Central Limit Theorem which is the second foundational theorem in probability.

**Theorem 2.2 (Central Limit Theorem).** *Let  $X_1, X_2, \dots, X_n$  be a sequence of i.i.d. random variables with expectation  $\mu$  and variance  $\sigma^2$ , then the distribution of*

$$\hat{\mu} - \mu \sim N(0, \frac{\sigma^2}{n})$$

as  $n \rightarrow \infty$ , where  $\hat{\mu} = \frac{1}{n} \sum_{i=1}^n X_i$ . Equivalently,

$$\frac{\hat{\mu} - \mu}{\frac{\sigma}{\sqrt{n}}} \sim N(0, 1)$$

as  $n \rightarrow \infty$ .

This suggests that if the sample size  $n$  is very large, the estimate  $\hat{\mu}$  should be close to  $\mu$ , with error  $O(\frac{1}{\sqrt{n}})$ .

We can make the argument more precise by using the idea of a confidence interval. By applying the unbiased estimators  $\hat{\mu}$  in (2.1) and  $\hat{\sigma}^2$  in (2.2), the confidence interval for the estimate  $\hat{\mu}$  with probability 0.95 can be gained from

$$\begin{aligned} \mathbb{P}\left(\left|\frac{\hat{\mu} - \mu}{\frac{\sigma}{\sqrt{n}}}\right| \leq 1.96\right) &= 0.95 \\ \mathbb{P}\left(\hat{\mu} - \frac{1.96\sigma}{\sqrt{n}} \leq \mu \leq \hat{\mu} + \frac{1.96\sigma}{\sqrt{n}}\right) &= 0.95 \end{aligned}$$

that is,

$$\left[\hat{\mu} - \frac{1.96\hat{\sigma}}{\sqrt{n}}, \hat{\mu} + \frac{1.96\hat{\sigma}}{\sqrt{n}}\right]. \quad (2.3)$$

This interval ensures the efficiency of the Monte Carlo method to approximate  $\mu$ . In

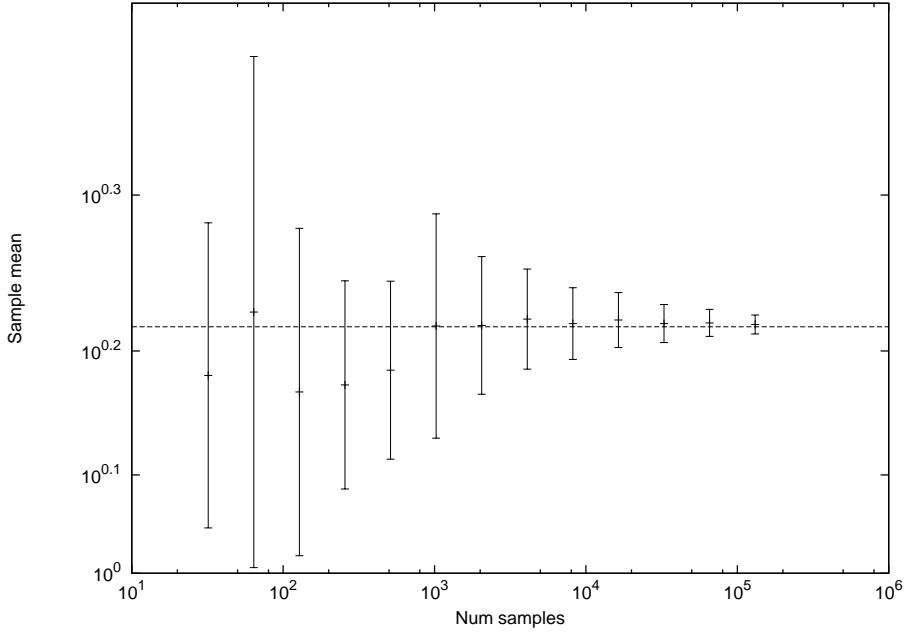


Figure 2.1: Monte Carlo approximation to  $\mathbb{E}(e^Z)$ , where  $Z \sim N(0, 1)$ . Vertical lines give computed 95% confidence intervals, middle points on the vertical lines are the approximations. Horizontal dashed line is at height  $\mathbb{E}(e^Z) = \sqrt{e}$ .

Figure 2.1 we give results from a Monte Carlo simulation of  $\mathbb{E}(e^Z)$ , where  $Z \sim N(0, 1)$ . In this case, we used 13 different sample sizes,  $n = 2^5, 2^6, \dots, 2^{17}$ . For each sample, the picture plots the computed mean  $\hat{\mu}$  with circles and 95% confidence interval with vertical lines. Compared with the theoretical expectation<sup>2</sup> of  $e^Z$ , we see as the sample size  $n$  increases the computed mean becomes more accurate and the confidence interval shrinks.

There are two points to note:

- The size of confidence interval reduces slowly. In fact, to reduce the error by 0.1, the number of sample  $n$  has to increase by 100. The stated estimation error is  $O(\frac{1}{\sqrt{n}})$ .
- It is required that  $n$  is sufficiently large so that the Central Limit Theorem approximation is accurate.

---

<sup>2</sup>If  $Z$  is a normal random variable with mean  $a$  and volatility  $b$ , then  $Y = e^Z$  has a log-normal distribution with mean  $e^{a+\frac{1}{2}b^2}$  and volatility  $(e^{b^2} - 1)e^{2a+b^2}$ .

## 2.3 Generating random numbers

In this section we briefly introduce algorithms at the core of Monte Carlo simulation methods for generating uniformly distributed random numbers and transforming them into a normal distribution. This algorithm may be run a million times for a single valuation, so its efficiency will be important.

- Linear Congruential Generator

The general linear congruential generator, firstly proposed by Lehmer (1951), has the form

$$x_{i+1} = (ax_i + c) \mod m$$

$$u_{i+1} = x_{i+1}/m$$

for some integers  $a$ ,  $m$  and  $c$  (although it is now customary to take  $c = 0$ ). For each  $i = 1, 2, \dots$ ,  $x_i$  is generated by an iterative process given an initial value  $x_0$  as ‘seed’ chosen from  $(0, m)$ , and the resulting values  $u_i$  always lie in the unit interval. Bratley, Fox and Schrage (1987) show a faster implementation of a linear congruential generator using only integer arithmetic and still avoiding overflow. Let

$$q = \lfloor m/a \rfloor, \quad r = m \mod a$$

so that

$$ax_i \mod m = a(x_i \mod q) - \lfloor \frac{x_i}{q} \rfloor r + (\lfloor \frac{x_i}{q} \rfloor - \lfloor \frac{ax_i}{m} \rfloor)m.$$

We can show  $(\lfloor \frac{x_i}{q} \rfloor - \lfloor \frac{ax_i}{m} \rfloor)$  only takes the values 0 and 1. This means that now the modular operator is only required by  $x_i$ , which can implemented faster than the calculation of  $ax_i \mod m$ . See a detailed discussion of the linear congruential generator in Glasserman (2003).

- Transformation Method: Normal Random Numbers

In the previous section, we saw how to generate random numbers with a uniform distribution. Now we introduce the Box-Muller (1958) method, which is the simplest technique for generating Normally distributed random numbers by

taking any uniformly distribution variables. Given two uniformly distributed random numbers  $x_1, x_2$ , two Normally distributed random numbers,  $y_1$  and  $y_2$  are given by:

$$y_1 = \cos(2\pi x_2) \sqrt{-2 \log x_1}$$

$$y_2 = \sin(2\pi x_1) \sqrt{-2 \log x_2}$$

## 2.4 Variance reduction techniques

One of the drawbacks of the Monte Carlo method arises from the slow decrease of error, at a rate inversely proportional to the square root of the number of simulations. Although any desired precision can be obtained by increasing the simulation trials, it is useful to provide more efficient ways to reduce error.

### 2.4.1 Control variates

One method to improve accuracy is known as the control variate approach. To compute the expectation  $E[X]$  of random variable  $X$ , we can estimate it through another independent random variable  $Y$ , satisfying the following conditions:

- the random variable  $Y$  has a known mean  $\mu$ ,
- and there is a strong correlation between the random variables  $X$  and  $Y$ .

Then, we generate random variable  $\hat{X}$  rather than  $X$ ,

$$\hat{X} = X - Y + \mu,$$

and estimate the expectation  $E[\hat{X}] = \frac{1}{n} \sum_{i=0}^n \hat{X}_i$ . This is because  $\hat{X}$  is an unbiased estimate of  $X$ , i.e.

$$E[\hat{X}] = E[X] - E[Y] + \mu = E[X],$$

but with lower variance than the original  $X$ , that is

$$\begin{aligned} Var[\hat{X}] &= Var[X] + Var[Y] - 2\rho_{XY}\sqrt{Var[X]Var[Y]} \\ &< Var[X], \end{aligned}$$

where the correlation  $\rho_{XY} > \frac{1}{2}\sqrt{\frac{Var[Y]}{Var[X]}}$ , which is implied by the second condition of  $Y$ . One of typical examples is to compute an arithmetic average price Asian call option with payoff  $X$ :

$$\max \left[ \frac{1}{n} \sum_{i=1}^n S(t_i) - K, 0 \right].$$

Let  $Y$  be the corresponding geometric average price Asian option with payoff

$$\max \left[ \frac{1}{n} \prod_{i=1}^n S(t_i) - K, 0 \right],$$

then the expectation  $\mathbb{E}[Y]$  has an explicit formula assuming  $S(t_i)$  follows a standard Brownian motion with constant drift and variance terms. Therefore, we may use  $Y$  as a control variate to estimate  $\mathbb{E}[X]$ . There are some other typical examples shown in Bolia and Juneja (2005), such as the European option pricing problem on a dividend paying stock. The control variates method is discussed in more detail and extended to multiple controls in Glasserman (2003). Rasmussen (2005) develops pricing American options using control variates.

### 2.4.2 Antithetic variates

Another method to improve convergence is through the use of antithetic variates. This produces antithetic pairs of random numbers,  $U$  and  $1-U$  from a uniform distribution, which ensures that the random numbers are symmetrically distributed with mean zero so that the variance from asymmetric sampling in the original simulation has been reduced. The implementation is straightforward: we generate a path with  $N$  standard normal random variables  $Z_i$ , and then directly gain another path with  $-Z_i$  for  $i = 0 \dots N-1$  which moves in the opposite direction. Both control variates and antithetic variates techniques are described in the paper by Boyle (1977). In the case of European options on discrete dividend-paying stock, Bolia and Juneja (2005) show that the use of both methods, antithetic variates and control variates, can considerably improve the accuracy of the estimators and shrink the confidence interval.

### 2.4.3 Importance sampling

Importance sampling (see Glasserman, 2003) is a popular method of variance reduction, with emphasis on generating important sample paths for the corresponding options. For example, consider a European call option with strike price  $K$ , which is deep out of the money ( $S(0) \ll K$ ). In such a situation, the accuracy of a standard Monte Carlo method suffers because most of the simulated sample paths expire out of the money and also some rare but large big payoffs could be missed. However, we can use importance sampling to generate important paths, that is  $S(T) > K$ . Assume that r.v.  $X$  follows the probability density function (pdf)  $f(x)$ , there exists another pdf  $g(x)$ , the expectation of  $X$  can be estimated as:

$$\begin{aligned} E[X] &= \int_{-\infty}^{\infty} xf(x)dx \\ &= \int_{-\infty}^{\infty} x \frac{f(x)}{g(x)} g(x)dx \\ &= \int_{-\infty}^{\infty} x W(x) g(x)dx \\ &= \hat{E}[XW(X)] , \end{aligned} \tag{2.4}$$

where  $w(x) = \frac{f(x)}{g(x)}$  is a likelihood ratio and is referred to as the weighting function. The third equality (2.4) implies a change of probability measure from  $f(x)$  to  $g(x)$ , and  $\hat{E}(\cdot)$  is the expectation under  $g(x)$ . Therefore, we can draw random variable  $X$  from  $g(x)$  and convert it to the estimator  $XW(X)$  which is unbiased to the estimator  $X$  from  $f(x)$ . To continue with the above example, the sample paths are simulated with the random increments from a specific uniform distribution  $U[a, b]$  (rather than the standard uniform distribution  $U[0, 1]$ ) such that  $S(T) > K$ . Then we compute the expectation of option price multiplied by their weighting  $W(x) = b - a$ . The variance of importance sampling is simply given by:

$$\begin{aligned} Var[XW(X)] &= \hat{E}[X^2W(X)^2] - \hat{E}^2[XW(X)] \\ &= \hat{E}[X^2W(X)^2] - E^2[X] \\ &= E[X^2W(X)] - E^2[X] , \end{aligned} \tag{2.5}$$

whilst the naive Monte Carlo method has the variance:

$$Var[X] = E[X^2] - E^2[X]. \quad (2.6)$$

From Eq (2.5), zero variance can be obtained when  $W(X) = \frac{E[X]}{X}$ , however,  $E[X]$  is unknown a priori. Comparing the two variances in Eq (2.5) and Eq (2.6), we can see that importance sampling reduces the variance when  $W(X) < 1$ , otherwise, it could also increase the variance. Consider our example again,  $W(X)$  is constant and equals  $b - a$ . From the analytical solution of underlying  $S(t)$ , we infer that  $b = 1$  and  $a > 0$  so that  $W(X) < 1$ , i.e.  $Var[XW(X)] < Var[X]$ , which shows that importance sampling gives a better estimator with lower variance over the naive Monte Carlo method. An optimal choice of the probability density function  $g(x)$  should minimize variance, which is the key to the efficiency of importance sampling. Bolia and Juneja (2005) and Glasserman (2003) illustrate this problem with different examples, such as one-dimensional up-and-in European put options and Bermudan options. Guasoni and Robertson (2008) derive an optimal change of drift terms for pricing Asian options, and show that importance sampling greatly improves the performance of the Monte Carlo method. In the standard Black-Scholes model, for both geometric and arithmetic average Asian options, the closed form explicit formulae of the change of drift are obtained by solving the corresponding Euler-Lagrange equation, which is a differential equation whose solution is the stationary value of a given functional. Their basic idea is to solve a variational problem  $u$ . Their paper is based on Glasserman, Heidelberger and Shahabuddin's (1999) work and extends it to a continuous time framework.

Besides the methods above, a number of effective techniques have been developed to reduce the variance of the estimates in Monte Carlo applications, such as moment matching and stratified sampling, which are described in detail by Glasserman (2003), Bratley et al. (1987) and Law and Kelton (1991).

## 2.5 Discretization methods

In this section, we will introduce discretization methods for the simulation of a stochastic process and demonstrate the convergence rate of the error.

### 2.5.1 The Euler method

The Euler method (Higham, 2004) is an explicit numerical method for approximating the solution of a stochastic differential equation, which is based on the idea of the Itô stochastic integral (El-Borai, El-Nadi, Mostafa and Ahmed, 2005) as in the following:

$$\int_{t=0}^T f(t, W(t))dW(t) = \lim_{N \rightarrow \infty} \sum_{i=1}^N f(t_i, W(t_i))(W(t_i) - W(t_{i-1})) ,$$

where  $W_t$  is a Brownian motion and  $N$  is defined as a finite number of shorter intervals of length  $\Delta t = T/N$  in the whole interval  $[0, T]$ .

We assume a stochastic process  $X(t)$  is the solution to the following generalised stochastic differential equation, which is

$$dX(t) = f(X(t))dt + g(X(t))dW(t) , \quad 0 \leq t \leq T, \quad (2.7)$$

where  $f(X(t))$  and  $g(X(t))$  are given functions of the stochastic process  $X(t)$ . Given the length of the interval  $T$ , the time step size  $\Delta t = T/N$  for some positive integer  $N$ , and  $t_i = t_{i-1} + \Delta t$  for  $i = 1, \dots, N$ , by integrating both sides of (2.7) from  $t_{i-1}$  to  $t_i$ , we can rewrite the stochastic differential equation in integral form as

$$X(t_i) = X(t_{i-1}) + \int_{t_{i-1}}^{t_i} f(X(s))ds + \int_{t_{i-1}}^{t_i} g(X(s))dW(s) , \quad (2.8)$$

which is the exact solution  $X(t_i)$ . Approximations  $X_i$  for  $X(t_i)$  using the Euler method can be expressed as:

$$\begin{aligned} X_i &= X_{i-1} + f(X_{i-1})\Delta t + g(X_{i-1})(W(t_i) - W(t_{i-1})) \\ &= X_{i-1} + f(X_{i-1})\Delta t + g(X_{i-1})\sqrt{\Delta t}Z_{i-1} , \end{aligned} \quad (2.9)$$

where  $Z_{i-1}$  is a normal random variable with mean 0 and variance 1 due to the basic properties of the Brownian motion  $W(t)$ . The approximation  $X_i$  approaches  $X(t_i)$  from the exact solution (2.8) as  $\Delta t$  reduces to zero.

There are many different, non-equivalent, definitions of convergence for sequences of random variables. The two most common and useful concepts in numerical stochastic differential equations are strong convergence and weak convergence, which are defined in Higham (2004) as follows:

A method is said to have *strong order* of convergence equal to  $p$  if there exists a constant  $C$  such that

$$\mathbb{E}|X_i - X(t_i)| \leq C\Delta t^p ,$$

for sufficiently small  $\Delta t$ ; similarly, a method has a *weak order* of  $p$  if there exists a constant  $C$  such that

$$|\mathbb{E}X_i - \mathbb{E}X(t_i)| \leq C\Delta t^p ,$$

where  $\mathbb{E}$  denotes the expected value.

In other words, the *strong convergence* is a convergence of the mean of the error and the *weak convergence* is convergence of the error of the mean. A discretization scheme normally has a lower strong order than the weak order. For the study of option pricing, the weak convergence is more relevant than the strong convergence, because we are interested in the difference between the estimate  $\mathbb{E}X_i$  and the exact value  $X(t_i)$ . As shown in Higham (2004), the Euler method typically has a strong order of 1/2 but it can achieve a weak order of 1.

### 2.5.2 The Milstein method

From a Taylor expansion, we can find that the approximation (2.9) expands the drift term to  $O(\Delta t)$  whilst the diffusion term up to  $O(\sqrt{\Delta t})$ . The Milstein (1975) method is derived through expanding the diffusion term to  $O(\Delta t)$ , being of the same order of the drift term. The approximation given by the Milstein method is in the form:

$$\begin{aligned} X_i = X_{i-1} + f(X_{i-1})\Delta t + g(X_{i-1})\sqrt{\Delta t}Z(t_{i-1}) \\ + \frac{1}{2}g'(X_{i-1})g(X_{i-1})\Delta t(Z_{i-1}^2 - 1) . \end{aligned} \quad (2.10)$$

Compared with the Euler method (2.9), the Milstein method adds the extra term  $\frac{1}{2}g'(X_{i-1})g(X_{i-1})\Delta t(Z_{i-1}^2 - 1)$ , which requires that  $g(X)$  is a smooth function (i.e. has a first derivative). Theorem 10.3.05 of Kloeden and Platen (1999) shows the Milstein method has strong order 1, which is higher than the strong order 1/2 of the Euler method. Higham (2001) provides a numerical test to compare the convergence orders of the Milstein method and the Euler method.

### 2.5.3 The second-order Milstein method

The second-order method proposed by Milstein (1979) can improve the accuracy of the approximation to converge weakly at  $O(\Delta t^2)$ . Consider the exact solution (2.8), using Itô's formula (Itô, 1951) to derive a exact representation for  $f(X(s))$  and  $g(X(s))$  with  $s \in [t, t + \Delta t]$ , which is

$$\begin{aligned} f(X(s)) &= f(X(t)) + \int_t^s (ff' + \frac{1}{2}g^2f'')du + \int_t^s gf'dW(u) , \\ g(X(s)) &= g(X(t)) + \int_t^s (fg' + \frac{1}{2}g^2g'')du + \int_t^s gg'dW(u) , \end{aligned}$$

where  $u \in [t, s]$ . We can see that the Euler method only approximates  $f(X(s)) \approx f(X(t))$  and  $g(X(s)) \approx g(X(t))$  by ignoring the integral terms. However, the second-order method approximates the values of two integral terms to produce a better approximation of  $f(X(s))$  and  $g(X(s))$ , which is

$$\begin{aligned} f(X(s)) &\approx f(X(t)) + \left\{ f(X(t))f'(X(t)) + \frac{1}{2}g^2(X(t))f''(X(t)) \right\} \int_t^s du \\ &\quad + g(X(t))f'(X(t)) \int_t^s dW(u) , \\ g(X(s)) &\approx g(X(t)) + \left\{ f(X(t))g'(X(t)) + \frac{1}{2}g^2(X(t))g(X(t))'' \right\} \int_t^s du \\ &\quad + g(X(t))g'(X(t)) \int_t^s dW(u) . \end{aligned}$$

Substituting these two approximations to the first term and the second term of integral in (2.8):

$$\begin{aligned} X(t + \Delta t) &\approx X(t) + f(X(t))\Delta t + g(X(t))\Delta t \\ &\quad + \left\{ f(X(t))f'(X(t)) + \frac{1}{2}g^2(X(t))f''(X(t)) \right\} \int_t^{t+\Delta t} \int_t^s du ds \end{aligned}$$

$$\begin{aligned}
 & + \left\{ g(X(t))f'(X(t)) \right\} \int_t^{t+\Delta t} \int_t^s dW(u) ds \\
 & + \left\{ f(X(t))g'(X(t)) + \frac{1}{2}g^2(X(t))g''(X(t)) \right\} \int_t^{t+\Delta t} \int_t^s du dW(s) \\
 & + \left\{ g(X(t))g'(X(t)) \right\} \int_t^{t+\Delta t} \int_t^s dW(u) dW(s),
 \end{aligned}$$

where double integrals can be resolved using stochastic calculus.

$$\begin{aligned}
 \int_t^{t+\Delta t} \int_t^s du ds &= \int_t^{t+\Delta t} (s-t) ds = \frac{1}{2}\Delta t^2, \\
 \int_t^{t+\Delta t} \int_t^s dW(u) ds &= \int_t^{t+\Delta t} (W(s) - W(t)) ds = \frac{1}{2}\Delta t \Delta W, \\
 \int_t^{t+\Delta t} \int_t^s du dW(s) &= \int_t^{t+\Delta t} (s-t) dW(s) = \frac{1}{2}\Delta t \Delta W, \\
 \int_t^{t+\Delta t} \int_t^s dW(u) dW(s) &= \int_t^{t+\Delta t} (W(s) - W(t)) dW(s) = \frac{1}{2}\Delta W^2 - \frac{1}{2}\Delta t,
 \end{aligned}$$

where  $\Delta W = W(t + \Delta t) - W(t)$ . Then, we can obtain the approximation  $X(t + \Delta t)$  of  $X_i$  as follows:

$$\begin{aligned}
 X_i &= X_{i-1} + f(X_{i-1})\Delta t + g(X_{i-1})\Delta W \\
 &+ \frac{1}{2} \left\{ f(X_{i-1})f'(X_{i-1}) + \frac{1}{2}g^2(X_{i-1})g''(X_{i-1}) \right\} \Delta t^2 \\
 &+ \frac{1}{2} \left\{ g(X_{i-1})f'(X_{i-1}) + f(X_{i-1})g'(X_{i-1}) + \frac{1}{2}g^2(X_{i-1})g''(X_{i-1}) \right\} \Delta t \Delta W \\
 &+ \frac{1}{2} \left\{ g(X_{i-1})g'(X_{i-1}) \right\} (\Delta W^2 - \Delta t),
 \end{aligned}$$

where  $\Delta W$  is normally distributed with mean 0 and variance  $\Delta t$ ; coefficient function  $f, g$  and their derivatives are evaluated at  $X_{i-1}$ .

Talay (1984) and Kloeden and Platen (1999) have shown that this scheme has a weak convergence order of 2. Moreover, the method can be extended to deal with a high-dimensional problem, which is discussed in Talay and Tubaro (1990) and Glasserman (2003). However, the second-order method requires smooth coefficient functions and calculation of the derivatives of the coefficient functions at each timestep, which increases the complexity of simulation, especially for those problems whose derivatives have to be estimated by numerical methods, such as finite-difference approximations. Therefore, there is an increase in the calculation time of simulation for each sample path, so the second-order method is usually slower than the Euler method.

### 2.5.4 The extrapolation method

The extrapolation method is described in Glasserman (2003) as an alternative approach to achieve a weak convergence  $O(\Delta t^2)$  using two estimates, which are calculated by the first-order convergence rate with different level timestep  $\Delta t$ , to extrapolate the more accurate estimate. The method is far easier to implement than the second-order method described previously. As the standard Euler method has weak order 1, Talay and Tubaro (1990) show that the relation between estimate  $X_i$  for and the exact value  $X(t_i)$  can be expressed as:

$$\begin{aligned}\mathbb{E}X_i^{(\Delta t)} &= \mathbb{E}X(t_i) + C\Delta t + O(\Delta t^2), \\ \mathbb{E}X_i^{(2\Delta t)} &= \mathbb{E}X(t_i) + 2C\Delta t + O(\Delta t^2),\end{aligned}$$

where  $C$  is the same constant in both cases;  $X_i^{(\Delta t)}$  represents the approximation using timestep  $\Delta t$  and  $X_i^{(2\Delta t)}$  is gained by setting timestep  $2\Delta t$ . By combining these two estimates, we can obtain an extrapolated estimate, that is

$$2\mathbb{E}X_i^{(\Delta t)} - \mathbb{E}X_i^{(2\Delta t)} = \mathbb{E}X(t_i) + O(\Delta t^2), \quad (2.11)$$

which has weak order of 2. This means that the combining estimate is more accurate than either of its two components. In fact, the extrapolation method can be applied to further increase the convergence order, which is discussed in Glasserman (2003).

We have introduced several basic discretization schemes in this section. In general, the extrapolation method is seen to have distinct advantages over the other methods in that it is easy to implement and relatively efficient. There are still many discretization methods which are derived from these basic schemes (see Kloeden and Platen, 1999). We suggest that an efficient method chosen for simulation depends on the specific features of the model we study. Sometimes even a simple change of variable  $X(t)$  can help to reduce the bias during the simulation, such as replacing underlying prices with the logarithm of the prices, which will be illustrated to simulate a jump diffusion process in Chapter 3.

## 2.6 Efficient Monte Carlo methods

As discussed in Section 2.4 and Section 2.5, Monte Carlo methods usually suffer error from the number of simulations  $M$  and the length of time intervals  $\Delta t$ . Under certain conditions on  $f(x)$  and  $g(x)$  (see Talay and Tubaro, 1990; Kloeden and Platen, 1999), it is well known that the sample mean-squared error<sup>3</sup> (MSE) of the estimate given by the Monte Carlo simulation associated with the Euler discretization is asymptotically of the form

$$\text{MSE} \approx C_1 M^{-1} + C_2 \Delta t^2 \quad (2.12)$$

for positive constant  $C_1$  and  $C_2$ . The first term represents the *variance* from sampling, and the second term is due to the *squared bias* of the Euler method with weak order 1. A more general form of MSE is given by Glasserman (2003), which is:

$$\text{MSE} \approx C_1 M^{-1} + C_2 \Delta t^{2p}. \quad (2.13)$$

Then an efficient Monte Carlo method is considered to minimize the value of the MSE (2.13).

With a limited budget of computation time, we have to consider how to make an efficient tradeoff between reducing the size of timesteps  $\Delta t$  and increasing the number of sample paths  $M$ . The total computation time  $s$  is roughly proportional to  $M/\Delta t$ , i.e.  $s \propto \frac{M}{\Delta t}$ , meaning the number of discrete time steps for total sample paths, thus the size of  $M/\Delta t$  is important. Duffie and Glynn (1995) show that an optimum root mean square error<sup>4</sup> (minimum RMSE) is gained by setting:

$$M \propto \Delta t^{-2p}, \quad (2.14)$$

then the minimum RSME is

$$\text{RMSE} \propto s^{-\frac{p}{2p+1}},$$

where the magnitude of RMSE is reduced when the convergence order  $p$  increases and tends to  $s^{-\frac{1}{2}}$  as  $p \rightarrow \infty$ . The expression (2.14) suggests that for the first-order

---

<sup>3</sup> $\text{MSE}(\hat{X}) = \mathbb{E}[(\hat{X} - X)^2]$  where  $\hat{X}$  is an estimator of  $X$ .

<sup>4</sup> $\text{RMSE}(\hat{X}) = \sqrt{\text{MSE}(\hat{X})}$ .

Euler method  $p = 1$ , when we reduce  $\Delta t$  by half, the number of sample paths should be quadrupled; for the second-order scheme  $p = 2$ , the number of sample paths is increased by a factor of  $2^4$ . They also illustrate several option pricing examples to show that the error reduction is somewhat halved using doubling the number of timesteps each time for the Euler method and the error is reduced by a factor of approximately 4 for the second-order method.

## 2.7 Quasi-Monte Carlo method

In contrast with ordinary Monte Carlo methods that compute an integral based on sequences of pseudo random numbers, quasi-Monte Carlo (QMC) methods take advantage of determined sequences with low discrepancy<sup>5</sup>, so the methods are also known as low-discrepancy methods. The famous advantage of the QMC methods is to achieve accuracy  $O(1/N)$  ( $N$  is the number of sample paths) which is higher than the accuracy  $O(1/\sqrt{N})$  associated with the normal Monte Carlo simulation. However, this clever method has been found to suffer a problem of dimensionality.

By the Koksma-Hlawka inequality (see Glasserman, 2003), the integration error for the QMC method over  $d$ -dimensional space is bounded by

$$\left| \frac{1}{N} \sum_{i=1}^N f(x_i) - \int_{[0,1]^d} f(x) dx \right| \leq Var(f) D^*(x_1, x_2, \dots, x_N) ,$$

where  $Var(f)$  is a bounded variation of function  $f(x)$  and  $D^*(x_1, x_2, \dots, x_N)$  is the discrepancy of the sequence. We can see the error of integration depends on the product of the term of the function variation and the term of the discrepancy of the sequence. As the variance is bounded, a low-discrepancy sequence results in a good approximation of the integration.

For one-dimensional problems, Glasserman (2003) suggests taking base- $b$  Van der

---

<sup>5</sup>Discrepancy is a measure of deviation from uniform distribution.

Corput sequences stated in Van Der Corput (1935), which is defined as:

$$\begin{aligned} k &= \sum_{j=0}^{\infty} a_j(k) b^j, \\ \psi_b(k) &= \sum_{j=0}^{\infty} \frac{a_j(k)}{b^{j+1}}, \end{aligned} \quad (2.15)$$

where  $k$  is a positive integer,  $a_j(k)$  is the coefficient with respect to the power  $j$  of the base  $b$ ,  $\psi_b(k)$  is called as the radical inverse function to map  $k$  to a point in interval  $[0, 1)$ . Note that the sum in (2.15) has a finite number of non-zero terms. The calculation of base-2 and base-3 sequences is illustrated in Table 2.1. The second

$k$	$k$ Binary	$\psi_2(k)$	$\psi_3(k)$
0	0	0	0
1	1	1/2	1/3
2	10	1/4	2/3
3	11	3/4	1/9
4	100	1/8	4/9
5	101	5/8	7/9
6	110	3/8	2/9
7	111	7/8	5/9
8	1000	1/16	8/9
9	1001	9/16	1/27
:	:	:	:

Table 2.1: Illustration of radical inverse function  $\psi_2(k)$  and  $\psi_3(k)$

column ‘ $k$  Binary’ represents numeric values on base-2, which can be expressed in the form of  $a_{j_{\max}} a_{j_{\max}-1} \cdots a_1 a_0$ . The basic idea of the sequence is to ‘fill the gap’ between existing values. For example, given 0 and 1/2, we take the median value between them as the next number for the base-2 sequence, that is 1/4. The van der Corput sequences have been extended to generate  $d$ -dimensional sequences by Halton (1960), which is :

$$x_r = (\psi_{b_1}(k), \psi_{b_2}(k), \dots, \psi_{b_d}(k)),$$

where  $\psi_b$  is given by Eq (2.15) and  $b_i$  is chosen as the first  $i$ -th prime number, for  $k = 0, 1, 2, \dots$ . For example, using the results in Table 2.1, we can construct a simple

two-dimensional Halton sequence, which is

$$(0,0), (1/2, 1/3), (1/4, 2/3), (3/4, 1/9), (1/8, 4/9), (5/8, 7/9), \\ (3/8, 2/9), (7/8, 5/9), (1/16, 8/9), (9/16, 1/27), \dots$$

The smaller primes taken as a base usually perform better than the larger ones so that for  $d$ -dimensional problem, we take the first  $d$  primes, such as 2, 3, 5, … . In fact, there is a significant decline in uniformity of Halton sequences with increasing dimension, because large primes have to be chosen for high-dimensional problems. Thus, other competitive methods are developed to construct the low discrepancy sequences in multi-dimensional space, most commonly, such as Faure and Sobol sequences (see more details in Glasserman, 2003). The basic idea for both sequences is to form a finer uniform partition of the unit interval  $[0, 1]$  and reorder them for each dimension. In contrast with different primes used as bases in Halton sequences, Faure sequences use a common base that is the smallest prime number greater or equal to the dimension itself, and multi-dimensional Sobol sequences only use base 2. Thus, with equal dimension, the bases used for these two methods are much smaller than the largest base used to construct Helton sequences. More specifically, a Faure sequence is constructed by permuting a Van der Corput sequence multiplied by different dimension itself. For each integer  $k$ , the expansion of base  $b$  is in the form:

$$k = \sum_{l=0}^r a_l(k) b^l.$$

Suppose there are  $r$  terms in the expansion of  $k$ , the point in  $i$ -th coordinate with  $i = 1, 2, \dots, d$  can be found from:

$$\begin{aligned} \psi_b^{(i)}(k) &= \sum_{j=1}^{\infty} \frac{y_j^{(i)}(k)}{b^{j+1}}, \\ y_j^{(i)}(k) &= \sum_{l=0}^{\infty} \binom{l}{j-1} (i-1)^{l-j+1} a_l(k) \mod b, \end{aligned}$$

where the summands vanish when  $l \geq r$  as  $a_l(k) = 0$ , then we only need consider the case of  $l < r$ ; the combination  $\binom{l}{j-1}$  is restricted by  $l \geq j - 1$  otherwise zero. This implies that both sums have a finite number of terms. The term  $y_j^{(i)}(k)$  can be

generated by the matrix-vector calculation, which is:

$$\begin{pmatrix} y_1^{(i)}(k) \\ y_2^{(i)}(k) \\ \vdots \\ y_r^{(i)}(k) \end{pmatrix} = C^{(i-1)} \begin{pmatrix} a_0(k) \\ a_1(k) \\ \vdots \\ a_{r-1}(k) \end{pmatrix} \pmod{b},$$

where the matrix  $C^{(i)}$  is a  $r \times r$  generator matrix in the form:

$$C^{(i)} = \begin{pmatrix} \binom{0}{0} i^0 & \binom{1}{0} i^1 & \binom{2}{0} i^2 & \cdots & \binom{r-1}{0} i^{r-1} \\ 0 & \binom{1}{1} i^0 & \binom{2}{1} i^1 & \cdots & \binom{r-1}{1} i^{r-2} \\ 0 & 0 & \binom{2}{2} i^0 & \cdots & \binom{r-1}{2} i^{r-3} \\ \vdots & \vdots & \vdots & \cdots & \vdots \\ 0 & 0 & 0 & \cdots & \binom{r-1}{r-1} i^0 \end{pmatrix},$$

and the generator matrix can be obtained using a recursive equation:

$$C^{(i)} = C^{(1)} C^{(i-1)},$$

for any  $i = 1, 2, \dots, d$ .

Now we turn to discuss an alternative method introduced by Sobol (1967). The Sobol sequence is constructed in a similar way as the Faure one by multiplying generator matrices by a vector of coefficients of a binary expansion of  $k$ , i.e. in base 2—the smallest prime number, which implies that it costs less computation time to generate the Sobol sequences than the Faure sequences with equal dimension. The key difference between two low discrepancy sequences is the construction of the generator matrices. For the Sobol sequence, the generator matrix is separately constructed by a primitive polynomial for each coordinate  $i$ ,  $i = 1, 2, \dots, d$ . Paskov and Traub (1995) first propose the QMC method with Halton and Sobol sequences to price a collateralized mortgage obligation (CMO) and show that the QMC method is superior to the regular Monte Carlo method. As suggested in Glasserman (2003), the Sobol sequences always produce results more accurately and quickly than other QMC sequence and Monte Carlo methods. The combination of the Sobol points with the Brownian bridge<sup>6</sup> construction is recommended.

---

<sup>6</sup>A Brownian bridge is a stochastic process  $B(t)$  with a conditional distribution on a Wiener process  $W(t)$  such that  $B(0) = B(1) = 0$ . For example:  $B(t) = W(t) - tW(1)$  is a Brownian bridge.

## 2.8 Monte Carlo for Greeks

As the model of stock prices we study later includes Gamma, we discuss using Monte Carlo to calculate the Greeks - the partial derivatives of the option value with respect to stock price. In particular, the first order differential, the delta  $\Delta = \frac{\partial V}{\partial S}$ , the second order differential, the gamma  $\Gamma = \frac{\partial^2 V}{\partial S^2}$  and the third order differential,  $\frac{\partial^3 V}{\partial S^3}$  are of interest.

Monte Carlo simulation can also be used to estimate option price derivatives. There are three standard methods: finite-difference approximations, the pathwise method and the likelihood ratio method.

### 2.8.1 Finite-difference approximation

The finite-difference approximation is a standard indirect method, which simulates a price process after a small perturbation in the parameter of interest. One makes two errors: one in the numerical computation of the expectation via the Monte Carlo, and another in the approximation of the derivative function via its finite difference approximation. To overcome the inefficiency, Broadie and Glasserman (1996) suggest using the likelihood ratio method. Another important drawback of the finite-difference approximation is that it performs poorly when the payoff function is insufficiently smooth. However, Fournie, Lasry, Lebuchoux, Lions and Touzi (1999) show that any Greek can be expressed as an expectation of a payoff function times a weight. The weight can be expressed in terms of the Malliavin derivative and is independent of the payoff function. This smooths the function to simulate because the value of Greeks is a numerical solution of the differential equations as usual. These features drive the high efficiency of simulation. Using this technique introduces some extra noise, and Fournie et al. (1999) propose that a localization of the Malliavin weight be used at the discontinuity of the payoff and elsewhere avoided. An additional discussion can be found in the paper by Benhamou (2002), in which some numerical results show the efficiency of this method; for instance if one computes the gamma of a corridor option, which is defined as an option that pays 1 dollar if the underlying

at maturity is within the range  $[S_{min}, S_{max}]$ .

### 2.8.2 Finite difference methods for Greeks

Three forms of finite difference technique are commonly considered: forward, backward and central differences (see the textbook Seydel, 2009). Here, we use central finite difference methods to value delta and gamma, which can be derived by Taylor series expansion

$$\begin{aligned}\Delta &= \frac{V(S + h, t) - V(S - h, t)}{2h} + O(h^2), \\ \Gamma &= \frac{V(S + h, t) - 2V(S, t) + V(S - h, t)}{h^2} + O(h^2),\end{aligned}\quad (2.16)$$

where  $h$  denotes the asset price space. Central finite difference approximations yield a more accurate approximation when  $h$  is small.

Next, we illustrate Monte Carlo methods coupled with the finite difference methods to estimate the Greeks. In order to check accuracy, we focus on European options whose delta and gamma are available by Black-Scholes formula exactly. From Figure(2.2(a)) to (2.2(b)), it is supposed  $S = 0.9, X = 1.0, T = 1, r = 0.04, \sigma = 0.1, h = 0.001$ . With adding paths,  $10000, 20000, 30000, \dots, 2 * 10^8$ , we note the estimate deltas and gammas for the European options by Monte Carlo converge to the exact values.

### 2.8.3 Pathwise method and the likelihood ratio method

Both the pathwise method and the likelihood ratio method are referred to as direct methods. The main advantage of direct methods over resimulations is increased computational speed. In the pathwise method, a simulation estimator is derived by differentiating the payoff function inside the expectation operator. In the likelihood ratio method, the parameter of the price function to be differentiated is treated as the parameter of the density function rather than the payoff function inside the expectation operator; see Glasserman (2003) for detailed descriptions of these methods. The approach using Malliavin calculus mentioned above can be viewed as an extension

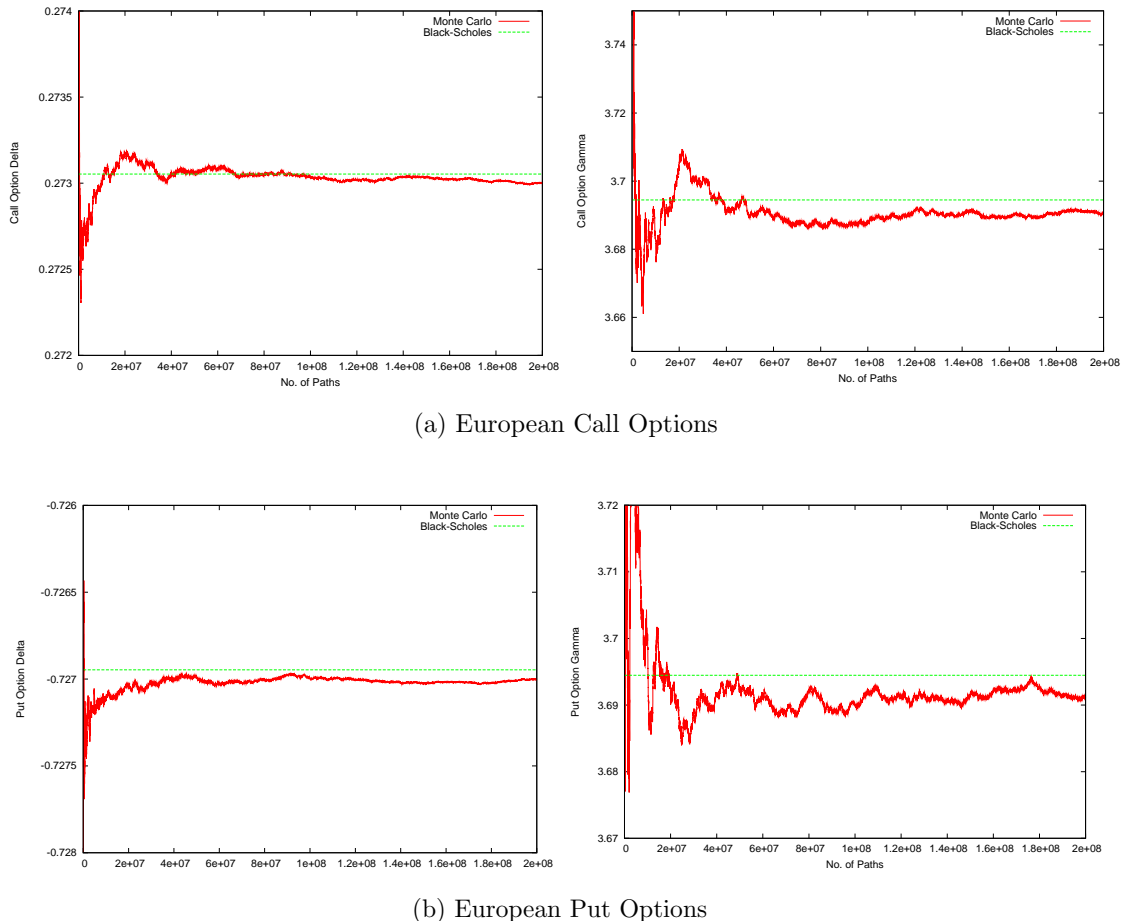


Figure 2.2: Monte Carlo approximation to delta of European call option,  $S = 0.9, X = 1.0, T = 1, r = 0.04, \sigma = 0.1$ , dashed line gives approximation by finite difference method, horizontal line is exact value from Black-Scholes formula

of the likelihood ratio method. Fournie, Lasry, Lebuchoux and Lions's (2001) paper proves that the weight that gives the minimum total estimator variance is the one given by the likelihood ratio method.

## 2.9 American options

Although Boyle (1977) first applied Monte Carlo in pricing European options, it was much later that the potential of Monte Carlo simulation for American-style options was suggested by Bossaerts (1989) and Tilley (1993). Monte Carlo simulation methods have been adapted to price American style options, a key breakthrough, and these

have been developed to be especially suitable for pricing path dependent options and in tackling high-dimensional problems.

### 2.9.1 Duality simulation

One technique introduced by Rogers (2002) is called a duality simulation approach based on a dual characterization of the optimal exercise problem. Rogers illustrates how to pick a suitable martingale  $M$  and take the pathwise maximum of the payoff less the martingale as the upper bound for the option price. The approach requires a suitable choice of Lagrangian martingale to give a good result. In his paper, through using the technique on four specific American style options, with even very simple choices of  $M$ , such as for corresponding European options, the accuracy achieved is surprising. The same dual simulation approach can be found in the working paper of Haugh and Kogan (2004), who provide a general algorithm for constructing upper and lower bounds on the true option price and show the bounds are tight. This means if the initial approximation is close to the true option value, the bounds are also guaranteed to be close. In this area, another important contribution is by Broadie and Glasserman (1997; 2004), who develop two stochastic mesh methods to generate errors bounds (in the form of confidence intervals) which converge to the correct price of Bermudan option which is a finitely exercisable American option. Their algorithm leads to exponential dependence of the computation time on the number of exercise opportunities rather than the number of assets. The method in Broadie and Glasserman (2004) requires the computation time to be linear in the number of exercise opportunities and quadratic in the number of simulation paths. In the spirit of the papers of Haugh and Kogan (2004) and Rogers (2002), a primal-dual simulation algorithm is proposed by Andersen and Broadie (2004) to handle any type of process dynamics, factor structure, and payout specification. Their algorithm uses an approximation to exercise policy, rather than an approximation to the option price, to estimate the bounds on the true price of the option. An advantage of working with the exercise policy is the situation where exercise strategies are known

and independent of option price. These authors also take the martingale part of supermartingale used in the original approach in Haugh and Kogan (2004) to gain more accurate estimates.

### 2.9.2 Regression simulation

Another popular method from a practitioner's view is based on the regression technique proposed in Carriere (1996), Tsitsiklis and Van Roy (2001) and Longstaff and Schwartz (2001). The regression approach is reasonably fast and widely applicable. Carriere (1996) presents a backward induction algorithm and applies it to calculate the early exercise premium. He shows that the estimation of the decision rule to exercise early is equivalent to the estimation of a series of conditional expectations. The conditional expectations are estimated by splines and local regressions. Tsitsiklis and Van Roy (2001) proposed a recursive algorithm that approximates the holding value functions by a linear weighted combination of basis functions directly. Longstaff and Schwartz (2001) present a simple and powerful approximation to the American option valuation problem. The main difference to Tsitsiklis and Van Roy (2001) is the use of least squares to approximate the conditional expectation payoff. The holder of an American option optimally compares the payoff from immediate exercise with the expected payoff from continuation. If the immediate payoff is higher, the holder will choose to exercise the option, otherwise, he will keep the option and wait for the next exercise opportunity. These authors apply least-squares regression to find a linear combination of basis functions of the current value of the underlying to estimate the next time step value. When using regression, the holder takes the underlying prices as  $x$  values and the discounting values of the future underlying price as  $y$  values. As the regression is only dependent on the paths for which the option is in the money, which significantly increases the efficiency of the algorithm and reduces computation times. Longstaff and Schwartz (2001) also extend the methodology to complex derivatives with many underlying factors and, in summary, the accuracy of the methodology depends on the choice of regression functions. In their empirical

analysis, the authors apply their method to price a wide class of derivatives instruments and show that it yields the best combination of price accuracy and efficiency against several methodologies employed. In detail, the convergence of least squares Monte Carlo is described in Cerrato and Cheung (2007), Clement, Lamberton and Protter (2002) and Rogers (2002). These papers show that the estimated conditional expectation approaches (with probability one) the true conditional expectation as the number of basis functions increases, and the number of basis functions determines the convergence rate of the algorithm. They also prove that the normalized estimation error is asymptotically Gaussian. For a standard put option, Moreno and Navas (2003) analyze the robustness of the least squares Monte Carlo method relative to the choice of the type and the number of basis functions. They find the algorithm is very robust when pricing the American put option and a reasonable approximate value can be obtained by a modest polynomial degree (between 3 and 20); actually, more terms can make least square regressions less accurate. Although the Longstaff and Schwartz method has proved successful and popular, it still suffers from the drawback of Monte Carlo convergence. Therefore, Duck, Newton, Widdicks and Leung (2005) enhance the performance of the least squares Monte Carlo through a convenient and useful procedure. They suggest a formula to describe the variance of the calculated option from the exact price. The extrapolation procedure entails three different numbers of paths. After evaluating the averaging put option, they use the proposed formula to improve the price. The averaging scheme with an extrapolation procedure does appear to converge better than an order of magnitude faster than the original scheme of Longstaff and Schwartz. Besides the least squares Monte Carlo estimator, there is another estimator proposed by Glasserman and Yu (2004), which is called the weighted Monte Carlo estimator. Broadly speaking, these two methods are similar, since both aim to evaluate the conditional expectations by a number of basis functions for regression and finally use Monte Carlo to extract the option price.

There are many other simulation-based methods proposed and, as with the regression approach, they can be used to evaluate the lower bounds on the Bermudan option value. Andersen (2000) illustrates a method that parameterizes the exercise

policy and then optimizes these parameters over a set of simulations to determine an approximation to the optimal exercise strategy. Jensen and Svenstrup (2005) propose a simplification of this exercise strategy, replacing a maximum value of all (still unexercised) core European options with a carefully chosen single option value. The numerical test in Jensen and Svenstrup (2005) shows that this simple strategy leads to a significant computational saving without losses of present values of the options. Another simulation technique based on parameterizing the exercise decision is addressed in Garcia (2003). This method uses a parametric representation of the early exercise decision. This can be constructed by using two different estimates, one of which is biased low, the other biased high; the two estimates are shown to be asymptotically unbiased. Very simple representations of the exercise policy can produce highly accurate option prices. The quantization method proposed in Bally, Pages and Printems (2002; 2005) is another competitive technique to treat higher-dimensional problems. Simulation methods based on dimensionality reduction or nonparametric representations of the early exercise region include Barraquand and Martineau (1995), Carr and Yang (2001), Clewlow and Strickland (1998), and Raymar and Zwecher (1997). Other papers by Tilley (1993), Barraquand and Martineau (1995), and Raymar and Zwecher (1997) incorporate different aspects of the usual backwards induction algorithm by stratifying the state space and finding the optimal exercise decision in each of the subsets of the state variables.

The Monte Carlo method for derivative securities has reached a fair degree of maturity. Nevertheless, challenges remain on several fronts. It is certain to be a continuing goal to develop a better asset price model that is a good fit to data observed in financial markets. Ever-improving computing technology will expand the amount and types of data that can be analyzed.

# Chapter 3

## Option Pricing with Jump Processes

*... there is evidence of non-stationarity in the variance. More work must be done to predict variances using the information available.*

*– Fischer Black and Myron Scholes*

*The valuation of option contracts and a test of market efficiency, 1972*

In this chapter, we investigate a jump diffusion model which relaxes some of the restrictive Black-Scholes-Merton model assumptions. Empirical studies have found that the Black-Scholes model based on Geometric Brownian Motion (GBM) suffers several defects. One is the asymmetric leptokurtic feature; that is, the return distribution obtained from market data has a higher peak and two (asymmetric) heavier tails than those of the normal distribution. The constant volatility assumed in the Black-Scholes model also contradicts an empirical phenomenon, namely the ‘volatility smile’ in options markets. Another defect is the continuity property of GBM which fails when markets crash or some large random fluctuations occur. Extensions proposed to model these phenomena can be classified into two groups: jumps and stochastic-volatility. The stochastic-volatility model was introduced by Hull and White (1987), then developed by Stein and Stein (1991) and Heston (1993). Also, stochastic volatility and stochastic interest rate models are presented by Amin and

Ng (1993) and Scott (2002). These models focus on adding more state variables, replacing some of the constant parameters used in the Black-Scholes model. The jump diffusion model is first suggested by Merton (1976), while Cox and Ross (1976) also provide a pure jump process instead of GBM. Statistical evidence in Ball and Torous (1985) and Huang and Tauchen (2005) suggest that jumps are significant in financial markets. Jarrow and Rosenfeld (1984) find the connection between jump risks and the Capital Asset Pricing Model (CAPM) and Jorion (1988) investigates the existence of jumps in foreign exchange and stock markets. Andersen and Andreasen (2000) use the jump-diffusion model to obtain excellent fits with stable parameter estimations for S&P500 market data. In recent years, some studies indicate the stochastic volatility model plus jumps leads to improved results. This is because stochastic-volatility is needed to determine the long-term trend of the volatility process, whilst jumps are able to model a series of instant changes in the underlying prices that are relatively large. Bakshi, Cao and Chen (1997) suggest an ideal framework is to include both jumps and stochastic volatility, which is also supported by Bates (1996). Eraker, Johannes and Polson (2003) recommend a model with jumps both in the underlying and the volatility. Andersen, Bollerslev, Diebold and Labys (2001) demonstrate a portion of realized jumps is caused by stochastic volatility. In his pioneering model, Merton (1976) proposes jumps according to a compound Poisson process with constant intensity and log-normally distributed jump sizes. Kou's (2002) work is similar to Merton's (1976) model, but with log-double-exponentially distributed jump amplitudes instead of log-normally distribution. Yan and Hanson (2006) and Zhu and Hanson (2005) treat the amplitudes as a log-uniformly distribution. Instead of a single class of jumps used in Merton (1976), Martzoukos (2003) derives a jump-diffusion model with multiple classes of jumps to describe different types of rare events and makes use of a joint probability distribution for each class of jumps. For European options, Merton (1976) derives an analytical expression but, for more exotic options or American options, no analytical solution exists under jump-diffusion models. Pricing derivatives on the jump diffusion models can also be related to solve the corresponding partial integro differential equation (PIDE). Duffy (2008) shows the relationship and propose

several numerical methods.

### 3.1 Background to the Merton jump diffusion (MJD) model

We start with the simple Merton (1976) jump diffusion model, written as:

$$dS = (r - \lambda\kappa)Sdt + \sigma SdW_S + SdJ, \quad (3.1)$$

where  $(r - \lambda\kappa)dt + \sigma dW_S$  is a Brownian motion with a drift term  $(r - \lambda\kappa)$  rather than  $r$  in the standard Black-Scholes model;  $\lambda$  represents the expected intensity of jumps during  $dt$  and  $\kappa$  is the expected magnitude of the jump size; the additional term  $dJ$  is a compound Poisson jump process to capture the rare events. There is no dependence between the diffusion term  $dW_S$  and the jump term  $dJ$ . Assuming the jump size is lognormally distributed, then an explicit analytical solution of European options with jumps derived in Merton (1976) can be written as:

$$F(S, \tau) = \sum_{n=0}^{\infty} \frac{e^{-\lambda'\tau} (\lambda'\tau)^n}{n!} BS_n(S, \tau; K, r', \sigma', \tau), \quad (3.2)$$

where  $\lambda' = \lambda(1 + \kappa)$ ,  $r' = r - \lambda\kappa + n * \log(1 + \kappa)/\tau$ ,  $\sigma' = \sqrt{\sigma^2 + \delta^2 n/\tau}$ ,  $\kappa = e^{\mu + \frac{1}{2}\delta^2} - 1$  and  $BS_n$  is the standard Black-Scholes formula of European options with the modified interest rate  $r'$  and volatility  $\sigma'$ . Here, two new parameters,  $\mu, \delta$ , represent the intensity of the jump process, namely the mean and standard deviation of the log jump size, respectively.

It is necessary to point out that the volatility of the Merton model is different from the Black-Scholes model. In the Black-Scholes case, the  $t$ -period standard deviation of log-return  $x_t$  is  $\sigma_{BS}\sqrt{t}$ , however in the Merton model, the standard deviation is  $\sqrt{(\sigma_{Merton}^2 + \lambda\mu^2 + \lambda\delta^2)t}$ . Normally, we will find an option price from the Merton model is higher than (or equal to) that from the Black-Scholes model because of the volatilities of both models, i.e. a larger volatility leads to higher option price:

$$\sigma_{BS}\sqrt{t} \leq \sqrt{(\sigma_{Merton}^2 + \lambda\mu^2 + \lambda\delta^2)t}. \quad (3.3)$$

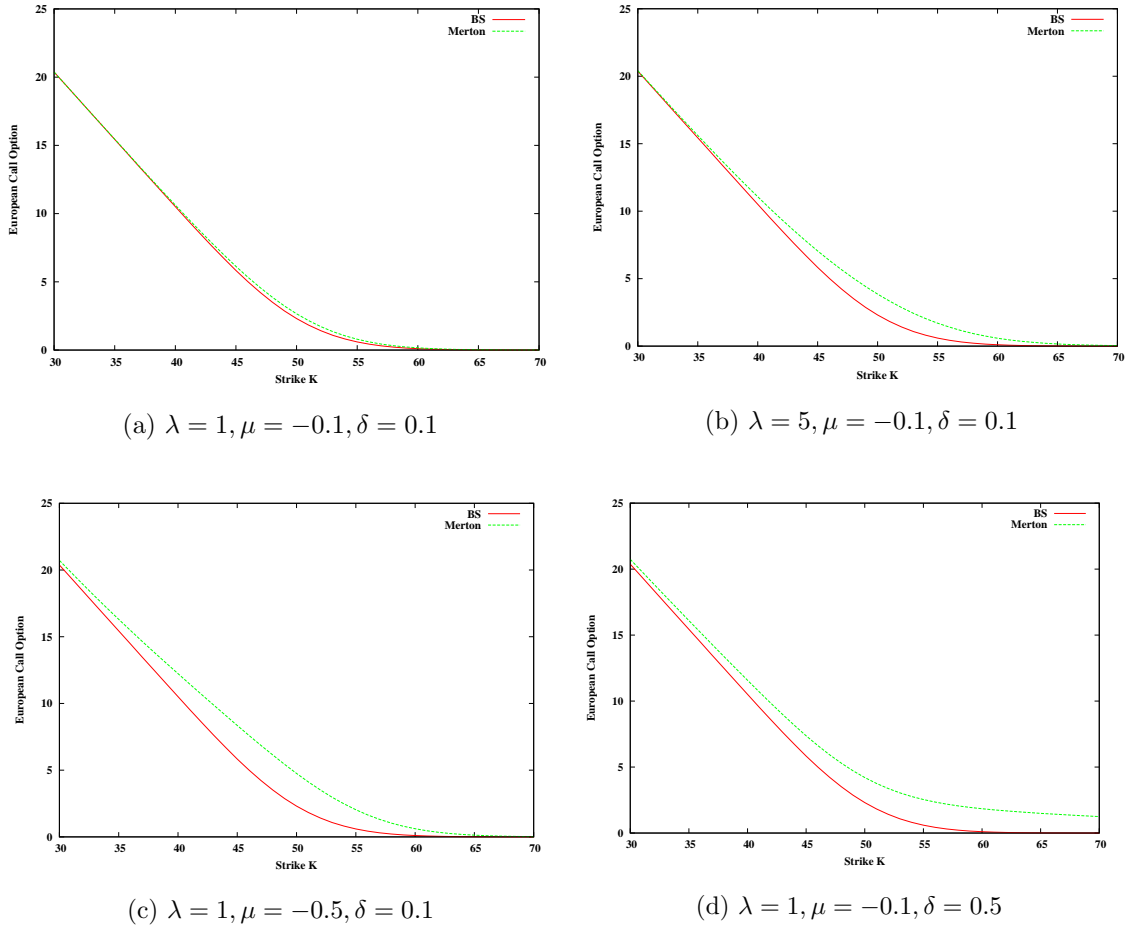


Figure 3.1: Pricing European call options by Merton and Black-Scholes models under different parameter sets (shown on the top of each graph). The other parameters applied here are  $S = 50, r = 0.05, \sigma = 0.2$  and  $T = 0.25$ .

Fig 3.1 provides the Merton option prices calculated by Eq (3.2) and also the corresponding standard Black-Scholes prices. Fig 3.1(a) and Fig 3.1(b) illustrate how the changes of  $\lambda$  impact on the Merton price accompanied by the Black-Scholes price. The Merton price generally increases in  $\lambda$  except for deep in or out-of-the-money (DITM/DOTM) options. The price difference between the two models is more pronounced for at-the-money (ATM) options. Similarly, we also provide the price impact from mean  $\mu$  and standard deviation  $\delta$  of the jump size in Fig 3.1(c) and Fig 3.1(d) compared with Fig 3.1(a). Reducing  $\mu$  from  $-0.1$  to  $-0.5$  has more influence on the option price than the changes of  $\lambda$  as the price increases even for DITM options. Furthermore, increasing  $\delta$  gives a higher price of DOTM options. In addition, if we

restrict  $\sigma_{BS}$  and  $\sigma_{Merton}$  in (3.3) such that

$$\sigma_{BS}\sqrt{t} = \sqrt{(\sigma_{Merton}^2 + \lambda\mu^2 + \lambda\delta^2)t},$$

then the option prices given by both models converge. For more detailed results, see Matsuda (2004).

Next, employing the option price formula (3.2), we fit FTSE100 data to estimate parameters which are needed in the Merton model and see how the formula works when compared with the Black-Scholes formula. The FTSE100 Index options are of European style. We focus on two specific options<sup>1</sup> which are detailed in Table 3.1<sup>2</sup>. Besides the option prices, the data file contains spot prices, strike prices and time to maturity, that is,  $S$ ,  $K$  and  $\tau$  are known parameters. We suggest employing a linear

Style	Call	Put
Strike	4000	6000
Start	06/08/2008	21/07/2008
Expiry	21/11/2008	21/11/2008
Sample Size	68	80

Table 3.1: FTSE100 Data information

least squares algorithm (LS) to estimate the unknown parameters by minimising the difference between model-derived prices and market prices. In other words, define an object function  $f(x)$  as:

$$f(x; S, K, \tau) = \sum_{i=1}^m (F_i^{\text{model}}(x) - F_i^{\text{market}}(x))^2, \quad (3.4)$$

subject to the bounds

$$l \geq x \geq u,$$

where  $x$  is a vector of unknown parameters:  $r, \sigma, \mu, \delta$  and  $\lambda$  in the Merton (1976) model, whilst there are only two parameters,  $r$  and  $\sigma$ , in the Black-Scholes (1973) model; the vectors  $l$  and  $u$  denote the lower and upper parameter bounds of  $x$ ;  $F^{\text{model}}$  is the option pricing formula, namely, either the Merton option pricing formula

<sup>1</sup>Both options chosen here are in the money.

<sup>2</sup>All data were obtained from DATASTREAM database.

(3.2) or the Black-Scholes formula (1973);  $F^{\text{market}}$  is the corresponding option price observed in the market, in this example, that is, the FTSE100 Index option price;  $m$  is the sample size given in Table 3.1. The problem of constrained minimization of  $f(x)$  can be solved by the Nag library function (nag\_opt\_bounds\_no\_deriv). Assuming the bounds are set as follows:

$$0.0 \leq r \leq 1.0 ,$$

$$0.0 \leq \sigma \leq 1.0 ,$$

$$-0.2 \leq \mu \leq 0.0 ,$$

$$0.0 \leq \delta \leq 1.0 ,$$

$$0.0 \leq \lambda \leq 5.0 ,$$

the resulting approximations of the parameters for the both models are presented in Table 3.2 and the option prices calculated by the option pricing formulae with the estimated parameters are shown in Fig 3.2.

Model	Merton		Black-Scholes	
	Call4000	Put6000	Call4000	Put6000
Style				
r	0.0000e+00	0.0000e+00	7.1961e-02	7.2847e-02
$\sigma$	3.3317e-01	0.0000e+00	1.6439e-01	1.6499e-01
$\mu$	-7.1758e-01	-9.6016e-01	n/a	n/a
$\delta$	6.0095e-01	2.8495e-01	n/a	n/a
$\lambda$	0.0000e+00	1.2668e-01	n/a	n/a
RMSE	67.3452	16.7612	50.5967	19.2470

Table 3.2: Parameter estimators

As shown in Table 3.2, the two sets of data suggest different values of the Merton-model-implied parameters. The call option data produce a non-jump pure diffusion model with  $r = 0$  and  $\lambda = 0$ , whilst the put option data results a pure jump diffusion model with  $r = 0$  and  $\sigma = 0$ . These inconsistent estimates might be explained by the short term sample period studied here. The entire sample period is just around two months during the global economic crisis of 2008, which might results in a zero interest rate. Compared with the Merton model, we observe that the estimates of the Black-Scholes model:  $r$  and  $\sigma$  are approximately equal from both sets of data. The RMSE value of the Black-Scholes model is less than that of the Merton model for

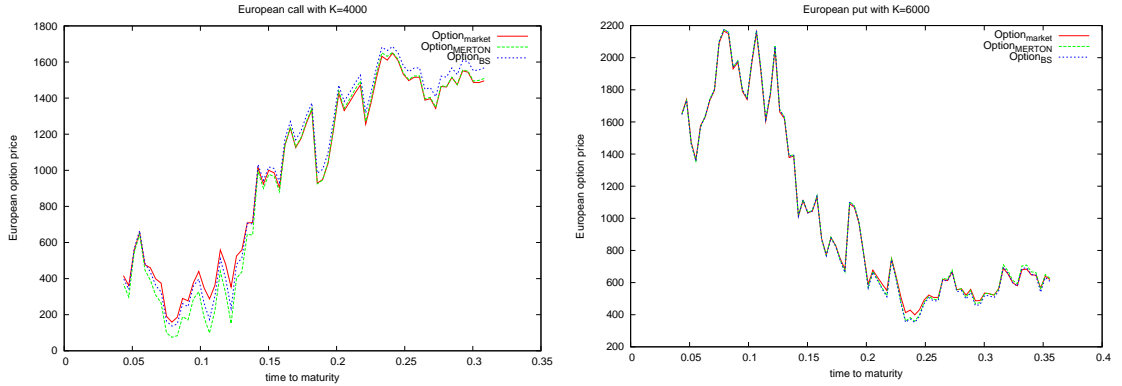


Figure 3.2: European Option Price from Merton Model against FTSE100 Index Option Price

pricing call options. More precisely, Fig 3.2 shows the Merton model underperforms the Black-Scholes model for pricing call options close to maturity. These results do not strongly support the proposition that the Merton model gives a better fit with FTSE100 Index options against the Black-Scholes model. The main explanations of the inferior performance of the Merton model are due to adequate sample size and the simple version of the Merton model used here. It might be improved by involving the stochastic volatility and market illiquidity which will be introduced in Chapter 4.

## 3.2 Generating sample paths in the MJD model

The option price formula (3.2) is only available for pricing vanilla European options. For other complex options on the Merton jump diffusion process (3.1), we are obliged to employ numerical methods, such as Monte Carlo simulation, to calculate the option prices. In this section, we give a brief introduction to a numerical method to generate sample paths under the simple Merton jump diffusion (3.1). Following Glasserman (2003), the solution of the SDE (3.1) is given by:

$$S(t) = S(0)e^{(r - \lambda\kappa - \frac{1}{2}\sigma^2)t + \sigma W_S(t)} \prod_{j=1}^{N(t)} Y_j , \quad (3.5)$$

where  $W_S(t)$  is a standard Brownian motion;  $N(t)$  is a Poisson process counting the number of jumps over  $[0, t]$ ;  $Y_1, Y_2, \dots$  are random numbers of the jump sizes from a lognormal distribution  $LN(\mu, \delta^2)$ ; we assume that  $W_S(t)$ ,  $N(t)$  and  $Y_j$  are

independent processes. Then the discrete time solution can be obtained at each time step  $t_i$  where  $i = 0, 1, \dots$ :

$$S(t_{i+1}) = S(t_i) e^{(r - \lambda\kappa - \frac{1}{2}\sigma^2)(t_{i+1} - t_i) + \sigma[W_S(t_{i+1}) - W_S(t_i)]} \prod_{j=N(t_i)+1}^{N(t_{i+1})} Y_j. \quad (3.6)$$

A simplification of the solution (3.6) can be found by taking logarithms of both sides of (3.6) and replacing  $\log S(t_i)$  with  $x(t_i)$ , which is

$$x(t_{i+1}) = x(t_i) + (r - \lambda\kappa - \frac{1}{2}\sigma^2)(t_{i+1} - t_i) + \sigma[W_S(t_{i+1}) - W_S(t_i)] + \sum_{j=N(t_i)+1}^{N(t_{i+1})} \log Y_j. \quad (3.7)$$

This representation is preferable, because it uses the sums of  $\log Y_j$  instead of the products of  $Y_j$ , and  $\log Y_j$  can be directly simulated from a normal distribution  $N(\mu, \delta^2)$ . The option price  $S(t_i)$  is estimated by exponentiating  $x(t_i)$ , which is easily implemented.

To generate sample paths  $x(t_i)$  following Eq (3.7), the diffusion term  $[W_S(t_{i+1}) - W_S(t_i)]$  can be simulated by the product of a standard normal random variable  $Z_i$  from  $N(0, 1)$  and the square root of the time difference  $\sqrt{t_{i+1} - t_i}$ . For the jump term, the number of jumps over  $[t_i, t_{i+1}]$  also has a Poisson distribution with mean  $\lambda(t_{i+1} - t_i)$ , therefore instead of simulating the jumps individually, we can estimate the total effect of the jumps over  $[t_i, t_{i+1}]$  by a normal random variable from  $N(\mu\xi_i, \delta^2\xi_i)$  with  $\xi_i$  is the realized possible random variable, that is,

$$\sum_{j=N(t_i)+1}^{N(t_{i+1})} \log Y_j \sim N(\mu\xi_i, \delta^2\xi_i) = \mu\xi_i + \delta\sqrt{\xi_i}N(0, 1).$$

The algorithm for simulation is given by the following steps:

1. generate  $Z_i \sim N(0, 1)$
2. generate  $\xi_i \sim Poisson(\lambda(t_{i+1} - t_i))$ ; if  $\xi_i = 0$ , set  $\eta_i = 0$  and go to Step 4
3. generate  $\bar{Z}_i \sim Normal(0, 1)$ ; set  $\eta_i = \mu\xi_i + \delta\sqrt{\xi_i}\bar{Z}_i$
4. set

$$x(t_{i+1}) = x(t_i) + (r - \lambda\kappa - \frac{1}{2}\sigma^2)(t_{i+1} - t_i) + \sigma\sqrt{t_{i+1} - t_i}Z_i + \eta_i \quad (3.8)$$

5. transfer to underlying price  $S$ 

$$S(t_i) = \exp(x(t_i)) .$$

Then, the standard Monte Carlo method is used with a number of sample paths generated by the above algorithm to compute the option price. An example is given in Fig 3.3. The straight line in each case is produced by Merton's analytical solution

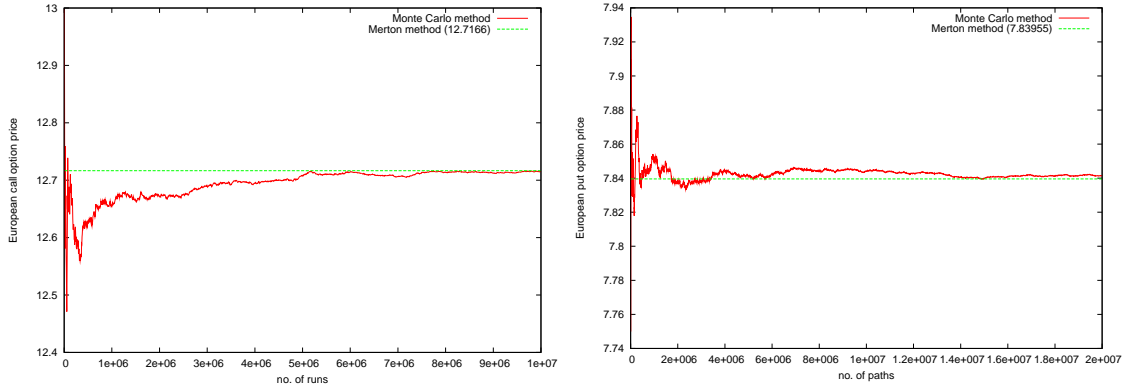


Figure 3.3: Pricing European options by Merton and Monte Carlo methods,  $S = K = 100, r = 0.05, \sigma = 0.2, T = 1, \lambda = 0.1, \delta = 0.8, \mu = -\delta^2/2$ .

(3.2) as a benchmark. Fig 3.3 shows that the Monte Carlo estimation converges to the Merton value with an increasing number of sample paths, which suggests the above algorithm is valid for estimating option prices.

### 3.3 Pricing 1D Bermudan put options using the MJD model

This section introduces the pricing of a Bermudan put option via Monte Carlo methods in a jump diffusion model. A Bermudan option allows the holder to exercise at a fixed number of dates, in contrast with an American option, which can be exercised at any time. As mentioned in Section 2.9, in recent years, the Monte Carlo method has been extended to handle early exercise for American and Bermudan options. We extend the Longstaff and Schwartz (2001), Least Squares Monte Carlo method (LSM) to incorporate the jump diffusion model, in particular the method of Duck et al. (2005) is employed to enhance accuracy.

Compared with the standard Black-Scholes model studied in Longstaff and Schwartz (2001) and Duck et al. (2005), our results show that the jump diffusion models required more computational time to achieve an accurate estimate of the Bermudan option price, and the Duck et al. (2005) method has a good performance in the jump diffusion models. We also provide a set of optimal parameter setting for the jump diffusion models.

According to London (2004), the LSM algorithm is divided into three parts: forward simulation of price paths by Monte Carlo, backwards production of cash flows for each path by comparing exercise values with values given by least-squares approximation over a collection of basis functions, and then calculation of the American option's price by averaging the discounted cash flows at time zero. With only 'in-the-money' paths included in the least squares regression, the performance of the algorithm is improved, with decreased computation time (see Longstaff and Schwartz, 2001).

### 3.3.1 Implementation

Consider an underlying process  $S$  that follows a jump diffusion equation (3.1). Using the algorithm for simulating a jump process introduced in Section 3.2, we provide a detailed LSM algorithm for pricing a one-dimensional Bermudan option as follows:

1. For pricing a Bermudan put with maturity  $T$ , strike  $K$  and  $N$  exercise opportunities on underlying  $S$ , we set up a discrete time framework using  $N^*$  timesteps of the equal size  $\Delta t = T/N^*$  with an integer  $n$ ,  $n = N^*/N$ , then each time point  $t_i = i\Delta t$  for  $i = 0, \dots, N^*$ . Assume that  $M$  sample paths are used in the least squares regression and the regression runs  $M_{run}$  times, independently.
2. Generate the Paths Matrix  $S_{ij}$  and Exercise Matrix  $X_{ij}$

Sample the  $M$  independent paths of the underlying price  $S_j(t_i)$  for  $j = 1, \dots, M$  by simple Euler discretization. As discussed in Section 3.2, the approximation of SDE (3.1) can be simplified to simulate the log price  $x(t)$  using Eq (3.8),

which can be rewritten as follows:

$$x_j(t_{i+1}) = x_j(t_i) + (r - \lambda\kappa - \frac{1}{2}\sigma^2)\Delta t + \sigma Z_j(t_i)\sqrt{\Delta t} \\ + [\mu\xi_j(t_i) + \delta\sqrt{\xi_j(t_i)}\bar{Z}_j(t_i)] , \quad (3.9)$$

where  $Z_j(t_i)$  and  $\bar{Z}_j(t_i)$  are independent standard normal random variables and  $\xi_j(t_i)$  is also a random variable arising from a Poisson distribution with parameter  $\lambda\Delta t$  for  $j$ -the sample path.

Then, we define a  $N \times M$  path matrix  $[S_{ij}]_{N \times M}$  and an exercise matrix  $[X_{ij}]_{N \times M}$  as follows:

$$S_{ij} = \exp(x_j(t_{i*n})) , \\ X_{ij} = \max(K - S_{ij}, 0) ,$$

for  $i = 0, \dots, N$  and  $j = 1, \dots, M$ . In addition, the number of random numbers required in this procedure is  $2n * N * M * M_{run}$ .

### 3. Calculate the Discounted Cash Flow Vector $DC_j$

We start from time  $t_N$  and assign the discounted cash flow  $DC_j = X_{Nj}$  for each path  $j = 1, \dots, M$ , then move backwards to recalculate the value of  $DC_j$  by a comparison of the exercise value and the continuation value of the option. Thus, for each exercise time points:  $t_{(N-1)n}, t_{(N-2)n}, \dots, t_n, t_0$ , first, the cash flow is discounted back  $n\Delta t$  in time as follows:

$$DC_j = DC_j e^{-rn\Delta t} .$$

Then the continuation value  $CV_j$  is estimated by a least squares regression of the discounted cash flow  $DC_j$  on the current value of underlying  $S_{ij}$  for ‘in-money’ paths, i.e.  $X_{ij} > 0$ . We use Chebyshev polynomials  $T_m$  as the basis function (see examples in Abramowitz and Stegun, 1972), which is

$$DC_j = \sum_{m=0}^{\bar{J}} a_m T_m(S_{ij}) , \quad (3.10)$$

where  $\bar{J}$  is the highest order of the polynomials and  $a_m$  are the parameters required to be determined by the observed data  $S_{ij}$  and  $DC_j$ . Once the  $a_m$  are

known, we can approximate the continuation value as follows:

$$CV_j = \sum_{m=0}^{\bar{J}} a_m T_m(S_{ij}) . \quad (3.11)$$

If  $X_{ij} > CV_j$ , we exercise the put option and replace the value  $DC_j = X_{ij}$ ; otherwise, we hold the option and keep the value of  $DC_j$ . We repeat this procedure until  $t_0$ .

4. Average the discounted cash flows over the  $M$  sample paths, that is,

$$P = \frac{1}{M} \sum_{j=1}^M DC_j .$$

5. Repeat Step 2 to Step 4 for  $M_{run}$  times and take the average value of  $P$  as the estimator of the Bermudan put price. There is an alternative procedure proposed in Duck et al. (2005) which is shown to achieve a more accurate estimated price. Their method, based on an extrapolation technique, can be easily implemented with three different sample sizes  $M$ . We will give a detailed description of the method and numerical examples in Section 3.5.4.

### 3.3.2 Sensitivity of option price to the choice of the parameters

In this section, we study the sensitivity of the input parameters used in the algorithm in Section 3.3.1 to the option price, which are the sample size  $M$  for the least squares regression, the expected number of jumps  $\lambda$  and the size of time steps  $\Delta t$  discussed respectively in the following:

1. Sample Size  $M$  Impact on Option Price

First, the choice of the sample size plays a critical role in the Least Squares Monte Carlo algorithm. In a case without jumps, as we increase exercise opportunities, the price of a Bermudan put option rises and tends to be an asymptotic value in the limit, which is the case of pricing an American option. This rule should hold in the case with jumps, so it can be used to test whether the choice

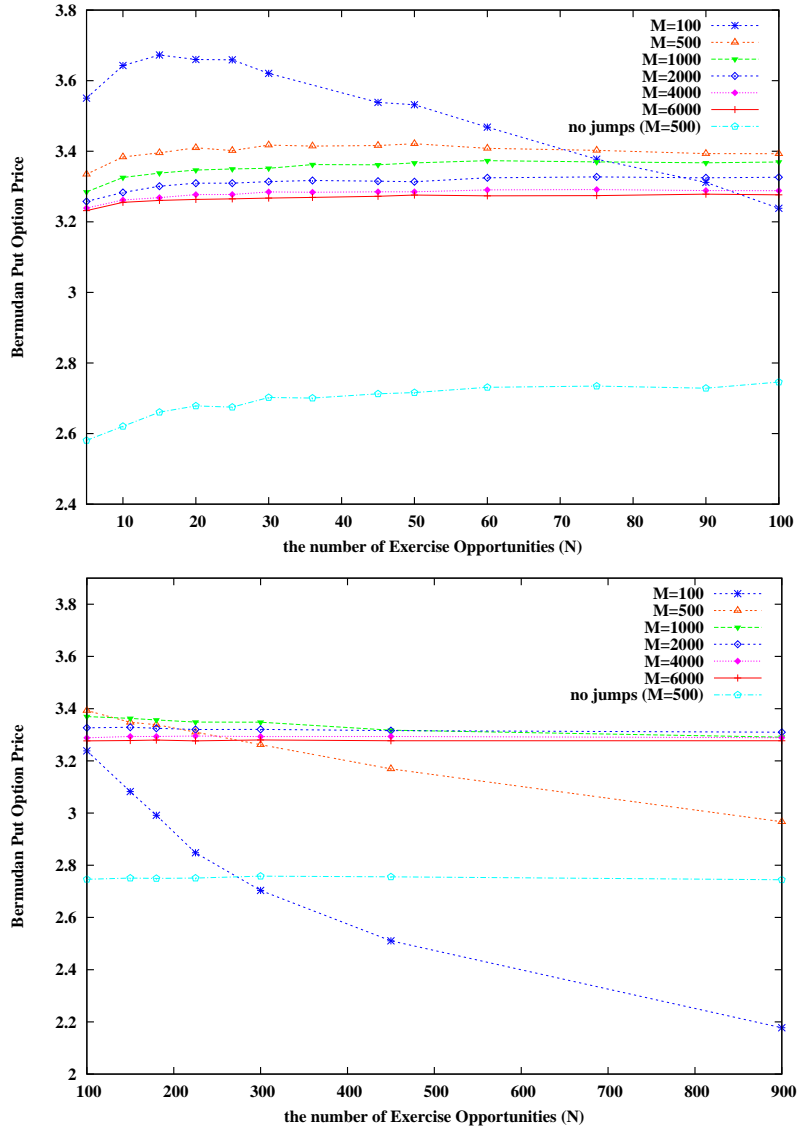


Figure 3.4: 1D-MJD: Bermudan put option respect to different sample sizes in the least squares calculation under the parameter setting:  $S = 100, K = 100, T = 0.25, r = 0.05, \sigma = 0.15, N^* = 900, \lambda = 0.1, \mu = -0.9, \delta = 0.45, M_{run} = 5000, \bar{J} = 6$ . The left panel shows the results for  $5 \leq N \leq 100$  and the right panel is for  $100 \leq N \leq 900$

of sample size  $M$  is appropriate to value the option price. Given  $M$  for the least squares algorithm, Fig 3.4 shows the Bermudan option prices with respect to the total number of exercise times  $N$  ranging from 5 to 900, assuming the total number of time steps  $N^*$  is taken to be 900 for this example. We also calculate the prices of the corresponding Bermudan options in the Black-Scholes model by setting  $\lambda = 0$  in the same algorithm, i.e. no jumps in the underlyings. Fig 3.4 shows that the choice of sample size  $M$  is important to achieve an acceptable Bermudan option price, because the option prices estimated by fewer sample paths, such as  $M = 100$  and 500, increase initially then decrease with increasing  $N$ . This decline is spurious and against the expected trend stated above. The problem can be easily resolved by increasing the sample size,  $M$ . As shown in Fig 3.4, the option price for  $M = 2000, 4000$  and 6000 slightly increases for relatively small values  $N$ , whilst for larger values of  $N$  the option price tends to be fairly constant, that can be recognised as the price of the corresponding American option price with infinite exercise opportunities. Compared with the Black-Scholes model where the sample size  $M = 500$  is sufficient to produce a reasonable price of the Bermudan option, the MJD model requires more sample paths to yield the Bermudan option price, due to more volatility involved in the underlying. The results in Fig 3.4 suggest that an adequate sample size is  $M = 2000$  for the least squares regression in the MJD model. When the sample size rises from 2000 to 6000, the option price slightly decreases and converges to an asymptotic value for the Bermudan option with  $N$  exercise opportunity. With a proper value of  $M$ , we find that the Bermudan prices in the MJD model are higher than the prices in the Black-Scholes model without jumps, which implies that the underlying asset becomes more volatile when including jump events.

Fig 3.5 shows a comparison of option prices between  $M_{run} = 5000$  and  $M_{run} = 10000$  for different values of  $M$ . In general, the computational time required for  $M_{run} = 10000$  is about twice as much as the time required for  $M_{run} = 5000$  (see

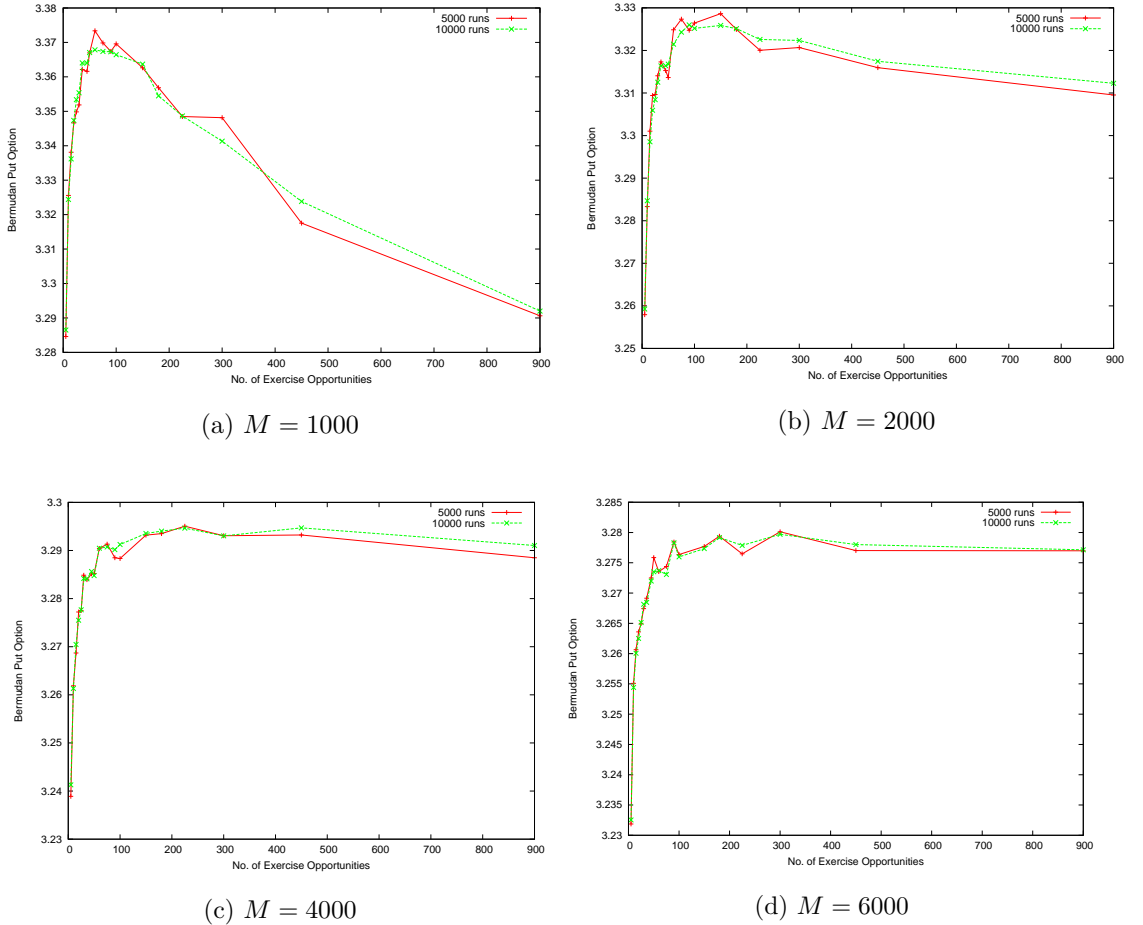


Figure 3.5: 1D-MJD: Pricing Bermudan put option with different sample sizes  $M$  and different runs  $M_{run}$ ,  $S = 100$ ,  $K = 100$ ,  $T = 0.25$ ,  $r = 0.05$ ,  $\sigma = 0.15$ ,  $N = 900$ ,  $\lambda = 0.1$ ,  $\mu = -0.9$ ,  $\delta = 0.45$

details in Appendix B). We find a clear decline in option prices for  $M = 1000$  and a slight drop for  $M = 2000$  and  $4000$ , but no decline for  $M = 6000$ . When  $M_{run}$  increases from 5000 to 10000, Fig 3.5 shows that there is no significant change of the option prices beyond  $M = 6000$ ; for the other values of  $M$  tested in this example,  $M_{run} = 10000$  leads to a slower decline of the option prices than that of  $M_{run} = 5000$ , which shows that  $M_{run} = 10000$  may improve the accuracy of the option pricing. Considering the cost of computation, we suggest that the optimal choice is  $M = 2000$  sample paths for each run of the least squares regression and the total number of run is  $M_{run} = 5000$ .

## 2. Timestep $\Delta t$ Impact on Option Price

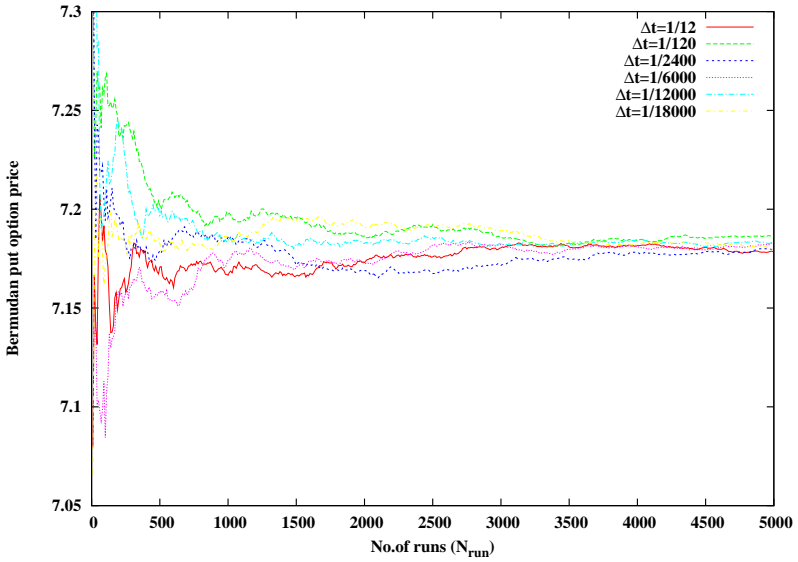


Figure 3.6: 1D-MJD: Pricing Bermudan put option with different sizes of timesteps  $\Delta t$  with the parameter setting:  $S = 100, K = 100, T = 1.0, r = 0.05, \sigma = 0.15, \lambda = 0.1, \mu = -0.9, \delta = 0.45, N = 12$  and  $M_{run} = 10000$

The timestep  $\Delta t$  is a factor for consideration in discrete-time approximation error for general Monte Carlo simulations. The algorithm in Section 3.3.1 suggests simulating underlying prices at each time point  $t_{i+1} = t_i + \Delta t$  to minimize discretization error by choosing a small value of  $\Delta t$ . Here, we show that, whatever  $\Delta t$  is applied, the simulated sample paths according to Eq (3.9) lead to accurate values for a Bermudan options. In Fig 3.6, varying values of  $\Delta t$  have been examined to estimate a Bermudan put option with  $N = 12$  exercise opportunities. We find that there is no obvious effect of  $\Delta t$  on the option prices. Indeed, the price given by  $\Delta t = 1/12$ , leading to the same time points as early exercises, is similar to those prices estimated by smaller values of  $\Delta t$ , because SDE (3.1) is solved exactly. Therefore, we can directly simulate the underlying price at each exercise time point, i.e. setting  $n = 1$  in the original algorithm in Section 3.3.1.

### 3.3.3 $\lambda$ impact on pricing option

The parameter  $\lambda$  in a jump process is a rate representing the expected number of arrivals per unit time. A higher  $\lambda$  implies more jumps during the option's life, which

implies more volatility associated with the underlying. As discussed in Section 3.1, using the analytical solution (3.2), we find that the prices of European-style options increase as  $\lambda$  values rise, just as expected for option prices as volatility is increased. Table 3.3 shows how the value of a Bermudan option changes with different values of  $\lambda$

$\lambda$	European put price	Bermudan put price ( $N = 12$ )	Bermudan put price ( $N = 30$ )
0	3.7146	4.2457	4.3004
1	27.4128	28.8465	28.9947
10	72.6870	74.4841	74.6463
20	86.3417	88.4513	88.5845

Table 3.3: 1D-MJD: Impact of  $\lambda$  on pricing Bermudan and European options under the following parameter setting:  $S = K = 100, T = 1, r = 0.05, \sigma = 0.15, \mu = -0.9, \delta = 0.45, M = 2000$  and  $M_{run} = 5000$ . The results for European options are calculated by Eq (3.2).

compared with a standard European put option in the same MJD model. Intuitively, the Bermudan option is more expensive than the European option. When  $\lambda$  rises, the price of the Bermudan option increases as in the case of the European price. Moreover, the option prices for  $\lambda \neq 0$  are much higher than the prices for  $\lambda = 0$ . This is because, when we set the mean of jump-size  $\mu$  to be negative, there is a high probability money can be made from trades with lower asset prices (immediately for those Bermudan option holders). Table 3.3 also provides two kinds of Bermudan options with the different number of exercise times:  $N = 12$  and  $N = 30$ . We can see that the option price given by  $N = 30$  is slightly higher than the price for  $N = 12$  in each case of  $\lambda$ , which is consistent with the previous results with regard to  $N$  in Fig 3.4.

### 3.4 Pricing multi-dimensional Bermudan put option using the MJD model

In this section, we extend our one-dimensional model in Section 3.3 to pricing a Bermudan option on multiple underlying assets with jumps. The main difficulty with pricing those options is to find the correlations of the intensities and sizes of

the jumps among different assets. There are three kinds of approaches: independent jumps, jumps with the same intensities but different sizes and jumps with different intensities and sizes. As an example of the first case, Merton (1976) set up a hedged portfolio with  $m$  stocks. He supposed the jump components of a stock's return were totally independent in the portfolio. For the second case, Duffie et al. (2000) illustrate a stochastic volatility model and apply the jumps into both the underlying and the volatility (referred to as SVJJ). In the SVJJ model, it is assumed that the jumps on the underlying arrive at the same time as those on the volatility process, that is, two processes are employed with the same number of jumps at time  $t$ ,  $N_t^v = N_t^s = N$ , and the correlated jump sizes are  $\xi^v \sim Exp(\mu^v)$  and  $\xi^s | \xi^v \sim Normal(\mu^s + \rho_J \bar{Z}^v, (\delta^s)^2)$ . Martzoukos (2003) introduces a foreign asset model with multiple classes of jumps. He assumes that the jumps from the same class can affect several or all asset prices with a correlation matrix of jump size for different assets, while the jumps from the different classes are totally independent. The same assumption has been applied by Clift (2007) in his thesis, who uses finite-difference methods to price options with a two-asset jump diffusion. Matei (2005) considers two kinds of jumps: idiosyncratic jumps and common jumps, which happen independently, in a multi-asset model. The former is determined by the specific asset itself, and leaves the other assets unaffected, whereas the latter affects all the assets at the same time, except for those specific assets. For common jumps, it is natural to consider the correlation of the jump sizes among different assets. The third approach concerning the correlation of the jump intensities is introduced in Chan's (2003) paper. He suggests that the number of jumps for the  $p$ -asset is  $N_p = N_p^* + \bar{N}$ , where  $N_p^*$  and  $\bar{N}$  are independent Poisson random variables with intensities  $\mu_p^*$  and  $\bar{\mu}$ . Based on Chan's (2003) and Clift's (2007) models, we consider the correlated intensities and sizes of jumps on assets  $S_p$  for  $p = 1 \cdots P$ . If the jumps happen at the same time, there is a correlation coefficient,  $\rho_J$ , for jump sizes which follows a multivariate normal distribution. We also consider a correlation coefficient,  $\rho_n$ , of jumps arrivals. For a multi-asset case,

the model under log-price scale,  $x_p = \log S_p$ , is obtained as follows:

$$dx_p = (r - \lambda_p \kappa_p - \frac{1}{2} \sigma_p^2) dt + \sigma_p dW_p + J_p dq_p , \quad (3.12)$$

where

$$\kappa_p = \exp(\mu_p + \frac{1}{2} \delta_p^2) - 1 ,$$

$$\xi_p^* \sim Poisson(\lambda_p dt) ,$$

$$\xi^* \sim Poisson(\bar{\lambda} dt) ,$$

$$dq_p = \xi_p^* + \xi^* ,$$

$$(J_1, \dots, J_P) \sim N(\mu_1, \dots, \mu_P; \delta_1^2, \dots, \delta_P^2; \Sigma_J) ,$$

which is a multivariate normal distribution of jump size on different assets, with a correlation matrix  $\Sigma_J$ ; similarly, the increments of Brownian motion  $dW_p$  are derived from a multivariate normal distribution with mean zero, which is

$$(dW_1, \dots, dW_P) \sim Normal(0; dt; \Sigma_W) ,$$

with the correlation matrix  $\Sigma_W$ , the vector of mean 0 and the vector of variance  $dt$ .

### 3.4.1 Implementation

The Monte Carlo method gains advantage over other numerical methods whose computational cost increases exponentially rather than linearly with an increasing number of underlyings. LSM is easily implemented and an effective choice in pricing options on multi-underlying Bermudan-style valuations. Consider a Bermudan put option on  $P$  correlated underlying assets, whose the payoff  $V$  is given by:

$$V = \max(0, K^1 - S^1(t_N), \dots, K^p - S^p(t_N), \dots, K^P - S^P(t_N)) , \quad (3.13)$$

where  $K^p$  is a strike price according to the  $p$ -th underlying asset. Now consider the Euler discretization of SDE (3.12) over small time intervals  $\Delta t$  where  $t_{i+1} = t_i + \Delta t$ , we gain the approximation as follows:

$$x^p(t_{i+1}) = x^p(t_i) + (r - \lambda^p \kappa^p - \frac{1}{2} (\sigma^p)^2) \Delta t + \sigma^p Z^p(t_i) \sqrt{\Delta t} + J^p(t_i) \Delta q^p(t_i) , \quad (3.14)$$

with a known risk-free  $r^p$  and volatility  $\sigma^p$  for each assets  $p = 1, \dots, P$ .  $Z^p(t_i)$  is a standard normal random variable with a symmetric correlation matrix  $\Sigma_W$  of underlyings given by:

$$\Sigma_W = \begin{pmatrix} 1 & \rho_{12}^{(W)} & \rho_{13}^{(W)} & \dots & \rho_{1P}^{(W)} \\ \rho_{21}^{(W)} & 1 & \rho_{23}^{(W)} & \dots & \rho_{2P}^{(W)} \\ \vdots & \vdots & \vdots & \vdots & \vdots \\ \rho_{P1}^{(W)} & \rho_{P2}^{(W)} & \rho_{P3}^{(W)} & \dots & 1 \end{pmatrix},$$

where  $\rho_{pq}^{(W)}$  denotes the correlation coefficient of the diffusion term  $dW$  between the  $p$ -th and the  $q$ -th assets, and  $\rho_{pq}^{(W)} = \rho_{qp}^{(W)}$ . Then, we can write the correlation between  $Z^p$  and  $Z^q$  as:

$$\mathbb{E}[Z^p Z^q] = \rho_{pq}^{(W)}.$$

Similarly, the jump sizes  $J^p(t_i)$  are dependent normal random variables with mean  $\mu^p$ , variance  $\delta^p$  and a symmetric correlation matrix  $\Sigma_J$ :

$$\Sigma_J = \begin{pmatrix} 1 & \rho_{21}^{(J)} & \rho_{31}^{(J)} & \dots & \rho_{P1}^{(J)} \\ \rho_{21}^{(J)} & 1 & \rho_{32}^{(J)} & \dots & \rho_{P2}^{(J)} \\ \vdots & \vdots & \vdots & \vdots & \vdots \\ \rho_{P1}^{(J)} & \rho_{P2}^{(J)} & \rho_{P3}^{(J)} & \dots & 1 \end{pmatrix}, \quad (3.15)$$

where  $\rho_{pq}^{(J)}$  denotes the correlation coefficient of the jump size  $J$  for the  $p$ -th and the  $q$ -th assets. By Cholesky factorization (see Wilmott, 2006), we can easily simulate the correlated random variables  $Z^p(t_i)$  and  $J^p(t_i)$ . Eq (3.12) shows  $\Delta q^p(t_i)$  is equal the sum of two independent random numbers from two Poisson distributions with mean rates  $\lambda^p \Delta t$  and  $\lambda \Delta t$  respectively. Then, it is straightforward to simulate a number of sample paths according to Eq (3.14) for each assets.

Here we produce  $P$  path matrices  $S_{ij}^p$  for  $i = 1, \dots, N$  and  $j = 1, \dots, M$ , then follow the payoff function (3.13) to work out the exercise matrix  $X_{ij}$ . The discounted cashflow vector  $DC_j$  can be calculated by a similar algorithm in section 3.3.1 with

replacing Eq (3.10) and (3.11) with

$$DC_j = \sum_{m_1=0}^{\bar{J}_1} \sum_{m_2=0}^{\bar{J}_2} \cdots \sum_{m_p=0}^{\bar{J}_p} \cdots \sum_{m_P=0}^{\bar{J}_P} \left( \kappa(m_1, m_2, \dots, m_p, \dots, m_P) \right. \\ \times a_{m_1, m_2, \dots, m_p, \dots, m_P} T_{m_1}(S_{ij}^1) T_{m_2}(S_{ij}^2) \cdots T_{m_p}(S_{ij}^p) \cdots T_{m_P}(S_{ij}^P) \left. \right), \quad (3.16)$$

and

$$CV_j = \sum_{m_1=0}^{\bar{J}_1} \sum_{m_2=0}^{\bar{J}_2} \cdots \sum_{m_p=0}^{\bar{J}_p} \cdots \sum_{m_P=0}^{\bar{J}_P} \left( \kappa(m_1, m_2, \dots, m_p, \dots, m_P) \right. \\ \times a_{m_1, m_2, \dots, m_p, \dots, m_P} T_{m_1}(S_{ij}^1) T_{m_2}(S_{ij}^2) \cdots T_{m_p}(S_{ij}^p) \cdots T_{m_P}(S_{ij}^P) \left. \right), \quad (3.17)$$

where  $T_{m_p}$  is the  $m$ -th Chebyshev polynomial corresponding to the  $p$ -th underlying;  $\bar{J}_p$  is the highest order of the polynomials of the  $p$ -th underlying, generally chosen as  $\bar{J}_1 = \bar{J}_2 = \cdots = \bar{J}_P = \bar{J}$ ; the  $a_{m_1, m_2, \dots, m_P}$  are the coefficients to be least square approximated;  $\kappa$  is an indicator function, which is

$$\kappa(m_1, m_2, \dots, m_p, \dots, m_P) = \begin{cases} 1 & \text{if } \sum_{p=1}^{p=P} (m_p) \leq \bar{J}, \\ 0 & \text{if } \sum_{p=1}^{p=P} (m_p) > \bar{J}. \end{cases}$$

We use the trace function to eliminate unnecessary computations and save calculation time. As mentioned in Duck et al. (2005), the choice of  $\bar{J}$  and  $M$  is important to option pricing. If  $\bar{J}$  is big enough and  $M$  is sufficiently large, LSM will produce an accurate estimate for the price of a Bermudan option.

### 3.4.2 Numerical results

In this section, we study the impact of the highest order of Chebyshev polynomials  $\bar{J}$  and sample size  $M$  on pricing two dimensional Bermudan options via three examples with the different numbers of exercise opportunities. The parameters employed in the examples are shown in Table 3.4. Fig 3.7 provides the results from pricing Bermudan put options for varying  $\bar{J}$  and  $M$  when exercise times  $N = 2, 10$  and  $25$ , respectively. It is (theoretically) expected that the red plane should be on the top, having the most exercise times ( $N = 25$ ), followed by the green surface ( $N = 10$ ) and the blue surface ( $N = 2$ ). However, this cannot hold when those values of  $J$  and

Parameter	Value
$S^p(t_0)$	100
$K^p$	100
$r$	0.05
$\sigma^p$	0.15
$T$	1.0
$\rho_{21}^{(W)}$	0.2
$\rho_{21}^{(J)}$	0.2
$\lambda^p = \bar{\lambda}$	0.1
$\mu^p$	-0.9
$\delta^p$	0.45
$n$	100
$\Delta t$	$1/(N * n)$
$p$	1, 2

Table 3.4: This set of parameters is used to demonstrate the numerical approach of pricing a Bermudan put under two assets with jump diffusion.

$M$  are relatively small. It is clear that increasing  $J$  and  $M$  reduces the error of the estimated option prices, while it also increases the computing budget. From Fig 3.7, we find that the option price will tend to rise as  $J$  increases, whereas the option price will reduce as  $M$  rises. Considering a trade-off between accuracy and computational cost, we recommend that the optimal choice is  $J = 12$  and  $M = 70000$ . For those proper values of  $J$  and  $M$ , the difference between the prices given by  $N = 10$  and  $N = 25$  is slight, while the price for  $N = 2$  is much lower than both of them. Moreover, the estimated price for  $N = 10$  and  $N = 25$  is more sensitive to the choice of  $J$  and  $M$  than the price of  $N = 2$ , which suggests that we usually need to choose larger values of  $J$  and  $M$  when pricing a Bermudan option with more exercise times.

### 3.5 Pricing 1D Bermudan put option using the double-jump stochastic volatility (SVJJ) model

As noted in Section 3.4, Duffie et al. (2000) derive an affine jump-diffusion model. Based on the variance model studied by Heston (1993), a two-factor jump process is derived to price options when jumps occur in both the underlying and volatility. The occurrences of jumps are governed by a Poisson process with intensity  $\lambda dt$ ; for

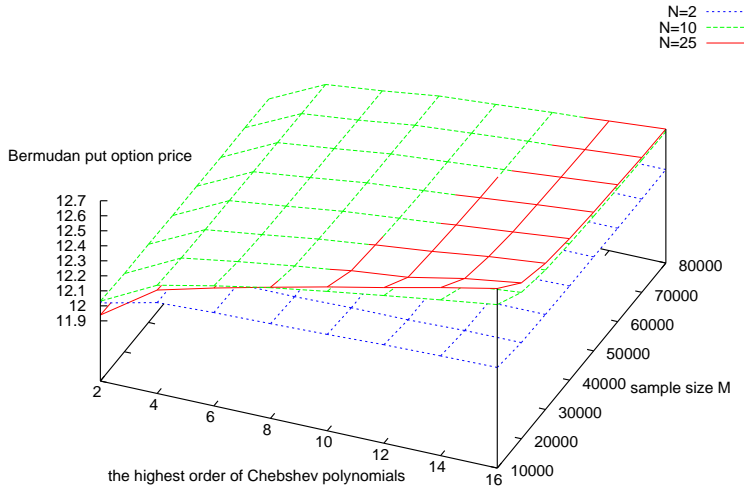


Figure 3.7: 2D-MJD: Bermudan put option prices depend on the highest order of Chebyshev polynomials  $\bar{J}$  and the sample size  $M$ . Every knot is obtained from 1000 runs.

the underlying asset, the jump sizes follow a normal distribution; for the volatility process, the jump sizes follow a positive exponential distribution. The model is referred to as SVJJ in Duffie et al. (2000), given by

$$dx = (r - \lambda\kappa_x - \frac{1}{2}v)dt + \sqrt{v}dW_x + J_x dq , \quad (3.18)$$

$$dv = \kappa_v(\theta_v - v)dt + \sigma_v\sqrt{v}dW_v + J_v dq , \quad (3.19)$$

where

$$dW_x dW_v = \rho_W dt ,$$

$$dq \sim Poisson(\lambda dt) ,$$

$$J_v \sim Exp(\mu_v) , \quad (3.20)$$

$$J_x \sim N(\mu_x + \rho_J J_v^*, \delta_x^2) , \quad (3.21)$$

$$\kappa_x = (\exp(\mu_x + \frac{1}{2}\delta_x^2) - 1)/(1 - \rho_J \mu_v) ,$$

where  $J_v^*$  is a realised volatility jump size. Note that the process of  $v$  is generated by a modified Cox, Ingersoll and Ross (1985) single-factor model (CIR), which is a mean-reverting square-root process with an extra jump term  $J_v dq$ . For a standard CIR model (no jump term), from the results of Feller (1951), it is possible to derive

the following condition that guarantees positive values of  $v$  in a continuous time case, which is:

$$2\kappa_v\theta_v > \sigma_v^2 \quad \text{with} \quad v(0) \geq 0 , \quad (3.22)$$

only for a one-dimensional model. However, the condition does not work in a discrete time case - see Higham and Mao (2005) and Xiao (2007). This implies that the value of  $v$  simulated by the modified CIR process (3.19) can be negative.

### 3.5.1 Implementation

The simulation for the SVJJ model is easily carried out, even with modelling of the additional process of variance  $v(t)$  on the asset. We can estimate the value of a Bermudan option using the algorithm introduced in Section 3.3.1 with the discrete form of Eq (3.23) and Eq (3.24) instead of Eq (3.9), which is:

$$\begin{aligned} x_j(t_{i+1}) &= x_j(t_i) + \left(r - \lambda\kappa_x - \frac{1}{2}v_j(t_i)\right)\Delta t + \sqrt{v_j(t_i)}Z_{x_j}(t_i)\sqrt{\Delta t} \\ &\quad + J_{x_j}(t_i)\xi , \end{aligned} \quad (3.23)$$

$$\begin{aligned} v_j(t_{i+1}) &= v_j(t_i) + \kappa_v(\theta_v - v_j(t_i))\Delta t + \sigma_v\sqrt{v_j(t_i)}\sqrt{\Delta t} \\ &\quad (\rho_W Z_{x_j}(t_i) + \sqrt{1 - \rho_W^2}\bar{Z}_{x_j}(t_i)) + J_{v_j}(t_i)\xi , \end{aligned} \quad (3.24)$$

where  $Z_{x_j}(t_i)$  and  $\bar{Z}_{x_j}(t_i)$  denote two independent standard normal random variables;  $\xi$  is the number of realized jumps and follows a Poisson distribution with mean  $\lambda\Delta t$ ; the jump sizes  $J_{v_j}(t_i)$  and  $J_{x_j}(t_i)$  are also random variables from the exponential (3.20) and normal distributions (3.21). As mentioned above, the formula (3.24) may produce unexpected negative values of  $v_j(t_{i+1})$ . If  $v_j(t_{i+1}) \leq 0$ , the formula fails to continue to calculate  $v_j(t_{i+2})$  due to the negative square root. Thus, we suggest discarding the  $j$ -th sample paths:  $x_j$  and  $v_j$ , and resimulating  $x_j$  and  $v_j$  from  $t_0$  until  $v_j(t_{i+1}) > 0$  for each time point  $t_{i+1}$ .

As long as one can gain the log prices  $x_j(t_i)$  by Eq (3.23) and Eq (3.24), the paths matrix  $S_{ij}$  is found by the transformation  $S_{ij} = \exp(x_j(t_i))$  and the exercise matrix  $X_{ij}$  of the option can be calculated. The remainder of the implementation is to perform the least squares regression, then average the estimated prices over  $M_{run}$

Parameter	Value
$S$	100
$K$	100
$r$	0.05
$T$	1.0
$\sigma_0(\sqrt{v_0})$	0.0870
$\kappa_v$	3.46
$\theta_v$	0.008
$\sigma_v$	0.14
$\rho_W$	-0.82
$\lambda$	0.47
$\mu_x$	-0.10
$\delta_x$	0.0001
$\mu_v$	0.0500
$\rho_J$	-0.38

Table 3.5: This set of parameters is used to demonstrate the numerical approach for pricing a Bermudan put on 1D SVJJ model, which is from Duffie et al. (2000)

times of independent runs, which is exactly the same as the descriptions of Step 3 and Step 5 in Section 3.3.1.

### 3.5.2 Pricing European options

Here, we present a numerical example to price European options by the method in Section 3.5.1. The parameters in the example are selected from Duffie et al. (2000) shown in Table 3.5. For the evaluation of European style options, the algorithm in Section 3.5.1 is directly applicable by setting the (only) exercise opportunity  $N = 1$ . Fig 3.8 provides results for the European options by Monte Carlo simulation compared with the exact prices from Lewis (2001). It is clear that the estimated prices converge to the exact value on increasing the total number of sample paths. This indicates that our algorithm works well in generating sample paths following Eq (3.23) and Eq (3.24).

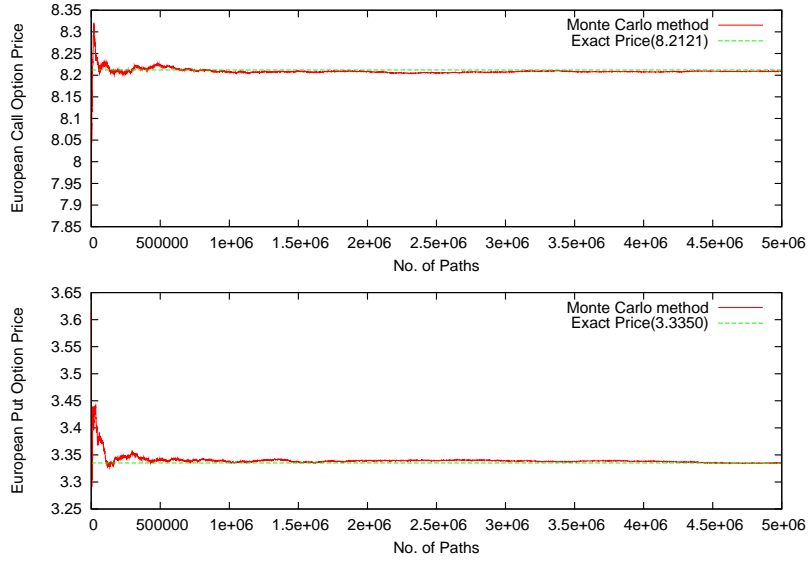


Figure 3.8: 1D-SVJJ: European call and put options pricing by Monte Carlo simulation using the parameters shown in Table 3.5. The x-axis refers to the number of paths which is determined by  $N^*$  in Section 3.3.1.

### 3.5.3 Exercise opportunities $N$ impact on pricing Bermudan options

Bermudan options allow the holder to exercise the options at specific times before the maturity date. Assuming there are a finite number of exercise opportunities  $N > 1$  over time  $[0, T]$ , we investigate the price impact of  $N$  in the SVJJ model. For

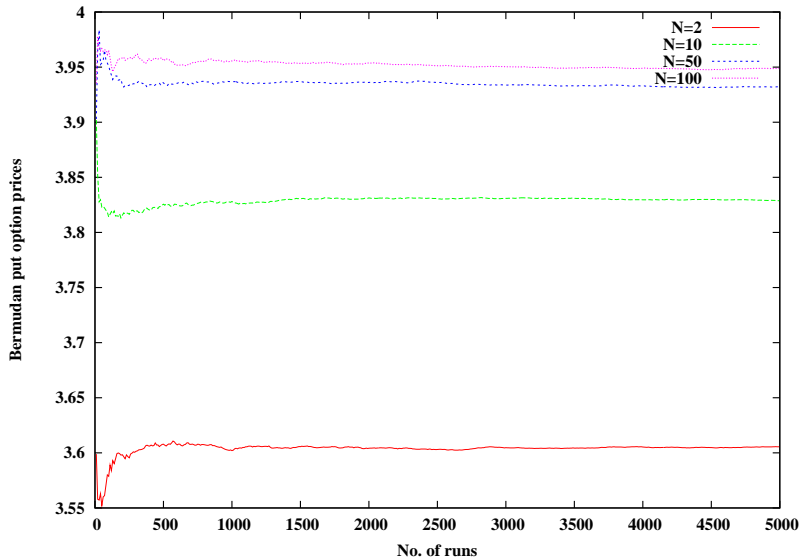


Figure 3.9: 1D-SVJJ: Bermudan put options pricing by Monte Carlo using the parameters shown in Table 3.5 and  $M = 2000$ ,  $\bar{J} = 6$

different exercise opportunities  $N$ , Fig 3.9 demonstrates the expected relationship for put option prices and  $N$ ; the more exercise opportunities, the more expensive the option. We find significant differences between the prices given by  $N = 2, 10$  and  $50$  (increased by 6.20% and 2.70% respectively) but a slight difference between  $N = 50$  and  $N = 100$  (increased by 0.42%). This implies that when  $N$  is large enough, the estimated price changes slightly and tends to a limit, which can be regarded as an estimate to an American option with infinite exercise opportunities.

### 3.5.4 Sensitivity of Bermudan options to the choice of numerical parameters

For pricing Bermudan options with early exercise, i.e.  $N > 1$ , we examine several numerical parameters affecting the option prices, which are the number of sample paths for least squares calculations  $M$ , the highest order of Chebyshev polynomials  $\bar{J}$  and the size of time steps  $\Delta t$ .

#### 1. Sample Size $M$ Impact on Option Price

As mentioned in Section 2.4, the convergence rate of standard Monte Carlo simulations is proportional to the square root of the number of sample paths employed in the least square algorithm, that is  $1/\sqrt{M}$  for each run in the LSM algorithm for pricing Bermudan options. Duck et al. (2005) find that the estimated option prices, which tend monotonically to the exact value as  $M$  increases, can be described by the following formula:

$$P_M = P_{exact} + \frac{\alpha_1}{\sqrt{M}} + \frac{\alpha_2}{M} + O(M^{-\frac{3}{2}}). \quad (3.25)$$

where the estimate  $P_{exact}$  is more accurate than  $P_M$  obtained from  $M$  sample paths and  $\alpha_1$  and  $\alpha_2$  are unknown parameters. Therefore, following the extrapolation technique proposed in Duck et al. (2005), we use three different sample sizes  $M$  to estimate  $\alpha_1$ ,  $\alpha_2$  and  $P_{exact}$ . Duck et al. (2005) and Xiao (2007) suggest that a better estimate  $P_{exact}$  can be efficiently yielded by  $M = 2000, 4000$  and  $8000$ , even on high-dimensional problems.

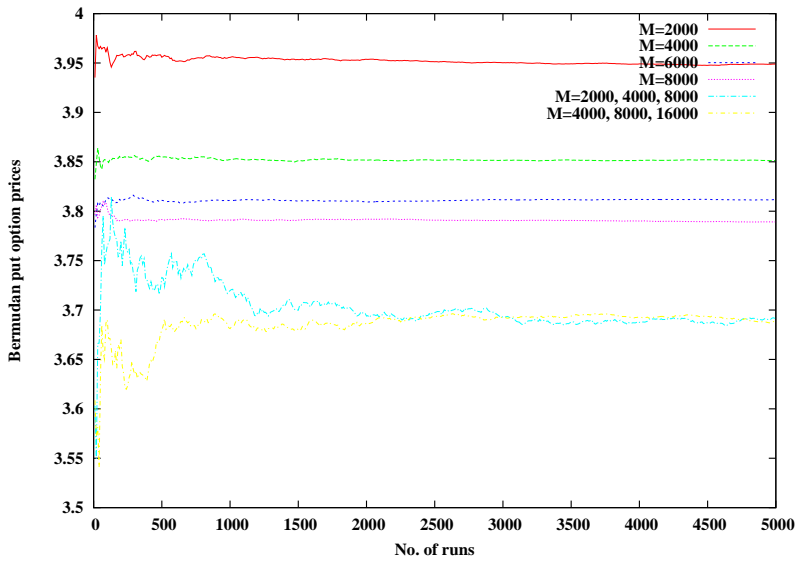


Figure 3.10: 1D-SVJJ: Bermudan put options pricing by Monte Carlo simulation using the parameters shown in Table 3.5 and  $N = 100$ ,  $\bar{J} = 6$ ,  $\Delta t = T/N$ .

In Fig 3.10, we illustrate the effects of extrapolation on option prices after 5000 runs. Without the extrapolation procedure, we find that the price of the Bermudan option generally reduces as  $M$  rises from 2000 to 8000 and the rate of the price changes tends to be small (reduced by 2.47%, 1.03% and 0.59% respectively). This implies that the option price converges to a limit which is lower than those estimates  $P_M$  and the limit can be obtained with sufficiently large  $M$ . Using the extrapolation procedure, we also gain two fluctuating lines for  $M = 2000, 4000, 8000$  and  $M = 4000, 8000, 16000$ . As anticipated, the prices vary considerably during the early runs because of the small sample sizes but tend to be consistent after sufficient runs. The extrapolated values are somewhat lower than the other estimates  $P_M$ , which are consistent with the limit suggested by  $P_M$ . Therefore, we can reasonably conclude that the extrapolation procedure is an efficient way to obtain an accurate estimate of the option price. Compared with two different settings of  $M$  for the extrapolation, the estimated prices are numerically equal so that  $M = 2000, 4000, 8000$  is a better choice for the extrapolation in the SVJJ model.

## 2. $\Delta t$ and $\bar{J}$ Impact on Option Prices

Moreover, to check the reliability of results by the method used above, we con-

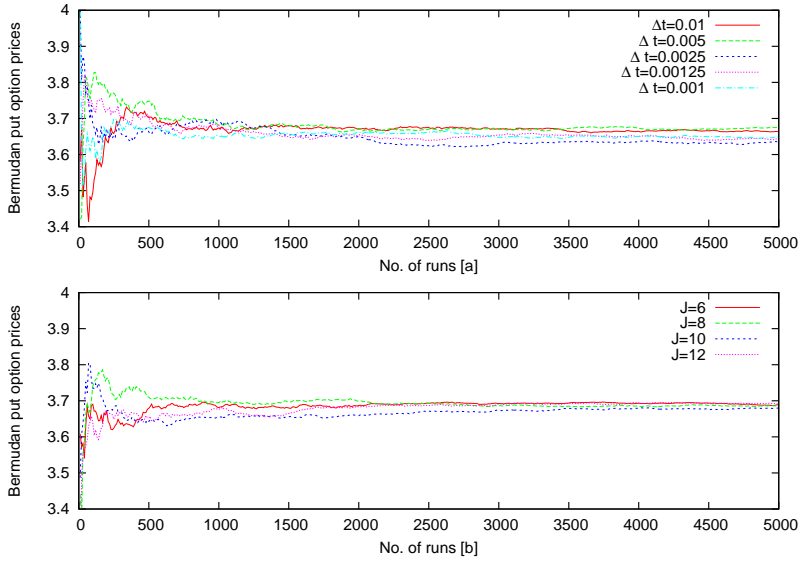


Figure 3.11: 1D-SVJJ: Bermudan put options pricing by Monte Carlo simulation using the parameters shown in Table 3.5 and  $N = 100$ , [a] using  $J = 6, M = 2000, 4000, 8000$  and [b] using  $\Delta t = T/N, M = 4000, 8000, 16000$

sider another two parameters, time steps  $\Delta t$  and the highest order of Chebyshev polynomials  $\bar{J}$  and show them in Fig 3.11. For pricing the Bermudan option with  $N = 100$  and  $T = 1$ , Fig 3.11 shows that the choice of  $\Delta t$  and  $\bar{J}$  has no significant impact on the option prices. Therefore the optimal parameter setting for the algorithm of pricing Bermudan option with the extrapolation technique is presented in Table 3.6.

Parameter	Value
$\Delta t$	0.01
$\bar{J}$	6
$M$	2000, 4000, 6000

Table 3.6: The optimal parameter setting is used in pricing a Bermudan put with the extrapolation procedure.

In Section 3.3, we recommend using  $\Delta t = T/N$  because for the 1D MJD model, SDE (3.1) has an analytic solution. Thus it can be exactly simulated, regardless of the choice of  $\Delta t$ . However, for the SVJJ model, the discretization error is introduced by the volatility process (3.24) if  $\Delta t$  is too large. Therefore, the accuracy of the estimated option price in the SVJJ model can be increased by reducing the value of  $\Delta t$ .

### 3.6 Pricing multi-dimensional Bermudan put option using the SVJJ model

Based on the discussions of Section 3.4 and Section 3.5, we consider an evaluation of a complex option under multiple assets following the SVJJ model. As described in Section 3.4, the times of jumps across assets are different over the same time horizon, while in Section 3.5 jumps are assumed to occur simultaneously in the processes of the asset price and its volatility. By combining Eq (3.12) with Eq (3.18) and Eq (3.19), the SVJJ model with multiple assets can be expressed in term of  $x_p = \log S_p$ , as follows:

$$dx_p = (r - \lambda_p \kappa_{x_p} - \frac{1}{2} v_p) dt + \sqrt{v_p} dW_{x_p} + J_{x_p} dq_p , \quad (3.26)$$

$$dv_p = \kappa_{v_p} (\theta_{v_p} - v_p) dt + \sigma_{v_p} \sqrt{v_p} dW_{v_p} + J_{v_p} dq_p , \quad (3.27)$$

where  $r$ ,  $\lambda_p$ ,  $\kappa_{v_p}$ ,  $\theta_{v_p}$  and  $\sigma_{v_p}$  are known constant for  $p = 1, \dots, P$ . The expectation of jump sizes in the asset prices  $\kappa_{x_p}$  is expressed as:

$$\kappa_{x_p} = (\exp(\mu_{x_p} + \frac{1}{2} \delta_{x_p}^2) - 1) / (1 - \rho_{x_p v_p}^{(J)} \mu_{v_p}) ,$$

with the correlation coefficient  $\rho_{x_p v_p}^{(J)}$  for jump sizes between  $x_p$  and  $v_p$ .

The correlated intensity of jump-arrivals is governed by two independent Poisson random variables:

$$\xi_p^* \sim Poisson(\lambda_p dt) , \quad (3.28)$$

$$\xi^* \sim Poisson(\bar{\lambda} dt) , \quad (3.29)$$

$$dq_p = \xi_p^* + \xi^* .$$

If  $dq_p = 0$ , then

$$J_{v_p} dq = 0 .$$

If  $dq_p \neq 0$ , then the magnitude of the jumps in the volatility process can be obtained from a gamma distribution (see Abramowitz and Stegun, 1972), which is

$$J_{v_p} dq_p \sim Gamma(dq_p, \mu_{v_p}) . \quad (3.30)$$

This is because for the integer  $dq_p$ , the gamma distribution represents the sum of  $dq_p$  independent exponentially distributed random variables with mean  $\mu_{v_p}$ .

We assume that  $J_{x_p}$  and  $J_{v_q}$  are independent random sizes of jumps, while  $J_{x_p}$  and  $J_{x_q}$  are correlated when  $p \neq q$ . Then, the jump sizes for the log-price process  $(J_{x_1}, \dots, J_{x_P})$  can be generated from multivariate normal distribution, which is

$$(J_1, \dots, J_P) \sim N(\bar{\mu}_{x_1}, \dots, \bar{\mu}_{x_P}; \delta_{x_1}^2, \dots, \delta_{x_P}^2; \Sigma_J), \quad (3.31)$$

where given a realised volatility jump size  $J_{v_p}^*$ , the mean  $\bar{\mu}_{x_p}$  can be estimated by

$$\bar{\mu}_{x_p} = \mu_{x_p} + \rho_{x_p v_p}^{(J)} J_{v_p}^*,$$

and  $\Sigma_J$  is a  $P \times P$  symmetric correlation matrix (3.15) in Section 3.4.

We also consider that the increments of Brownian motion are normally distributed as follows:

$$(dW_{x_1}, dW_{v_1}, \dots, dW_{x_P}, dW_{v_P}) \sim N(0; dt; \Sigma_W), \quad (3.32)$$

where 0 and  $dt$  stand for mean and variance respectively, and  $\Sigma_W$  is a  $2P \times 2P$  symmetric correlation matrix in the following form:

$$\sum_W = \begin{pmatrix} 1 & \rho_{x_1 v_1}^{(W)} & \rho_{x_1 x_2}^{(W)} & \rho_{x_1 v_2}^{(W)} & \cdots & \rho_{x_1 x_P}^{(W)} & \rho_{x_1 v_P}^{(W)} \\ \rho_{x_1 v_1}^{(W)} & 1 & \rho_{x_2 v_1}^{(W)} & \rho_{v_1 v_2}^{(W)} & \cdots & \rho_{x_P v_1}^{(W)} & \rho_{v_1 v_P}^{(W)} \\ \rho_{x_1 x_2}^{(W)} & \rho_{x_2 v_1}^{(W)} & 1 & \rho_{x_1 x_2}^{(W)} & \cdots & \rho_{x_2 x_P}^{(W)} & \rho_{x_2 v_P}^{(W)} \\ \rho_{x_1 v_2}^{(W)} & \rho_{v_1 v_2}^{(W)} & \rho_{x_2 v_2}^{(W)} & 1 & \cdots & \rho_{x_P v_2}^{(W)} & \rho_{v_2 v_P}^{(W)} \\ \vdots & \vdots & \vdots & \vdots & \vdots & \vdots & \vdots \\ \rho_{x_1 x_P}^{(W)} & \rho_{x_P v_1}^{(W)} & \rho_{x_2 x_P}^{(W)} & \rho_{x_P v_2}^{(W)} & \cdots & 1 & \rho_{x_P v_P}^{(W)} \\ \rho_{x_1 v_P}^{(W)} & \rho_{v_2 v_P}^{(W)} & \rho_{x_2 v_P}^{(W)} & \rho_{v_2 v_P}^{(W)} & \cdots & \rho_{x_P v_P}^{(W)} & 1 \end{pmatrix},$$

with  $\rho_{x_i v_j}^{(W)} = \rho_{x_i x_j}^{(W)} \rho_{x_j v_j}^{(W)}$  for  $i, j = 1, \dots, P$ .

### 3.6.1 Implementation

The implementation of pricing a multi-dimensional Bermudan option in the SVJJ model is similar to the way proposed in Section 3.4.1 with the additional processes of the volatilities. Let  $N$  be the number of possible exercise times during the option

life  $T$ , and  $V$  be the payoff function of the option. Therefore, following the procedure in Section 3.4.1, in the discrete-time framework with  $N$  time steps of equal size  $\Delta t = T/N$ , we derive the discrete form of Eq (3.27) and Eq (3.27) as follows:

$$\begin{aligned} x_j^p(t_{i+1}) &= x_j^p(t_i) + (r - \lambda^p \kappa_x^p - \frac{1}{2} v_j^p(t_i)) \Delta t + \sqrt{v_j^p(t_i)} Z_x^p(t_i) \sqrt{\Delta t} \\ &\quad + J_x^p(t_i) \xi^p(t_i), \end{aligned} \quad (3.33)$$

$$\begin{aligned} v_j^p(t_{i+1}) &= v_j^p(t_i) + \kappa_v^p (\theta_v^p - v_j^p(t_i)) \Delta t + \sigma_v^p \sqrt{v_j^p(t_i)} Z_v^p(t_i) \sqrt{\Delta t} \\ &\quad + J_v^p(t_i) \xi^p(t_i), \end{aligned} \quad (3.34)$$

for  $i = 0, \dots, N-1$  and  $j = 1, \dots, M$ . The number of realized jumps during the time interval  $[t_i, t_{i+1}]$  is  $\xi^p(t_i)$  in the  $p$ -th asset and volatility processes, which is estimated by the sum of two random numbers from the Poisson distributions (3.28) and (3.29); according to the expressions (3.30) and (3.31) we can evaluate the magnitudes of the jumps occurring in the interval:  $J_v^p(t_i) \xi^p(t_i)$  and  $J_x^p(t_i) \xi^p(t_i)$  respectively; the correlated random variables  $Z_x^p(t_i)$  and  $Z_v^p(t_i)$  for  $p = 1, \dots, P$  can also be modelled from a multivariate normal distribution (3.32). Therefore, the log-price process  $x(t_i)$  can be directly generated by Eq (3.34). Following the same algorithm as described in Section 3.4.1, the Bermudan option can be estimated by averaging the results obtained from  $M_{run}$  times of the LSM procedure.

### 3.6.2 Numerical results

In this section, we illustrate the algorithm in Section 3.6.1 by pricing a two-dimensional Bermudan option in the SVJJ model. The parameters used here are given by Table 3.7 and the payoff function of the option is  $V$ , which is

$$V = \max(K_1 - S_1, K_2 - S_2, 0).$$

#### 1. Exercise opportunities $N$ Impact on Option Price

We investigate how option prices change with respect to the number of exercise opportunities,  $N$ . Fig 3.12 shows that the option prices calculated by our algorithm with sample size  $M = 2000$  are convergent after a number of runs. From

Parameter	Value
$S^p(t_0)$	100
$K^p$	100
$r$	0.05
$T$	1.0
$\sigma_0^p = \sqrt{v_0^p}$	0.0870
$\kappa_v^p$	3.46
$\theta_v^p$	0.008
$\sigma_v^p$	0.14
$\lambda^p = \bar{\lambda}$	0.235
$\mu_x^p$	-0.10
$\delta_x^p$	0.0001
$\mu_v^p$	0.0500
$\rho_{xv}^{(J)}$	-0.38
$\rho_{xx}^{(J)}$	0.2
$\rho_{xx}^{(W)} = \rho_{vv}^{(W)}$	0.2
$\rho_{x_p v_p}^{(W)}$	-0.82
$p$	1, 2

Table 3.7: This set of parameters is used to demonstrate the numerical approach of pricing a Bermudan put on 2D SVJJ model

Fig 3.12, we can see that the Bermudan option ( $N \geq 2$ ) prices are significantly higher than the observed European option price ( $N = 1$ ). The Bermudan option becomes more expensive as  $N$  increases, whilst the increment of the option prices tends to be small when  $N$  is large enough, where an approximation for the corresponding American price is obtained.

## 2. Sample Size $M$ Impact on Option Price

Fig 3.13 provides the results of option prices for different sample sizes  $M$  without extrapolation and then shows the estimated price by the extrapolation procedure with the optimal parameters in Table 3.6. Similar to the results in Fig 3.10, the estimate of the put option value reduces as  $M$  increases. Compared with the raw method with a single value  $M$ , the extrapolated method ( $M = 2000, 4000, 8000$ ) produces the lowest price that is more variable during early runs, but is shown to be convergent as the number of runs increases, which implies that the extrapolation technique also performs well when solving a multi-dimensional problem to achieve an accurate estimate effectively.

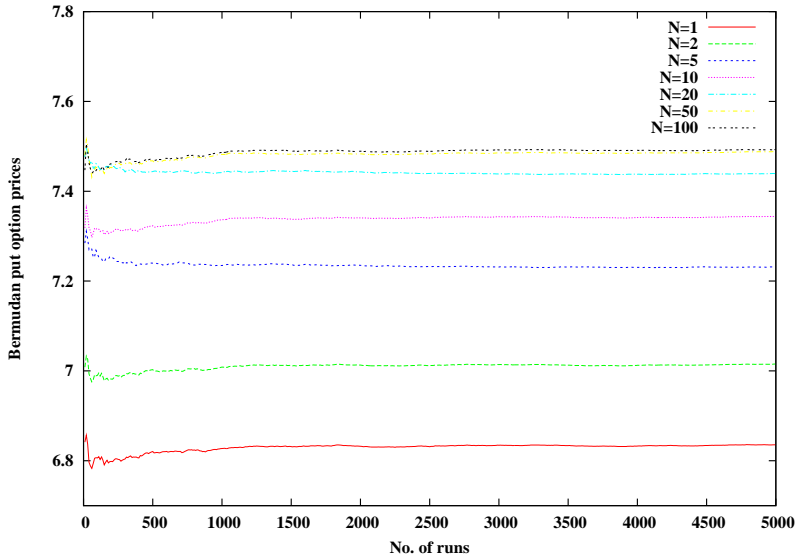


Figure 3.12: 2D-SVJJ: Pricing Bermudan put options on the two underlyings with respect to the number of exercise opportunities  $N$  using parameter list showed in Table 3.7,  $\bar{J} = 6$ ,  $\Delta t = 0.01$  and  $M = 2000$ .

### 3.7 Comparison of jump diffusion models

Jump diffusion models are considered as an approach to relax the Black-Scholes model. We have discussed different jump diffusion models in this chapter, which are derived from the fundamental Merton (1976) jump model. More specifically, we illustrate a LSM algorithm to price Bermudan options under the MJD model and the SVJJ model and extend it to a multi-dimensional problem to price Bermudan basket options. In this section, we compare different models in terms of option pricing under certain parameter settings as seen in Table 3.8. The parameters listed in Table 3.8 are based on those parameters used to price two-dimensional options in the SVJJ model in Section 3.6.2, and the values of the parameters for the other models are taken to make these models comparable in general. We choose the value for  $\sigma_0^p$  in the constant volatility models, such as the BS models and MJD models, equal to the value for the long-term level  $\theta_v^p$  in the stochastic volatility models, i.e. SVJJ models. Also the expectation of the intensity of jumps  $\lambda$  in one-dimensional models equals the sum of  $\lambda^p$  and  $\bar{\lambda}$  in two-dimensional models, that is,  $\lambda = \lambda^p + \bar{\lambda}$ .

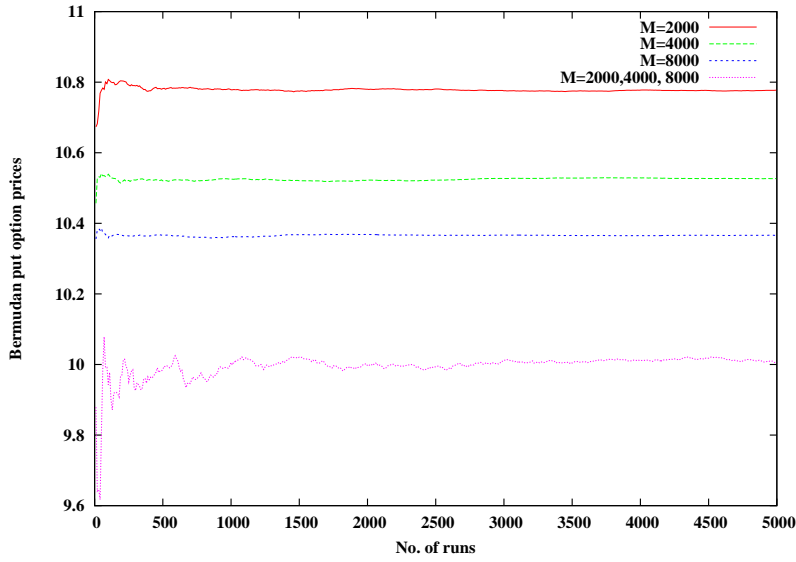


Figure 3.13: 2D-SVJJ: Bermudan put options pricing by Monte Carlo using parameter list showed in Table 3.7,  $J = 6$ , exercise opportunities  $N = 100$  and  $\Delta t = 0.01$ .

Parameter	1D-BS	1D-MJD	1D-SVJJ	2D-BS	2D-MJD	2D-SVJJ
$S^p(t_0)$	100	100	100	100	100	100
$K^p$	100	100	100	100	100	100
$r$	0.05	0.05	0.05	0.05	0.05	0.05
$T$	1.0	1.0	1.0	1.0	1.0	1.0
$\sigma_0^p = \sqrt{v_0^p}$	$\sqrt{0.008}$	$\sqrt{0.008}$	0.0870	$\sqrt{0.008}$	$\sqrt{0.008}$	0.0870
$\kappa_v^p$	n/a	n/a	3.46	n/a	n/a	3.46
$\theta_v^p$	n/a	n/a	0.008	n/a	n/a	0.008
$\sigma_v^p$	n/a	n/a	0.14	n/a	n/a	0.14
$\lambda (\lambda^p = \bar{\lambda})$	n/a	0.47	0.47	n/a	0.235	0.235
$\mu_x^p$	n/a	-0.10	-0.10	n/a	-0.10	-0.10
$\delta_x^p$	n/a	0.0001	0.0001	n/a	0.0001	0.0001
$\mu_v^p$	n/a	n/a	0.0500	n/a	n/a	0.0500
$\rho_{xv}^{(J)}$	n/a	n/a	-0.38	n/a	n/a	-0.38
$\rho_{xx}^{(J)}$	n/a	n/a	n/a	n/a	0.2	0.2
$\rho_{xx}^{(W)} = \rho_{vv}^{(W)}$	n/a	n/a	n/a	0.2	0.2	0.2
$\rho_{xv}^{(W)}$	n/a	n/a	-0.82	n/a	n/a	-0.82
$p$	1	1	1	1, 2	1, 2	1, 2

Table 3.8: Parameter setting for different jump models and Black-Scholes models, which are one-dimensional Black-Scholes model (1D-BS), one-dimensional Merton jump diffusion model (1D-MJD) and one-dimensional stochastic volatility jump diffusion model (1D-SVJJ), and their two-dimensional versions: 2D-BS, 2D-MJD, and 2D-SVJJ.

Table 3.9 shows the resulting prices of put options with and without extrapolation with respect to the number of exercise opportunities  $N$ . From Table 3.9, we

Model	$N$	$M^{ext}$	$M = 2000$	$M = 4000$	$M = 8000$
1D-BS	1	1.56989130836	1.57172972200	1.57156537756	1.57126211127
	2	1.83017513710	1.83464969367	1.83426412149	1.83352898324
	10	2.01329588241	2.04481473990	2.03542299443	2.02886207045
	50	2.06569368846	2.11020323982	2.08736672051	2.07611884962
	100	2.05948412345	2.12467582135	2.09925653993	2.08444493126
1D-MJD	1	2.41324307718	2.40023758711	2.39773717863	2.39912393701
	2	2.69694670509	2.70383435596	2.70047940248	2.69877589575
	10	2.94884600029	2.96990521753	2.95250901041	2.94582208699
	50	3.00476323316	3.05435747793	3.02230512143	3.00840395206
	100	3.00527852296	3.07017245759	3.03579333146	3.01916968461
1D-SVJJ	1	3.36058142049	3.35158677589	3.35260028812	3.35412742858
	2	3.60991595365	3.60668419642	3.59919491046	3.59811710844
	10	3.72388085676	3.83187905320	3.77823298342	3.75130654889
	50	3.65536581505	3.93120728964	3.84510310739	3.78687429867
	100	3.67918799555	3.95401450826	3.85309003471	3.79194048088
2D-BS	1	2.75862314578	2.74876260006	2.74931149457	2.75086921783
	2	3.07473929655	3.08897843215	3.07641938973	3.07173305375
	10	3.29338320608	3.39139104304	3.34660584631	3.32297761295
	50	3.33725977524	3.51448392431	3.43408620691	3.39148141871
	100	3.32371962082	3.53340717165	3.44758088882	3.39909765279
2D-MJD	1	5.03082461948	5.05202123532	5.05524692936	5.05281081995
	2	5.20520584521	5.25421502592	5.23346230660	5.22198704936
	10	5.32698175737	5.52402193573	5.44764046257	5.40296547549
	50	5.35169616022	5.63126355620	5.51746505624	5.45295491796
	100	5.34304283637	5.64071551573	5.52322462010	5.45529830428
2D-SVJJ	1	6.84287868988	6.83576925240	6.83958954113	6.84142190184
	2	6.92155965963	7.01529939522	6.98068726802	6.95979099533
	10	6.95980393695	7.34388227010	7.19910501027	7.11287368836
	50	6.86741732955	7.48826871869	7.27264749177	7.13706929262
	100	6.82807813448	7.49256206851	7.26917148315	7.12559435893

Table 3.9: comparison of put prices in different jump models. The results shown in the column  $M^{ext}$  are given by the simulation with the extrapolation scheme for  $M = 2000, 4000$  and  $8000$ . All the results are obtained after  $M_{run} = 5000$  runs.

can clearly see that the approximated option prices in two-dimensional models are generally significantly higher than the corresponding option prices estimated in one-dimensional models, because there are more chances to profit from holding a basket

put option with payoff  $u = \max(K_1 - S_1, K_2 - S_2, 0)$  than in holding a standard put options whose payoff is  $u = \max(K_1 - S_1, 0)$ . Both jump models: MJD and SVJJ produce higher prices than the standard Black-Scholes model prices. Compared with the MJD models, the SVJJ models produce higher option values due to a stochastic volatility process. With respect to  $N$ , there is an increase in the option price as the number of exercise opportunities arises in all the models, which is consistent with the results without extrapolation in Table 3.9.

As for the extrapolation method, in each jump model we find that the option prices evaluated by the extrapolation technique are lower than the corresponding prices generated without using extrapolation. When pricing Bermudan options with  $N > 1$ , there is an obvious advantage with the extrapolation method: the prices using extrapolation are more accurate than the prices given by the raw algorithm. This advantage increases as the number of exercise opportunities  $N$  increases.

# Chapter 4

## Feedback Models with Illiquidity

*Futures and options are the tail wagging the dog. They have also escalated the leverage and volatility of the markets to precipitous, unacceptable levels.*

– John Shad

*Wall Street Journal. 1988*

### 4.1 Background

As mentioned in Section 3.1, the simple Merton (1976) jump diffusion model seems not to fit the quoted option prices significantly better than the standard Black-Scholes model. In this chapter, we discuss another kind of model, concerning market liquidity, to relax the restrictive Black-Scholes assumptions in a different way.

In the past, most academic discussion concerning asset pricing models has been based on complete markets, with sufficient liquidity to allow the purchase or sale of any amount of the underlying asset at any time, without causing significant movement in the asset's price. The generalised asset pricing model described in the seminal paper by Black and Scholes (1973) may be expressed as,

$$dS = \mu(S, t)Sdt + \sigma(S, t)SdW , \quad (4.1)$$

where  $dW$  is a Wiener process,  $\mu(S, t)$  is the function of expected return and  $\sigma(S, t)$  is

the volatility function. In the original model, it is assumed that  $\mu$  and  $\sigma$  are constants in a risk-neutral world, and  $\mu$  is replaced by the risk-free rate,  $r$

$$dS = rSdt + \sigma SdW . \quad (4.2)$$

Through the application of Ito's lemma and a hedging argument, now studied in textbooks (e.g. see Hull, 2009; Wilmott et al., 1995) the Black-Scholes-Merton partial differential equation (PDE) is derived, from which, when boundary conditions have been applied, a huge range of financial options can be priced and upon which much of the literature on option pricing is based. For options maturing under one year on stocks or stock indices, this modelling approach has been successful as a first approximation in practical option pricing.

The assumptions of constant volatility and constant risk-free interest rate were both relaxed in favour of stochastic modelling in other strands of the literature. Constant volatility is known to be too restrictive an assumption, leading to the practical observation of “volatility smiles”. Similarly, constant interest rate becomes inappropriate for all but short-term options (perhaps under a year to maturity). However, a less well researched area by far is the assumptions of perfect elasticity for the supply and demand of underlying traded assets. Financial models which are based on the assumption that an investor trading a large number of assets cannot impact the price movement, may fail when market liquidity vanishes. The literature on illiquidity can roughly be divided into two approaches: (i) studies on price impact due to large traders, and (ii) studies on price impact due to immediacy provision by market makers. In the models falling into the first category, larger traders can move the price by their actions on pricing and hedging. Jarrow (1992) finds conditions on the economy consisting of a money market and a stock market that exclude market manipulation strategies. Jarrow (1994) develops the standard theory of pricing and hedging of derivative securities, with a feedback effect from the large trader's position. In a discrete-time framework, he denotes the impact of the large trader's activities on the price process via a reaction function, which is an exponential function with respect

to the large trader's share and option holdings. He demonstrates that market manipulation strategies exist using the derivative securities if there are no additional conditions on the price process. The conditions shown in his model are (i) there is a limit to the number of the total holdings imposed on the large trader's position, and (ii) the stock, money market fund, and derivative security markets have to be synchronous to prevent manipulation strategies. Jarrow's results have been extended to the continuous time framework by Frey (1996), Frey and Stremme (1997), Platen and Schweizer (1998) and Bank and Baum (2004). Frey (1996) focuses on the additional assumption in Jarrow (1994): the synchronous market condition to derive a full pricing theory in a finitely-elastic market. Moreover, he finds that the cost of hedging derivatives is influenced by the position held by larger traders. Frey and Stremme (1997) consider the feedback effects on market volatility and provide the tracking error, i.e. the discrepancy between the cost of the standard Black-Scholes hedging portfolio and the actual modelling value of a European call option. The tracking error is shown to be largest for ATM options, and to vanish for DITM and DOTM options. Frey and Patie (2002) present more details on the performance of different hedging strategies, and show that a optimal hedging portfolio is more accurate than the standard Black-Scholes hedge as the tracking error is relatively small. The feedback effect is also used to explain the 'smile pattern' and 'skewness pattern' of the implied volatility of the underlying assets in Platen and Schweizer (1998) and Frey and Patie (2002). Sircar and Papanicolaou (1998) derive a different nonlinear PDE that depends on the exogenous income process of the reference traders and the relative size of the program traders. Schonbucher and Wilmott (2000) analyze the influence of dynamic strategies on pricing, hedging and replication of an option in a general equilibrium model. Liu and Yong (2005) examine whether the put-call parity is satisfied in the modified PDE and deduce a special form of put-call parity due to the initial transaction costs considered. Rather than using the reaction function of the direct feedback effect in Jarrow (1994), Cuoco and Cvitanic (1998) and Cvitanic and Ma (1996) study a diffusion model for price dynamics by making the drift and volatility coefficient depend on the large traders' trading strategy.

The second approach involves the price impact due to provisions of immediacy by market makers, which is studied in Cetin, Jarrow and Protter (2004), Rogers and Singh (2006) and Cetin and Rogers (2006). These models capture the features of a short-term price impact of large traders using the equalisation of supply and demand in the short-term market, i.e. the price impact disappears instantaneously when there are no large volume trades. Bakstein and Howison (2003) adopt a similar approach to Rogers and Singh (2006), but the former study leads to feedback effects, which the latter study was trying to avoid. Another model in this category is the work of Cetin, Jarrow, Protter and Warachka (2006), who modelled the illiquidity cost as a stochastic supply curve with the underlying asset price depending on order flow.

The study presented in this thesis is based on the first approach to study the price impact, where the volume traded by ‘large traders’ cannot be absorbed by the market without price changes and there exists feedback effects from trading strategies. In particular, we illustrate the effects on pricing derivatives.

## 4.2 Modelling framework

We propose an asset pricing model in an illiquid market, which is also employed in Liu and Yong (2005) and Glover (2008). Rather than working on a modified PDE for pricing derivatives as used in these previous works, we focus on deriving a modified stochastic differential equation of the underlying asset. The asset model presented here is as follows:

$$dS = \mu S dt + \sigma S dW_S + \lambda S d\Phi , \quad (4.3)$$

where  $S$  is the underlying price,  $\mu$  and  $\sigma$  are the constant drift and volatility respectively and  $W_S$  is a standard Brownian motion.  $\Phi$  represents the number of shares held by a single ‘large trader’, which is a smooth, differentiable function of  $S$  and  $t$ . The ‘large trader’ can be interpreted as a market maker who can take arbitrarily large positions or a group of small traders who follow the same trading strategies.  $\lambda S$  can be interpreted as some function specifying how illiquid the market is, where  $\lambda$  is the illiquidity coefficient. The term  $\lambda S d\Phi$  is considered as the price impact made by the

trader when she follows some strategy in buying or selling the asset. Compared with the model used in Glover (2008), our model includes an extra ‘ $S$ ’ in the last term on the right of Eq (4.3) to model the impact of the market illiquidity as the market value of trading shares, rather than just the number of the shares. With the additional  $S$ , the amount of the trading shares  $d\Phi$  has been mapped to the corresponding impact on the share price movement. In addition, the quantity  $\frac{1}{\lambda S}$  is referred to as the ‘market depth’, which is the size of a order needed to cause one unit of asset price change in the market.

As  $\Phi(S, t)$  is smooth and differentiable, using Ito’s Lemma we obtain

$$d\Phi(S, t) = \Phi_t dt + \Phi_S dS + \frac{1}{2} \Phi_{SS} (dS)^2 .$$

Substituting this into Eq (4.3), we obtain, as  $dt \rightarrow 0$ ,

$$(1 - \lambda S \Phi_S) dS = (\mu S + \lambda S \Phi_t) dt + \sigma S dW_S + \frac{1}{2} \Phi_{SS} dS^2 ,$$

and so

$$dS = \frac{\mu S + \lambda S \Phi_t}{1 - \lambda S \Phi_S} dt + \frac{\sigma S}{1 - \lambda S \Phi_S} dW_S + \frac{1}{2} \frac{\Phi_{SS}}{1 - \lambda S \Phi_S} dS^2 . \quad (4.4)$$

Then squaring Eq (4.4) gives

$$dS^2 = \frac{\sigma^2 S^2}{(1 - \lambda S \Phi_S)^2} dt + o(dt) \quad (4.5)$$

as  $dt \rightarrow 0$ . Substituting Eq (4.5) into Eq (4.4), we arrive at an adjusted price model:

$$dS = \hat{\mu}(S, t) dt + \hat{\sigma}(S, t) dW_S , \quad (4.6)$$

where

$$\begin{aligned} \hat{\sigma}(S, t) &= \frac{\sigma S}{1 - \lambda S \Phi_S} , \\ \hat{\mu}(S, t) &= \frac{\mu S + \lambda S \Phi_t}{1 - \lambda S \Phi_S} + \frac{1}{2} \frac{\lambda \hat{\sigma}^2 S \Phi_{SS}}{1 - \lambda S \Phi_S} . \end{aligned} \quad (4.7)$$

In the case of delta hedging, we can identify the number of shares  $\Phi(S, t)$  to hedge a derivative  $V(S, t)$ . Note that the SDE (4.6) is different from the one shown in Glover (2008) due to involving  $S \Phi_S$  term instead of  $\Phi_S$ . Then, following a similar analysis in Glover (2008), we discuss two kinds of feedback models for different trading

strategies. First, we assume that the price taker who does not know the existence of the market illiquidity applies delta hedging as in the derivation of the standard Black-Scholes formula, i.e.  $\Delta = V_S^{BS}$  which has an analytical form:  $\Delta = N(d_1)$  for call options whilst  $\Delta = 1 - N(d_1)$  for put options<sup>1</sup>, where  $N(\cdot)$  is the standard normal distribution function. We call this case ‘first-order feedback’ which is used to model the price impact of the sub-optimal hedging strategy of the price taker. For more complicated cases, the hedging strategy taken by the market maker who realises the illiquidity impact on the underlying price follows the modified SDE (4.6), i.e.  $\Delta = V_S$  for which we need to appeal to numerical methods for solution. This case, called ‘full feedback’, is subject studied in Chapters 7 and 8. Therefore, under a risk-neutral measure, instead of Eq (4.6) one of many simple dynamic of the asset movement is given by

$$dS = rSdt + \frac{\sigma S}{1 - \lambda SV_{SS}^{BS}} dW_S , \quad (4.8)$$

in the case of the first-order feedback SDE, or for the full feedback SDE,

$$dS = rSdt + \frac{\sigma S}{1 - \lambda SV_{SS}} dW_S , \quad (4.9)$$

where  $r$  is the instantaneous risk-free interest rate. The second derivative of  $V$  with respect to  $S$  affects the modified volatility ( $V_{SS}^{BS}$  denotes the value of the ‘gamma’ in Black-Scholes model) together with the illiquidity coefficient  $\lambda$ . The case of  $\lambda = 0$  implies that the market is perfectly liquid and vanilla option prices can be calculated by the standard Black-Scholes formula. Rather than the non-linear PDE applied in Frey and Patie (2002), we have not put any constraints on the volatility term in Eq (4.8) and Eq (4.9), which might cause numerical problems when the volatility term tends to zero or infinity. To deal with these circumstances, we will include additional constraints on the simulation algorithm of specific models in later chapters.

In the following chapters, we will illustrate how to use the Monte Carlo method to simulate the path following the stochastic processes (4.8) and (4.9) and analyse the results of option pricing. Chapter 5 investigates the first-order feedback model (4.8) with a constant illiquidity  $\lambda$  while a stochastic illiquidity  $\lambda$  is studied in Chapter 6;

---

<sup>1</sup>where  $d_1$  is defined as  $\frac{\log(S/K)+(r+\frac{1}{2}\sigma^2)(T-t)}{\sigma\sqrt{T-t}}$ .

Chapters 7 and 8 consider the full feedback model (4.9) with constant  $\lambda$  and stochastic illiquidity  $\lambda$  respectively.

# Chapter 5

## First-Order Feedback Model with Constant Illiquidity

We start with the simplest model, which is first-order feedback with constant illiquidity  $\lambda$ . In such an illiquid market, a trader does realize that the market is illiquid but hedges his position as in an original Black-Scholes model. The price impact of his trade volume is related to  $V_{SS}^{BS}$  in a modified SDE. Recall the effective dynamic process (4.8) of the underlying using a risk-neutral measure:

$$dS = rSdt + \frac{\sigma S}{1 - \lambda SV_{SS}^{BS}} dW_S ,$$

and for pricing a European call option with a standard payoff function  $(S - K)^+$  at maturity,<sup>1</sup> the corresponding  $V_{SS}^{BS}$  (the Gamma) is derived from the Black-Scholes formula (for more details of the derivation, see Higham, 2004), which is

$$\begin{aligned} V_{SS}^{BS} &= \frac{e^{-\frac{1}{2}d_1^2}}{\sigma S \sqrt{2\pi(T-t)}} , \\ d_1 &= \frac{\log(S/K) + (r + \frac{1}{2}\sigma^2)(T-t)}{\sigma \sqrt{T-t}} , \end{aligned} \tag{5.1}$$

and we notice the same form of  $V_{SS}^{BS}$  given by a European put option. The modified volatility term in SDE (4.8) can capture the underlying price dynamics affected by the delta hedging of large investors who are assumed to trade the number of stocks  $V_S^{BS}$  raised from the standard Black-Scholes formula. We study in detail how the

---

<sup>1</sup>Denoted as  $\max(S - K, 0)$

modified volatility term has an impact on option pricing in Section 5.2, particularly for changes in the denominator of the volatility term.

The rest of the chapter is organised as follows: Section 5.1 introduces how to use Monte Carlo simulation to evaluate option prices under the stock process given by (4.8). Section 5.2 presents results we find using this model. In Section 5.3 we compare our model with that proposed in Glover (2008).

## 5.1 Implementation

In this section, we illustrate how to apply Monte Carlo simulation for pricing a European call option  $V(0)$  at time  $t = 0$ . The first step is to apply the Euler scheme to approximate the SDE (4.8) at discrete times  $t = 0, t_1, t_2, \dots, T$ . As the value of  $V_{SS}^{BS}(S, t_i)$  can be calculated in time, the underlying price  $S(T)$  at terminal time  $T$  is easily obtained. The payoff of a call option  $V(T)$  is estimated by the standard payoff function  $(S_T - K)^+$  and the value of the option  $V(0)$  at initial time  $t = 0$  is found by discounting the payment  $V(T)$  via the factor  $e^{-rT}$  with a constant risk-free interest rate  $r$ . The process has to be repeated to obtain a sufficient number of the  $V(0)$  values, and then we treat the average value of these  $V(0)$  as a reasonable estimator of the call price. The following algorithm describes the procedure in detail:

1. Divide the life of option  $[0, T]$  into  $N$  small time periods  $[t_i, t_{i+1}]$  with equal duration  $\Delta t$ , i.e.  $t_{i+1} = t_i + \Delta t$ , where  $i = 0, \dots, N - 1$  and  $t_0 = 0, t_N = T$ .
2. Generate  $M$  independent paths of the underlying price  $S_j(t_i)$  for  $j = 1, \dots, M$  by simple Euler discretization. The approximation of SDE (4.8) is given by

$$S_j(t_{i+1}) = S_j(t_i) + rS_j(t_i)\Delta t + \frac{\sigma S_j(t_i)}{1 - \lambda S_j(t_i)V_{SS}^{BS}(S_i, t_i)}(W_j(t_{i+1}) - W_j(t_i)) ,$$

for each path  $j$ . Because Brownian motion has independent normally distributed increments, the simulation of  $W_j(t_{i+1}) - W_j(t_i)$  is equal to a standard normal random variable  $Z_j(t_i)$  multiplied by the square root of the time increment  $\Delta t$ . Therefore the approximation described above can be rewritten

as:

$$S_j(t_{i+1}) = S_j(t_i) + rS_j(t_i)\Delta t + \frac{\sigma S_j(t_i)}{1 - \lambda S_j(t_i)V_{SS_j}^{BS}(S_i, t_i)} Z_j(t_i) \sqrt{\Delta t}. \quad (5.2)$$

Hence, for pricing the option by this algorithm, we need  $NM$  standard normal random numbers in total.

3. Estimate the value of  $V_{SS_j}^{BS}(t_i)$  at time  $t_i$  by the corresponding Black-Scholes formula for Greeks as follows:

$$V_{SS_j}^{BS}(S_i, t_i) = \frac{e^{-\frac{1}{2}d_1^2}}{\sigma S_j(t_i) \sqrt{2\pi(T - t_i)}}, \quad (5.3)$$

$$d_1 = \frac{\log(S_j(t_i)/K) + (r + \frac{1}{2}\sigma^2)(T - t_i)}{\sigma \sqrt{T - t_i}}.$$

Therefore, the process to estimate of the terminal price  $S_j(T)$  is quite straightforward.

- The formula (5.3) implies that the Gamma (i.e.  $V_{SS_j}^{BS}(S_i, t_i)$ ) increases for options being in-the-money and reaches a peak for at-the-money options, whilst the Gamma decreases for options being away from the money. The Gamma also increases as expiration approaches, and for a near-the-money option, the value  $V_{SS_j}^{BS}(S_i, t_i)$  becomes large close to expiry. For a discrete model, the maximum value

$$[V_{SS_j}^{BS}(S_i, t_i)]_{\max} = \frac{e^{(r+\sigma^2)\Delta t}}{\sigma K \sqrt{2\pi\Delta t}}$$

occurs when  $S_i = Ke^{-(r+\frac{3}{2}\sigma^2)\Delta t}$  and  $t_i = T - \Delta t$ . This suggests that an extremely large value of  $V_{SS_j}^{BS}(t_i)$  is possible during the period close to maturity  $T$ .

- Moreover, we find that for some values of  $V_{SS_j}^{BS}(S_i, t_i)$ , the denominator of the volatility term,  $1 - \lambda SV_{SS}^{BS}$  in SDE (4.8) can be close to zero, which leads to a high variance of the underlying. The affected underlying prices could jump down to a negative value or jump up to a high level. Either of these is undesirable, because negative stock prices cause arbitrage opportunities (and it also leads to problems in calculating  $d_1$  to simulate the

following price), while abnormally high underlying prices lead to an unrealistic price or an overpricing of call options. Compared with the jumps described in Chapter 3, the jumps we discuss here are caused by abrupt changes in the volatility term rather than those jumps modelled by the additional term of jump individually. Thus, different from those well controlled jumps, we need to take some measure to remove the paths affected by those abnormal jumps from the simulation.

To implement the algorithm, for each path  $j$ , the price  $S_j(t_i)$  has to be checked at each time point  $t_i$ . If the current price  $S_j(t_i)$  satisfies:

$$S_j(t_i) < 0 \quad \text{or} \quad S_j(t_i) > \bar{S} ,$$

where  $\bar{S}$  denotes the highest underlying price which can be accepted, then we interrupt to simulate the  $j$ -th path by setting the related option price  $V_j(0) = 0$ , then carry on the next simulation of the  $(j + 1)$ -th sample path. In addition, the total number of abandoned paths occurring in the algorithm will be referred to as  $m$  which is subtracted from the total number of samples  $M$  when we compute the average value of the option price. We call this procedure a price cap and floor scheme, and one of its applications in real markets is called as ‘circuit breakers’. This is a trading restriction to halt trading when the prices rise or fall too far, too soon, such as the May 6, 2010 ‘Flash Crash’ that the Dow Jones Industrial Average (DJIA) fell almost 1,000 points within a few minutes.

In Fig 5.4, we show that the results of option prices obtained from the algorithm without the capping scheme are problematic as the estimated prices are hard to converge as the number of sample paths increases.

4. Calculate the terminal payoff  $V_j(T)$  using  $(S_j(T) - K)^+$  and multiply the discount factor  $e^{-rT}$  to compute the discounted payoff  $V_j(0)$  at time 0 for  $j = 1, \dots, M$ .
5. Take the average of the discounted payoff on  $M - m$  live paths (those not

abandoned) as the estimator of the option price  $V(0)$ , i.e.

$$\bar{V}(0) = \frac{1}{M-m} \sum_{j=1}^M V_j(0).$$

We assume that the law of large number holds in the presence of caps and floors, which implies  $\bar{V}(0) \rightarrow V(0)$ .

Notice that the algorithm described above does not assume any particular type of financial derivative.

## 5.2 Numerical results

### 5.2.1 Denominator of the volatility term

As the Gammas,  $V_{SS}^{BS}$ , can be evaluated directly by the analytic form Eq (5.1), we are concerned with the value of the denominator of the volatility term in Eq (4.8), in particular  $SV_{SS}^{BS}$ . In Fig 5.1, the value of  $SV_{SS}^{BS}$  is plotted with respect to the varying spot price  $S$  and current time  $t$  with time-step  $\Delta t = 0.2$ . The value of Gamma  $V_{SS}^{BS}$

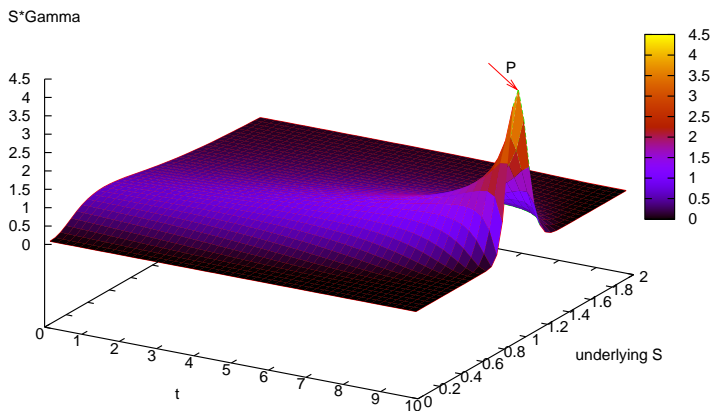


Figure 5.1: Value of  $SV_{SS}^{BS}$  with respect to  $S$  &  $t$ , assuming  $K = 1, r = 0.04, \sigma = 0.2, T = 10$  and  $\Delta t = 0.2$

is extremely small if the spot price  $S$  does not hit the strike price  $K$ , thus the value of Gamma multiplied the spot price  $S$  is still small. If  $S$  hits close to the strike price  $K$ , then the value of the product  $SV_{SS}^{BS}$  is close to the value of  $KV_{SS}^{BS}$ .

In the remaining section, we give a detailed discussion on the denominator of volatility term as follows:

- The value of  $SV_{SS}^{BS}$  is positive because for call and put options in the Black-Scholes model, the Gamma  $V_{SS}^{BS}$  is always positive.
- For any fixed time point  $t$ , when  $S \rightarrow Ke^{-(r+\frac{1}{2}\sigma^2)(T-t)}$ , the value of  $SV_{SS}^{BS}$  reaches a peak; otherwise, the value of  $SV_{SS}^{BS}$  decreases to zero. We can find the value of  $S$  where the Gamma takes on the maximum value by setting the first derivative

$$\frac{\partial}{\partial S}(SV_{SS}^{BS}) = -\frac{d_1 e^{-\frac{1}{2}d_1^2}}{SK\sigma^2(T-t)\sqrt{2\pi}} = 0,$$

which yields the maximum value at the point  $S = Ke^{-(r+\frac{1}{2}\sigma^2)(T-t)}$ :

$$[SV_{SS}^{BS}]_{\max} = \frac{1}{\sigma\sqrt{2\pi(T-t)}}.$$

- The maximum value  $[SV_{SS}^{BS}]_{\max}$  increases monotonically as  $t$  increases. There is a significant increase of the maximum function as  $t$  becomes close to  $T$ . Thus, the peak value of  $P$  shown in Fig 5.1 is equal to  $\frac{1}{\sigma\sqrt{2\pi\Delta t}}$  at position  $(Ke^{-(r+\frac{1}{2}\sigma^2)\Delta t}, T - \Delta t)$  and the size of the peak value is proportional to the inverse square root of  $\Delta t$ .
- As shown in Glover (2008), the denominator of the volatility term can vanish for pairs  $(S, t)$  that satisfy the following equation:

$$1 - \lambda SV_{SS}^{BS}(t, S) = 0, \quad (5.4)$$

using the Black-Scholes formula, this can be written:

$$1 - \frac{\lambda S}{\sigma S \sqrt{2\pi\tau}} \exp\left(-\frac{\left(\log(S/K) + (r + \frac{1}{2}\sigma^2)\tau\right)^2}{2\sigma^2\tau}\right) = 0,$$

where  $\tau = T - t$  presents time to expiry, thus  $S$  can be expressed in the explicit form of  $\tau$ :

$$S(\tau) = K \exp\left(-(r + \frac{1}{2}\sigma^2)\tau \pm \sigma\sqrt{\tau}\sqrt{2\log\lambda - \log(2\pi\sigma^2\tau)}\right), \quad (5.5)$$

in the range  $0 \leq \tau \leq \tau^*$ , for some  $\tau^*$ , which is

$$\tau^* = \frac{\lambda^2}{2\pi\sigma^2}, \quad (5.6)$$

whereas for  $\tau > \tau^*$  the denominator does not vanish.  $\tau^*$  is increasing in  $\lambda$  so that  $\tau^*$  would be larger than  $T$  for  $\lambda > \sqrt{2\pi\sigma^2 T}$ . In such a situation, the denominator can vanish at any time  $t \in [0, T]$ . Fig 5.2 illustrates the solution (5.5) for  $\lambda = 0.1, 0.5$  and  $1.0$  and shows the corresponding vanishing time range  $\tau \in [0, \tau^*]$ . There is a significant increase in the region as we expect and the denominator would vanish only if the underlying price  $S \rightarrow K$  as  $\tau \rightarrow 0$ .

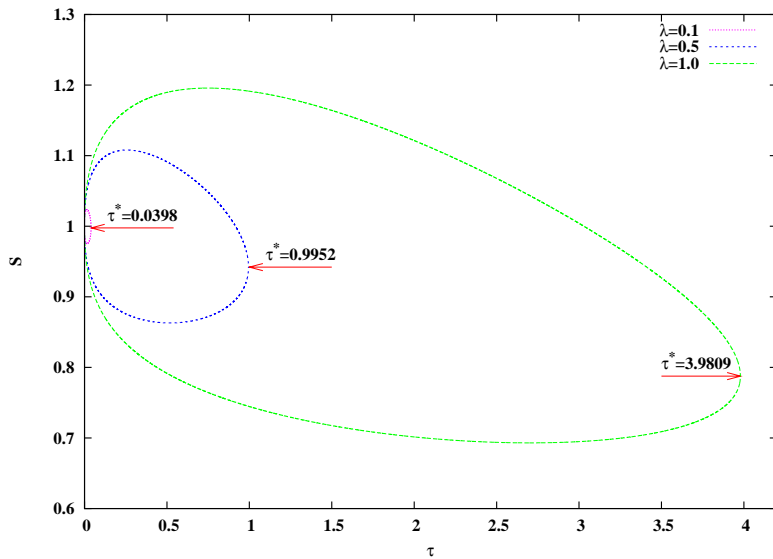


Figure 5.2: Location of  $(S, \tau)$  for Eq (5.5) to vanish the denominator with different  $\lambda$ , assuming  $K = 1, r = 0.04, \sigma = 0.2$

- The discussion above is based on the continuous-time framework, whereas we focus on a discrete-time model and explore in detail the impact of the vanishing of the denominator on simulation. In fact, there is a rare occurrence of zero denominator and a near zero denominator can be observed more frequently in the simulation, which is still of interest to us. As described in Section 5.1, the simulation for the underlying movement could produce negative prices. The reason for this is just because a small denominator caused by some pair of  $(S, \tau)$ , leads to a high variance of the underlying process. This implies that the time period when we encounter abandoned paths should be consistent with the

vanishing time range found in Fig 5.2. To illustrate this point, we undertake a similar analysis to the continuous-time model and record the abandoning region where there exist abandoned paths. The pair of  $(S, \tau)$  in the abandoning region satisfies the following inequality:

$$|1 - \lambda SV_{SS}^{BS}| \leq \varepsilon , \quad (5.7)$$

where  $\varepsilon$  denotes some small positive value. The absolute value taken here is because either a positive or negative small value of the denominator causes problematic simulated paths and renders the model invalid. If  $\varepsilon = 0$ , the inequality (5.7) reduces to the form of the equation (5.4) and the solution shown in Eq (5.5).  $\varepsilon$  also is a measure of how large the variance is. The inequality (5.7) can be easily solved leading to:

$$\bar{S}_{in}(\tau) \leq S(\tau) \leq \bar{S}_{out}(\tau) , \quad (5.8)$$

or

$$\underline{S}_{in}(\tau) \leq S(\tau) \leq \underline{S}_{out}(\tau) , \quad (5.9)$$

where

$$\bar{S}_{in}(\tau) = K \exp \left( -\left(r + \frac{1}{2}\sigma^2\right)\tau + \sigma\sqrt{\tau} \sqrt{2 \log \lambda - \log(2\pi\sigma^2\tau(1-\varepsilon)^2)} \right) , \quad (5.10)$$

$$\underline{S}_{in}(\tau) = K \exp \left( -\left(r + \frac{1}{2}\sigma^2\right)\tau - \sigma\sqrt{\tau} \sqrt{2 \log \lambda - \log(2\pi\sigma^2\tau(1-\varepsilon)^2)} \right) , \quad (5.11)$$

$$\bar{S}_{out}(\tau) = K \exp \left( -\left(r + \frac{1}{2}\sigma^2\right)\tau + \sigma\sqrt{\tau} \sqrt{2 \log \lambda - \log(2\pi\sigma^2\tau(1+\varepsilon)^2)} \right) , \quad (5.12)$$

$$\underline{S}_{out}(\tau) = K \exp \left( -\left(r + \frac{1}{2}\sigma^2\right)\tau - \sigma\sqrt{\tau} \sqrt{2 \log \lambda - \log(2\pi\sigma^2\tau(1+\varepsilon)^2)} \right) . \quad (5.13)$$

Then  $\bar{S}_{in}(\bar{S}_{out})$  and  $\underline{S}_{in}(\underline{S}_{out})$  refer to the boundaries of the upper and lower abandoning regions, and the subscripts ‘*in*’ and ‘*out*’ refer to the inner and outer bounds of the abandoning region. This means that the pairs of  $(S, \tau)$  that satisfy either (5.8) or (5.9) could result in abandoned paths, otherwise they cannot cause negative prices.

Analogously to (5.5), valid bounds (5.10)-(5.13) exist if and only if  $\tau \in [0, \tau_{out}^*]$  where  $\tau_{out}^* = \frac{\lambda^2}{2\pi\sigma^2(1-\varepsilon)^2}$ . Comparing with the vanishing time range  $\tau \in [0, \tau^*]$

where  $\tau^* = \frac{\lambda^2}{2\pi\sigma^2}$  in (5.6), the time period of abandoned paths  $[0, \tau_{out}^*]$  is somewhat wider than the vanishing time range because  $\tau_{out}^* > \tau^*$  for  $\varepsilon > 0$ .

It is important to set an appropriate level of  $\varepsilon$  to define an abandoning region. In a discrete-time stochastic underlying process  $S(t_i)$  with individual time  $t_i$ ,  $i = 0, \dots, N$ , we assume the negative price,  $S(t_{n+1}) < 0$ , is observed at some time  $t_{n+1}$ , which is  $S(t_i) \geq 0$  for any  $i \leq n$ . Then, by Euler's method,  $S(t_{n+1})$  can be estimated by the prior price  $S(t_n) > 0$  and the known parameters  $r$ ,  $\sigma$  and  $\Delta t$ :

$$S(t_{n+1}) = S(t_n) + rS(t_n)\Delta t \pm \frac{\sigma}{\varepsilon} S(t_n)\sqrt{\Delta t}Z < 0 ,$$

where  $Z$  is a standard normal random variable. Dividing both sides of the inequality by  $S(t_n)$  gives:

$$1 + r\Delta t \pm \frac{\sigma}{\varepsilon}\sqrt{\Delta t}Z < 0 , \quad (5.14)$$

then the inequality (5.14) would hold if

$$\varepsilon < \frac{\sigma|Z|}{\sqrt{1/\Delta t + r\sqrt{\Delta t}}} < \frac{\sigma|Z|_{\max}}{\sqrt{1/\Delta t + r\sqrt{\Delta t}}} , \quad (5.15)$$

where  $|Z|_{\max}$  is the maximum value of  $|Z|$ . The standard normal distribution ensures the probability of the random variable  $Z \leq 3.5$  is 99.977%, so we can take  $|Z|_{\max} = 3.5$  with 99% confidence as  $Z$  follows a continuous distribution. Notice that the range of  $\varepsilon$  given by the inequality (5.15) would lead to negative underlying prices; therefore, a proper value  $\varepsilon$  to prevent negative prices should be equal to  $\varepsilon^*$ , which is defined as:

$$\varepsilon^* = \frac{\sigma|Z|_{\max}}{\sqrt{1/\Delta t + r\sqrt{\Delta t}}} . \quad (5.16)$$

With  $\varepsilon = \varepsilon^*$ , the abandoning region for negative prices is determined by (5.8)-(5.9).

To investigate how this abandoning region works for negative prices, we generate  $10^6$  sample paths which start from the price  $S = 1$  at  $t_0 = 0$  and estimate the price changes at the following  $N = 2000$  discrete time points  $t_i = i \Delta t$ ,

$i = 0, \dots, N$  until maturity  $T = 10$  with the same other parameters used in Fig 5.2. At the same time, without any caps for large prices, we only abandon the paths that produce negative prices and record their location  $(S(\tau_i), \tau_i)$  with the time left  $\tau_i = T - t_i$ , then we count the number of abandoned paths at each  $\tau_i$  for  $i = 0, \dots, N$ . Then setting  $\varepsilon^* = 0.05$  estimated by Eq (5.16) implies the occurrence of abandoned paths if the instantaneous variance was higher than  $20\sigma$ . Fig 5.3 presents the results about the location and number of abandoned paths for  $\lambda = 0.1, 0.5$  and  $1.0$ . The abandoning region and the vanishing line (green lines), namely the lines shown in Fig 5.2, are also indicated in the right panel. The results from the left panel clearly suggest that abandoned paths due to negative prices occur during the period  $\tau \in [0, \tau^* + s]$  for some constant  $s$ , which is not just the vanishing time range  $[0, \tau^*]$  but also somewhat wider than this range. In fact,  $s = \varepsilon^*$  because the right panel of Fig 5.3 shows that all the scattered points  $(S(\tau_i), \tau_i)$  (red points) leading to negative prices are located within this estimated abandoning region between the inner and outer bounds (blue lines) for the three cases  $\lambda = 0.1, 0.5$  and  $1.0$ . Fig 5.3 also indicates that the abandoning region  $[0, \tau^* + \varepsilon^*]$ , i.e.  $[0, \tau_{out}^*]$ , is extended with a larger  $\lambda$ , which leads to more abandoned paths than what was found in the case of smaller  $\lambda$ . This is the reason why there is an increase in the total number of abandoned paths, which are 540 (0.054%), 7702 (0.770%) and 33366 (3.337%) for  $\lambda = 0.1, 0.5$  and  $1.0$  respectively, although the number of abandoned paths is a relatively small percentage of the total sample paths  $M = 10^6$ . For each  $\lambda$ , the cumulative number of abandoned paths reaches the peak when  $\tau$  approaches  $\tau^*$  and decreases rapidly towards both sides. This can be explained by the shape of the abandoning region which is widest around  $\tau^*$  and becomes narrow as  $\tau$  tends to zero. Moreover, the peak time is around  $\tau^*$  rather than  $\tau_{in}^*$  which is  $\frac{\lambda^2}{2\pi\sigma^2(1+\varepsilon)^2}$  because naturally the closer points are to the vanishing lines (green lines), the more likely they cause negative prices. Notice that Fig 5.3(a) are somewhat different from the others because the abandoning region for  $\lambda = 0.1$  is indeed small relative to  $\Delta t$ .

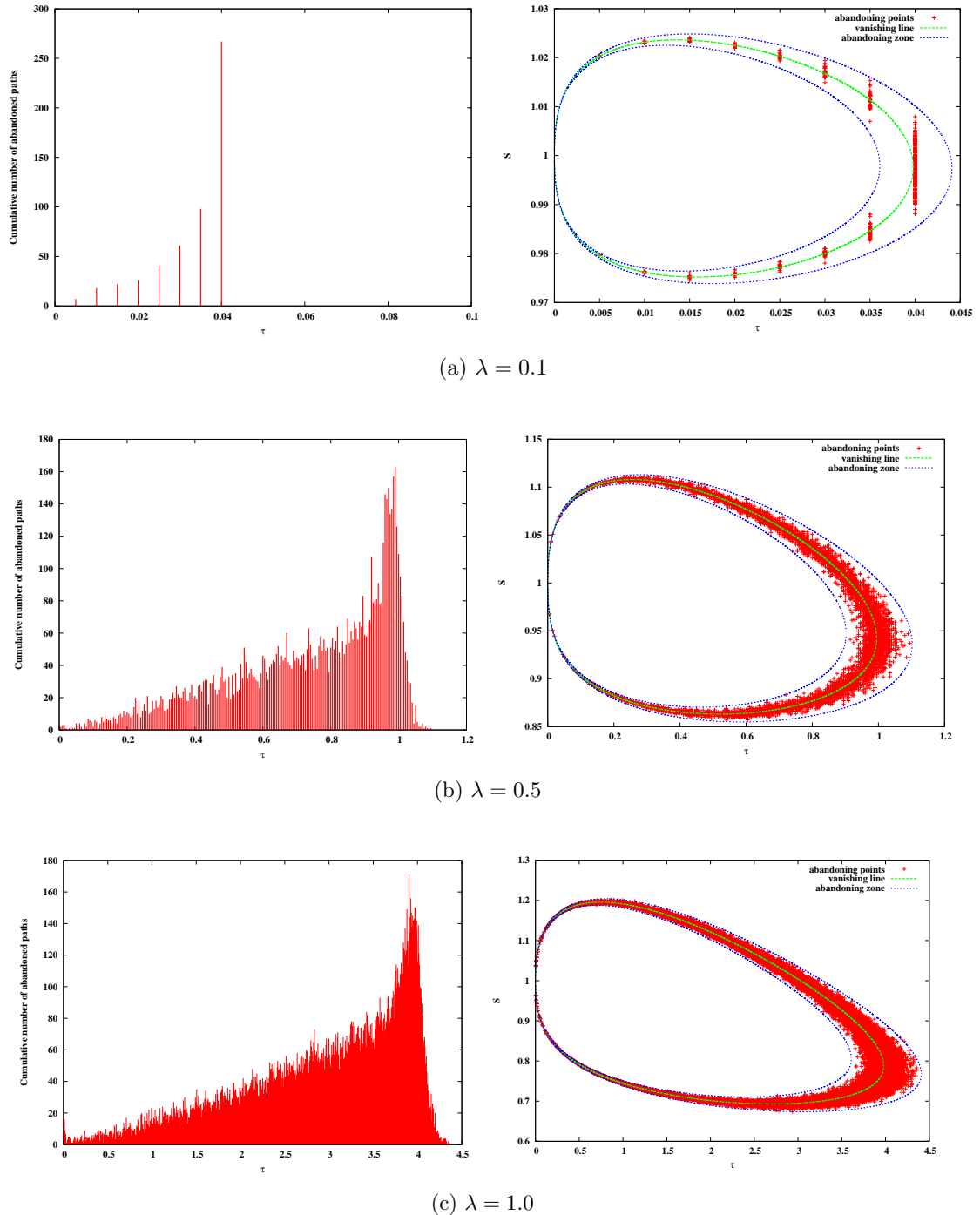


Figure 5.3: The cumulative number of abandoned paths caused by negative price with respect to time-to-expiry  $\tau$  & the corresponding location of negative prices, assuming  $S_0 = K = 1, r = 0.04, \sigma = 0.2, T = 10, N = 2000, dt = 0.005, M = 10^6$

### 5.2.2 Put-call parity

The put-call parity condition (henceforth, PCP) formalised by Stoll (1969) should hold in the first-order feedback model, i.e.

$$C + Ke^{-r\tau} = P + S , \quad (5.17)$$

where  $C$  denotes the call price;  $P$  the price of the put and  $S$  the current stock price. This can be illustrated using the linear PDE of a derivative portfolio  $V$  proposed in Glover (2008):

$$\frac{\partial V}{\partial \tau} + \frac{1}{2} \frac{\sigma^2 S^2}{(1 - \lambda SV_{SS}^{BS})^2} \frac{\partial^2 V}{\partial S^2} + rS \frac{\partial P}{\partial S} - rV = 0 . \quad (5.18)$$

Setting up a portfolio  $V = V_1$  such that  $V_1 = P + S - Ke^{-r\tau}$ , then the above PDE (5.18) yields:

$$\frac{\partial P}{\partial \tau} + \frac{1}{2} \frac{\sigma^2 S^2}{(1 - \lambda SP_{SS}^{BS})^2} \frac{\partial^2 P}{\partial S^2} + rS \frac{\partial P}{\partial S} - rP = 0 , \quad (5.19)$$

with the payoff of  $V_1$  at maturity:

$$V_1(\tau = 0) = \begin{cases} S - K & \text{if } S > K, \\ 0 & \text{otherwise,} \end{cases}$$

which is the same payoff as the call option. The PDE for the call option  $V_2 = C$  is:

$$\frac{\partial C}{\partial \tau} + \frac{1}{2} \frac{\sigma^2 S^2}{(1 - \lambda SC_{SS}^{BS})^2} \frac{\partial^2 C}{\partial S^2} + rS \frac{\partial C}{\partial S} - rC = 0 , \quad (5.20)$$

which shows  $V_1 = V_2$  as both of them have the same payoff function and satisfy the same form of PDE, i.e.

$$C = P + S - Ke^{-r\tau} .$$

However, following the implementation shown in Section 5.1, if we only discard the paths with negative prices, the PCP would still fail to hold in the first-order feedback model due to the existence of the paths with artificially high prices as discussed in Section 5.2.1. Similar to negative prices, high prices are also caused by small values of the denominator, where the denominator with the same sign as the standard normal random variable leads to a positive and significant jump in the underlying,

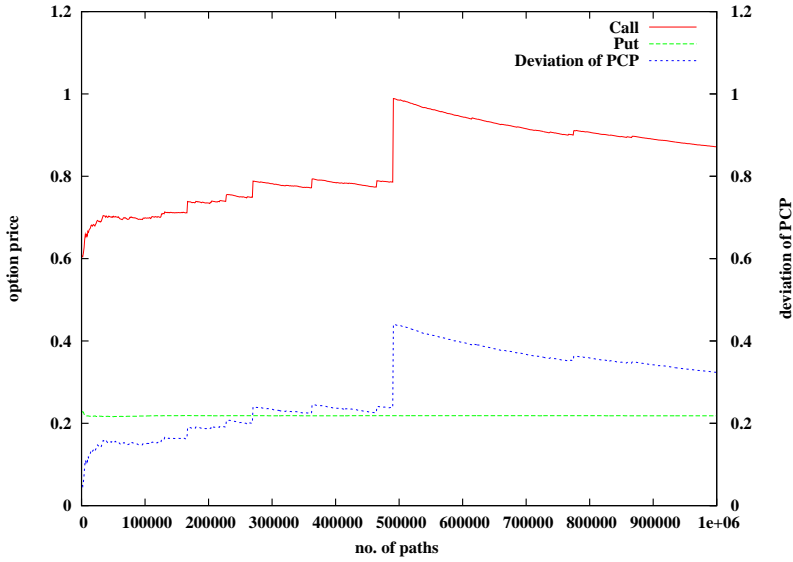


Figure 5.4: Pricing European options and examining the violation of PCP under the identical underlying price process with the following parameters:  $\lambda = 1$ ,  $S_0 = K = 1$ ,  $r = 0.04$ ,  $\sigma = 0.2$ ,  $T = 10$  and  $N = 2000$  after  $M = 10^6$

i.e. a sudden dramatic increase performed in the underlying price process. Fig 5.4 shows the numerical results for pricing a call/put option at  $t = 0$  with the identical underlying  $S_t$  in such a situation, and also indicates the corresponding deviation of PCP, which is estimated by  $\text{Dev} = C + Ke^{-rT} - P - S_0$ . The parameter setting is applied in this example as follows:  $\lambda = 1$ ,  $S_0 = K = 1$ ,  $r = 0.04$ ,  $\sigma = 0.2$ ,  $T = 10$ ,  $N = 2000$  and  $M = 10^6$ . As we study a simulation-based estimator, the error arising from a finite sample size will still have an impact on option pricing and a deviation of PCP. The law of big numbers ensures the error can be reduced asymptotically as the number of samples increases so that the option price tends to converge to the accurate reliable value and the deviation of PCP theoretically reduces. However, this trend clearly never happens to the call price in Fig 5.4 by simply increasing the number of paths, because there are some large fluctuations produced randomly for pricing the call option. However, for the put option, the price becomes stable as the number of paths increases. The reason for this phenomenon is that there are high underlying prices appearing randomly which affect, on average, the value of a call option, whereas they have relatively little impact on pricing a put option. The positive deviation of the PCP has a similar shape to the call price from the figure,

which reveals that the failure of PCP is mainly due to the over-priced call option obtained from the model.

Intuitively, the resolution we seek in order to make the PCP successful is to set a maximum threshold value of the underlying price in the first-order feedback model, which means that we need to abandon the paths whose prices exceed the maximum value besides those paths whose prices are negative. As mentioned in the algorithm in Section 5.1, the maximum value is called the cap of the underlying  $S(t)$ , written as  $\bar{S}$ , in the subsequent discussion. Notice  $\bar{S}$  can be made a function of time,  $t$ , rather than a constant, however we study with a constant cap  $\bar{S}$  over the whole option life  $T$  for simplicity. Once  $S(t) > \bar{S}$  through simulation of sample paths, we discard these paths and restart with a new simulation. After  $N$  simulations, only live paths are taken into account when calculating the value of the option. Fig 5.5 shows the impact of constant caps  $\bar{S}$  on pricing options compared with the situation without any caps by setting the same parameters shown in Fig 5.4. The corresponding results for the deviation of PCP are given in Fig 5.6. As anticipated, the estimated price tends

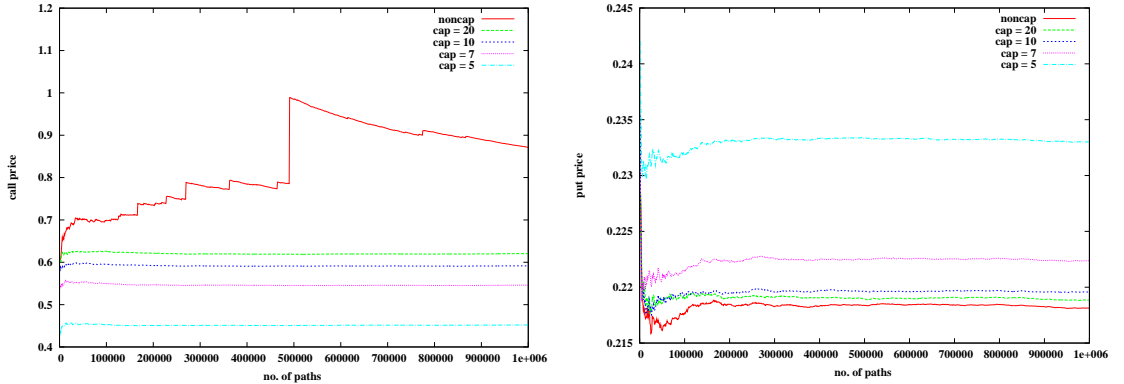


Figure 5.5: European option pricing depends on the number of samples paths with varying caps  $\bar{S}$  assumed parameters:  $\lambda = 1$ ,  $S_0 = K = 1$ ,  $r = 0.04$ ,  $\sigma = 0.2$ ,  $T = 10$  and  $N = 2000$  after  $M = 10^6$  runs. The left panel for a European call option and the right one for a European put option.

to converge to a limit by increasing the number of sample paths when pricing a call option by embedding a cap to protect the underlying price  $S(t)$  from the extremely high level, i.e.  $S(t) < \bar{S}$ , as shown in the left panel of Fig 5.5. It also suggests a decrease in  $\bar{S}$  would reduce the value of a call option but increase the value of a put option, as shown in the right panel of Fig 5.5. The small increase in the put

price is because the put option's payoffs taken from those paths with over-capped price <sup>2</sup> are zero, in general. Therefore, eliminating those paths leads to a modest increase in the expected value of the put option. As all of the caps employed here are able to help to produce a convergent option price, we have to judge the four restrictions,  $\bar{S} = 5, 7, 10$  and  $20$ , by examining their deviation from PCP, which is shown in Fig 5.6. By increasing the number of sample paths, the deviation of PCP

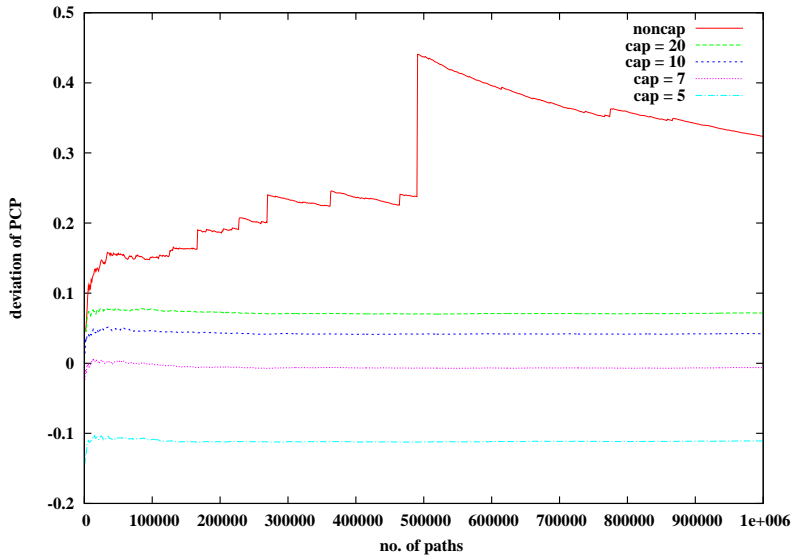


Figure 5.6: The violation of PCP depends on the number of samples paths with varying caps  $\bar{S}$  assumed parameters:  $\lambda = 1$ ,  $S_0 = K = 1$ ,  $r = 0.04$ ,  $\sigma = 0.2$ ,  $T = 10$  and  $N = 2000$  after  $M = 10^6$  runs.

given by the model with a cap apparently converges to some limit. The limits of the deviation given by the different caps are generally small, but these limits are still different and are positively related to  $\bar{S}$ . We notice the case of  $\bar{S} = 5$  has a negative value of the deviation and the magnitude of the deviation is even higher than the case of  $\bar{S} = 20$  because of underpricing the call and relatively overpricing the put. Therefore, a reliable cap should aim to give a small absolute deviation of PCP so that  $\bar{S} = 7$  where the deviation is closest to zero has been chosen as the proper cap subject to this specific parameter setting.

We employ a simple Euler scheme (5.2) in the simulation algorithm, leading to the usual discretization error  $O(1/\sqrt{N})$  on estimating the option prices which can be eliminated by taking a sufficient number of time steps (see details in Section 2.5).

<sup>2</sup>Denotes the prices over the value of the cap applied.

Table 5.1 shows the option values and deviation of PCP for various time-steps  $N$  (2000, 5000, 10000 and so on) for the two caps  $\bar{S} = 7$  and  $\bar{S} = 10$  considered before. From Fig 5.6 we see that  $\bar{S} = 7$  gives a slightly negative deviation of PCP and for  $\bar{S} = 10$  the deviation is relatively larger but positive. The results are estimated by  $10^6$  simulation trials under a similar set of parameters listed in Table 5.1. When

(a)  $\bar{S}=7$

$N$ time steps	European Call	European Put	Deviation of PCP	No. of abandoned paths
2000(-)	0.54572(-)	0.22242	-0.00638(-)	53548
5000(0.008)	0.53950(0.006)	0.22229	-0.01247(0.006)	49751
10000(0.012)	0.53472(0.011)	0.22269	-0.01765(0.011)	47160
50000(0.017)	0.52847(0.017)	0.22190	-0.02312(0.017)	43287
100000(0.019)	0.52758(0.018)	0.22194	-0.02404(0.018)	42268

(b)  $\bar{S}=10$

$N$ time steps	European Call	European Put	Deviation of PCP	No. of abandoned paths
2000(-)	0.59141(-)	0.21959	0.04214(-)	40423
5000(0.008)	0.58520(0.006)	0.21921	0.03631(0.006)	36631
10000(0.012)	0.58126(0.010)	0.21931	0.03227(0.010)	34335
50000(0.017)	0.57319(0.018)	0.21919	0.02432(0.018)	24013
100000(0.019)	0.57256(0.019)	0.21891	0.02397(0.018)	7137

Table 5.1: European option pricing and Deviation of PCP with respect to the number of time-steps  $N$  for (a)  $\bar{S} = 7$  & (b)  $\bar{S} = 10$ , assumed parameters:  $\lambda = 1$ ,  $S_0 = K = 1$ ,  $r = 0.04$ ,  $\sigma = 0.2$ ,  $T = 10$  and  $M = 10^6$ . The numbers in the parentheses of the first column are the discretization bias estimated by  $1/\sqrt{N} - 1/\sqrt{N_{2000}}$  where  $N_{2000} = 2000$  and others are the value differences from the one given by  $N = 2000$ .

the number of time steps  $N$  increases, for both caps, the call prices reduce more significantly than the put prices that seem to be stable. This suggests that the discretization error has an impact on the deviation from PCP as the estimated price of the call option can affect the deviation. As shown in parentheses, the changes of the deviation become less when  $N$  increases, which indicate that the deviation is reasonably convergent to a limit as  $N \rightarrow \infty$ . For  $\bar{S} = 7$ , the absolute deviation becomes larger as  $N$  increases. Conversely, for  $\bar{S} = 10$ , the absolute deviations are smoothly reduced by increasing  $N$  from 2000 to 100000. Then, when  $N = 100000$  in the table, the absolute deviation given by the cap  $\bar{S} = 10$  is smaller than that one given by  $\bar{S} = 7$ . For this example, a suitable cap to make the PCP successful is in

the range between 7 and 10 subject to the number of time steps  $N$  chosen. We also provide the number of abandoned paths with  $\bar{S} = 7$  and  $\bar{S} = 10$  in the last column of Table 5.1. It shows that the number of abandoned paths is decreasing as  $N$  increases. Compared with  $\bar{S} = 7$ ,  $\bar{S} = 10$  leads to less abandoned paths and its decrease is more rapid than  $\bar{S} = 7$ .

We previously noted that either over-capped prices or negative prices are triggered by a nearly zero denominator,  $\varepsilon = 1 - \lambda SV_{SS}^{BS} \rightarrow 0$ , where  $\varepsilon$  can be positive or negative, therefore the location  $(S, \tau)$  which has the potential for over-capping prices can be deduced by a similar analysis to that used to estimate the abandoning region with  $\varepsilon^*$  for negative prices (shown in Eq (5.16)). Consider a underlying price process  $S(t_i)$  generated at discrete time  $t_i = i\Delta t$ ,  $i = 0, \dots, N$  with equal time steps  $\Delta t$ . If  $S(t_{m+1}) > \bar{S}$  and  $S(t_i) \leq \bar{S}$  for any  $i \leq m$ , then the following inequalities must be satisfied:

$$\begin{aligned}\frac{Z_m}{\varepsilon} &> \frac{\bar{S}/S(t_m) - 1 - r\Delta t}{\sigma\sqrt{\Delta t}}, \\ \frac{Z_m}{\varepsilon} &> 0,\end{aligned}$$

where  $Z_m$  is a standard normal random variable to simulate  $S(t_{m+1})$ . The second inequality ensures the same signs of  $Z_m$  and  $\varepsilon$ , i.e.  $\frac{Z_m}{\varepsilon} = \frac{|Z_m|}{|\varepsilon|}$ , then the inequalities simply become:

$$\frac{|Z_m|}{|\varepsilon|} > \frac{\bar{S}/S(t_m) - 1 - r\Delta t}{\sigma\sqrt{\Delta t}}. \quad (5.21)$$

We will prove that if the inequality (5.21) holds, then

$$\varepsilon \rightarrow 0 \quad \text{or} \quad S(t_m) > \bar{S}/(1 + r\Delta t).$$

For any given value of  $S(t_m)$  such that  $0 < S(t_m) < \bar{S}/(1 + r\Delta t)$ , (5.21) can be written as:

$$|\varepsilon| < \frac{\sigma\sqrt{\Delta t}|Z_m|}{\bar{S}/S(t_m) - 1 - r\Delta t}, \quad (5.22)$$

which suffices to show that  $|\varepsilon| \rightarrow 0$  because the right hand of the inequality (5.22) tends to zero as the expectation value of  $|Z_m| \rightarrow 0$ ; otherwise, for any given value of  $S(t_m)$  such that  $\bar{S}/(1 + r\Delta t) < S(t_m) < \bar{S}$ , we derive an opposite inequality:

$$|\varepsilon| > \frac{\sigma\sqrt{\Delta t}|Z_m|}{\bar{S}/S(t_m) - 1 - r\Delta t}, \quad (5.23)$$

which always holds for any  $\varepsilon$  as the right hand of the inequality (5.23) is negative. Eq (5.22) implies, for  $0 < S(t_m) < \bar{S}/(1 + r\Delta t)$ , that over-capped prices can only be obtained when  $|\varepsilon| \rightarrow 0$ , which is exactly the same as the vanishing line mentioned in Section 5.2.1. Eq (5.23) suggests for  $\bar{S}/(1 + r\Delta t) < S(t_m) < \bar{S}$ , then  $S(t_m)$  is so close to the cap  $\bar{S}$  that any pair of  $(S(t_m), t_m)$  would cause the following price  $S(t_{m+1}) \geq \bar{S}$ . To confirm that the location of high prices corresponds to the region of vanishing denominator and the region where  $S(t_m)$  closes to  $\bar{S}$ , we show the location of high prices and negative prices in Fig 5.7 with  $\lambda = 1$ ,  $\bar{S} = 10$  and the other parameters listed in the figure. The left panel indicates that all of the region of

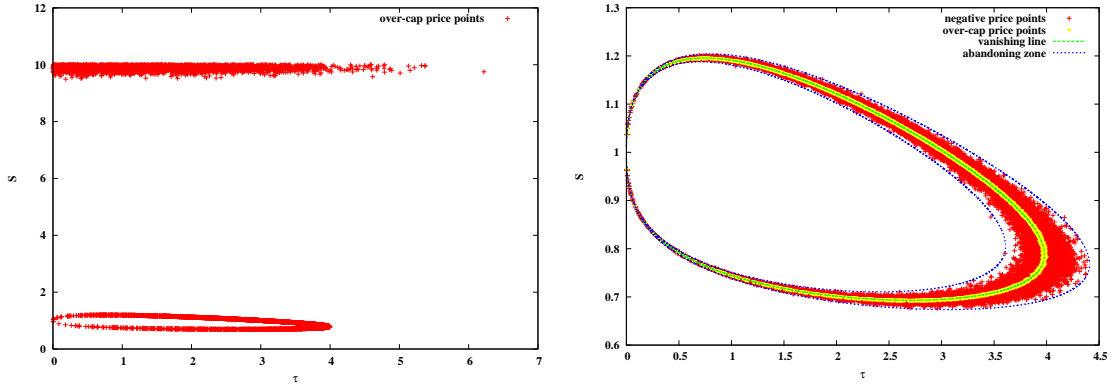


Figure 5.7: The number of abandoned paths with respect to time-to-expiry  $\tau$ , assuming  $S_0 = K = 1$ ,  $r = 0.04$ ,  $\sigma = 0.2$ ,  $T = 10$ ,  $N = 2000$ ,  $dt = 0.005$ ,  $M = 10^6$

the over-capped prices (red points) observed during the simulation, which is clearly divided into two regions: the upper region is close to the cap  $\bar{S} = 10$  and the bottom region is around the strike  $K = 1$ . The points in the upper region cause abandoned paths because  $S \approx \bar{S}$ , which is consistent with the condition  $S(t_m) > \bar{S}/(1+r\Delta t)$ . For the points in the enclosed region, we increase the scale in the right panel, which also provides the location of negative prices (red points), the estimated abandoning region for negative prices (between blue lines) and the vanishing region (green line). We find that the yellow points of the over-capped prices are uniformly and densely distributed throughout the green line of the vanishing region. This shows that the over-capped prices are actually caused by extremely small absolute values of  $\varepsilon$ . Therefore, the distribution of over-capped prices is much more concentrated around the vanishing line given by Eq (5.5), whilst the distribution of negative prices is nearly in the

entire abandoning regions. As shown in Fig 5.7, the abandoning zone covers all the negative prices and all the over-capped prices in the lower region, which implies that  $|\varepsilon| < \varepsilon^*$ . Moreover, in the total of 40427 abandoned paths found after simulating  $10^6$  sample paths, the number of the abandoned paths led by over-capped prices is only 6861 whilst the number of paths with negative prices is 33566, which shows the over-capped prices occur less frequently than the negative prices in the simulation.

### 5.2.3 Illiquidity $\lambda$ impact on pricing option

In this subsection, we focus on how the option prices are changed by the illiquidity  $\lambda$ . To be clear, we denote the volatility term, as follows:

$$\sigma_{tot}(\lambda) = \frac{\sigma}{1 - \lambda SV_{SS}^{BS}} .$$

It has a hyperbolic variation with  $\lambda$  with a singularity at  $\lambda = \frac{1}{SV_{SS}^{BS}}$ . Then the absolute value of  $\sigma_{tot}$  is monotonically increasing and always larger than  $\sigma$  in the region  $0 \leq \lambda < \frac{1}{SV_{SS}^{BS}}$  and monotonically decreasing in the region  $\lambda > \frac{1}{SV_{SS}^{BS}}$ , eventually becoming smaller than  $\sigma$ . It seems that the modified volatility  $\sigma_{tot}$  changes with the sign of the denominator: the volatility increases in  $\lambda$  for positive denominators and decreases in  $\lambda$  for negative denominators.<sup>3</sup> Recall the explicit form of the zero denominator (5.5):

$$S(\tau) = K \exp \left( - \left( r + \frac{1}{2}\sigma^2 \right) \tau \pm \sigma \sqrt{\tau} \sqrt{2 \log \lambda - \log(2\pi\sigma^2\tau)} \right) ,$$

subject to the restriction  $\tau \in (0, \tau^*)$ , where  $\tau^*$  is given by (5.6):

$$\tau^* = \frac{\lambda^2}{2\pi\sigma^2} ,$$

which suggests that the vanishing period  $(0, \tau^*)$  increases with the square of  $\lambda$  (shown in Fig 5.2). We find that negative denominators are given by those pairs  $(S, \tau)$  in the area enclosed by the curves (5.5) and the denominators remain positive for  $\tau \in (\tau^*, T]$ . Due to the two opposite effects of  $\lambda$  on option pricing, the length of the

---

<sup>3</sup>The negative denominator forces the stock price changes in the opposite direction of the change indicates by the Wiener process  $dW$ .

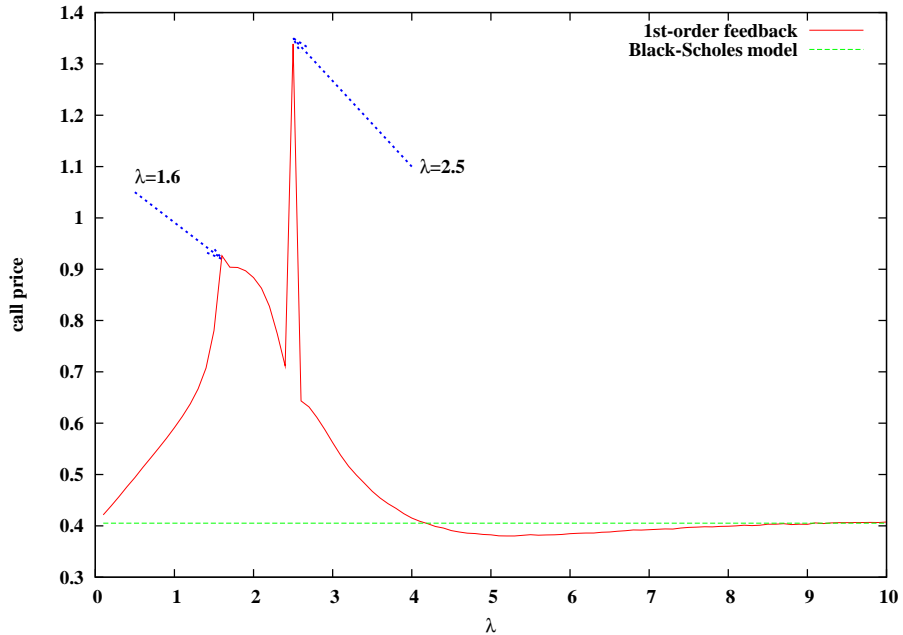
period  $(0, \tau^*)$  is important in deciding which effect dominates the price process: if the vanishing period is extended over half the maturity, we suggest that the negative relation between option prices and  $\lambda$  is stronger than the positive relation, otherwise, there is a stronger positive relation between them. Therefore, for  $\tau^* = T/2$ , let the particular value of  $\lambda$  be  $\lambda^*$ , which is:

$$\lambda^* = \sigma\sqrt{\pi T} . \quad (5.24)$$

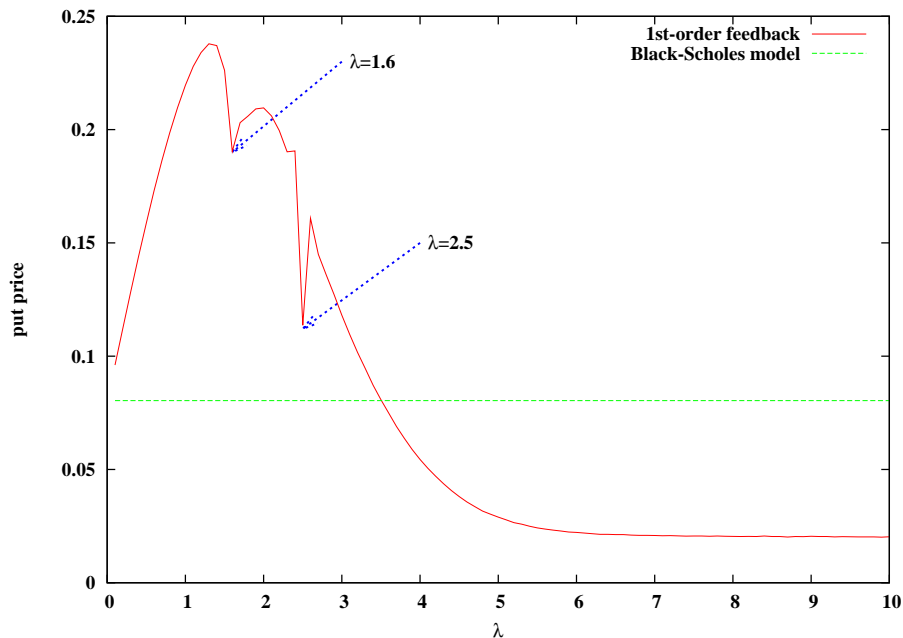
Using the similar parameters:  $S_0 = K = 1$ ,  $r = 0.04$ ,  $\sigma = 0.2$ ,  $T = 10$ ,  $N = 2000$  and  $M = 10^6$ , then  $\lambda^*$  is approximated as 1.121. There is another specific value of  $\lambda$ , denoted by  $\hat{\lambda}$ , which makes  $(S(\tau), \tau)$  lie in the vanishing circle when  $\tau = T$ . By Eq (5.5) with known  $S(\tau) = K = 1$  as  $\tau = T$ , such  $\hat{\lambda}$  can be expressed in an explicit form:

$$\hat{\lambda} = \sigma\sqrt{2\pi T} \exp\left(\frac{(r + \frac{1}{2}\sigma^2)^2 T}{2\sigma^2}\right) .$$

Fig 5.8 provides evidence of the impact of  $\lambda$  on pricing European call options in the upper panel and European put options in the bottom panel. The Black-Scholes prices for a perfect liquid market are also indicated by straight green lines in these figures for comparison. We set a cap  $\bar{S} = 10$  in order to avoid those paths with abnormally large underlying prices in this example and all the results presented in the figures are estimated by  $10^6$  sample paths. In Fig 5.9, we also provide average values of the volatility  $\sigma_{tot}$  with respect to each  $\lambda$  and the corresponding deviation of PCP. From Fig 5.8, we find clear evidence that  $\lambda$  has two opposite effects on option prices. Consistent with the estimator  $\lambda^* \approx 1.1$  suggested above, we notice in the range  $\lambda < 1.1$ , the option price is strictly increasing in  $\lambda$ , which is by implication larger than the corresponding price given by the Black-Scholes formula. However, for  $\lambda > 1.1$ , the option price is decreasing in  $\lambda$  in general, and eventually drops down below the Black-Scholes price. The price changes are consistent with the volatility in Fig 5.9(a), which shows the average volatility is increasing as  $\lambda$  and reaches a peak around  $\lambda^* = 1.1$ , whilst for  $\lambda > \lambda^*$  the volatility approximately tends to decrease with  $\lambda$  and would be even lower than the constant volatility value  $\sigma = 0.2$  for the Black-Scholes model when  $\lambda > 3$ . The reason for such a low volatility is because



(a) Call Option



(b) Put Option

Figure 5.8: Option prices with respect to the illiquidity  $\lambda$  for the parameter setting:  $\bar{S} = 10$ ,  $S = K = 1$ ,  $r = 0.04$ ,  $\sigma = 0.2$ ,  $T = 10$  and  $N = 2000$  after  $M = 10^6$ . The green lines presents the results for the Black-Schole model to compare with the first-order feedback model

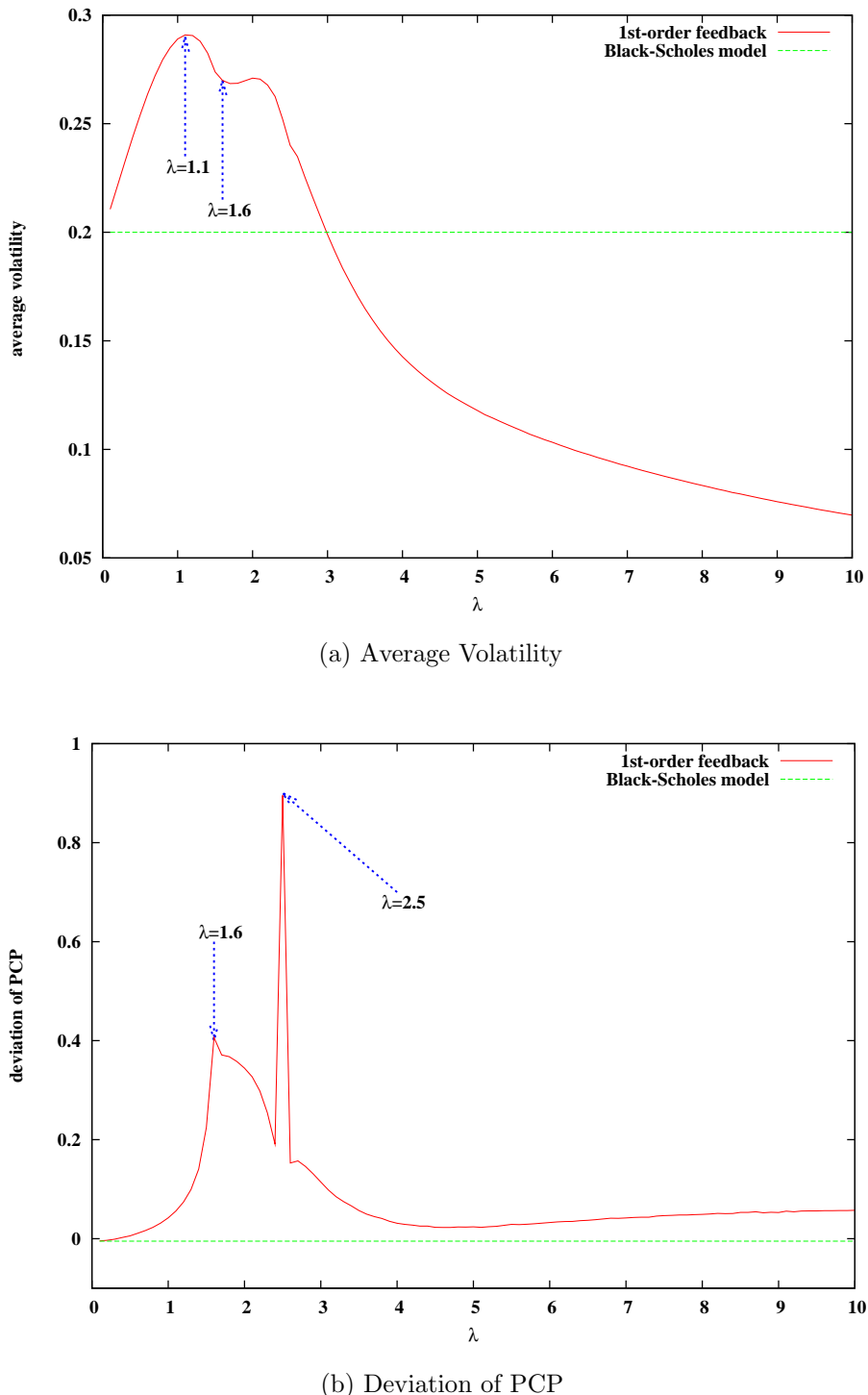


Figure 5.9: Average volatility & deviation of PCP with respect to the illiquidity  $\lambda$  using the same parameter setting as the previous Fig 5.8. The green lines presents the results for the Black-Schole model to compare with the first-order feedback model

the absolute value of the denominator of the volatility is larger than 1 when  $\lambda$  is sufficiently large. It is clear that the case of  $\lambda > 1.1$  is more complicated because we found kinks around  $\lambda = 1.6$  and  $\lambda = 2.5$ . At or near these kinks, the call price jumps up while the put price just falls slightly. The biggest positive jump occurs at  $\lambda = 2.5$  which is nearly equal to the value of  $\hat{\lambda}$ , mainly because the denominator  $1 - \lambda SV_{ss} \approx 0$  at the initial time  $t_0$ . Fig 5.10 reinforces this point by a comparison of  $\lambda = 1.0$  and  $\lambda = 2.5$ . In detail, we find the paths simulated by the first-order model

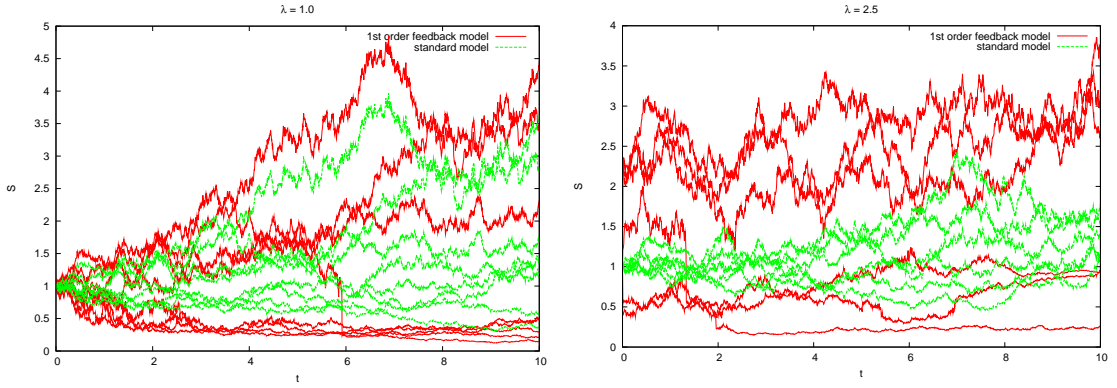


Figure 5.10: Random paths with illiquidity  $\lambda = 1.0$ ,  $\lambda = 2.5$  and  $\lambda = 0.0$ . The red paths stand for 1st order feedback model and the green paths for standard Black-Scholes model (i.e.  $\lambda = 0.0$ ). Use the same parameter setting as the previous Fig 5.8.

can fluctuate much more than the standard Black-Scholes model. For the particular case of  $\lambda = 2.5$ , the underlying prices  $S(t_1)$  become more volatile than the case of  $\lambda = 1$ , which causes the highest abandonment rate (around 47%) when  $\lambda = 2.5$ . As the restriction of the price:  $0 \leq S \leq 10$  with  $S(t_0) = 1$ , there is more opportunities for call options to earn money than put options. Furthermore, the deviation from PCP shown in Fig 5.9(b) has a similar shape to the call prices with two significant kinks occurring near  $\lambda = 1.6$  and  $\lambda = 2.5$ , which implies that the deviation from PCP is mainly determined by the estimate of the call option rather than the put option. We also provide the impact of  $\lambda$  on the deviation from PCP with different sizes of the cap:  $\bar{S} = 5, 7$  and  $10$  in Fig 5.11. This suggests the lower deviation is given by the lower cap, which is consistent with the findings in Section 5.2.2, so that using a suitable cap can ensure that the PCP is reasonably well satisfied for a given  $\lambda$ . However, the idea of using a constant cap to fix all cases with different  $\lambda$

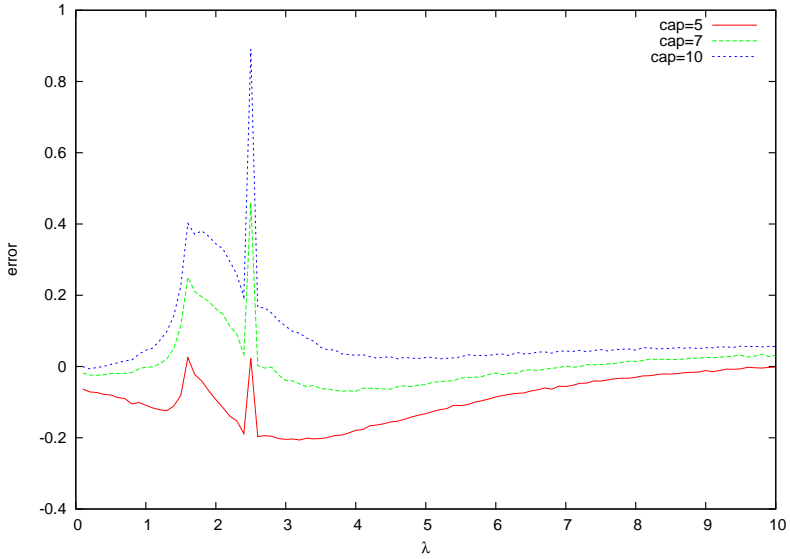


Figure 5.11: Error of put-call parity changes with respect to illiquidity  $\lambda$  in the cases of different caps  $\bar{S}$  with parameters:  $S = K = 1$ ,  $r = 0.04$ ,  $\sigma = 0.2$ ,  $T = 10$  and  $N = 2000$  after  $M = 10^5$

is unrealistic. The deviation curves still have a similar shape for different caps in Fig 5.11 with two kinks near  $\lambda = 1.6$  and  $\lambda = 2.5$ .

To sum up, in the first-order feedback model, the option will become more expensive when the market becomes more illiquid in a reasonable range  $\lambda \in [0, \lambda^*]$ , where there is a positive relation between  $\lambda$  and option prices. For  $\lambda > \lambda^*$ , the option prices will have a negative relation with  $\lambda$ , consequently, it will be cheaper than in a liquid market.

### 5.3 Comparison with Glover (2008) model

There is a slightly different SDE employed in Glover (2008), which is:

$$dS = rSdt + \frac{\sigma S}{1 - \lambda V_{SS}^{BS}} dW, \quad (5.25)$$

where  $\lambda$  is some constant. The difference arises because his model only captures the price impact of the trading volume, but we extend it to account for the price impact of the present market value of the trading. Therefore, we apply a similar scheme introduced in Section 5.1 to estimate option prices and check the deviation from PCP. The parameters have been used in Glover (2008):  $K = 1$ ,  $r = 0.04$ ,  $\sigma = 0.2$

and  $T = 1$  with different  $\lambda = 0, 0.09, 0.1, 1, 2, 5$  and  $10$ . The additional parameters for our simulation are set as:  $S = 1, N = 2000, M = 10^6$ . It is pointed out in Glover (2008) that there exists a vanishing denominator region, which has a similar form to Eq (5.5), namely:

$$S(\tau) = K \exp \left( -\left( r + \frac{3}{2}\sigma^2 \right)\tau \pm \sigma\sqrt{2\tau} \left[ (r + \sigma^2)\tau + \log \left( \frac{\lambda}{\sigma K \sqrt{2\pi\tau}} \right) \right]^{\frac{1}{2}} \right). \quad (5.26)$$

Notice that for a given  $\tau$ , we can gain two distinct values of  $S(\tau)$  unless  $\tau = 0$  or the following equation is satisfied:

$$(r + \sigma^2)\tau + \log \left( \frac{\lambda}{\sigma K \sqrt{2\pi\tau}} \right) = 0, \quad (5.27)$$

which gives a single value of  $S(\tau)$ . Let  $\tau = \tau^*$  be a solution to Eq (5.27), then the vanishing region is written as  $(0, \tau^*)$ , and for  $\tau > \tau^*$ , there is no chance to obtain vanishing denominators. However, we cannot explicitly solve for  $\tau^*$  from Eq (5.27), which is different from our model where  $\tau^*$  can be expressed by Eq (5.24). This implies that a finite value of  $\tau^*$  must be found in our model, but it might not exist in Glover (2008) model. If there is a solution  $\tau^*$  to Eq (5.27) and  $\tau^* \in \mathbb{R}$ , then  $\lambda$  must satisfy:

$$\lambda \leq \sigma K \sqrt{2\pi\tau}, \quad (5.28)$$

otherwise, the equation (5.27) cannot be solved, and for any  $\tau$ , there always exist two distinct values of  $S(\tau)$  given by Eq (5.26). Glover (2008) studies the period of close to maturity for relatively small  $\lambda$ , such as  $\lambda = 0.1$  and  $0.09$  under the parameter setting given above. The inequality (5.28) suggests that  $\lambda \leq 0.50\sqrt{\tau}$ . For maturity  $T = 1$ , if we need the length of the vanishing region  $\tau^*$  which is less than  $T$ , then

$$\lambda \leq \sigma K \sqrt{2\pi\tau} \leq \sigma K \sqrt{2\pi T} = 0.50. \quad (5.29)$$

Fig 5.12 shows the vanishing region with respect to  $\lambda$  in the range  $0.09$  to  $10$  for the Glover (2008) model and our model. We find that the region expands significantly as  $\lambda$  increases. For smaller values  $\lambda = 0.09$  and  $0.1$  that satisfy the condition (5.29),  $\tau^*$  is shown to be around  $0.03$  and  $0.04$  respectively in the two magnified figures, which suggests that the vanishing regions given by both models are limited and relatively

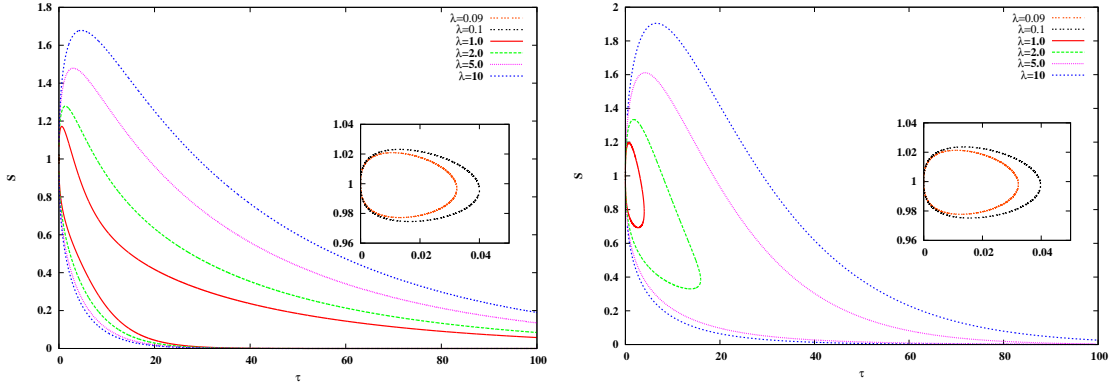


Figure 5.12: Comparison of Glover (2008) model (left hand) and our model (right hand): vanishing regions with respect to varying  $\lambda$  under the parameters:  $S = K = 1$ ,  $r = 0.04$ ,  $\sigma = 0.2$ ,  $T = 10$  and  $N = 2000$  after  $M = 10^6$

narrow. However, when  $\lambda$  increases to 1, the length of the regions become significantly different. In particular for  $\lambda = 1$ ,  $\tau^*$  given by our model is around 3.979, while  $\tau^*$  cannot be found in the range  $(0, 100)$  for the Glover (2008) model. This implies that choices of maturity  $T$  would significantly affect pricing option from these two models as they have such different  $\tau^*$ . In fact, in this setting of parameters,  $\tau^*$  does not exist for the Glover (2008). The reason for this is shown in the following proof:

Let  $f(\tau)$  be the left side of Eq (5.27), that is:

$$\begin{aligned} f(\tau) &= (r + \sigma^2)\tau + \log\left(\frac{\lambda}{\sigma K \sqrt{2\pi\tau}}\right), \\ &= (r + \sigma^2)\tau + \log\left(\frac{\lambda}{\sigma K \sqrt{2\pi}}\right) - \frac{1}{2}\log\tau, \end{aligned}$$

then, the first derivative and the second derivative can be obtained:

$$\begin{aligned} f'(\tau) &= (r + \sigma^2) - \frac{1}{2\tau}, \\ f''(\tau) &= \frac{1}{2\tau^2} > 0. \end{aligned}$$

The second derivative test:  $f''(\tau) > 0$  indicates that  $f(\tau)$  has a local minimum, which is

$$f(\tau)_{\min} = \log\lambda + \log\left(\frac{\sqrt{e(r + \sigma^2)}}{\sigma K \sqrt{\pi}}\right), \quad \text{when } \tau = \frac{1}{2(r + \sigma^2)}. \quad (5.30)$$

Then  $f(\tau)_{\min}$  increases monotonically with increase in  $\lambda$ . To ensure that there exists at least one value of  $\tau$  to satisfy Eq (5.27), it requires that

$$f(\tau)_{\min} \leq 0,$$

which means

$$\lambda \leq \frac{\sigma K \sqrt{\pi}}{\sqrt{e(r + \sigma^2)}} .$$

Under the parameters used in Fig 5.12, the range of  $\lambda$  is estimated to be  $\lambda \leq 0.760$ . This is clear that  $\lambda = 1$  is beyond the range, therefore, there is no solution  $\tau$  (i.e.  $\tau^*$ ) to Eq (5.28) in this case.

To compare both models easily, we focus on analysing the changes of put options, rather than call options which are more problematic due to the dependency on the sizes of caps. In Fig 5.13, there are two different maturities  $T = 1$  (top panels) and

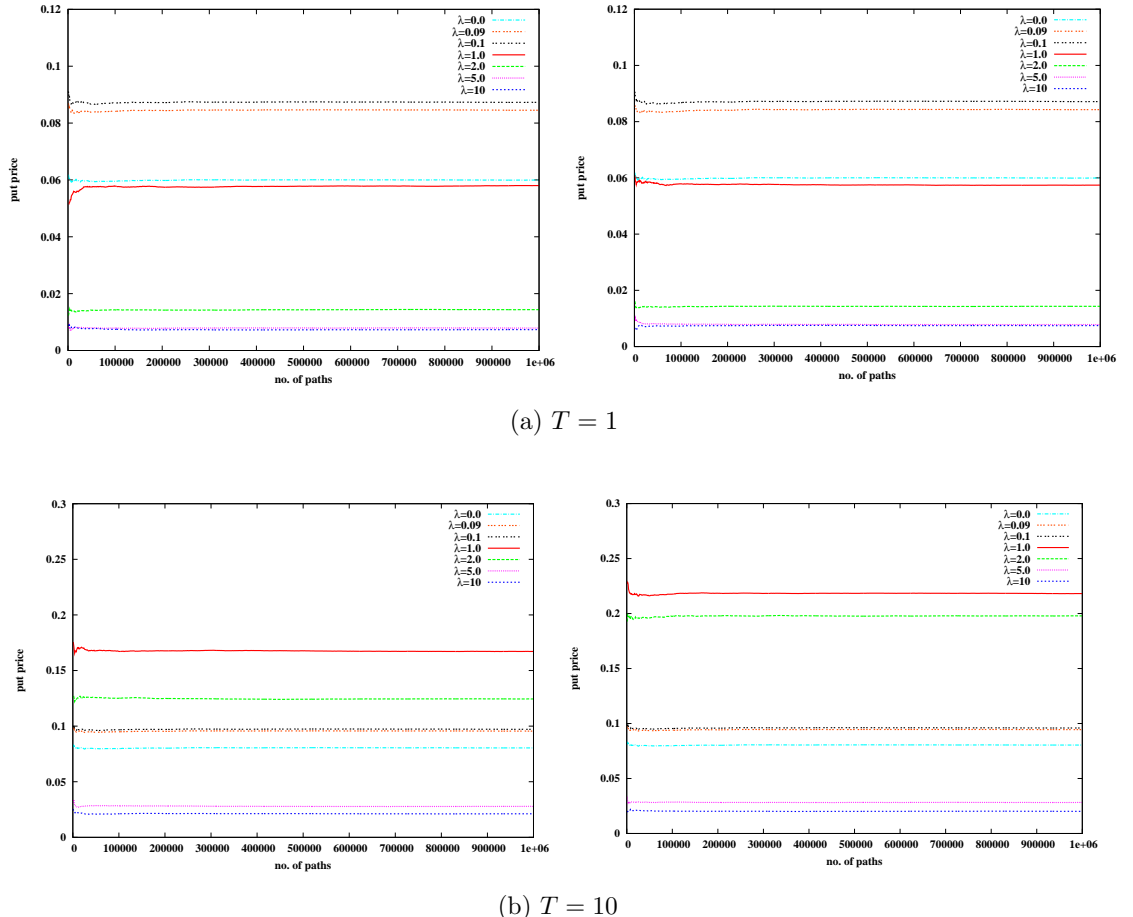


Figure 5.13: Comparison of Glover (2008) model (left hand) and our model (right hand): put prices for  $T = 1$  (a) and  $T = 10$  (b) with respect to varying  $\lambda$  under the parameters:  $S = K = 1$ ,  $r = 0.04$ ,  $\sigma = 0.2$ ,  $T = 10$  and  $N = 2000$  after  $M = 10^6$

$T = 10$  (bottom panels) employed to estimate put prices. In the case of the maturity

$T = 1$ , both models have a similar value of  $\tau^* < T$  for smaller values of  $\lambda$  (0.09 and 0.1) whilst for larger values of  $\lambda$  (1, 2, 5 and 10),  $T$  is clearly shorter than  $\tau^*$  for both models so that they have a similar impact of  $\tau^*$ . Therefore, we find that the option prices shown in the top panels are very close to each other. Except for the choices  $\lambda = 0.09$  and 0.1, the other prices for  $T = 1$  are lower than the corresponding Black-Scholes prices and apparently reduced monotonically as  $\lambda$  increases, which is also shown in Glover (2008). Thus, it is natural to consider that for both models the put price first increases for relatively small  $\lambda$  then decreases when  $\lambda > \lambda^*$ , as discussed in the previous section.

In the case of  $T = 10$ , the prices estimated by our model are clearly higher than the prices given by the Glover (2008) model when  $\lambda = 1$  and  $\lambda = 2$ , because the maturity is long enough to show the difference of  $\tau^*$  for two models:  $\tau^*$  in our model is less than 20 and much smaller than that in Glover's model (see Fig 5.12), which implies that the underlying in our model has more possibility of hitting the vanishing circle. Both models produce higher put prices than Black-Scholes prices when  $\lambda < 5$  because of the existence of the vanishing regions. When  $\lambda = 5$  and  $\lambda = 10$ , the prices become close again as the corresponding value of  $\tau^*$  for both models are large, which also implies that their prices are lower than the Black-Scholes price as the vanishing regions are hard to hit. The put prices for  $T = 10$  are still decreasing as  $\lambda$  increases in results that all the values of  $\lambda$  here are nearly larger than  $\lambda^*$ . We also give the results of call options and deviations of PCP in Fig 5.14 and show without caps, the estimated prices of call options cannot converge by increasing the number of paths, due to the presence of extremely high prices in the underlying. Call options are overpriced by both models by the unexpected big jumps, and the deviations of PCP in the bottom panel are obviously seen to be seriously affected by the corresponding call prices. Therefore, in both models used here for pricing a call option, we suggest estimating the associated put price and then extract the call price from put-call parity.

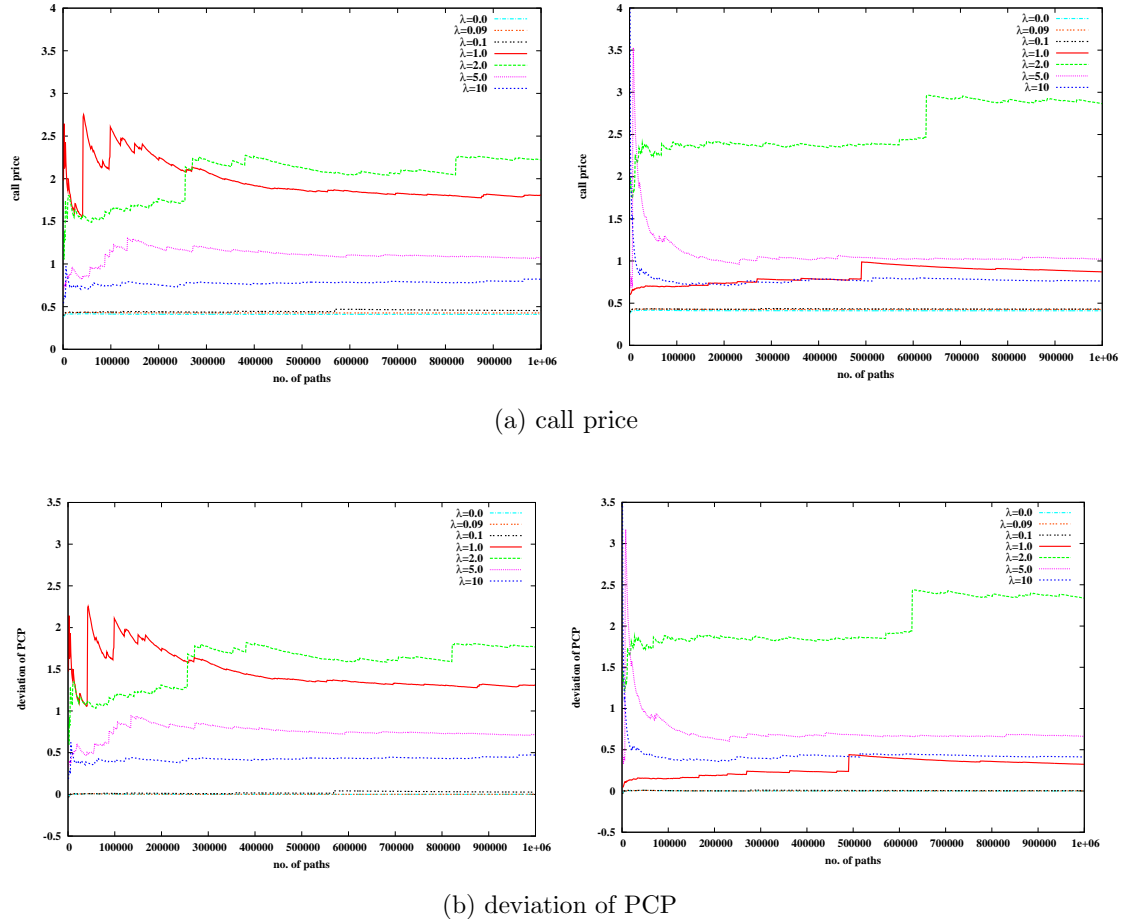


Figure 5.14: Comparison of Glover (2008) model (left hand) and our model (right hand): call prices (a) and deviation of PCP (b) with respect to varying  $\lambda$  under the parameters:  $S = K = 1$ ,  $r = 0.04$ ,  $\sigma = 0.2$ ,  $T = 10$  and  $N = 2000$  after  $M = 10^6$

# Chapter 6

## First-Order Feedback Model with Stochastic Illiquidity

The question of whether market illiquidity is not constant has been discussed in a number of papers. Frey and Patie (2002) proposed a function of illiquidity,  $\lambda$ , dependent on underlyings rather than constant  $\lambda$  in Frey (2000). Esser and Monch (2002) suggest that  $\lambda$  should be strictly positive and follow a stochastic process, which is specified as a mean-reverting square-root process with a natural long-term level of the illiquidity, i.e. a CIR model (see Cox et al., 1985). Furthermore, illiquidity is assumed to have an impact on trading strategies. Liao, Chen and Chou (2005) develop a stochastic liquidity balance model which is influenced by changes of economic states and their liquidity model is also mean-reverting but allows negative values to indicate liquidity crises. In this chapter, we introduce a two-dimensional SDE of underlyings derived from Esser and Monch (2002) with the standard Black-Scholes delta-hedging strategy, and illustrate an application to pricing European options. Assume the underlying price  $S$  and the market illiquidity  $\lambda$  are followed by two stochastic processes with correlation coefficient  $\rho$ , which are

$$\begin{aligned} dS &= \mu S dt + \sigma S dW^S + \lambda S d\Phi, \\ d\lambda &= \kappa(\theta - \lambda)dt + \zeta \sqrt{\lambda} dW^\lambda, \end{aligned} \tag{6.1}$$

where  $\mu$  and  $\sigma$  denote the constant drift and volatility for the underlying  $S$ ;  $\Phi$  is the number of shares traded by large investors;  $\lambda$  follows a one-factor CIR model which ensures the mean-reversion of illiquidity  $\lambda$  towards the long-run value  $\theta$  with speed of adjustment  $\kappa$  and the volatility of this process  $\zeta$ .  $dW^S$  and  $dW^\lambda$  are two correlated Brownian motions with correlation coefficient  $\rho$  as follows:

$$dW^S dW^\lambda = \rho dt .$$

The  $\rho$  could be positive or negative, whose effects on option pricing will be addressed in Section 6.2.2. Using Cholesky decomposition, Eq (6.1) can be rewritten with two uncorrelated standard Brownian motions  $W$  and  $\bar{W}$

$$\begin{aligned} dS &= \mu S dt + \sigma S dW + \lambda S d\Phi , \\ d\lambda &= \kappa(\theta - \lambda) dt + \rho \zeta \sqrt{\lambda} dW + \sqrt{1 - \rho^2} \zeta \sqrt{\lambda} d\bar{W} . \end{aligned} \quad (6.2)$$

To present a complete derivation, we assume the illiquidity  $\lambda$  has an impact on the number of shares  $\Phi(t, S, \lambda)$  held by large investors, then by applying Ito's lemma to the function of  $\Phi(t, S, \lambda)$ , we should find

$$\begin{aligned} d\Phi &= \Phi_t dt + \Phi_S dS + \Phi_\lambda d\lambda \\ &\quad + \frac{1}{2} (\Phi_{SS} dS^2 + \Phi_{\lambda\lambda} d\lambda^2 + 2\Phi_{\lambda S} d\lambda dS) \\ &= \Phi_t dt + \Phi_S dS + \Phi_\lambda d\lambda + \frac{1}{2} \Phi_{\lambda\lambda} \zeta^2 \lambda dt \\ &\quad + \frac{1}{2} \Phi_{SS} dS^2 + \Phi_{\lambda S} d\lambda dS , \end{aligned}$$

where the subscripts are used to denote partial derivatives. Substituting this into Eq (6.2) leads to

$$\begin{aligned} (1 - \lambda S \Phi_S) dS &= \left( \frac{\mu}{\lambda} + \Phi_t + \kappa(\theta - \lambda) \Phi_\lambda + \frac{1}{2} \Phi_{\lambda\lambda} \zeta^2 \lambda \right) \lambda S dt \\ &\quad + (\sigma + \lambda \Phi_\lambda \rho \zeta \sqrt{\lambda}) S dW \\ &\quad + \lambda \Phi_\lambda \sqrt{1 - \rho^2} \zeta \sqrt{\lambda} S d\bar{W} \\ &\quad + \frac{1}{2} \lambda S \Phi_{SS} dS^2 + \lambda S \Phi_{\lambda S} d\lambda dS . \end{aligned} \quad (6.3)$$

Assuming the SDE of  $S$  has the general form:

$$dS = b(t, S, \lambda) dt + v(t, S, \lambda) S dW + \bar{v}(t, S, \lambda) S d\bar{W} , \quad (6.4)$$

which implies, as  $dt \rightarrow 0$ ,

$$\begin{aligned} dS^2 &= (v^2 + \bar{v}^2)S^2 dt, \\ d\lambda dS &= (\rho v + \sqrt{1 - \rho^2}\bar{v})\zeta\sqrt{\lambda}S dt. \end{aligned}$$

Comparing the coefficients of each term,  $v$ ,  $\bar{v}$  and  $b$  can be obtained from

$$v(t, S, \lambda) = \frac{\sigma}{1 - \lambda S \Phi_S} + \rho \frac{\lambda \Phi_\lambda \zeta \sqrt{\lambda}}{1 - \lambda S \Phi_S}, \quad (6.5)$$

$$\bar{v}(t, S, \lambda) = \sqrt{1 - \rho^2} \frac{\lambda \Phi_\lambda \zeta \sqrt{\lambda}}{1 - \lambda S \Phi_S}, \quad (6.6)$$

$$\begin{aligned} b(t, S, \lambda) &= \frac{\lambda S}{1 - \lambda S \Phi_S} \left[ \frac{\mu}{\lambda} + \Phi_t + \kappa(\theta - \lambda)\Phi_\lambda + \frac{1}{2}\Phi_{\lambda\lambda}\zeta^2\lambda \right. \\ &\quad \left. + \frac{1}{2}\Phi_{SS}S^2(v^2 + \bar{v}^2) + \zeta\sqrt{\lambda}\Phi_{\lambda S}S(\rho v + \sqrt{1 - \rho^2}\bar{v}) \right]. \end{aligned} \quad (6.7)$$

Therefore, the dynamics of  $S$  and  $\lambda$  are given by

$$dS = b(t, S, \lambda)dt + v(t, S, \lambda)SdW + \bar{v}(t, S, \lambda)Sd\bar{W}, \quad (6.8)$$

$$d\lambda = \kappa(\theta - \lambda)dt + \rho\zeta\sqrt{\lambda}dW + \sqrt{1 - \rho^2}\zeta\sqrt{\lambda}d\bar{W}, \quad (6.9)$$

where  $v(t, S, \lambda)$ ,  $\bar{v}(t, S, \lambda)$  and  $b(t, S, \lambda)$  are prescribed in Eq (6.5)-(6.7). Moreover, in the risk-neutral world, we deduce the SDEs with a drift adjustment as

$$\begin{aligned} dS &= rSdt + \left( \frac{\sigma}{1 - \lambda S \Phi_S} + \rho \frac{\lambda \Phi_\lambda \zeta \sqrt{\lambda}}{1 - \lambda S \Phi_S} \right) SdW \\ &\quad + \sqrt{1 - \rho^2} \frac{\lambda \Phi_\lambda \zeta \sqrt{\lambda}}{1 - \lambda S \Phi_S} Sd\bar{W}, \end{aligned} \quad (6.10)$$

$$d\lambda = \kappa(\theta - \lambda)dt + \rho\zeta\sqrt{\lambda}dW + \sqrt{1 - \rho^2}\zeta\sqrt{\lambda}d\bar{W}. \quad (6.11)$$

Again, price takers in the first-order feedback model are assumed to use a sub-optimal delta hedging according to the standard Black-Scholes formula, i.e.  $\Phi_S = V_{SS}^{BS}$ . For simplicity, we consider the function of  $\Phi$  is independent of the illiquidity  $\lambda$  i.e.  $\Phi_\lambda = 0$ , where the liquidity has no impact on the strategy of the larger trader. This leads to a simple form of equation system for the first-order feedback models, as follows:

$$dS = rSdt + \frac{\sigma S}{1 - \lambda S V_{SS}^{BS}} dW, \quad (6.12)$$

$$d\lambda = \kappa(\theta - \lambda)dt + \rho\zeta\sqrt{\lambda}dW + \sqrt{1 - \rho^2}\zeta\sqrt{\lambda}d\bar{W}. \quad (6.13)$$

Naturally, for the full feedback model,  $V_{SS}^{BS}$  is replaced by  $V_{SS}$ .

The remainder of the chapter is organized as follows: Section 6.1 briefly introduces the implementation of the first-order feedback model with stochastic illiquidity and Section 6.2 presents a detailed analysis with respect to the denominator of the volatility term and option pricing in the stochastic illiquidity model is compared with the constant illiquidity case.

## 6.1 Implementation

We apply a Monte Carlo scheme to implement pricing of the two-dimensional problem, i.e. the first-order feedback with stochastic illiquidity  $\lambda(t)$  as detailed in Eq (6.12)-(6.13). The algorithm used here is quite similar to that applied in Section 5.1 for simulating the underlying  $S(t)$ , but with varying  $\lambda(t)$  at time points  $t_1, \dots, t_N$  which are also estimated by a simple Euler discretization of Eq (6.13). For a European call option price  $V(t)$ , a detailed implementation is given as follows:

1. Set  $N$  discrete time points  $t_i$  for  $i = 0, \dots, N$  in time interval  $[0, T]$  with the same increment, i.e.  $t_{i+1} = t_i + \Delta t$  for the sake of easy implementation.
2. Generate  $M$  sample paths  $S_j(t_i)$  for  $j = 1, \dots, M$  by a simple Euler discretization. As  $dW$  is an increment of Brownian motion  $W$ , by the basic property of Brownian motion we can gain its estimate:  $Z\sqrt{\Delta t}$  with a standard normal random variable  $Z \sim N(0, 1)$ . Then the approximation of Eq (6.12) can be obtained as follows:

$$S_j(t_{i+1}) = S_j(t_i) + rS_j(t_i)\Delta t + \frac{\sigma S_j(t_i)}{1 - \lambda_j(t_i)S_j(t_i)V_{SS_j}^{BS}(t_i)} Z_j(t_i) \sqrt{\Delta t},$$

where the second differential  $V_{SS_j}^{BS}(t_i)$  is directly given by the Black-Scholes formula for Gamma, given in Eq (5.3). Notice there is the same serious problem as in the constant illiquidity model: the possibility of nearly vanishing denominators of the volatility term would cause either negative prices or abnormally high prices. As the illiquidity  $\lambda$  is now variable, the problem seems to be more complicated. As before, we discard those paths with negative prices or above-cap prices and set the relative option prices  $V_j(t_0) = 0$ . The total number of

abandoned paths is stored as  $m$ .

3. Simulate the corresponding value of  $\lambda_j(t_i)$  at each time point  $t_i$  for each path  $S_j$  based on the square-root diffusion shown in Eq (6.13), as follows:

$$\begin{aligned}\lambda_j(t_{i+1}) = & \lambda_j(t_i) + \kappa(\theta - \lambda_j(t_i))\Delta t + \rho\zeta\sqrt{\lambda_j(t_i)}Z_j(t_i)\sqrt{\Delta t} \\ & + \sqrt{1 - \rho^2}\zeta\sqrt{\lambda_j(t_i)}\bar{Z}_j(t_i)\sqrt{\Delta t},\end{aligned}\quad (6.14)$$

where  $\bar{Z}_j(t_i)$  is a standard normal random number and independent of  $Z_j(t_i)$ .

As discussed in Section 3.5 for modelling stochastic volatility in jump diffusion processes, the continuous-time CIR model is able to prevent  $\lambda$  from negative values with a suitable parameter setting which does not work for a discrete-time version. Thus, similar to the measure taken to deal with the occurrence of negative values of volatility in Section 3.5.1, if  $\lambda_j(t_{i+1}) < 0$  in the  $j$ th path, we resimulate the sample paths for  $\lambda_j(t_i)$  and  $S_j(t_i)$  from  $t_1$  to  $t_N$ .

4. Calculate the option payment at maturity  $V_j(t_N) = (S_j(t_N) - K, 0)^+$  and discount it back to initial time  $t_0$  by the discount factor  $e^{-rT}$  to get the price of option  $V_j(t_0)$  for each paths  $S_j$ .
5. Then the expected option price is estimated as the averaged value of option prices  $V_j(t_0)$ , i.e.

$$\bar{V}(t_0) = \frac{1}{M-m} \sum_{j=1}^M V_j(t_0),$$

where  $m$  is the number of discarded paths during the procedure. Then, the law of large numbers ensures that the estimator  $\bar{V}(t_0)$  converges to the exact expected value  $V(t_0)$ .

## 6.2 Comparison between constant and stochastic illiquidity parameter

Esser and Monch (2002) suggest that the stochastic  $\lambda$  model shown (6.12)-(6.13) should have little difference with the corresponding constant  $\lambda$  model due to excluding

the impact of  $\lambda$  on the trading strategy, i.e. setting  $\Phi_\lambda = 0$ . However, we do obtain some differences between the two models from our numerical results. In the remainder of this section, we discuss the difference between the two models in two ways: the changes of the denominator of the volatility term, which includes an analysis of abandoning paths and put-call parity; and an impact of the choice of parameters on option pricing.

### 6.2.1 Denominator of the volatility term

As with the constant illiquidity model, there is also a possibility of finding vanishing denominators from the stochastic illiquidity model. To make the results from these two models comparable, we assume the same default parameters<sup>1</sup> for both models:  $S_0 = K = 1$ ,  $r = 0.04$ ,  $\sigma = 0.2$ ,  $T = 10$ ,  $N = 2000$ ,  $M = 10^6$ ,  $\kappa = 0.35$ ,  $\zeta = 0.2$  and  $\theta = 1$ ; the stochastic illiquidity  $\lambda$  starts from  $\lambda_0 = 1$  and the constant illiquidity  $\lambda^c = 1$ ; the correlation between the underlying process and its illiquidity is considered to be zero, i.e.  $\rho = 0$ . Unless otherwise stated, these parameters will be applied throughout this section.

#### 1. Negative Prices of Underlyings

As described in Chapter 5, the first-order constant illiquidity model has a vanishing zone to cause abnormal price moves, which is given by (5.5):

$$S(\tau) = K \exp \left( -\left( r + \frac{1}{2}\sigma^2 \right)\tau \pm \sigma\sqrt{\tau} \sqrt{2\log\lambda - \log(2\pi\sigma^2\tau)} \right),$$

and the corresponding abandoning region for negative prices has been found by (5.10)-(5.11). The scales of the vanishing zone  $(0, \tau^*)$  and abandoning region  $(0, \tau_{out}^*)$  are totally independent of the option's maturity  $T$  and they are only dependent on the critical value of time-to-expiry  $\tau^* = \frac{\lambda^2}{2\pi\sigma^2}$  and  $\tau_{out}^* = \frac{\lambda^2}{2\pi\sigma^2(1-\varepsilon)^2}$  respectively;  $\lambda$  here is assumed to be constant. However, when  $\lambda$  follows a stochastic process the duration will be extended to the whole option life  $T$ .

Fig 6.1 is used to illustrate this point using three examples with  $T = 1$  (a),

---

<sup>1</sup>The parameters for stochastic illiquidity are taken from Esser and Monch (2002).

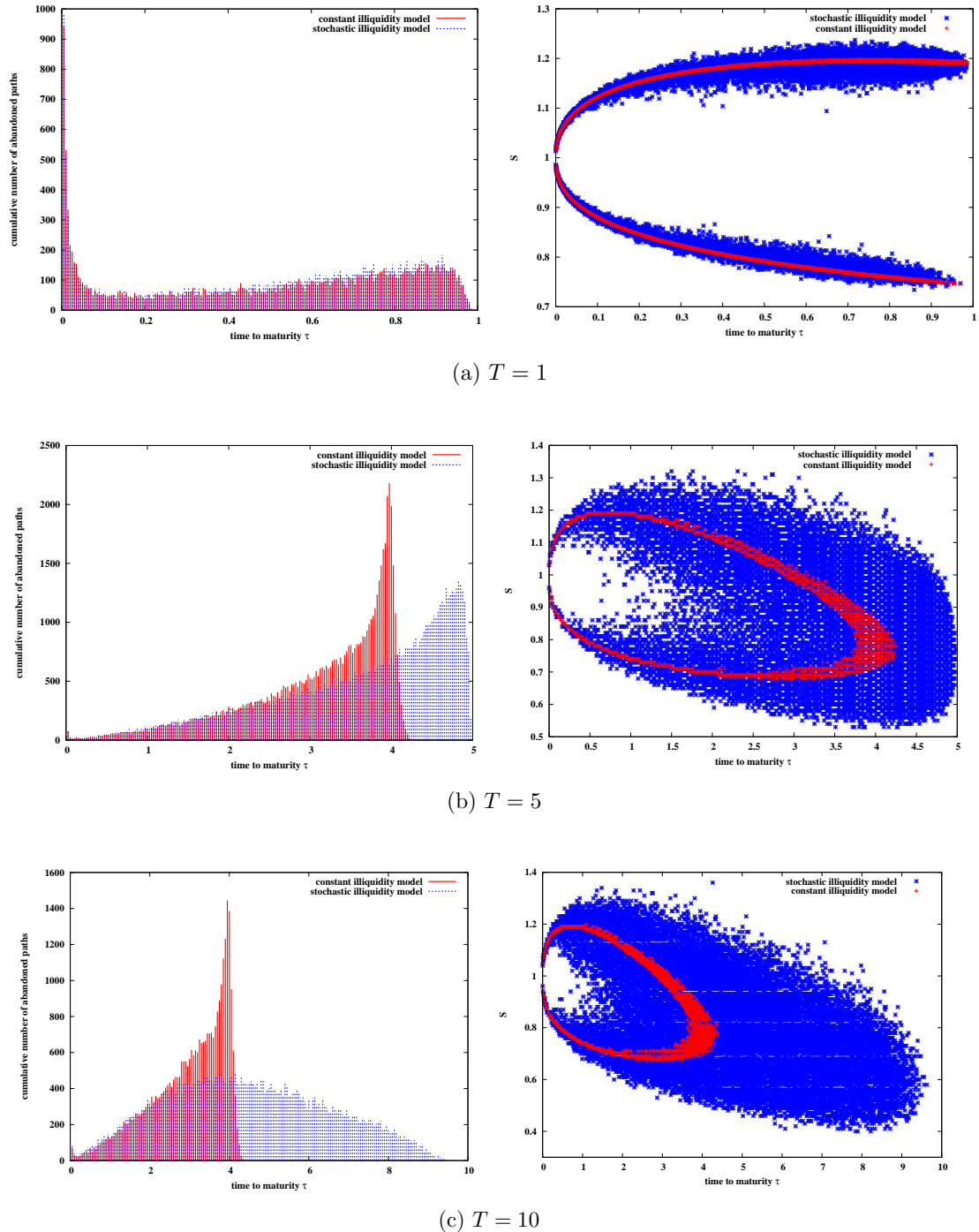


Figure 6.1: The cumulative number of abandoned paths caused by negative price with respect to time-to-expiry  $\tau$  & the corresponding location of negative prices. The results are given by  $10^6$  simulated paths

5 (b) and 10 (c). We provide histograms of the distribution of the number of abandoned paths and scatter plots of the location  $(\tau, S)$  leading to negative prices. For the case with constant illiquidity  $\lambda^c = 1$ , the estimators of  $\tau^*$  and  $\tau_{out}^*$  are 3.98 and 4.41 respectively. Therefore, the example aims to show the abandoning region for negative prices in pricing options with a short-term maturity  $T = 1$ , a medium-term maturity  $T = 5$  and a long-term maturity  $T = 10$  in two models<sup>2</sup>. Fig 6.1(a) with  $T = 1 < \tau^*$  indicates both models have the same time period of finding negative prices as the maturity  $T$ , but the stochastic illiquidity model has a somewhat wider abandoning zone than the constant illiquidity model. The distributions of the cumulative number of abandoned paths seem to be similar and the total number of abandoned paths in the stochastic illiquidity is only slightly higher than that with constant illiquidity, as seen in Table 6.1. As shown in Fig 6.1(b), when  $T = 5$ , the

Maturity $T$	Constant Illiquidity	Stochastic Illiquidity
1	18146	19678
5	65640	81721
10	33315	51624

Table 6.1: The number of abandoned paths with negative prices in  $10^6$  sample paths.

abandoning zone of the stochastic illiquidity in the scatter plot is somewhat wider than the constant illiquidity. Moreover, the abandoning range  $\tau \in (0, \tau_{out}^*)$  is only satisfied by the constant illiquidity model, rather than the stochastic illiquidity whose range is still  $\tau \in (0, T)$ . The number of abandoned paths presented in the histogram shows there is a strong peak around  $t = T - \tau^*$  for the constant illiquidity model, while the stochastic illiquidity model has a moderate peak at earlier times  $t \approx 0$ . When the maturity increases again in Fig 6.1(c), the constant illiquidity model retains the same shape for the abandoning zone and the distribution of the number of abandoned paths as the case of  $T = 5$ . However, in the stochastic illiquidity model, we find an extended abandoning zone for all  $\tau \in (0, T)$  with  $T = 10$ , and the maximum cumulative

<sup>2</sup>Notice that  $T = 5$  is close to 4.41 for  $\tau_{out}^*$  calculated in the constant illiquidity model.

number of negative paths occurs at the critical time  $t = T - \tau^*$ .

The main results from Fig 6.1 reveal that negative prices are found during the entire life in the stochastic illiquidity model, whereas they are only obtained when  $\tau \in (0, \tau_{out}^*)$  in the constant illiquidity model. For each level of maturity, the abandoning zone of the stochastic illiquidity model is shown to be wider than for the constant illiquidity case. Thereby, the stochastic illiquidity model generally produces many more negative prices than the constant illiquidity model, as shown in Table 6.1. In the case of  $T \leq \tau_{out}^*$ , the stochastic illiquidity model still generates more abandoned paths but the difference in the number of abandoned paths between the two models is relatively small. Both models obtain the maximum number of negative prices when  $T \approx \tau^*$ .

We are also interested in values of  $\lambda$  when negative prices occur in the stochastic illiquidity model. Fig 6.2 gives the relative location  $(\tau, \lambda)$  when the underlying

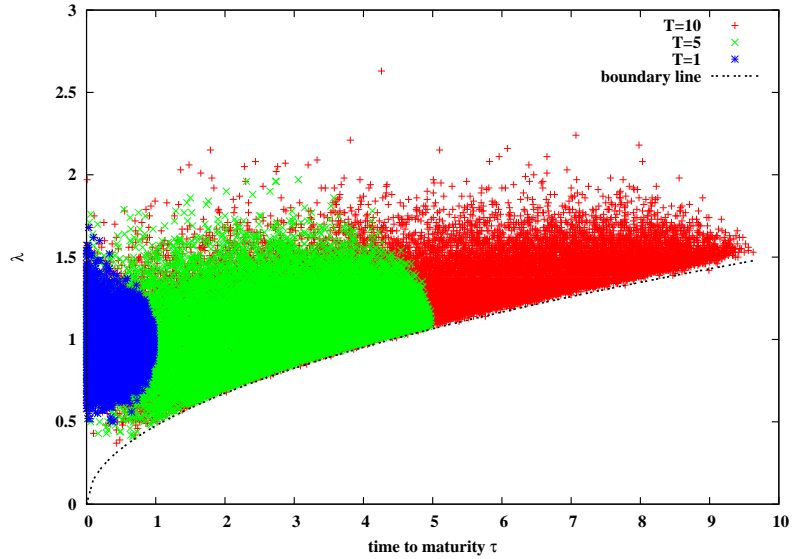


Figure 6.2: The location of  $\lambda$  for negative prices with varying maturity  $T$ . The scattered points are given by the results of  $M = 10^6$  runs.

prices  $S(\tau) < 0$  with the same parameters used in Fig 6.1. The scatter plot shows a clear boundary line to divide the plane into two regions: the data above the boundary line could result in negative prices otherwise the data below the boundary should never produce negative prices. The economic implication of

the results is that there exists an arbitrage opportunity when the point  $(\tau, \lambda)$  is above the boundary line. This is because negative prices cause arbitrage opportunities. The boundary can be explained as follows.

As mentioned, negative prices are caused by a nearly vanishing denominator,  $|1 - \lambda SV_{SS}^{BS}| < \varepsilon$ , whose solution is given by (5.8)-(5.13). However, the expressions (5.10)-(5.13) become invalid once

$$\lambda < \sqrt{2\pi\sigma^2\tau(1 - \varepsilon)^2} .$$

Therefore, those pairs  $(\tau, \lambda)$  that satisfy the inequality would not cause negative prices, which implies the boundary line is given by

$$\lambda = \sqrt{2\pi\sigma^2\tau(1 - \varepsilon)^2} .$$

In Fig 6.2 the boundary line estimated by  $\varepsilon = 0.05$  is shown to confirm this.

## 2. Put-Call Parity

Under the stochastic volatility assumption, put-call parity remains valid in the illiquid market. This can be illustrated by a PDE approach, as follows:

As discussed in the beginning of this chapter, the risk-adjusted process are given by Eq (6.12) and (6.13). Applying Itô's lemma, we can find the change of derivative's price  $V(S, \lambda, t)$  is:

$$\begin{aligned} dV(S, \lambda, t) = & \left[ \frac{\sigma^2 S^2}{2(1 - \lambda SV_{SS}^{BS})^2} \frac{\partial^2 V}{\partial S^2} + \frac{\rho\sigma\zeta\sqrt{\lambda}S}{1 - \lambda SV_{SS}^{BS}} \frac{\partial^2 V}{\partial S \partial \lambda} + \frac{\zeta^2\lambda}{2} \frac{\partial^2 V}{\partial \lambda^2} \right. \\ & \left. + rS \frac{\partial V}{\partial S} + \kappa(\theta - \lambda) \frac{\partial V}{\partial \lambda} + \frac{\partial V}{\partial t} \right] dt \\ & + \left[ \frac{\sigma S}{1 - \lambda SV_{SS}^{BS}} \frac{\partial V}{\partial S} + \rho\zeta\sqrt{\lambda} \frac{\partial V}{\partial \lambda} \right] dW \\ & + \left[ \sqrt{1 - \rho^2}\zeta\sqrt{\lambda} \frac{\partial V}{\partial \lambda} \right] d\bar{W}, \quad (6.15) \end{aligned}$$

given by two independent Brownian motion  $W$  and  $\bar{W}$ . By analogy with Glover (2008) using standard hedging arguments, we construct a portfolio including one underlying asset and two call options with different maturities<sup>3</sup>. Following

---

<sup>3</sup>This is because there is no underlying asset with which to hedge for the illiquidity risk. We need two options to eliminate two sources of uncertainty  $dW$  and  $d\bar{W}$ .

the standard arbitrage arguments, the derivative price  $V(S, \lambda, t)$  with two state variables must obey the following PDE:

$$\begin{aligned} & \frac{\sigma^2 S^2}{2(1 - \lambda SV_{SS}^{BS})^2} \frac{\partial^2 V}{\partial S^2} + \frac{\rho \sigma \zeta \sqrt{\lambda} S}{1 - \lambda SV_{SS}^{BS}} \frac{\partial^2 V}{\partial S \partial \lambda} + \frac{\zeta^2 \lambda}{2} \frac{\partial^2 V}{\partial \lambda^2} + rS \frac{\partial V}{\partial S} \\ & + (\kappa(\theta - \lambda) - f(S, \lambda, t)) \frac{\partial V}{\partial \lambda} + \frac{\partial V}{\partial t} - rV = 0 , \end{aligned} \quad (6.16)$$

where the unspecified term  $f(S, \lambda, t)$  represents the market price of the illiquidity risk as the illiquidity itself cannot be traded. Define a European call option  $V^C(S, \lambda, t)$  and put option  $V^P(S, \lambda, t)$ . As  $V^P(S, \lambda, t)$  satisfies the above PDE, we can substitute the put-call parity formula:

$$V^P(S, \lambda, t) = V^C(S, \lambda, t) - S + Ke^{-r(T-t)}$$

into the PDE, then we can obtain:

$$\begin{aligned} & \frac{\sigma^2 S^2}{2(1 - \lambda SV_{SS}^{BS})^2} \frac{\partial^2 V^C}{\partial S^2} + \frac{\rho \sigma \zeta \sqrt{\lambda} S}{1 - \lambda SV_{SS}^{BS}} \frac{\partial^2 V^C}{\partial S \partial \lambda} + \frac{\zeta^2 \lambda}{2} \frac{\partial^2 V^C}{\partial \lambda^2} + rS \frac{\partial V^C}{\partial S} \\ & + (\kappa(\theta - \lambda) - f(S, \lambda, t)) \frac{\partial V^C}{\partial \lambda} + \frac{\partial V^C}{\partial t} - rV^C = 0 , \end{aligned}$$

which is true as the call option  $V^C(S, \lambda, t)$  also satisfies the modified Black-Scholes equation (6.16). This suggests that a European option can be replicated by the portfolio:  $V^C - S + Ke^{-r(T-t)}$  which has the same payoff as the put option at maturity. The solution to the Black-Scholes PDE shows that put-call parity still holds. However, as mentioned in the constant illiquidity case, the problem with put-call parity still exists in the crude simulation model with a stochastic illiquidity, in that the model is seen to produce abnormally high underlying prices. Fig 6.3 shows evidence that for both models there are some unexpectedly high underlying prices that disrupt the convergence in pricing a call option, when the number of sample paths is increasing and these lead to deviations in put-call parity by both models. The stochastic illiquidity model appears to overprice the call options more than the constant illiquidity model.

We can find an improved value of a call option by two methods. One approach has been introduced in the constant illiquidity model, which is to set a cap  $\bar{S}$

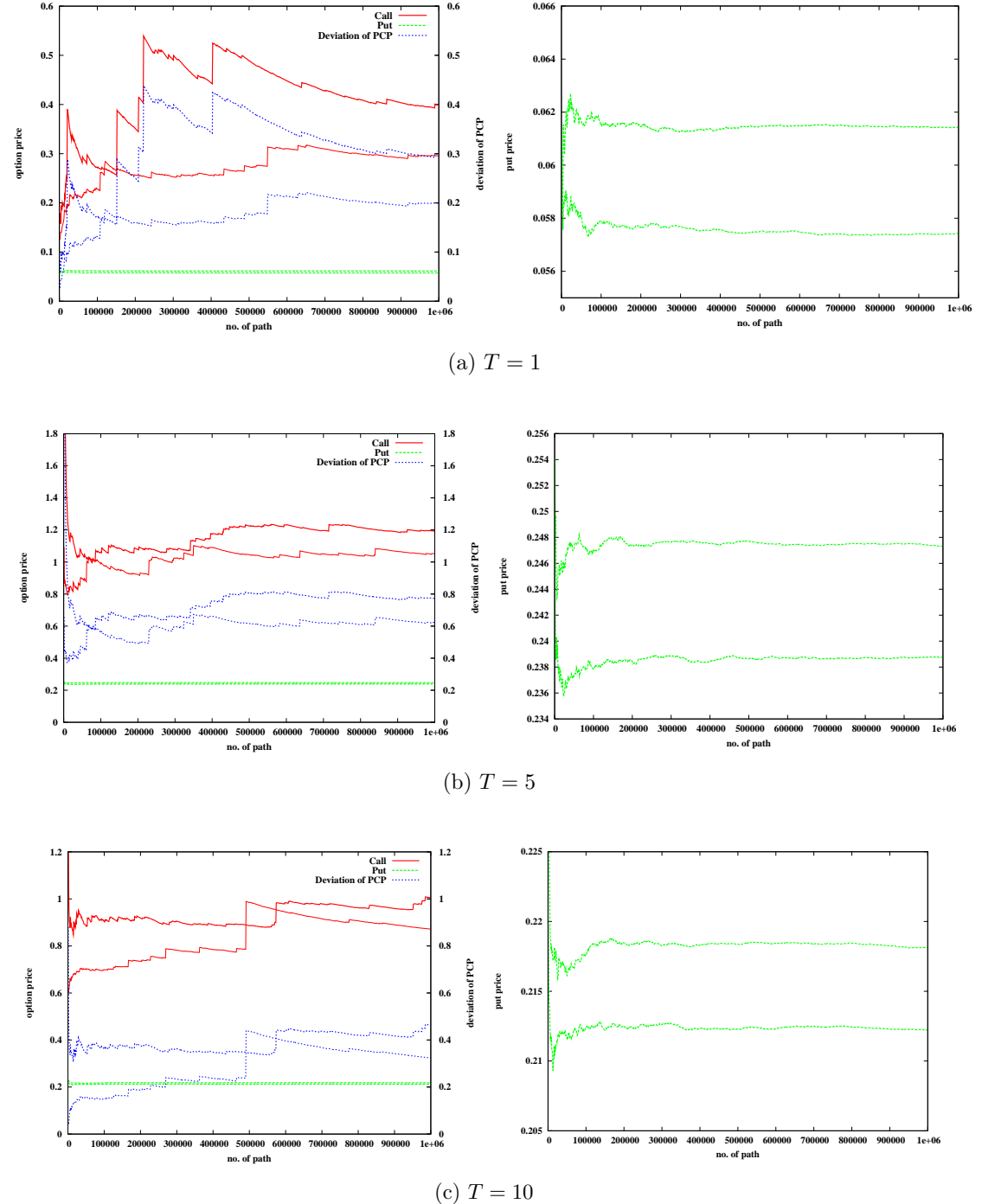


Figure 6.3: Pricing European options and examining the violation of PCP under the identical underlying price process. The thicker lines are for the stochastic illiquidity model and the thinner lines for the constant illiquidity model.

such that we restrict  $S < \bar{S}$ . The chosen value of the cap  $\bar{S}$  should ensure the smallest absolute deviation from the put-call parity. Another approach is to estimate the value of the call option via pricing the corresponding put option. Because put-call parity is shown to hold and the estimated price of the put option tends to be more convergent and reliable with an increasing number of the sample paths, as seen in the right panel of Fig 6.3, in the remainder of this chapter we will focus on pricing put options. Then the implied call prices can be computed by put-call parity with these known put prices.

### 6.2.2 Sensitivity of option price to the choice of parameters

In this section, we discuss the impact of the parameters applied in a stochastic illiquidity model on option pricing, which includes maturity  $T$ , moneyness  $S/K$ , correlation coefficient  $\rho$  between two dynamic processes, the adjustment speed  $\kappa$  and the volatility  $\zeta$  for illiquidity. Again, the remaining parameters are set as follows:  $S_0 = K = 1$ ,  $r = 0.04$ ,  $\sigma = 0.2$  and  $N = 2000$ . Assuming the constant illiquidity value  $\lambda^c = 1$ , then for the stochastic illiquidity we let the illiquidity start from  $\lambda_0$  and denote the long-term illiquidity  $\theta$  with the same value as the constant illiquidity  $\lambda^c$ , i.e.  $\lambda_0 = \theta = \lambda^c = 1$ . We will focus on European put options in the remaining section.

#### 1. $T$ Impact on Option Price

A European put option price varies with the maturity  $T$ : the price generally increases in time to maturity for a relatively short-term maturity  $T$ , but decreases in time to maturity for a long-term maturity, such as greater than 10 years, as seen in Fig 6.4. The figure presents the results of three models: constant  $\lambda$ , stochastic  $\lambda$  and  $\lambda = 0$ . A peak of the option price appears when  $T = 5$ : when  $T < 5$  the option price is increasing as  $T$  rises; then for  $T \geq 5$  the option price is slightly decreasing as  $T$  rises. We notice that there is a decline in the put price for the constant illiquidity model when  $T = 4$  because the maturity is close to the length of the vanishing region  $\tau^*$  which has been

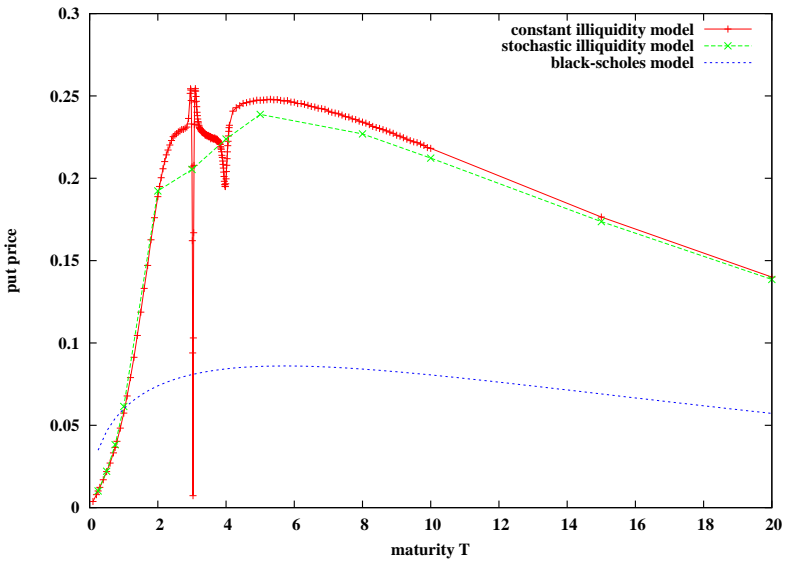


Figure 6.4: The difference of put prices with stochastic  $\lambda$  and constant  $\lambda$  depends on varying maturity  $T$  under the parameters:  $\kappa = 0.35$ ,  $\zeta = 0.2$ ,  $\rho = 0$  and others shown in the section. The standard Black-Scholes prices are evaluated for the following parameters:  $S_0 = K = 1$ ,  $r = 0.04$ ,  $\sigma = 0.2$ . The scattered points is given by the results of  $M = 10^6$  runs.

explained in Chapter 5. Compared with Black-Scholes prices, the prices given by the illiquidity models are lower when  $T \leq 1$ , which implies that the volatility for the illiquidity models is reduced (and smaller than  $\sigma$ ). This is because for a short-term maturity,  $T < 1$ , the value of  $V_{SS}^{BS}$  estimated by the Black-Scholes formula is usually large as the time-to-maturity  $\tau$  is small and the spot price  $S$  stays around the strike  $K$ , so that the denominator of the volatility term  $|1 - \lambda S V_{SS}^{BS}| > 1$ . Then when  $T > 1$ , the put prices from the illiquidity increase deeply and exceed the Black-Scholes prices, which implies that for long-term options, the illiquidity risk increases the volatility of underlying assets. Fig 6.4 indicates the relation of option pricing between constant and stochastic illiquidity models. The price with stochastic  $\lambda$  is slightly higher than that with fixed  $\lambda$  when  $T \leq 3$ , while for a long-term maturity, such as  $T > 3$ , the stochastic illiquidity model gives a lower option price than the constant illiquidity model. Moreover, due to the mean-reverting behaviour of the stochastic  $\lambda$ , the difference between option prices obtained from these two illiquid models vanishes for an extremely long-term maturity  $T$ , such as  $T = 20$  shown in Fig 6.4.

## 2. Moneyness $S/K$ Impact on Option Price

The example shown in Fig 6.5 highlights the impact of moneyness on put option prices, with particular parameters below the figure. The left panel compares

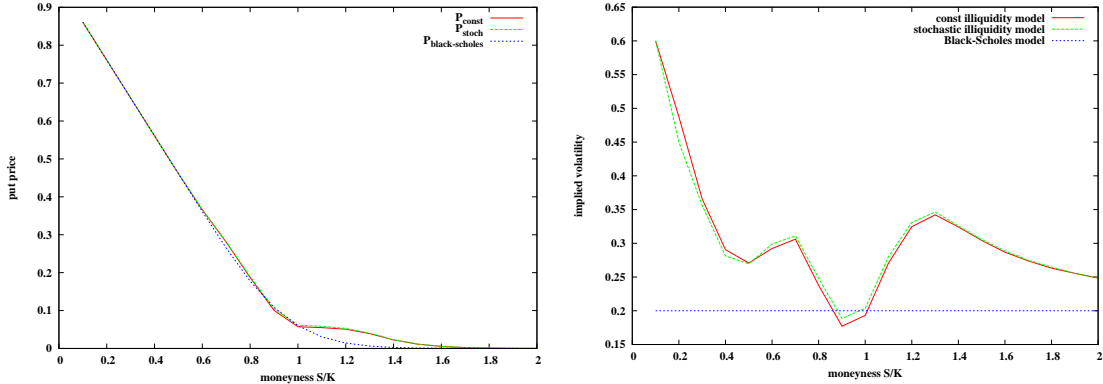


Figure 6.5: Put prices with stochastic  $\lambda$  and constant  $\lambda$  depends on varying moneyness under the parameters:  $K = 1$ ,  $T = 1$ ,  $\kappa = 0.35$ ,  $\zeta = 0.2$ ,  $\rho = 0$  and others shown in the section. The scattered points is given by the results of  $M = 10^6$  runs

the put prices produced by the three models: constant illiquidity, stochastic illiquidity and standard Black-Scholes models using varying moneyness ( $S/K$ ). We find that the two illiquidity models give similar prices for put options with respect to various moneyness. Compared with the Black-Scholes prices, both models generally produce higher prices except the range:  $0.9 < S/K < 1$ . In the range of  $0.7 < S/K < 0.9$  and  $1 < S/K < 1.6$ , the illiquidity models produce option prices which clearly exceed the standard Black-Scholes prices and the deviations from the Black-Scholes prices are more pronounced in the range  $1 < S/K < 1.6$  than those in the range  $0.7 < S/K < 0.9$ . This implies that an OTM option has more chance to produce a profit at expiry than an option that is in the money when its underlying is illiquid. However, both option prices given by the illiquidity models are close to the Black-Scholes price when the option is deep in ( $S/K \ll 0.7$ ) or deep out of the money ( $S/K \gg 1.6$ ). The analysis of the deviations from the Black-Scholes prices suggest that the illiquidity model can generate a smile and skew pattern implied volatility using the Black-Scholes formula. From the right panel of Fig 6.5, in general, the implied volatility is shown to be higher than the constant volatility of the Black-Scholes model. In

the range of the ratio  $0.7 < S/K < 1.2$ , the implied volatility presents a strong U-shaped pattern in the figure, which we may regard as a volatility smile. For DOTM options ( $S/K > 1.3$ ), the relative implied volatility is shown to be decreasing as  $S/K$  increases, which is because the absolute magnitude of the option price bias becomes very small. Fig 6.6 shows the difference between the

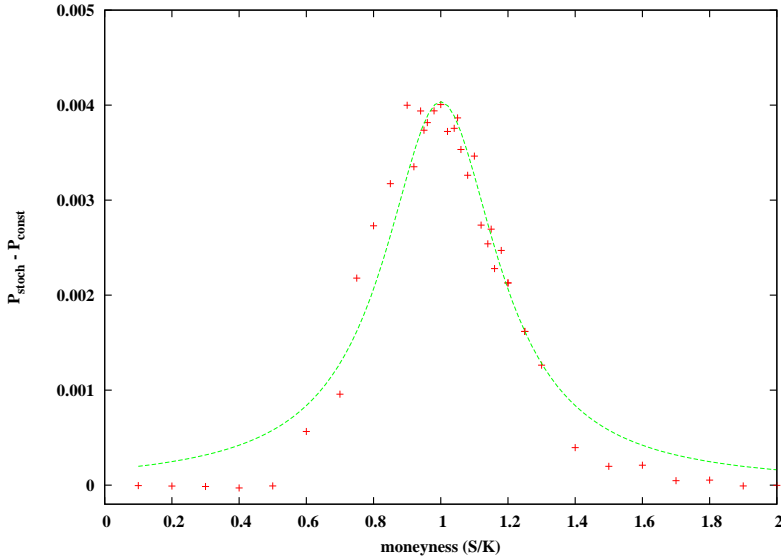


Figure 6.6: The difference of put prices with stochastic  $\lambda$  and constant  $\lambda$  depends on varying moneyness using the results from Fig 6.5. The scattered points is given by the results of  $M = 10^6$  runs; the smoothed curve line is produced by least-squares fitting & the fitting function is assumed as  $f(x) = \frac{a}{b+(x-1)^2}$ .

two illiquidity models for varying moneyness  $S/K$ . The difference is relatively small and positive, which means that the stochastic  $\lambda$  case produces slightly higher prices than the constant  $\lambda$  case. We can use a least squares method to fit the points in the figure with a simple function:

$$f(x) = \frac{a}{b + (x - 1)^2} ,$$

where the  $x$  values are taken as the moneyness  $S/K$  and the values of  $f(x)$  as the price bias between the two illiquidity models. The parameters  $a$  and  $b$  are estimated by the least squares fitting. The bell-shaped curve given by the fitting function shown in Fig 6.6 indicates the bias is more pronounced in the case of ATM options, whilst for DITM or DOTM options, stochastic  $\lambda$  gives a similar value of the options to when  $\lambda$  is constant.

### 3. $\rho$ Impact on Option Price

The correlation  $\rho$  indicates the strength and direction of the relationship between the two random variables for  $\lambda$  and  $S$ . The range of  $\rho$  is  $[-1, 1]$ , then the dependence between the two variables increases with the absolute value of  $\rho$ ;  $\rho = 1$  indicates the identical random variable used to simulate the following  $\lambda$  and  $S$ ;  $\rho = -1$  allows the use of the same variables but with the opposite sign;  $\rho = 0$  implies that the two variables are completely independent; for other values of  $\rho$ , there is a certain degree of the dependence between two variables. In Fig 6.7, we examine the impact of  $\rho$  on option pricing and compare with the

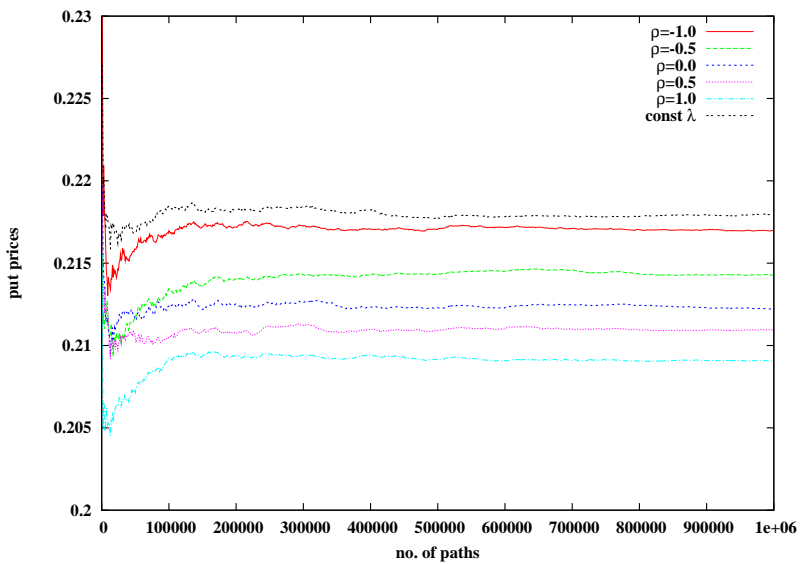


Figure 6.7: The prices of put option with respect to the correlation  $\rho$  under the parameters:  $S_0 = K = 1$ ,  $T = 10$ ,  $\kappa = 0.35$ ,  $\zeta = 0.2$  and others shown in the section.

corresponding constant illiquidity model. It is found clearly that the put option price is monotonically decreasing as the correlation  $\rho$  increases, i.e. a higher correlation between the two dynamic processes reduces the total volatility of the underlying which is:

$$\sigma_{tot} = \frac{\sigma}{1 - \lambda SV_{SS}^{BS}} . \quad (6.17)$$

The highest prices are achieved by setting  $\rho = -1$  but still lower than the price for the constant illiquidity  $\lambda = 1$ . The stochastic illiquidity generally produces a lower put price than the constant illiquidity under the parameter setting here.

In the positive correlation case  $\rho > 0$ , high stock prices  $S$  are associated with high illiquidities  $\lambda$ , which cause lower  $\sigma_{tot}$  than the constant illiquidity model. Low stock prices are associated with low illiquidities  $\lambda$ , which lead to  $\sigma_{tot}$  (6.17) closer to  $\sigma$  than the constant illiquidity model. As both these effects reduce the total volatility, the stochastic illiquidity model produces a lower option price than the constant illiquidity model. When the correlation  $\rho$  is negative, the effects on the total volatility are reduced. This leads to a relatively higher volatility  $\sigma_{tot}$  than the case of the positive  $\rho$ .

#### 4. $\kappa$ Impact on Option Price

The adjustment speed  $\kappa$  in (6.13) determines the speed of  $\lambda$  towards the long-term level of illiquidity  $\theta$ . Increasing  $\kappa$  would make  $\lambda$  likely take a value around  $\theta$ , which leads to the same effect as the constant illiquidity  $\lambda^c$ .

Fig 6.8(a) shows that the put price increases with  $\kappa$  and when  $\kappa = 100$  is relatively large, the price is much closer to the price with  $\lambda^c$  (black line). This is because the higher adjustment speed  $\kappa$  ensures that the illiquidity  $\lambda$  returns quickly to the long-term value  $\theta$ , which in this case is assumed to equal  $\lambda^c$ . As  $\kappa \rightarrow \infty$  the stochastic illiquidity behaves like a constant  $\theta$  and its option price is the same as that of  $\lambda^c$ .

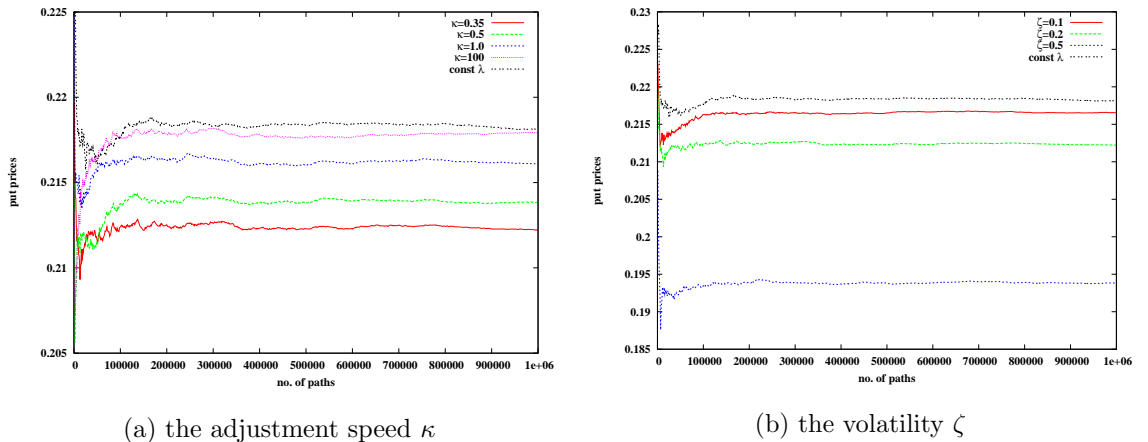


Figure 6.8: The prices of put option with respect to the adjustment speed  $\kappa$  and the volatility  $\zeta$  under the parameters:  $T = 10$ ,  $\rho = 0$  ( $\zeta = 0.2$ ,  $\kappa = 0.35$ ) and others shown in the section.

### 5. $\zeta$ Impact on Option Price

The volatility of the illiquidity  $\zeta$  refers to the deviation of random variables  $\lambda$  from the long-term value  $\theta$ . Then, compared with  $\kappa$ ,  $\zeta$  has the opposite effect on pricing option, i.e. the price is clearly decreasing as  $\zeta$  increases. As shown in Fig 6.8(b), for  $\zeta = 0.1, 0.2$  and  $0.5$ , the highest put price is given by the lowest volatility  $\zeta = 0.1$ , moreover the constant illiquidity  $\lambda^c$  yields the highest price than others  $\zeta$ . In fact, the constant illiquidity case can be obtained by setting  $\zeta = 0$  assuming  $\theta = \lambda_0$ , because Eq (6.14) employed to simulate the illiquidity process reduces to:

$$\lambda_j(t_{i+1}) = \lambda_j(t_i) = \lambda_0 ,$$

for  $i = 0, \dots, N-1$ , which is equal to the value of  $\lambda^c$  in the constant illiquidity model.

From the above we can see that all of the parameters can cause a difference in option prices between the stochastic illiquidity model and the constant illiquidity model, especially the maturity  $T$  which mainly determines if the prices given by the stochastic illiquidity model are higher than those from the constant case. However the stochastic illiquidity parameters, such as  $\kappa$  and  $\zeta$ , just have a relatively modest effect on the option pricing as the differences are somewhat small. Moreover, we also find that the constant illiquidity is a specific case of the stochastic illiquidity process when we choose larger  $\kappa$ , lower  $\zeta$  or more negative correlation  $\rho$ .

#### 6.2.3 Illiquidity $\theta$ impact on pricing option

As we mentioned before, in order to make the stochastic illiquidity model and the constant illiquidity model comparable, we assume the long term illiquidity  $\theta$  and the initial value  $\lambda_0$  have the same value as the constant illiquidity  $\lambda^c$  and, i.e.  $\lambda^c = \theta = \lambda_0$ . With respect to the impact of the stochastic illiquidity on the option prices, we focus on the price's sensitivity to the value of  $\theta$ . Because only the European put option interests us, no caps are applied to the model here. As the maturity  $T$  is an important factor in affecting the differences in put prices between both models, we also test the

option price behaviour with respect to varying maturities in Fig 6.9, which are the close-to-expiry option with  $T = 0.1$ , the short-term option with  $T = 1$  and the long-term option with  $T = 10$ . The other parameters chosen for the examples in the section are similar to those used in the previous sections, as follows:  $S_1 = K = 0$ ,  $r = 0.04$ ,  $\sigma = 0.2$ ,  $\rho = 0$ ,  $\kappa = 0.35$ ,  $\zeta = 0.2$ ,  $N = 2000$  and  $M = 10^6$ .

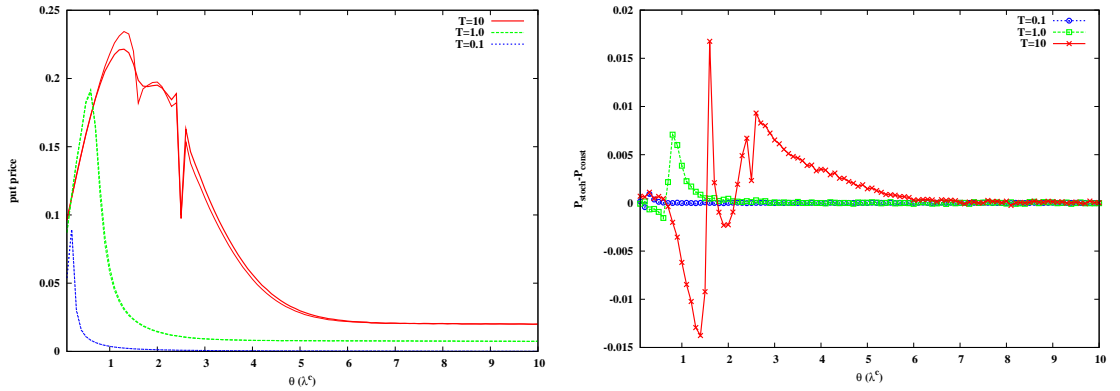


Figure 6.9: Pricing a European put option depends on long-term illiquidity  $\theta$  (or  $\lambda^c$ ) with different maturity  $T = 0.1, 1.0$  and  $10$  in the left panel. The corresponding differences in the put prices between two models are given in the right panel, which is calculated by the formula  $P_{stoch} - P_{const}$ . The thicker line indicates the stochastic illiquidity model and the thinner line for the constant illiquidity model.  $\theta$  is taken as  $0.1, 0.2, 0.3, \dots, 9.9, 1.0$

We notice in the right panel of Fig 6.9 that the option prices estimated by both models with a fixed maturity  $T$  are slightly different and the largest difference is less than 0.02, which shows that the stochastic illiquidity does not significantly influence the option value. For either option with short-term maturities or larger values of  $\theta$ , there is no difference between the two option prices, which indicates that both models have the same price impact in such situations. From the left panel of Fig 6.9, for each  $T$  there is an approximately skewed bell-shaped curve of option prices with respect to  $\theta$  (or  $\lambda^c$  for the constant illiquidity model), which is increasing in  $\theta$  before the peak price is reached at some  $\theta^*$  and afterwards the option price is generally decreasing in  $\theta$  as the variance of the underlying is relatively small. The right panel also indicates that there are more significant differences when  $\theta$  takes a value around  $\theta^*$ . The value of  $\theta^*$  is clearly relative to the maturity  $T$  and following the result in Section 5.2.3,  $\theta^*$

can be estimated by Eq (5.24):

$$\theta^* = \lambda^* = \sigma\sqrt{\pi T}, \quad (6.18)$$

as we assume  $\theta = \lambda^c$ . Table 6.2 suggests the reference values of  $\theta^*$  estimated by

Maturity $T$	Reference $\theta^*$	Approximate $\theta^*$	Approximate $\lambda^*$
0.1	0.11	0.2	0.2
1.0	0.35	0.6	0.6
10	1.12	1.3	1.3

Table 6.2: Comparison of reference value  $\theta^*$  calculated by Eq (6.18) with the approximate value by simulation with  $10^6$  sample paths.

Eq (6.18) are roughly consistent with the approximate values of  $\theta^*$  observed from the simulation, and the table also provides evidence that the values of  $\theta^*$  and  $\lambda^*$  approximated from the simulation are equal. In the case of  $T = 10$ , there are several critical values of  $\lambda$  that lead to jumps, such as  $\lambda^c = 2.5$ , which is mentioned in the first-order feedback model with a constant illiquidity (Section 5.2.3). The corresponding stochastic illiquidity model appears to have the same jumps but with slightly smaller sizes because of varying  $\lambda$ . We also provide the results of abandoned paths (i.e. those

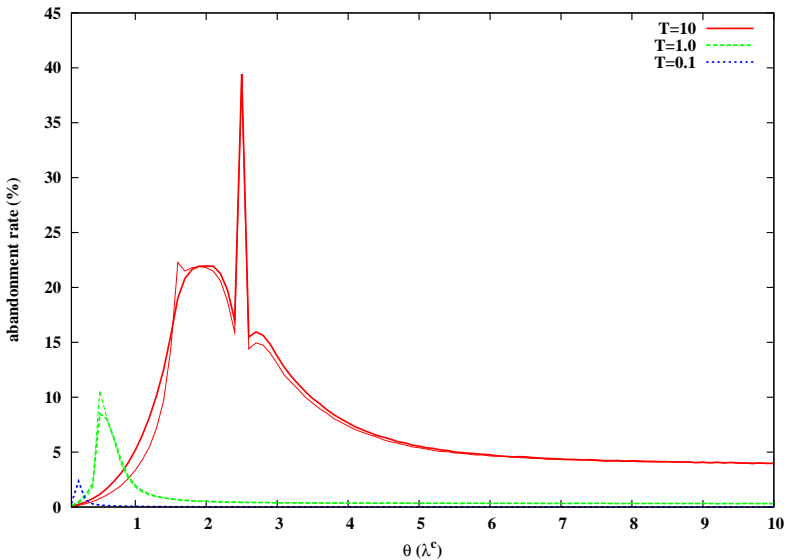


Figure 6.10: Abandonment rate of paths depends on long-term illiquidity  $\theta$  (or  $\lambda^c$ ) with different maturity  $T = 0.1, 1.0$  and  $10$  in the left panel. The thicker line indicates the stochastic illiquidity model and the thinner line for the constant illiquidity model.  $\theta$  is taken as  $0.1, 0.2, 0.3, \dots, 9.9, 1.0$ . These results are as result of  $10^6$  sample paths.

paths with negative prices) during the simulation in Fig 6.10. The abandonment rate has a skewed bell-shaped curve excluding some kinks, which is similar to the option price curve in the left panel of Fig 6.9. This is because a higher abandonment rate implies a higher volatility of the underlying, which increases the option prices.

### 6.3 First-order feedback wrap-up

Chapters 5 and 6 have introduced and analyzed first-order feedback models with constant and stochastic illiquidity parameter using a Monte Carlo simulation. To implement the simulation, we require some additional restrictions on the simulation process due to a problematic denominator of the volatility term in the feedback models. The sensitivity of the option price to different parameters has been discussed for each model and the comparison of option prices given by the both models are presented as well. We also investigate put-call parity in these first-order feedback models and provide an approach to decrease the error from put-call parity occurring in the model simulation. The problem is mainly caused by mispricing call options, hence we suggest to calculate the call option price using the corresponding put option price.

Following the analysis of the first-order feedback models, in the next chapter we will present a detailed analysis of the full feedback models in a simulation study.

# Chapter 7

## Full Feedback Model with Constant Illiquidity

In this chapter we move to study an even more challenging model: a full feedback model which is used to describe the situation in which traders realize that the market is not perfectly liquid and perform the hedge according to a modified asset model. The full feedback SDE has been derived by

$$dS = rSdt + \frac{\sigma S}{1 - \lambda SV_{SS}} dW_S , \quad (7.1)$$

where the term  $V_{SS}$  is derived by the modified SDE itself rather than by the Black-Scholes formula, which leads to more difficulties in the implementation than the case of the first-order feedback models discussed in the previous chapters; the illiquidity coefficient  $\lambda$  is initially assumed to be constant. Following the analysis in Glover (2008), the related non-linear PDE to the full feedback problem is

$$\frac{\partial V}{\partial t} + \frac{1}{2} \frac{\sigma^2 S^2}{(1 - \lambda SV_{SS})^2} \frac{\partial^2 V}{\partial S^2} + rS \frac{\partial V}{\partial S} - rV = 0 . \quad (7.2)$$

Here, we will illustrate how to use the Monte Carlo method to simulate the path following the stochastic process (7.1).

## 7.1 Implementation

The main additional problem in producing paths with SDE (7.1) is the need to calculate the second derivative  $V_{SS}$  at each timestep  $t_i$ . We can approximate  $V_{SS}$  by a three-point difference (assuming  $x_1 > x_2 > x_3$ ), i.e.

$$\frac{\partial^2 f}{\partial x^2} \approx \frac{\frac{f(x_1)-f(x_2)}{x_1-x_2} - \frac{f(x_2)-f(x_3)}{x_2-x_3}}{\frac{1}{2}(x_1-x_3)}, \quad (7.3)$$

where the error in this approximation can be derived using a Taylor expansion. Assuming  $h = x_1 - x_2$  and  $\hat{h} = x_2 - x_3$  with the spacing  $h$  and  $\hat{h}$ , we first obtain the expansions of  $\frac{f(x_1)-f(x_2)}{x_1-x_2}$  and  $\frac{f(x_2)-f(x_3)}{x_2-x_3}$ .

$$\begin{aligned} \frac{f(x_1) - f(x_2)}{x_1 - x_2} &= f'(x_2) + \frac{1}{2!} f^{(2)}(x_2)h + \frac{1}{3!} f^{(3)}(x_2)h^2 + \frac{1}{4!} f^{(4)}(x_2)h^3 + \dots, \\ \frac{f(x_2) - f(x_3)}{x_2 - x_3} &= f'(x_2) - \frac{1}{2!} f^{(2)}(x_2)\hat{h} + \frac{1}{3!} f^{(3)}(x_2)\hat{h}^2 - \frac{1}{4!} f^{(4)}(x_2)\hat{h}^3 + \dots, \end{aligned}$$

then we have

$$\begin{aligned} \frac{\frac{f(x_1)-f(x_2)}{x_1-x_2} - \frac{f(x_2)-f(x_3)}{x_2-x_3}}{\frac{1}{2}(x_1-x_3)} &= f^{(2)}(x_2) + \frac{1}{3!} f^{(3)}(x_2) \frac{h^2 - \hat{h}^2}{\frac{1}{2}(h + \hat{h})} + \frac{1}{4!} f^{(4)}(x_2) \frac{h^3 + \hat{h}^3}{\frac{1}{2}(h + \hat{h})} \\ &\quad + \frac{1}{5!} f^{(5)}(x_2) \frac{h^4 - \hat{h}^4}{\frac{1}{2}(h + \hat{h})} + \dots, \end{aligned}$$

then the error of the approximate of  $\frac{\partial^2 f}{\partial x^2}$  at  $x_2$  is given by :

$$\frac{\frac{f(x_1)-f(x_2)}{x_1-x_2} - \frac{f(x_2)-f(x_3)}{x_2-x_3}}{\frac{1}{2}(x_1-x_3)} - \frac{\partial^2 f}{\partial x^2} = \frac{1}{3!} f^{(3)}(x_2) \frac{h^2 - \hat{h}^2}{\frac{1}{2}(h + \hat{h})} + \frac{1}{4!} f^{(4)}(x_2) \frac{h^3 + \hat{h}^3}{\frac{1}{2}(h + \hat{h})} + \dots.$$

Notice, when  $h = \hat{h}$ , we have a second order approximation with  $O(h^2)$ . However, the requirement is not applied in our algorithm, hence, in general, the approximate of  $\frac{\partial^2 f}{\partial x^2}$  have the first order error  $O(h^*)$  where  $h^*$  corresponds to the maximum local spacing, i.e.  $h^* = \max(h, \hat{h})$ .

The method of three point differencing requires us to simulate three sample paths with slightly different initial prices:  $S_0 + h$ ,  $S_0$  and  $S_0 - h$  with exactly the same random increment  $\Delta W_S$  at each time  $t_i$ . Then, for a particular set of random numbers, we start by forward simulating three sample paths of underlyings using a liquid model i.e.  $\lambda = 0$  in Eq (7.1), then backward calculate the corresponding  $V_{SS}$  at each timestep

$t_i$ . Making use of the results of  $V_{SS}$ , we reproduce the three sample paths under the illiquid model of Eq (7.1), we then calculate  $V_{SS}$  from these three paths at each time point  $t_i$  and the option value  $V(0)$  at initial time. The process is iterated using these renewal values of  $V_{SS}$  for each time to obtain a convergent value of  $V(0)$ . Then the final set of  $V_{SS}$  is accepted by the particular set of random numbers. We then take the average of a (large) number of estimators of  $V(0)$  from different sets of random numbers. The general algorithm for a European call option is presented as follows:

1. Set up a discrete time framework by dividing the option's life  $T$  into  $N$  time steps, i.e.  $t_i$  for  $i = 0, 1, \dots, N$  with  $t_0 = 0$ ,  $t_N = T$  and equal increments  $t_i = t_{i-1} + \Delta t$ . Suppose there are  $M$  sample paths in total, let  $j$  be the  $j$ -th time of the simulation with  $j = 1, 2, \dots, M$ . There would be some abandoned paths during the simulation for three reasons: the underlying price is negative; the prices of the three sample paths cross at some time; and the convergent value  $V(0)$  cannot be achieved for some set of random numbers. Therefore, a counter  $m$ , with  $m = 0$  at the beginning of the simulation is used to check the number of abandoned paths during the whole simulation.
2. Initialize  $V_{SS}$  using Eq (7.1) when  $\lambda = 0$ 
  - choose one set of standard normal random variables for the  $j$ -th run of the simulation ( $j \leq M$ ):  $Z_j(t_i)$  for  $i = 0, 1, \dots, N - 1$ .
  - to calculate  $V_{SS}(t_i)$  by the finite-difference method, we have to concurrently produce three sample paths  $S_j^+(t_i)$ ,  $S_j(t_i)$  and  $S_j^-(t_i)$  rather than one path in the first-order feedback case (and standard Monte Carlo computation). Those paths can be simulated by a simple Euler discretization as follows:

$$S_j^+(t_{i+1}) = S_j^+(t_i) + rS_j^+(t_i)\Delta t + \sigma S_j^+(t_i)Z_j(t_i)\sqrt{\Delta t} ,$$

$$S_j(t_{i+1}) = S_j(t_i) + rS_j(t_i)\Delta t + \sigma S_j(t_i)Z_j(t_i)\sqrt{\Delta t} ,$$

$$S_j^-(t_{i+1}) = S_j^-(t_i) + rS_j^-(t_i)\Delta t + \sigma S_j^-(t_i)Z_j(t_i)\sqrt{\Delta t} ,$$

where  $i = 0, 1, \dots, N - 1$  and

$$S_j^+(t_0) = S_0 + h, \quad S_j(t_0) = S_0 \quad \text{and} \quad S_j^-(t_0) = S_0 - h$$

for some small increment  $h$  serves as a price space for the underlying. Notice that each path uses the same random variable  $Z_j(t_i)$  at time point  $t_i$ . Then the prices of a call option at time  $t_i$  can be directly evaluated for each path, which are:

$$V_j^+(t_i) = e^{-r(T-t_i)} \max(S_j^+(t_N) - K, 0), \quad (7.4)$$

$$V_j(t_i) = e^{-r(T-t_i)} \max(S_j(t_N) - K, 0), \quad (7.5)$$

$$V_j^-(t_i) = e^{-r(T-t_i)} \max(S_j^-(t_N) - K, 0), \quad (7.6)$$

with the strike price  $K$  and exponential discount factor  $e^{-r(T-t_i)}$ .

- approximate the corresponding  $V_{SS_j}(t_i)$  at time  $t_i$  by the three point difference method, which is given by

$$V_{SS_j}(t_i) = \frac{\frac{V_j^+(t_i) - V_j(t_i)}{S_j^+(t_i) - S_j(t_i)} - \frac{V_j(t_i) - V_j^-(t_i)}{S_j(t_i) - S_j^-(t_i)}}{\frac{1}{2}(S_j^+(t_i) - S_j^-(t_i))}, \quad (7.7)$$

for  $i = 0, 1, \dots, N - 1$ . The error in this approximation is  $O(h^2)$  as  $h \rightarrow 0$ .

Then we set these values of  $V_{SS_j}(t_j)$  as initial values used to simulate SDE (7.1) with  $\lambda > 0$ .

### 3. Back to Eq (7.1) with a non-zero $\lambda$

- substitute the initial  $V_{SS_j}(t_i)$  into Eq (7.1) and reproduce the three asset paths as follows:

$$S_j^+(t_{i+1}) = S_j^+(t_i) + rS_j^+(t_i)\Delta t + \frac{\sigma S_j^+(t_i)Z_j(t_i)\sqrt{\Delta t}}{1 - \lambda S_j^+(t_i)V_{SS_j}(t_i)}, \quad (7.8)$$

$$S_j(t_{i+1}) = S_j(t_i) + rS_j(t_i)\Delta t + \frac{\sigma S_j(t_i)Z_j(t_i)\sqrt{\Delta t}}{1 - \lambda S_j(t_i)V_{SS_j}(t_i)}, \quad (7.9)$$

$$S_j^-(t_{i+1}) = S_j^-(t_i) + rS_j^-(t_i)\Delta t + \frac{\sigma S_j^-(t_i)Z_j(t_i)\sqrt{\Delta t}}{1 - \lambda S_j^-(t_i)V_{SS_j}(t_i)}, \quad (7.10)$$

where  $i = 0, 1, \dots, N - 1$  and the same set of random variable  $Z_j(t_i)$  used in Step 2. Similar to the first-order feedback model, the underlying prices

from (7.8-7.10) could be negative when the term  $1 - \lambda SV_{SS}$  in Eq (7.1) is estimated to be nearly zero<sup>1</sup>. Therefore we discard the path by adding the counter  $m$  to  $m + 1$  once its price becomes negative and set the value of the option  $V_j(t_0) = 0$  for this run, then restart with the next run  $j + 1$  from Step 2. Otherwise, we can directly obtain the prices of the call option:  $V_j^+(t_i)$ ,  $V_j(t_i)$  and  $V_j^-(t_i)$  for each path at time  $t_i$  from Eq (7.4) to Eq (7.6).

- calculate the new  $V_{SS_j}(t_i)$  at each timestep by Eq (7.7) and record the call price  $V_j(t_0)$  at time zero. Notice that to avoid vanishing denominators in Eq (7.7), any two values of the underlying prices:  $S_j^+(t_i)$ ,  $S_j(t_i)$  and  $S_j^-(t_i)$  cannot be the same. This was not a problem when  $\lambda = 0$  in Step 2, however for a non-zero  $\lambda$ , the underlying prices estimated by Eq (7.8-7.10) could be nearly equal at some time  $t_i$ . We discard the crossed path once those values are equal and set  $m = m + 1$  and  $V_j(t_0) = 0$ , then restart the next run from Step 2. When the prices of the underlying are nearly equal, we would obtain a large value of  $V_{SS_j}(t_i)$  (namely extreme values of the Gamma), which could occur at any time  $t_i$  rather than  $t \rightarrow T$  in the Black-Scholes formula. The extreme values of Gamma could cause a sudden and considerable reduction in the total volatility of the underlying.
- repeat the above two steps to gain a new option price  $V_j(t_0)$  until the price  $V_j(t_0)$  converges, i.e. the error between the current price and the price received from last iteration is less than a prescribed tolerance  $\epsilon = 10^{-5}$ . In the algorithm we also set the maximum number of iterations as  $I_{\max} = 1000$  to save computational costs and detect non-convergent paths. If the current price  $V_j(t_0)$  is convergent before the limit  $I_{\max}$  is arrived, the current price  $V_j(t_0)$  is treated as the final price in the  $j$ -th run given by the set of random variables  $Z_j(t_i)$ ; otherwise, we discard the nonconvergent path and set the counter  $m = m + 1$  and  $V_j(t_0) = 0$ , then move to the next run  $j + 1$  which starts from Step 2 with a new set of random variables.

---

<sup>1</sup>The term cannot be zero in a discrete time framework as mentioned in Chapter 5

## 4. Estimate the Option Value

- repeat the above scheme from Step 2 to Step 3 until  $j > M$ .
- take the average of the option prices  $V_j(t_0)$  as the estimated price, i.e.

$$V_0 = \frac{1}{M-m} \sum_{j=1}^M V_j(t_0) , \quad (7.11)$$

as  $M - m$  indicates the number of those 'living' paths.

We found that this procedure could produce more invalid paths (such as crossed paths: any two of these three prices  $S_j^+(t_{i+1})$ ,  $S_j^+(t_{i+1})$  and  $S_j^+(t_{i+1})$  are equal, nonconvergent paths those that cannot produce a convergent option price after a maximum number of iteration in Step 3, negative price and large price paths in this full feedback model) than the first-order feedback case where paths are abandoned only because of the occurrence of negative prices or extremely large prices. The number of abandoned paths during simulation is discussed in more detail in Section 7.3.1. In addition, the algorithm above can also be used to pricing different financial derivatives, such as risky bonds discussed in Liu (2009).

## 7.2 Smoothed payoffs

### 7.2.1 A problem with using standard payoff functions

If the algorithm described above works correctly, we should find that the estimate  $\hat{V}_{SS}(t_0)$  converges to the corresponding real Gamma  $V_{SS}(t_0)$  from the Black-Scholes formula when  $\lambda = 0$ , which can be expressed as follows:

$$\begin{aligned} \hat{V}_{SS}(t_0) &\doteq \frac{1}{M-m} \sum_{j=1}^M [V_{SS_j}(t_0)] \\ &= \frac{1}{M-m} \sum_{j=1}^M [e^{-rT} V_{SS_j}(t_N)] \\ &= \hat{V}_{SS_j}(t_0)] \\ &\rightarrow V_{SS}(t_0) , \end{aligned}$$

for  $M \rightarrow \infty$ . However, due to the random occurrence of large values of  $V_{SS}(t_0)$ , a large number of sample paths are required to achieve the limit of  $V_{SS}(t_0)$  following the algorithm with a standard payoff function. This can be shown in the left panel of Fig 7.1(a) where a numerical example is used to illustrate how the estimate  $\hat{V}_{SS}(t_0)$  changes as  $M$  increases. In Fig 7.1(a), the estimate of  $V_{SS}(t_0)$  is nearly zero (around

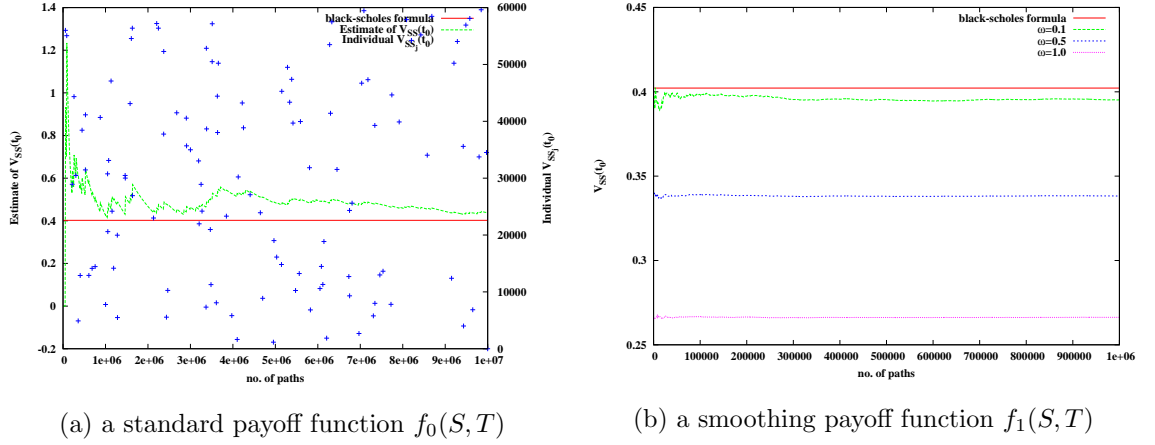


Figure 7.1: Estimate of  $V_{SS}(t_0)$  for a European call option in a perfect liquid market, i.e.  $\lambda = 0$  with a standard payoff function  $f_0(S, T) = \max(S(T) - K, 0)$  in the left panel and with a smoothing payoff function  $f_1(S, T) = \frac{K(S(T)-K+\sqrt{(S(T)-K)^2+\omega^2})}{K+\sqrt{K^2+\omega^2}}$  in the right panel under the same parameter setting:  $S(t_0) = K = 1$ ,  $r = 0.04$ ,  $\sigma = 0.2$ ,  $T = 10$ ,  $N = 2000$ .

$10^{-5}$ ) at the beginning of the simulation and it abruptly jumps to a high level of  $V_{SS}(t_0)$ , followed by a general fall before the next jump occurs. This is because, for each path  $j$ , the individual value of  $V_{SS_j}(t_i)$  estimated by Eq (7.7) is always zero for  $i = 0, 1, \dots, N - 1$ , except that those paths hit the strike price,  $K$ , i.e. satisfying the condition  $S_j^+(t_N) > K$  and  $S_j^-(t_N) < K$ . These exceptions do not happen frequently, as seen in the figure, but still result in a significant increase in the value of  $\hat{V}_{SS}(t_0)$ , when there is a limit on the number of sample paths. Such jumps affect the speed of the convergence of the estimated prices. Thus, from Fig 7.1(a), we see that  $10^6$  sample paths still cannot resolve the estimate of  $V_{SS}(t_0)$ , compared to the benchmark value given by the Black-Scholes formula. After  $10^7$  sample paths, the estimate of  $V_{SS}(t_0)$  does indeed converge to the Black-Scholes price, because these jumps have less impact on the estimate  $V_{SS}(t_0)$  over a significantly large number of sample paths.

Therefore, we seek for a way of improving of the speed the convergence of the estimate  $V_{SS}(t_i)$  for each time point,  $t_i$ .

### 7.2.2 Resolution

The problem described above arises because the standard payoff function of a European call option comprises two straight lines which intersect each other when  $S_j(t_N) = K$ . If these three paths  $S_j^+(t_i)$ ,  $S_j(t_i)$  and  $S_j^-(t_i)$  expire either in the money or out the money concurrently, then  $V_{SS_j}(t_0)$  is equal to zero<sup>2</sup>. The only possibility to gain a non-zero estimate of  $V_{SS_j}(t_0)$  occurs when  $S_j^+(t_N)$ ,  $S_j(t_N)$  and  $S_j^-(t_N)$  do not lie in the same line, i.e. the underlying price hits close to the strike price. In such a situation, the non-zero Gamma is relatively large so that there are sharp jumps on the average cumulative estimate  $\hat{V}_{SS}(t_0)$  in the figure.

To overcome this limitation of the convergence, we use a sufficiently smooth payoff function, which has a finite second derivative everywhere. We achieve this using a smoothing function, that ensures we obtain non-zero  $V_{SS}$ , which helps to enhance the illiquidity effect on the stochastic process. Following Glover (2008), we assume similar smoothing payoff functions with a parameter  $\omega$  in Table 7.1. Compared with

Model	$f_0(S, T)$	$f_1(S, T)$	$f_2(S, T)$
European Call	$\max(S - K, 0)$	$\frac{K(S-K+\sqrt{(S-K)^2+\omega^2})}{K+\sqrt{K^2+\omega^2}}$	$\frac{S-K+\sqrt{(S-K)^2+\omega^2}}{2}$
European Put	$\max(K - S, 0)$	$\frac{K(K-S+\sqrt{(S-K)^2+\omega^2})}{K+\sqrt{K^2+\omega^2}}$	$\frac{K-S+\sqrt{(S-K)^2+\omega^2}}{2}$

Table 7.1: Smoothing payoff function for different derivatives used in Glover (2008)  $f_2(S, T)$  and our model  $f_1(S, T)$ . The standard payoff function is defined as  $f_0(S, T)$ .

the Glover's payoff functions  $f_2(S, T)$  which is also used in Frey (1996), our payoff  $f_1(S, T)$  is much closer to the value given by the standard payoff function, in particular for the case of put options when the underlying price  $S = 0$ , where  $f_1(S, T)$  gives the same value  $K$  as the standard payoff function whilst  $f_2(S, T)$  cannot (see Fig 7.2(b)).

Fig 7.2 provides the different payoffs' change depends on the smoothing parameter  $\omega$ , where  $\omega = 0.0, 0.4, 0.8$  and  $1.0$ . For European put options, both smoothed payoffs

<sup>2</sup>However, computer round-off error occurs in the calculation of  $V_{SS_j}(t_0)$  for those paths with  $S_j^-(t_N) > K$ , which leads to a nearly zero estimate (around  $10^{-5}$ ) rather than zero.

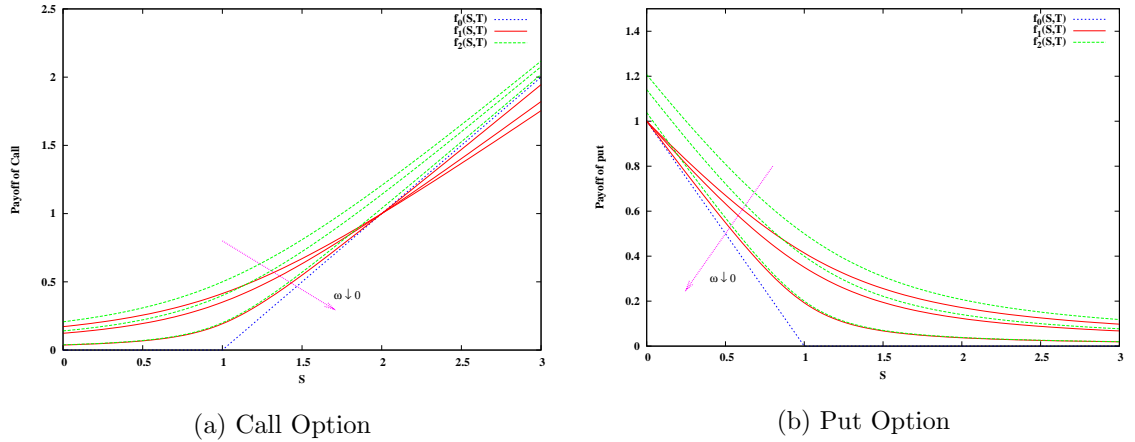


Figure 7.2: Different smoothing payoff functions depend on the illiquidity  $\omega$ , which are the standard payoff function  $f_0(S, T)$ , Glover's smoothed payoff  $f_2(S, T)$  and the modified smoothed payoff  $f_1(S, T)$ .

are higher than the standard payoff value and strictly decreasing with decreases in  $\omega$ ; for European call options, the payoff value  $f_1(S, T)$  shows different behaviours with respect to  $\omega$  in two region of  $S$ : for  $S < 2K$ , all values of  $f_1(S, T)$  lie above the standard payoff  $f_0(S, T)$  and decreasing as  $\omega$  reduces, whilst for  $S > 2K$  the smoothed function  $f_1(S, T)$  lies below  $f_0(S, T)$  and increasing as  $\omega$  reduces. We note that the largest difference between the smoothing payoffs and the standard payoff occurs at the singular point  $S = K$ . This indicates that the smoothing parameter  $\omega$  has significantly more impact on the pricing ATM options than DOTM and DITM options. To apply the smoothed payoff  $f_1(S, T)$ , we replace Eq (7.4)-(7.6) in Step 2 of Implementation (Section 7.1) with

$$\begin{aligned} V_j^+(t_i) &= e^{-r(T-t_i)} \frac{K \left( S_j^+(t_N) - K + \sqrt{(S_j^+(t_N) - K)^2 + \omega^2} \right)}{K + \sqrt{K^2 + \omega^2}}, \\ V_j(t_i) &= e^{-r(T-t_i)} \frac{K \left( S_j(t_N) - K + \sqrt{(S_j(t_N) - K)^2 + \omega^2} \right)}{K + \sqrt{K^2 + \omega^2}}, \\ V_j^-(t_i) &= e^{-r(T-t_i)} \frac{K \left( S_j^-(t_N) - K + \sqrt{(S_j^-(t_N) - K)^2 + \omega^2} \right)}{K + \sqrt{K^2 + \omega^2}}. \end{aligned}$$

Fig 7.1(b) shows the estimated values of Gamma  $V_{SS}(t_0)$  using the smoothed payoff  $f_1(S, T)$ . The convergence of the estimated  $V_{SS}(t_0)$ , which used to be problematic in the algorithm with the standard payoff  $f_0(S, T)$ , has been greatly justified. As the

value of  $\omega$  reduces to zero, the estimate of  $V_{SS}(t_0)$  approaches the value from the Black-Scholes formula.

Now we study the case of non-zero  $\lambda$  with the smoothed payoff  $f_1(S, T)$ . The estimated prices of European call and put options are presented in Table 7.2 with  $S(t_0) = K = 1$  and  $\lambda = 0.1$ . Clearly, the results are consistent with those for the

$\omega$	European Call	European Put	Deviation of PCP
0.0	0.40998	0.08043	-0.00013
0.2	0.45439	0.10457	0.02014
0.4	0.45688	0.13594	-0.00874
0.6	0.47713	0.17195	-0.02450
0.8	0.49837	0.20736	-0.03867
1	0.51658	0.24034	-0.05344

Table 7.2: The impact of  $\omega$  on the price of European options under the parameter setting:  $\lambda = 0.1$ ,  $S(t_0) = K = 1$ ,  $r = 0.04$ ,  $\sigma = 0.2$ ,  $T = 10$ ,  $N = 2000$ . The results is given by  $10^6$  simulated paths and the last column data are given by  $Dev = C + Ke^{-rT} - P - S(t_0)$ .

payoff function in Fig 7.2, which yields higher prices of ATM options if  $\omega$  is increasing. This is not surprising, because if illiquidity is small (e.g.  $\lambda = 0.1$ ), the prices of the options are mostly dominated by the smoothed payoff functions, whose values are increasing in the smoothing parameter  $\omega$ . But if larger values of  $\lambda$  are chosen (e.g.  $\lambda = 1$ ) some difficulties with the simulation procedure can arise, which is discussed in more detail in Section 7.3. In addition, Fig 7.2(a) also suggests that DITM call options  $S(t_0) > 2K$  should have an opposite effect between the option price and  $\omega$ , i.e. the price reduces as  $\omega$  increases. The last column in Table 7.2 also shows the deviation of put-call parity again exists in the full feedback model without any caps imposed on the underlying prices.

## 7.3 Problems arising from smoothed function - failure paths

In this section, with respect to the deviation of put-call parity, we will concentrate on European put options and focus on deeper analysis of failure paths when using smoothed payoff functions, computing with the dynamic of the underlying asset  $S(t)$  in Eq (7.1) and the terminal condition  $f_1(S, T)$  of the European put  $V(S, t)$  in Table 7.1.

The algorithm utilising a smoothed payoff function for the full feedback case was found to lead to two phenomena: many more abandoned paths than the first-order feedback model using the standard payoff function  $f(S, T)$  in Table 7.1, and extremely large values of the Gamma; the two phenomena are not unconnected. Because Monte Carlo simulation is based on the law of large numbers, a high number of abandoned paths does increase the cost of computation and can even contaminate the simulation, with too many paths being unusable. Our studies show there exists a relation between a smoothing parameter  $\omega$  and the illiquidity parameter  $\lambda$  chosen to reduce the path abandonment rate for the simulation.

### 7.3.1 Abandoned paths

We study the number of abandoned paths which lead to the difficulties in pricing options. There are three standard rules to judge which paths should be discarded, as explained in Section 7.1. One of these is the paths with negative or large prices due to nearly vanishing denominators of the volatility term in (7.1), which are also found in the first-order feedback model. Another is crossed paths, i.e. any two of the three prices  $S^+(t_j)$ ,  $S(t_j)$  and  $S^-(t_j)$  are nearly equal, which invalidates the calculation of the Gamma. Another is the paths which cannot provide a convergent price for the option (for example, the convergence could not be less than  $10^{-6}$  after 1000 iterations). To alleviate these failures of the algorithm, it is the best to abandon the paths once they cross, go negative, are extremely large or lead to nonconvergent. At the

same time, we count the number of abandoned paths out of all the simulated paths. Fig 7.3 shows that the abandonment rate approaches some level as the number of

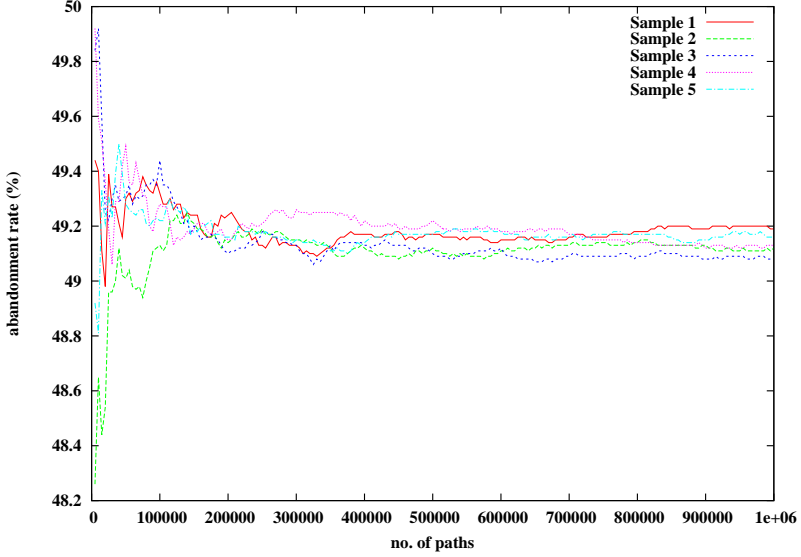


Figure 7.3: Abandonment rate of paths in pricing a European put with  $S(t_0) = K = 1$ ,  $r = 0.04$ ,  $\sigma = 0.2$ ,  $T = 10$ ,  $\lambda = \omega = 1$  and  $N = 2000$

paths increases, which the abandoned paths take up nearly 49% of all the paths in the case  $\lambda = \omega = 1$ . With the benefit of saving processing time, we can estimate the abandonment rate after  $10^5$  paths run. Table 7.3 gives a detailed breakdown of the abandonment rate when pricing a European put option. It is divided into

dt	Abandonment	Crossed	Unconvergent	Negative	Over-Cap 10
1/200	49.19	27.00	0.06	74.24	n/a
1/500	49.06	41.23	0.05	61.80	n/a
1/1000	48.95	50.34	0.05	54.38	n/a
1/200	49.28	23.17	0.03	65.66	23.56
1/500	49.15	37.25	0.04	56.88	21.06
1/1000	49.03	46.68	0.03	51.13	19.37

Table 7.3: Three Causes & Four Causes Contribution to Abandonment Paths (%) for pricing a European put with  $S(t_0) = K = 1$ ,  $r = 0.04$ ,  $\sigma = 0.2$ ,  $T = 10$ ,  $\lambda = \omega = 1$  and  $N = 2000, 5000, 10000$ . The results are given by  $10^6$  simulations based on 64-bit machines

two parts, which depend upon whether the over-capped price is considered or not. We notice that the total number of abandoned paths does not change significantly if sample paths with over-capped prices are discarded during the simulation. Without

discarding the over-capped prices, the data shows an increase in the number of abandoned paths due to the other three reasons. This implies that the abandoned paths with large prices are strictly related to the paths with negative prices, unconvvergent prices and nonconvvergent prices. Thus, some of the results in the following tests are obtained without discarding the paths with large prices.

Our experiment also confirms that abandoned paths are usually associated with changes of the sign of the denominator, i.e.  $1 - \lambda SV_{SS}$  in SDE (7.1), which is considered as an indicator. Fig 7.4 provides 16 independent samples with  $10^6$  paths

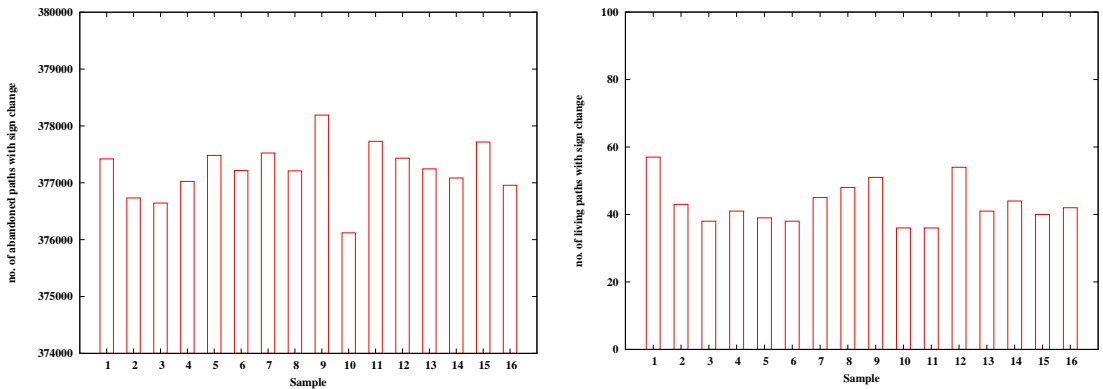


Figure 7.4: The number of abandoned (living) paths with the changes of the sign of the denominator pricing a European put with  $S(t_0) = K = 1$ ,  $r = 0.04$ ,  $\sigma = 0.2$ ,  $T = 10$ ,  $\lambda = \omega = 1$  and  $N = 2000$ . Each sample is given by  $10^6$  paths.

each. The number of the living paths that experience sign change in the denominator is normally less than 60 out of  $10^6$  sample paths, while those abandoned paths with a sign change total more than 376000, which is a high percentage (around 80%) of the total number of the abandoned paths. The results in Fig 7.4 show that the non-abandoned paths rarely change their denominators' signs, so it is intuitive to put some constraint on the denominator to avoid abandoned paths, such as  $1 - \lambda SV_{SS} > 0$ , which is mentioned by Glover (2008) with the smoothing payoff function  $f_2(S, T)$  in Table 7.1. We rewrite his model as:

$$\begin{aligned} dS &= rSdt + \frac{\sigma S}{1 - \lambda V_{SS}} dW_S , \\ V(S, T) &= \frac{1}{2}(K - S + \sqrt{(K - S)^2 + \omega^2}) , \end{aligned}$$

where the denominator of his SDE is  $1 - \lambda V_{SS}$ , assuming the illiquidity function as

the constant  $\lambda$  rather than  $\lambda S$  in our model. By the maximum principle, Glover finds a critical value of  $\lambda$  (i.e.  $\lambda = 2\omega$ ) and shows the condition:

$$\lambda < 2\omega$$

can prevent the dominator of the volatility term from vanishing. Following similar analysis, we derive the condition suitable for our case with the smoothing payoff  $f_1(S, T)$ , which is

$$\lambda S < \omega(1 + \sqrt{1 + (\omega/K)^2}) .$$

Let the upper bound for underlying price  $S$  be  $\bar{S}$ , then a relation between  $\lambda$  and  $\omega$  is given by

$$\lambda < \omega(1 + \sqrt{1 + (\omega/K)^2})/\bar{S} .$$

To demonstrate that this condition works well, Fig 7.5 illustrates abandonment rates for pricing a put option for different values of  $\lambda$  and  $\omega$ . Fig 7.5(b) is for Glover's

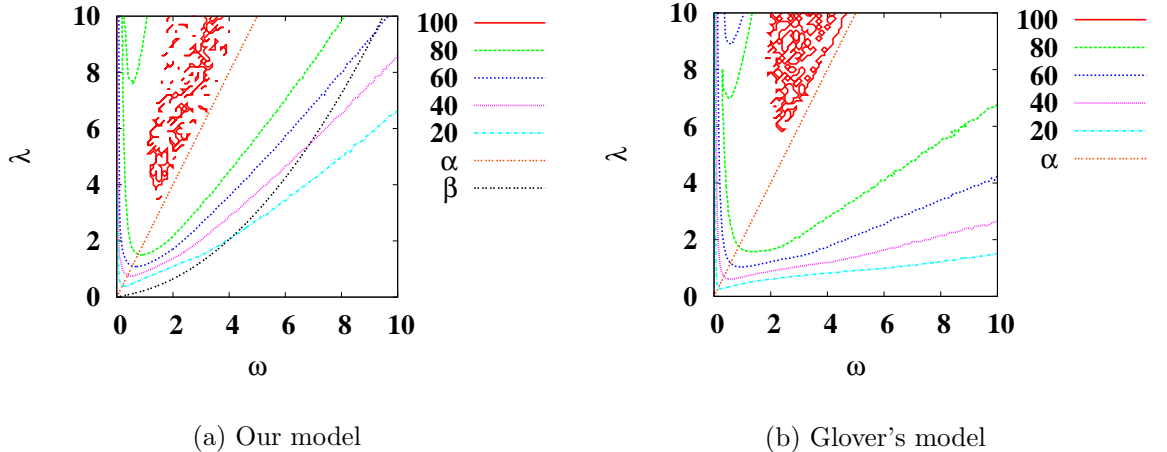


Figure 7.5: Contour figures of abandonment rate in the  $\omega$  versus  $\lambda$  plane for pricing a European put with  $S = K = 1, r = 0.04, \sigma = 0.2, T = 10, N = 2000$  and  $\bar{S} = 10$ . The red dash lines  $\alpha$  stand for the condition line  $\alpha : \lambda = 2\omega$  while the black curve  $\beta$  stands for the condition line  $\beta : \lambda < \omega(1 + \sqrt{1 + (\omega/K)^2})/\bar{S}$ . The data is given by  $10^5$  sample paths.

(2008) model and Fig 7.5(a) is ours. The contour lines with 100 correspond to 100% abandonment rate and are located in the upper-left corners of both graphs, which means the points  $(\lambda, \omega)$  lying in this area would bear the highest risk of abandonment. In the remainder of the domain, the abandonment rate is generally declining and the

‘safest’ points appear in the lower-right corner where the abandonment rate is less than 20%. In Fig 7.5, by comparison with the condition line  $\alpha$  given by  $\lambda = 2\omega$  and the line  $\beta$  given by  $\lambda = \omega(1 + \sqrt{1 + (\omega/K)^2})/\bar{S}$ , we can easily find that the condition  $\lambda < 2\omega$  excludes the contour lines with 100% rates as both of them are above the condition line  $\alpha$ . Moreover, we can apply the condition  $\lambda < \omega(1 + \sqrt{1 + (\omega/K)^2})/\bar{S}$  in Fig 7.5(a), and this condition ensures the maximum abandonment rate is less than 60%. From the two contour graphs, we can generally say that Fig 7.5(a) has fewer discarded paths because the blank area below the blue contour line with 20% is much larger than that on the right. This means our model has an advantage of producing valid paths over Glover’s model in the simulation study.

As for the discrete-time model we study here, the size of the time-step is also a factor increasing the number of abandoned paths. One way to overcome this is naturally to choose sufficiently small time-steps. For our full feedback model, Table 7.3 shows that the percentage of the total of abandoned paths is reduced slightly by reducing the time-steps  $\Delta t$ , but its effect is not significant. According to the reasons for abandoning paths, i.e. those that are crossed paths, nonconvergent paths, negative paths or over-capped paths, we found that reducing time-steps  $\Delta t$  would lead to an obvious decline in the number of negative and overcap paths as we might expect, but it would also increase the number of crossed paths. As a result, the total abandonment rates remain at the same level. In addition, nonconvergent paths are too infrequent to be considered here.

We also examine how the moneyness of options would change abandonment rates. As shown in Fig 7.6, for the fixed strike price  $K = 1$ , the abandonment rate can be shown as a convex-shape curve with respect to the spot price  $S$ , with the peak around  $S = 0.7$ , which indicates that ITM options (even ATM options) are more likely to produce the abandoned paths whilst DITM options are not. This is because for DITM options, the smoothing payoff function is much closer to the standard payoff function (see Fig 7.2(b)), then the value of  $V_{SS}$  is too small to significantly reflect the impact of the illiquidity on the underlying process. Besides the moneyness, we consider two numerical parameters in the algorithm, the increment of spot prices  $h$

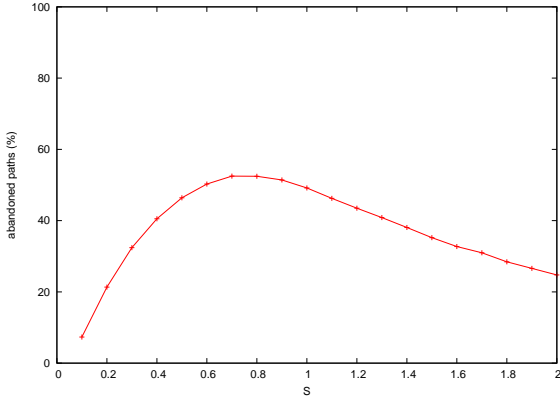


Figure 7.6: Abandonment rate of paths with different  $S$  when pricing a European put with  $K = 1, r = 0.04, \sigma = 0.2, T = 10, N = 2000$  and  $\lambda = \omega = 1$

and the tolerator  $\epsilon$  for judging the convergence of the pricing. Table (7.4) indicates  $h$  nearly has a little effect on the abandonment rate, whilst the rate increases slightly by reducing  $\epsilon$ .

Abandonment Rate (%)	Increment $h$			Abandonment Rate (%)	Tolerator $\epsilon$			
	$10^{-1}$	$10^{-3}$	$10^{-5}$		$10^{-3}$	$10^{-4}$	$10^{-5}$	$10^{-6}$
	49.54	49.33	49.32		45.71	48.92	49.67	56.41

Table 7.4: Abandonment rate of paths with different  $h$  &  $\epsilon$  when pricing a European put with  $S = K = 1, r = 0.04, \sigma = 0.2, T = 10, N = 2000$  and  $\lambda = \omega = 1$

### 7.3.2 Extreme values of Gamma

In this section, we describe more details on the interesting phenomenon of extreme large values of Gamma. When calculating Gammas by Eq (7.7), as mentioned in Section 7.1 we note that the denominator could be small enough to result in abnormally large values of Gamma when the paths become close. Fig 7.7 illustrates how this situation happens. In the left panel, we monitor a particular path with a large Gamma appearing around  $t = 7$ . The corresponding difference:  $S^+ - S$ ,  $S - S^-$  and  $\frac{1}{2}(S^+ - S^-)$  given in the right panel suggests the smallest absolute difference (around  $2.5 \times 10^{-8}$ ) should occur around  $t = 7$  (indicated by an arrow in the figure), which is consistent with the time when extreme values of Gamma show up in the left panel.

Actually, the extreme values of Gamma are caused by the smallest multiplication of these differences:  $|(S^+ - S)(S^+ - S^-)(S - S^-)|_{min}$ , rather than the differences

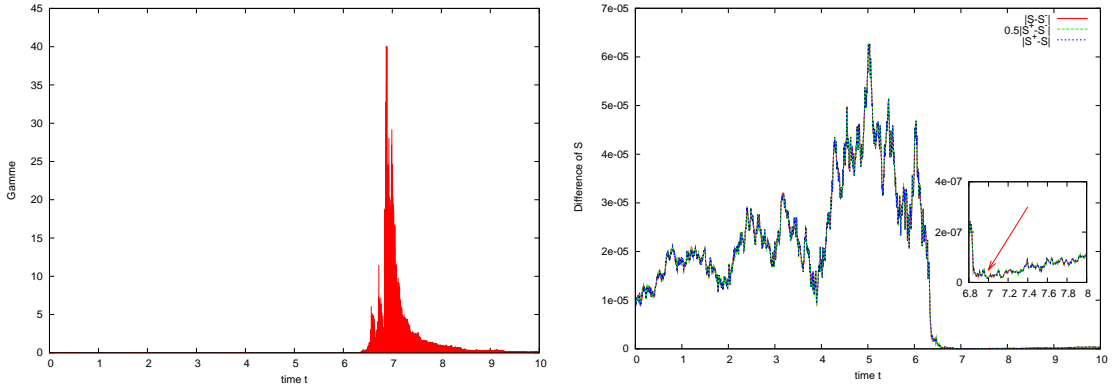


Figure 7.7: A particular path with extreme values of Gamma in pricing a European put with  $S = K = 1, r = 0.04, \sigma = 0.2, T = 10, \lambda = \rho = 1$  and  $N = 2000$

themselves:  $|(S^+ - S)|_{min}$ ,  $|(S^+ - S^-)|_{min}$  or  $|(S - S^-)|_{min}$ . Fig 7.8 gives an example to illustrate this point. For a particular path with extreme values of Gamma, in the left panel, we plot the values of Gamma against the individually differences:  $(S^+ - S)$ ,  $(S - S^-)$  and  $\frac{1}{2}(S^+ - S^-)$ . Most values of Gamma are significantly larger when the  $S$  values are close, but in this region we still find there are relatively small values of Gamma. Meanwhile, we can check the product of these differences for the same path in the right panel of Fig 7.8. When the product of differences is close to zero, the values of Gamma are certainly quite large. Hence, we can deduce that extreme values of Gamma can only be produced by the smallest value of  $|(S^+ - S)(S^+ - S^-)(S - S^-)|_{min}$ .

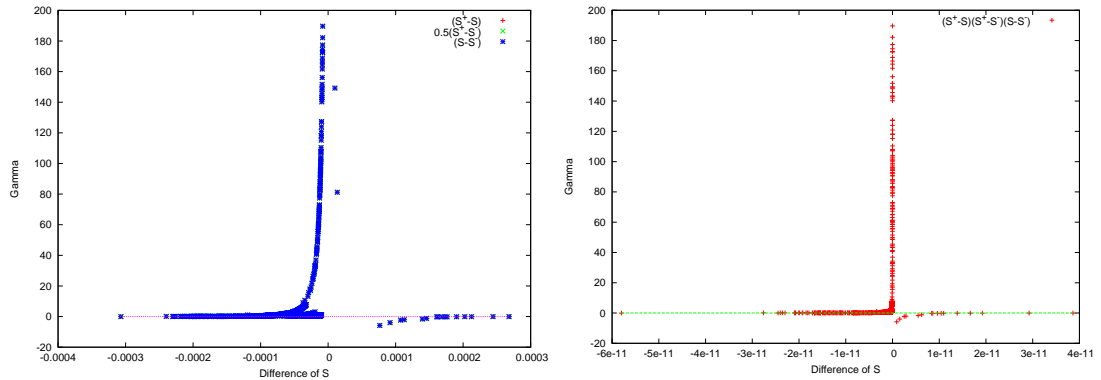


Figure 7.8: A particular path with extreme values of Gamma in pricing a European put with  $S = K = 1, r = 0.04, \sigma = 0.2, T = 10, \lambda = \rho = 1$  and  $N = 2000$

The main effect of the extreme values of Gamma on the asset process is to eliminate the volatility term of SDE (7.1) and change the risky asset to the riskless asset. For instance, the underlying price shown in the left panel of Fig 7.9 moves like a riskless asset before  $t = 5.5$  and then follows a stochastic process. This strange movement is explained by the right panel, which shows the existence of extreme values of Gamma in the corresponding time horizon. The ‘Extra Values of Gamma Effect’ could be used to realize more specific financial circumstance in practise. Moreover,

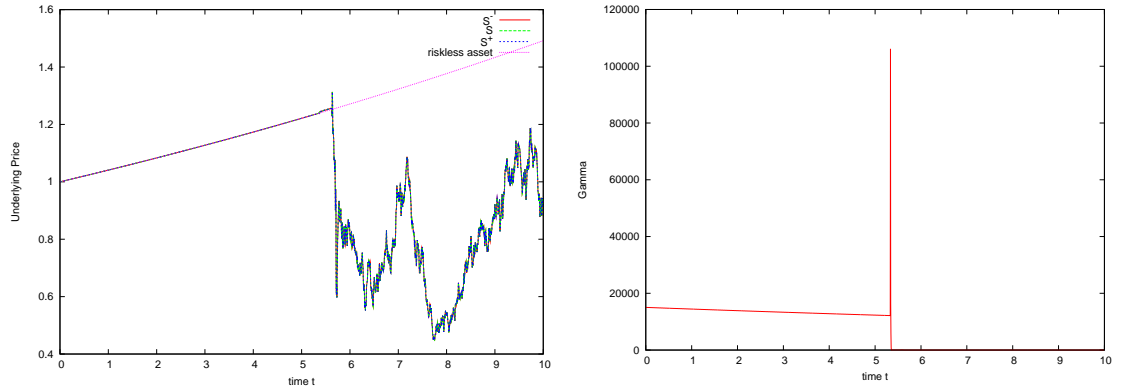


Figure 7.9: A particular path with extreme values of Gamma in pricing a European put with  $S = K = 1, r = 0.04, \sigma = 0.2, T = 10, \lambda = \rho = 1$  and  $N = 2000$

Fig 7.10(a) describes a cumulative distribution of extreme values of Gamma on different time intervals using  $10^5$  sample paths. The histogram has a lower peak in the middle, and higher values on the right side than the left side, which means it is more likely that extreme values of Gamma occur when options are close to maturity. We also investigate the maximum size of the Gammas along each path. The result presented in the Fig 7.10(b) shows the largest concentration of Gammas is in the range  $[10 : 100]$ , and the observation of extremely large values of Gamma (larger than  $10^5$ ) is rare.

The extreme values of Gamma effect also contributes to the number of abandoned paths in the algorithm. Once the value of Gamma was extremely large (for example  $|V_{SS}(t_i)| > 100$ ), the denominator always changed from positive to negative. As mentioned earlier in Section 7.3.1, a change in sign of the denominator  $1 - \lambda S V_{SS}$  in the simulation would usually be found in abandoned paths rather than living

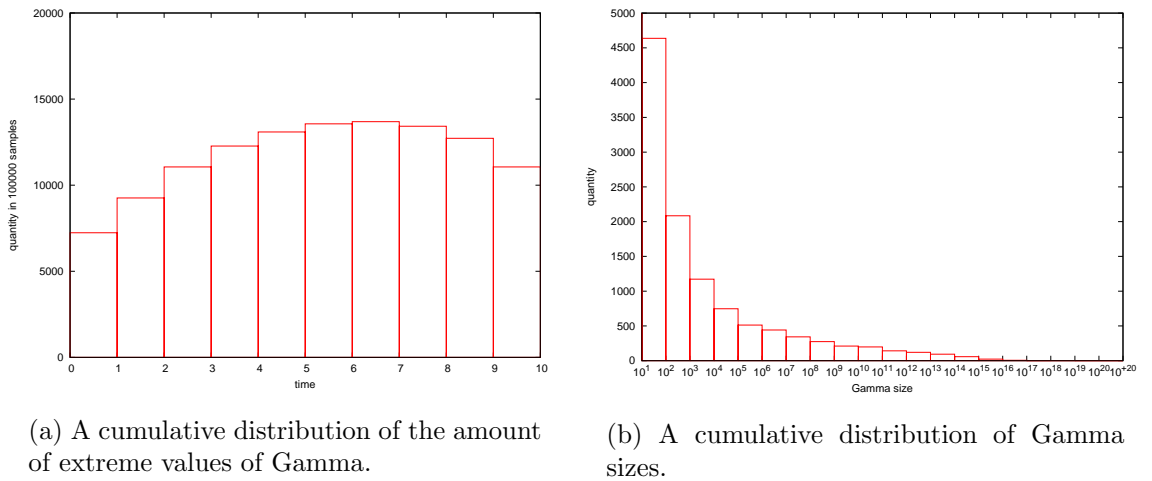


Figure 7.10: A test by  $10^5$  sample paths with  $S = K = 1, r = 0.04, \sigma = 0.2, T = 10, \lambda = \rho = 1$  and  $N = 2000$

paths. For large values of Gamma (says  $10 \leq V_{SS}(t_i) \leq 100$ ), if the sign does not change, we can still suppose that these Gammas allow more chances for a nearly zero denominator:  $1 - \lambda S V_{SS} \rightarrow 0$ , which could lead to a abandoned path. In such a case, there would be a significant increase in the volatility term, which would make the underlying price suddenly rise above a common price level or drop to a negative price. When there is a drop in the underlying price, the order of  $S^+ > S > S^-$  would be disrupted, as the highest price  $S^+$  reduces more sharply than the other two, so these three paths would be more lively to cross each other (intersect) in the future simulation. Consider both the range of the extreme values of Gamma. Intuitively, we may anticipate there exists a relationship between the extreme values of Gamma and the number of abandoned paths. Fig 7.11 indicates the number of abandoned paths and the number of living paths associated with extreme values of Gamma over total  $10^6$  sample paths in multiple independent tests (17 times). Similar to the results of the sign of the denominator shown in Fig 7.4, we find that in the  $10^6$  simulation paths for each test, there were few living paths with extreme values of Gamma (less than 60) but a large number of the abandoned paths with extreme values of Gamma, which is higher than 50% of the total number of the abandoned paths. This strongly suggests that most paths where large values of Gamma occur could always be abandoned.

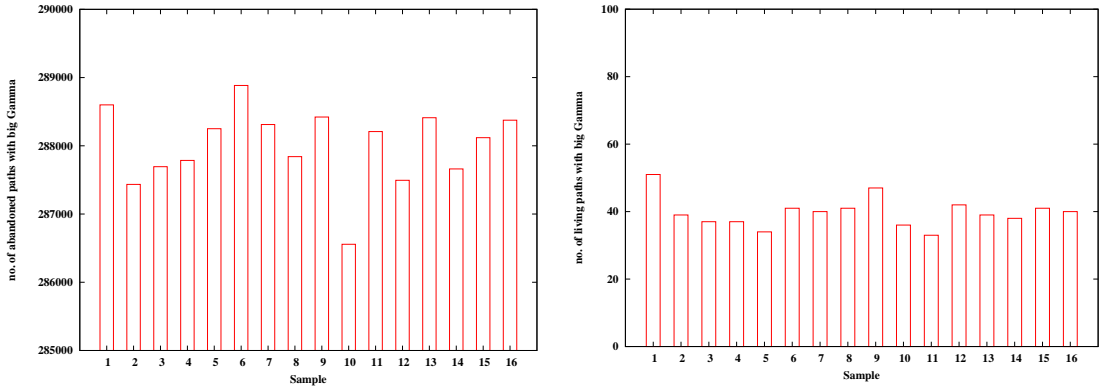


Figure 7.11: The number of abandoned (living) paths with extreme values of Gamma in pricing a European put with  $S(t_0) = K = 1$ ,  $r = 0.04$ ,  $\sigma = 0.2$ ,  $T = 10$ ,  $\lambda = \omega = 1$  and  $N = 2000$ . Each sample is given by  $10^6$  paths.

## 7.4 Illiquidity $\lambda$ impact on pricing option

In this section, we investigate an impact of illiquidity on the option prices using a standard payoff or a smoothed payoff. We also check if estimated prices of call and put options satisfy put-call parity. As shown in Glover (2008), put-call parity should still hold in the full feedback model. Following PDE (7.2), we find that the non-linear PDE differs from the standard Black-Scholes PDE only as the volatility term, which is a function of the stock price and the second derivatives for the option price, i.e.  $\sigma = \sigma(t, S, V_{SS})$ . Since the second derivative of the put and call options coincide, the put-call parity should still hold in our full feedback model.

### 7.4.1 Option pricing with standard payoffs

We start with illiquidity  $\lambda$  effects on pricing European options with standard payoff functions  $f_0(S, T)$  in Table 7.1. As mentioned in Section 7.2, the standard payoffs can cause extremely small values of Gamma, which will eliminate illiquidity effects on pricing options. Fig 7.12 shows how the option price changes with respect to the different  $\lambda$  (0, 0.5, 1, 3 and 5) under the parameter setting:  $S = K = 1$ ,  $r = 0.04$ ,  $\sigma = 0.2$ ,  $T = 10$ ,  $N = 2000$  and  $h = \epsilon = 10^{-5}$ . Even without any caps on underlying prices, both option prices converge to a particular value as the number of paths  $M$  increases, which indicates our algorithm is reliable and valid. It also suggests

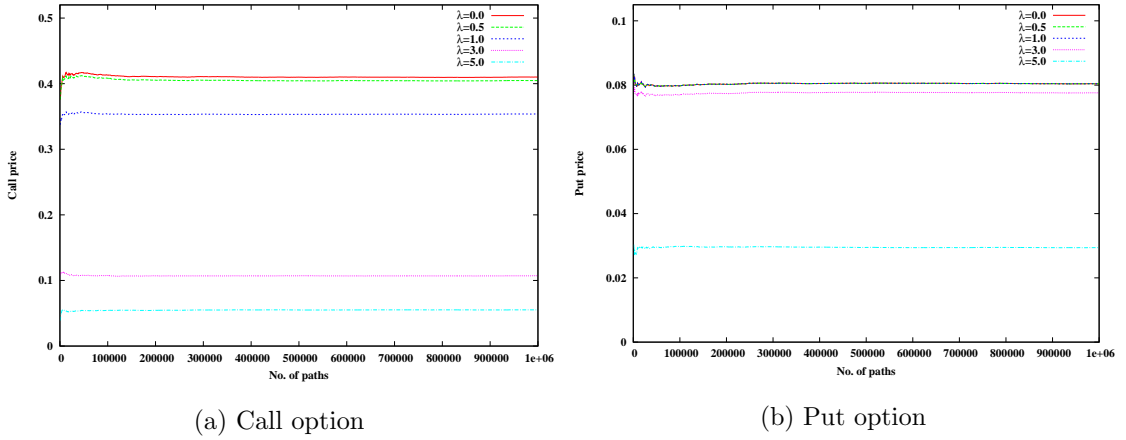


Figure 7.12: European option prices depend on the illiquidity  $\lambda$ . Note the green line with  $\lambda = 0.5$  is close to the red line with  $\lambda = 0.0$  in the case of call & the three lines: blue ( $\lambda = 1$ ), green ( $\lambda = 0.5$ ) and red ( $\lambda = 0.0$ ) are close in the case of put.

that there is a negative correlation between the option price and the illiquidity  $\lambda$ , i.e. the option price is lower with the larger  $\lambda$ . This is because with  $\lambda$  in the denominator  $1 - \lambda SV_{SS}$  of the volatility term, larger  $\lambda$  would make the magnitude of the denominator larger than one, then the volatility be reduced, so the option price would be lower. However, for those small values of  $\lambda$ , such as  $\lambda = 0.5$ , from Fig 7.12 the option price for the illiquidity model is much closer to the option price in the perfectly liquid market. As the standard payoff function  $f_0(S, T)$  is applied here, the illiquidity model frequently produces nearly zero Gammas if the underlying price does not hit the strike price at maturity. This results in little illiquidity effect on the underlying dynamics, and is also the reason we suggest for using the smoothed payoff function  $f_1(S, T)$  rather than the standard payoff function  $f_0(S, T)$ .

We test more values of  $\lambda$  and show these results in Fig 7.13. It is clear that  $\lambda$  in the range  $[0, 1]$  makes little impact on the put option value and only a slight difference on the call's value. As  $\lambda$  increases the call price is reduced much more than the corresponding put prices, which results in the usual problems with call-put parity. As shown in Fig 7.13, the deviation from put-call parity is due to the sharp decrease in the price of the call option. This also implies that large prices of the underlying would not be a problem in the full feedback model, so using a cap to control the

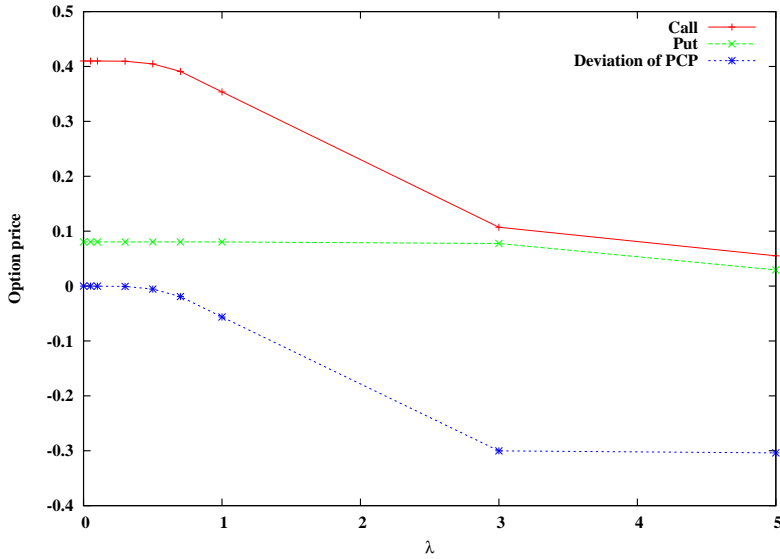


Figure 7.13: European option price depends on the illiquidity  $\lambda$ : 0, 0.1, 0.3, 0.5, 0.7, 1, 3 and 5 and the corresponding violation of put-call parity. We use the same parameter setting as Fig 7.12. All points are produced by  $10^6$  sample paths.

underlying price which is applied in the first-order feedback model is not a means to solve the put-call parity problem. Under the same parameter setting, Table 7.5 provides the total number of abandoned paths and the number of abandoned paths with respect to different effects during the simulation. The number of abandoned paths for the call option price evaluation is generally much higher than that of the put option. The data in the ‘Abandonment’ column shows there is a significant increase in the number of abandoned paths as  $\lambda$  becomes larger. For the case of  $\lambda = 5$ , the abandonment rate is up to 54% for call options and 28% for put options. Among the three different reasons listed in the table, the cause of ‘negative’ paths has the highest percentage, especially for larger values of  $\lambda$ , for which over half of the abandoned paths are discarded as they produce negative prices. For small values of  $\lambda$ , there are no abandoned paths but the corresponding option prices in Fig 7.13 are shown to be close to the Black-Scholes price. From Fig 7.13 and Table 7.5, it is suggested that the option price is related to the number of abandoned paths, which is that the more abandoned paths we obtain in the simulation, the lower option prices are estimated.

$\lambda$	Abandonment	Crossed	Unconvergent	Negative
0	0(0)	0(0)	0(0)	0(0)
0.05	7(0)	0(0)	7(0)	0(0)
0.1	3(0)	0(0)	2(0)	1(0)
0.3	49(0)	0(0)	18(0)	31(0)
0.5	970(0)	11(0)	132(0)	827(0)
0.7	4922(0)	83(0)	314(0)	4528(0)
1	21747(0)	569(0)	1402(0)	1.981e+04(0)
3	401025(41014)	2.348e+04 (1797)	1.327e+05 (1.738e+04)	2.469e+05 (2.218e+04)
5	541575(279926)	3.496e+04 (3.068e+04)	2.366e+05 (8.966e+04)	2.73e+05 (1.619e+05)

Table 7.5: The number of the abandoned paths in the full feedback model with constant  $\lambda$ . The data in parentheses stand for put options and others for call options.

We also examine the effect of  $\lambda$  on option pricing in the five moneyness categories: DITM, ITM, ATM, OTM and DOTM, and relative results with a liquid model. In Fig 7.14, we compare the ranges between the illiquid prices ( $\lambda = 1$ ) and the liquid prices ( $\lambda = 0$ ) given by the Black-Scholes formula for variant moneyness and indicate their percentage reduction due to illiquidity. Consistent with the liquid market, a higher spot price,  $S$ , raises the price of call options in the illiquid market. The reduction indicated in the figure decreases as the moneyness ( $S/K$ ) of the option decreases, which suggests that the impact of  $\lambda$  is most pronounced for DITM options. For DOTM options, due to the standard payoff function, it is more likely that  $V_{SS} \approx 0$  which will eliminate the illiquidity effect so that there is little difference between our model and the standard Black-Scholes model. Intuitively, if one sells a DOTM option which is most likely to be valueless at maturity, she does not need to trade any more shares to hedge the option so that in this sense the market is perfectly liquid without the large trading volume.

### 7.4.2 Option pricing with smoothed payoffs

We now consider the impact of  $\lambda$  on option pricing when the option payment is set as a smoothing function  $f_1(S, T)$  in Table 7.1, instead of the standard payoff  $f_0(S, T)$ . As discussed in Section 7.3.1, there exists a restriction for  $\lambda$  and the smoothing

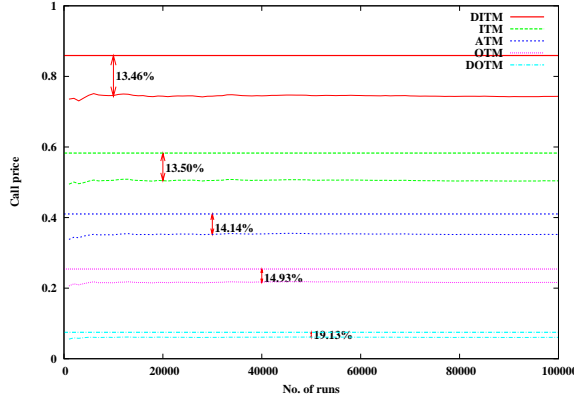


Figure 7.14: Pricing a European Call Option in various moneyness: DITM ( $S = 1.5$ ), ITM ( $S = 1.2$ ), ATM ( $S = 1.0$ ), OTM ( $S = 0.8$ ) and DOTM ( $S = 0.5$ ) in a liquid market (thicker lines) or an illiquid market (thinner lines). The following parameters are used:  $K = 1.0$ ,  $\rho = 1.0$ ,  $T = 10$ ,  $r = 0.04$  and  $\sigma = 0.2$

parameter  $\omega$  to avoid a number of abandoned paths through our path generation algortihem, which is:

$$\lambda < \omega(1 + \sqrt{1 + (\omega/K)^2})/\bar{S} .$$

There are rarely abnormally large prices of the underlying asset found to affect the convergence of pricing option in the full feedback model. We can generally assume  $\bar{S} = 10$  to approximate a non-abandoned range of  $\lambda$  using the above inequality. Then, for two kinds of smoothing parameters: a small value  $\omega = 0.1$  and a slightly large value  $\omega = 1.0$ , the inequality suggests the non-abandoned range of  $\lambda$ :  $\lambda < 0.020$  and  $\lambda < 0.241$  respectively. Following the discussion on the standard payoffs, we illustrate a similar example using a smoothing function in Fig 7.15 and Table 7.6.

The results in Table 7.6 show that when  $\lambda$  is small enough, i.e.  $\lambda$  lies in the non-abandoned range, simulations generate few abandoned paths, but the option prices given by these  $\lambda$  are much closer to the prices given by  $\lambda = 0$ , as shown in Fig 7.15. When  $\lambda$  lies beyond this range, some simulated paths have been abandoned and the number of abandoned paths increases greatly with an increase in  $\lambda$ . The option prices given by these values of  $\lambda$  are apparently quite different from the price for  $\lambda = 0$ . When  $\omega = 0.1$ , both call and put option prices increase slightly, and then generally decrease. For larger values of  $\lambda$ , such as 3 or 5, both options become valueless and also a large number of abandoned paths arise in the simulation. This

$\lambda$		$\omega = 0.1$			$\omega = 1.0$				
		Abandoned	Crossed	Unconvergent	Negative	$\lambda$	Abandoned	Crossed	Unconvergent
0	0	0	0	0	0	0	0	0	0
0.005	0	(0)	(0)	(0)	(0)	0.05	(0)	(0)	(0)
	0	(0)	(0)	(0)	(0)	0	(0)	0	(0)
0.01	0	0	0	0	0	0.1	854	78	788
	0	(0)	(0)	(0)	(0)	0	(0)	0	(0)
0.02	604	23	71	515	0.2	87710	1.242e+04	34	7.688e+04
	(244)	(21)	(85)	(143)	(124)	(8)	(4)	(4)	(114)
0.03	6930	309	1967	4692	0.3	360738	7.559e+04	99	2.946e+05
	(3526)	(9189)	(1481)	(1879)	(4284)	(421)	(24)	(24)	(3860)
0.04	22767	1118	9522	1.228e+04	0.4	588848	1.369e+05	212	4.682e+05
	(13673)	(835)	(7002)	(5928)	(25356)	(4037)	(74)	(74)	(2.137e+04)
0.05	49631	2492	2.678e+04	2.064e+04	0.5	670870	1.571e+05	194	5.315e+05
	(31703)	(2547)	(1.822e+04)	(1.117e+04)	(71276)	(1.619e+04)	(66)	(66)	(5.563e+04)
0.1	121721	9965	6.892e+04	4.366e+04	0.6	720984	2.115e+05	268	5.249e+05
	(99930)	(2.063e+04)	(4.988e+04)	(3.109e+04)	(138798)	(4.021e+04)	(45)	(45)	(1.001e+05)
0.3	220731	3.735e+04	7.545e+04	1.102e+05	0.7	758066	2.983e+05	398	4.761e+05
	(146794)	(4.506e+04)	(1.285e+04)	(9.241e+04)	(221077)	(7.672e+04)	(59)	(59)	(1.479e+05)
0.5	307497	7.576e+04	6.314e+04	1.725e+05	0.8	787800	3.396e+05	968	4.628e+05
	(183205)	(7.387e+04)	(1.914e+04)	(9.365e+04)	(312176)	(1.032e+05)	(57)	(57)	(2.134e+05)
0.7	439932	1.114e+05	6.036e+04	2.74e+05	0.9	812254	3.264e+05	1876	5e+05
	(221872)	(9.63e+04)	(3.839e+04)	(9.061e+04)	(404800)	(1.132e+05)	(114)	(114)	(2.964e+05)
1.0	668473	1.633e+05	6.015e+04	4.551e+05	1.0	832763	2.968e+05	2124	5.557e+05
	(281534)	(1.205e+05)	(6.6e+04)	(9.86e+04)	(491230)	(1.327e+05)	(178)	(178)	(3.647e+05)
3.0	814978	2.144e+05	7.291e+04	5.427e+05	3.0	971685	1.362e+05	1353	8.501e+05
	(600169)	(2.723e+05)	(1.382e+05)	(1.98e+05)	(966976)	(4.657e+05)	(1.059e+04)	(1.059e+04)	(5.092e+05)
5.0	844152	2.197e+05	6.712e+04	5.721e+05	5.0	955909	9.326e+04	3.426e+04	8.384e+05
	(634821)	(2.948e+05)	(1.343e+05)	(2.17e+05)	(989314)	(4.62e+05)	(1.797e+04)	(1.797e+04)	(5.302e+05)

Table 7.6: The number of the abandoned paths for European options in  $10^6$  sample paths. The data in parentheses stand for put options and others for call options.

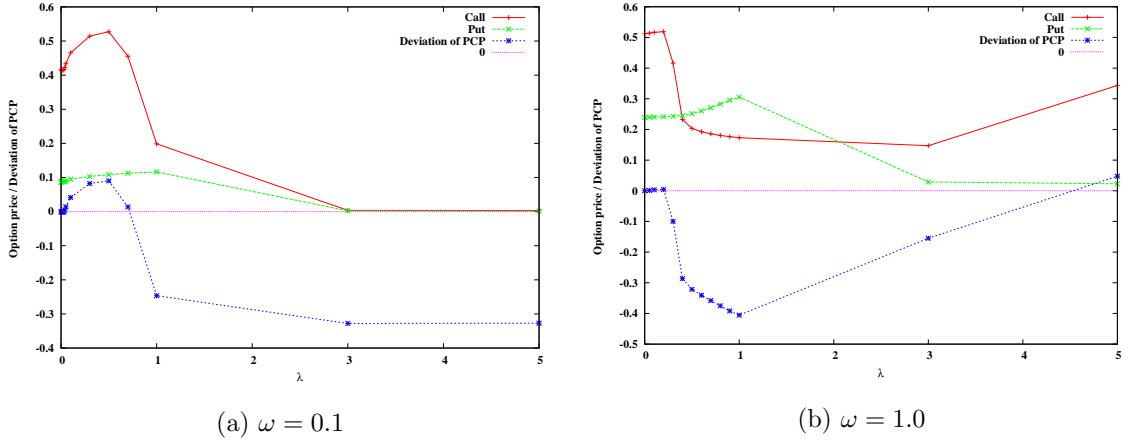


Figure 7.15: European option prices depend on the illiquidity  $\lambda$  and the deviation from put-call parity.

can be explained because, in a highly illiquid stock market, the movement of stock price depends on hedging strategies by market traders, which leads to related option market breakdown. When  $\omega = 1.0$ , Table 7.6 shows the underlying price processes are more sensitive to values of  $\lambda$  in that some  $\lambda$  cause over 95% abandonment rate, which is so poor as to be almost meaningless. This is a potential reason why we obtain irrational behaviour of option prices presented in Fig 7.15(b). When  $\omega = 1$ , the value of ATM call option could become lower than the responding value of the put option for some values of  $\lambda$ , which indicates that the put-call parity fails to hold.

With regard to the put-call parity, we derive a modified relationship between call and put options related to the smoothing payoff  $f_1(S, T)$  with  $\omega > 0$ , as follows:

$$C + \Psi(K, \omega)Ke^{-rT} = P + \Psi(K, \omega)S(t_0) , \quad (7.12)$$

where

$$\Psi(K, \omega) = \frac{2K}{K + \sqrt{K^2 + \omega^2}} < 1 .$$

Then, the deviation from modified put-call parity is estimated by:

$$Dev := C + \Psi(K, \omega)Ke^{-rT} - P - \Psi(K, \omega)S(t_0) . \quad (7.13)$$

Note that the results shown in Fig 7.15 are evaluated without using any caps in the simulation, then we can calculate the deviation by Eq (7.13). Otherwise, another form

of put-call parity for a barrier option should be considered (see details in Wilmott, 2007). As Fig 7.15 shows the deviation is negative for the most chosen values of  $\lambda$  except for some values of  $\lambda$ , such as 0.5 in the case of  $\omega = 0.1$ .

To show the over-capped price is not a significant factor to the deviation from put-call parity, we test how a cap  $\bar{S} = 10$  works in the case of  $\lambda = 0.5$  and  $\omega = 0.1$ . Fig 7.16 indicates that using the cap the value of call option has been slightly reduced

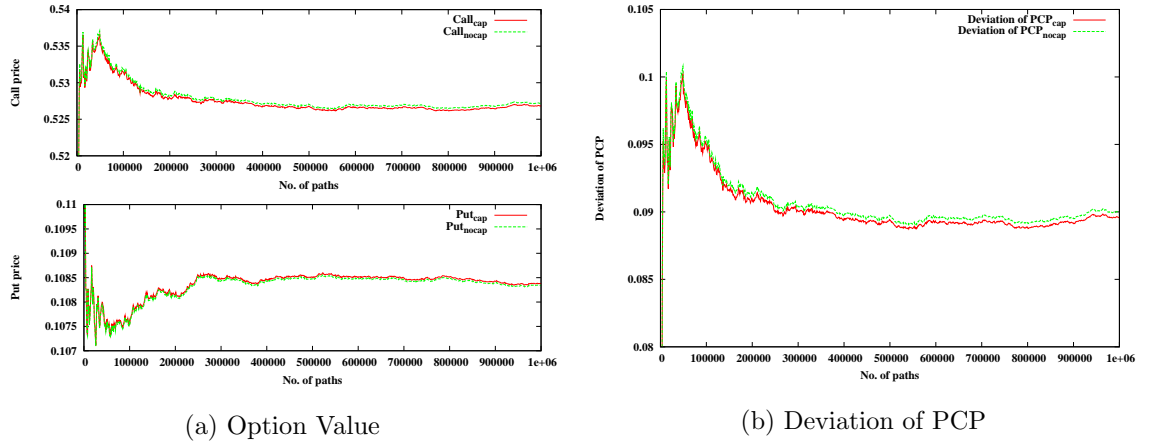


Figure 7.16: Comparison of European option prices and the corresponding deviation of the put-call parity between full feedback model with a cap  $\bar{S} = 10$  and without any caps. The other parameters are the same values as Fig 7.15.

while the value on put options is minimal. As a result, the deviation from put-call parity is less than the model without any caps. However, the deviation presented in Fig 7.16 is still too large to be acceptable. For the negative values of deviation, the capping apparently does not work, which means that capping is not an efficient way to reduce the bias from the put-call parity in the full feedback model.

Fig 7.17 shows the histogram<sup>3</sup> of the log returns in the full feedback model with  $\lambda = 1$ , which is calculated separately for call and put options by  $10^5$  sample paths. Compared with the exact probability density function for  $\lambda = \omega = 0$  indicated by green lines in the figure, we find that when  $\omega = 0$  the histogram of the call option is only slightly different from the density function, while the histogram of the put option perfectly fits the density function. Thus, the distributions of the lognormal return for call and put options are so close to each other that the option prices estimated by

<sup>3</sup>This illustration is motivated by Heston (1993)

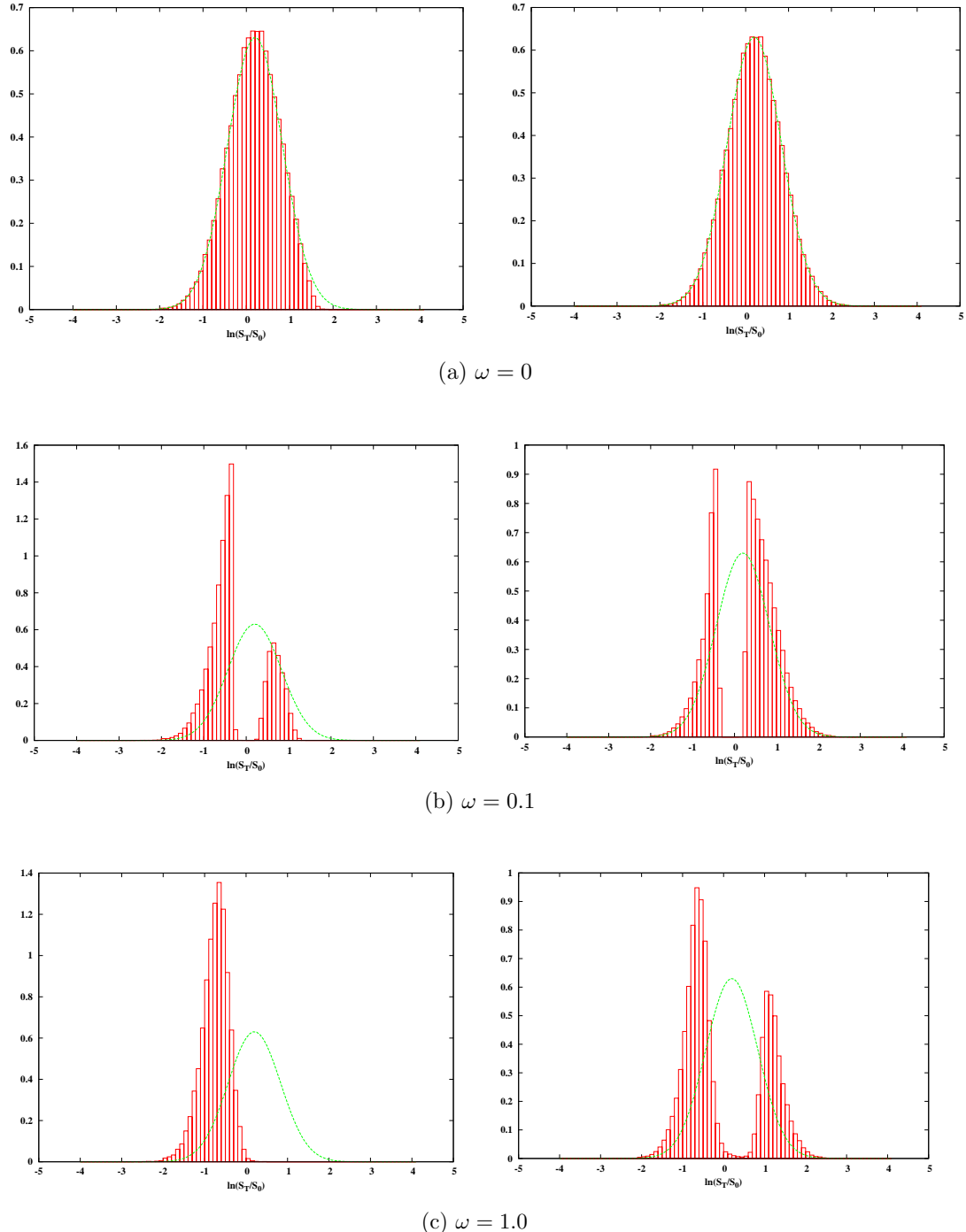


Figure 7.17: Histogram for  $\ln(S_T/S_0)$  from  $10^5$  sample paths, with lognormal density function for perfect liquid assets, i.e.  $\lambda = \omega = 0$ . Top:  $\omega = 0$ , middle:  $\omega = 0.1$  and bottom:  $\omega = 1$ .

this pair of  $\lambda$  and  $\omega$  almost satisfy put-call parity, as shown in Fig 7.13. However, the problem as mentioned in Section 7.4.1 is that using a standard payoff rarely realises the impact of illiquidity on the price moves. When non-zero smoothing parameters are applied, the histograms for the illiquid market are significantly different from the curve of the density function for the perfectly liquid market, which shows that the smoothed payoff aids modelling the effect of illiquidity on the movement of stock prices. In the standard Black-Scholes model, the stock price change is unrelated to the strike price of options. However, from the histograms, we find in the full feedback model, the stock price at maturity rarely hits the strike price<sup>4</sup>, and the terminal stock price  $S_T$  is more likely less than the strike price when pricing call options and greater than the strike prices when pricing put options. This suggests that the full feedback model tends to produce a lower option price as the stock price tends to move in the direction where the option will expire worthless. It is also seen that there are two distinct histograms for pricing call and put options. Moreover, the distinction for  $\omega = 1$  is more obvious than for  $\omega = 0.1$ . To put it another way, we check the prices of both options using the exact same values of Gamma  $V_{SS}$  which are calculated using the put option value at each time step, because from Fig 7.17 the distribution of histogram given by a put option is nearly symmetric around zero when  $\omega = 0.1$ . The results of the option values shown in Fig 7.18 indicate that the bias from put-call parity is clearly not equal to zero, so the estimated prices using the same values of  $V_{SS}$  still cannot satisfy put-call parity. However, as we apply the same values of  $V_{SS}$ , the bias of put-call parity given in Eq (7.13) can be written as follows:

$$\begin{aligned}
 Bias &= \frac{1}{M-m} \sum_{i=1}^{M-m} f_1^c(S_T^i) e^{-rT} - \frac{1}{M-m} \sum_{i=1}^{M-m} f_1^p(S_T^i) e^{-rT} \\
 &\quad + \Psi K e^{-rT} - \Psi S_0 \\
 &= \frac{1}{M-m} \sum_{i=1}^{M-m} \Psi(S_T^i - K) e^{-rT} + \Psi K e^{-rT} - \psi S_0 \\
 &= \frac{1}{M-m} \sum_{i=1}^{M-m} \Psi S_T^i e^{-rT} - \Psi S_0
 \end{aligned}$$

---

<sup>4</sup>In Fig 7.17, we assume the strike price  $K = 1$  for call and put options.

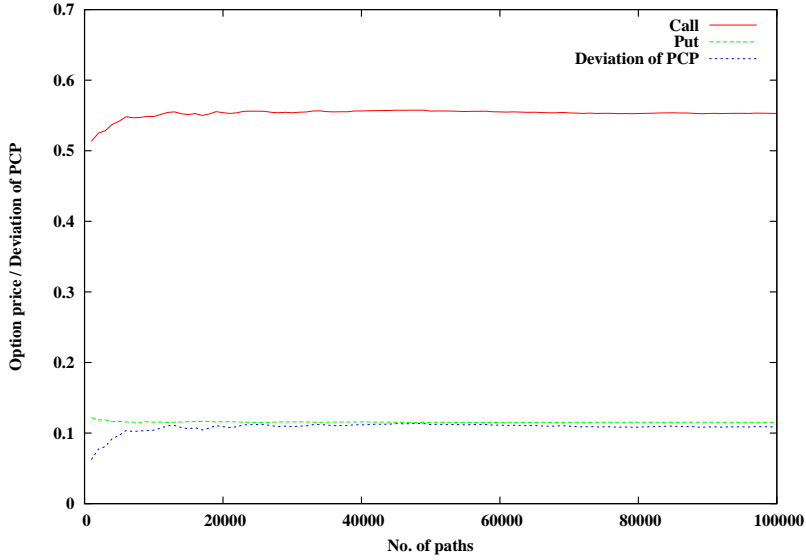


Figure 7.18: European option prices and the corresponding deviation of the put-call parity when the same values of  $V_{SS}$  are used in the full feedback model. We assume  $\lambda = 1$ ,  $\omega = 0.1$  and cap  $\bar{S} = 10$ ; the other parameters are the same values as Fig 7.17.

$$= \Psi e^{-rT} \left( \frac{1}{M-m} \sum_{i=1}^{M-m} S_T^i - S_0 e^{rT} \right) ,$$

where  $f^c$  and  $f^p$  indicate the smoothing payoffs for call and put options;  $M$  is the total number of sample paths and  $m$  is the number of abandoned paths among the total samples. The bias observed from the previous examples implies that

$$\frac{1}{M-m} \sum_{i=1}^{M-m} S_T^i \neq S_0 e^{rT} .$$

Therefore, to ensure the put-call parity holds, we introduce a new parameter called ‘implied rate’  $\hat{r}$  instead of  $r$ , such that

$$\hat{r} = \frac{1}{T} \ln \left( \frac{1}{M-m} \sum_{i=1}^{M-m} S_T^i / S_0 \right) ,$$

which gives the put-call parity in the form:

$$C + \Psi(K, \omega) K e^{-\hat{r}T} = P + \Psi(K, \omega) S(t_0) .$$

This parity will definitely hold and the ‘implied rate’  $\hat{r}$  arises because the riskless rate,  $r$ , fails to work in the full feedback illiquidity market.

## 7.5 Summary

This chapter introduces the full feedback model and illustrates the implementation of Monte Carlo. An alternative payoff function has been suggested in our algorithm. Compared with a standard payoff, it has been shown to produce a more convergent estimate of option price. However, the smoothed payoff might lead to an increase in the number of abandoned paths in the simulation. We have given a proper range that a smoothing parameter  $\omega$  should be chosen from, which is dependent on the illiquidity  $\lambda$ . We also present a detailed analysis of the impact of  $\lambda$  on option pricing with respect to the standard and smoothed payoffs, respectively. In addition, we discuss the existence of put-call parity in the simulation case.

In the next chapter, stochastic illiquidity is introduced into the full feedback model and a similar analysis is investigated.

# Chapter 8

## Full Feedback Model with Stochastic Illiquidity

In this section, we extend the full feedback model in Chapter 7 by introducing stochastic illiquidity. Following a similar analysis made in Chapter 6, we obtain the system of stochastic differential equation for the new model, which is:

$$dS = rSdt + \frac{\sigma S}{1 - \lambda SV_{SS}} dW , \quad (8.1)$$

$$d\lambda = \kappa(\theta - \lambda)dt + \rho\zeta\sqrt{\lambda}dW + \sqrt{1 - \rho^2}\zeta\sqrt{\lambda}d\bar{W} , \quad (8.2)$$

where  $W$  and  $\bar{W}$  are two independent Brownian motions.

### 8.1 Implementation

The valuation algorithm for option pricing under the stochastic processes (8.1) and (8.2) is based on the algorithm introduced in Chapter 7 which is extended to a two-dimensional framework with stochastic illiquidity  $\lambda$ . It consists of the following steps: initialize Gamma values  $V_{SS_i}$  at each discrete time points  $t_i$ ,  $i = 0, 1, \dots, N$  from the corresponding liquid asset paths ( $\lambda = 0$ ) with a set of  $N$  standard normal random numbers  $Z_i$ ; generate three illiquid asset paths (8.1) with the exact same random increment  $dW_i = \sqrt{dt}Z_i$  but with slightly different initial prices  $S_0 + h$ ,  $S_0$  and  $S_0 - h$ , and simulate a correlated sample path of the illiquidity movement (8.2)

with two independent sets of random variables  $Z_i$  and  $\bar{Z}_i$ ; estimate the option price from the valid asset paths, i.e. those paths are positive, convergent and never cross. The algorithm can be briefly described as follows:

1. Choose  $N$  time steps with equal size  $\Delta t$ , i.e.  $t_{i+1} = t_i + \Delta t$ ,  $i = 0, 1, \dots, N$ .

Set the total number of runs as  $M$ , then  $S_{ij}$  and  $\lambda_{ij}$  denote the asset price and the illiquidity at time  $t_i$  in the  $j$ -th run, where  $j = 1, 2, \dots, M$ . Add a counter  $m$  of the number of invalid paths during the simulation. Define the difference of the initial prices of the underlying asset as  $h$  and the convergence tolerance of option prices as  $\epsilon$  in each run, which  $h$  and  $\epsilon$  are both small values.

2. Initialize  $V_{SS_{ij}}$

- in each run, we generate a set of  $N$  standard normal random numbers  $Z_{ij}$ ,  $i = 0, 1, \dots, N - 1$ , then simulate the three liquid asset paths  $S_{ij}^+$ ,  $S_{ij}$  and  $S_{ij}^-$  by the following equations:

$$\begin{aligned} S_{(i+1)j}^+ &= S_{ij}^+ + rS_{ij}^+ \Delta d + \sigma S_{ij}^+ Z_{ij} \sqrt{\Delta t}, \\ S_{(i+1)j} &= S_{ij} + rS_{ij} \Delta d + \sigma S_{ij} Z_{ij} \sqrt{\Delta t}, \\ S_{(i+1)j}^- &= S_{ij}^- + rS_{ij}^- \Delta d + \sigma S_{ij}^- Z_{ij} \sqrt{\Delta t}, \end{aligned}$$

where

$$S_{0j}^+ = S_0 + h, \quad S_{0j} = S_0 \quad \text{and} \quad S_{0j}^- = S_0 - h.$$

As the case of constant illiquidity  $\lambda$ , we consider a smoothing payoff function  $f_1(S_{Nj})$  in Table 7.1:

$$\begin{aligned} \text{European Call} \quad f_1(S_{Nj}) &= \frac{K(S_{Nj} - K + \sqrt{(S_{Nj} - K)^2 + \omega^2})}{K + \sqrt{K^2 + \omega^2}}, \\ \text{European Put} \quad f_1(S_{Nj}) &= \frac{K(K - S_{Nj} + \sqrt{(S_{Nj} - K)^2 + \omega^2})}{K + \sqrt{K^2 + \omega^2}}, \end{aligned}$$

which give a standard payoff by setting  $\omega = 0$ . Thus, the values of option  $V_{ij}^+$ ,  $V_{ij}$  and  $V_{ij}^-$  are estimated by discounting maturity payments, which

are:

$$V_{ij}^+ = e^{-r(T-t_i)} f_1(S_{Nj}^+) , \quad (8.3)$$

$$V_{ij}^- = e^{-r(T-t_i)} f_1(S_{Nj}^-) , \quad (8.4)$$

$$V_{ij}^- = e^{-r(T-t_i)} f_1(S_{Nj}^-) . \quad (8.5)$$

- approximate the Gammas  $V_{SS_{ij}}$  by:

$$V_{SS_{ij}} = \frac{\frac{V_{ij}^+ - V_{ij}}{S_{ij}^+ - S_{ij}} - \frac{V_{ij}^- - V_{ij}}{S_{ij}^- - S_{ij}}}{\frac{1}{2}(S_{ij}^+ - S_{ij}^-)} , \quad (8.6)$$

which are assigned to the initial values of  $V_{SS_{ij}}$  to simulate the illiquid asset paths, i.e.  $\lambda \neq 0$ .

### 3. Simulate sample paths for the illiquid asset (8.1)

- generate the illiquidity path with a new set of  $N$  standard normal random variables  $\bar{Z}_{ij}$  as follows:

$$\lambda_{(i+1)j} = \lambda_{ij} + \kappa(\theta - \lambda_{ij})\Delta t + \zeta\sqrt{\lambda_{ij}}\sqrt{\Delta t}(\rho Z_{ij} + \sqrt{1-\rho^2}\bar{Z}_{ij}) ,$$

- iterate to generate the following asset paths:

$$\begin{aligned} S_{(i+1)j}^+ &= S_{ij}^+ + rS_{ij}^+\Delta t + \frac{\sigma S_{ij}^+ Z_{ij} \sqrt{\Delta t}}{1 - \lambda_{ij} S_{ij}^+ V_{SS_{ij}}} , \\ S_{(i+1)j}^- &= S_{ij}^- + rS_{ij}^-\Delta t + \frac{\sigma S_{ij}^- Z_{ij} \sqrt{\Delta t}}{1 - \lambda_{ij} S_{ij}^- V_{SS_{ij}}} , \\ S_{(i+1)j}^- &= S_{ij}^- + rS_{ij}^-\Delta t + \frac{\sigma S_{ij}^- Z_{ij} \sqrt{\Delta t}}{1 - \lambda_{ij} S_{ij}^- V_{SS_{ij}}} , \end{aligned}$$

At each iteration, the corresponding Gammas  $V_{SS_{ij}}$  are recalculated by Eq (8.3)-(8.6). We consider that the option price  $V_{0j}$  is convergent when the error of option price  $V_{0j}$  between two iterations is lower than the tolerance  $\epsilon$ . If the convergence criterion is not satisfied, we repeat the process using the updated values of  $V_{SS_{ij}}$  until it reaches the maximum number of the iteration  $I_{\max}$ .

- The iteration can be also stopped if  $S_{(i+1)j}^+$ ,  $S_{(i+1)j}$  and  $S_{(i+1)j}^-$  are negative or two of them are close. The total number of the abandoned paths are assigned to the counter  $m$ .

4. Estimate the option price  $V_0$  by

$$V_0 = \frac{1}{M-m} \sum_{j=1}^M V_{0j} .$$

In the remainder of this chapter, we will focus on comparing the impact of stochastic illiquidity on pricing options with a constant illiquidity by several numerical examples. The analysis follows on two different payoffs, which are standard payoffs  $\omega = 0$  and smoothing payoffs  $\omega \neq 0$ . The default setting of parameters chosen here is the same as those in Chapter 6 and Chapter 7, which is shown in Table 8.1. The parameters

Parameters	Constant Illiquidity	Stochastic Illiquidity
$S(t_0)$	1.0	1.0
$K$	1.0	1.0
$T$	10	10
$r$	0.04	0.04
$\sigma$	40.2	0.2
$N$	2000	2000
$M$	$10^6$	$10^6$
$\lambda^c$	1.0	—
$\lambda_0$	—	1.0
$\theta$	—	1.0
$\kappa$	—	0.35
$\zeta$	—	0.2
$\rho$	—	0.0

Table 8.1: Default parameter setting for constant illiquidity model and stochastic illiquidity model.  $\lambda^c$  stands for the default value of constant illiquidity.

for the dynamic process of the illiquidity are taken from Esser and Monch (2002). Note that the values of long-term level of illiquidity  $\theta$  and initial illiquidity  $\lambda_0$  at  $t_0$  are the same as the constant illiquidity  $\lambda^c$ , which ensures that the two models are comparable.

## 8.2 Standard payoffs $\omega = 0$

### 8.2.1 Illiquidity $\lambda$ impact on option pricing

As mentioned in Chapter 7, the most significant shortcoming of standard payoffs applied in pricing option is barely to reflect the influence of the illiquidity on the underlying movement. Figure 8.1 shows both models produce a similar trend of option prices as  $\theta$  ( $\lambda^c$ ) increases. Hence, under a stochastic illiquidity process, when

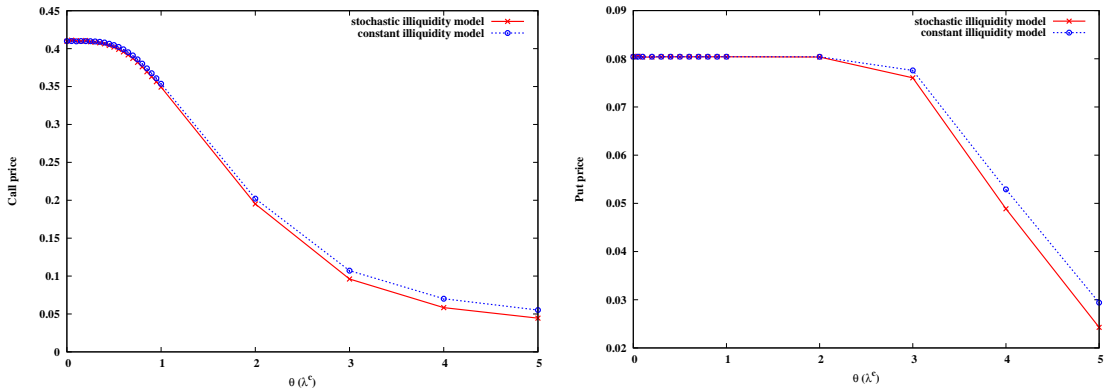


Figure 8.1: Option price depends on illiquidity using the standard payoffs in the stochastic (constant) illiquidity full feedback model. We assume  $\theta = \lambda_0 = \lambda^c$ .

$\theta$  ( $\lambda^c$ ) is relatively small, the option prices are still nearly the same as the Black-Scholes prices due to the standard payoffs here. For larger values of  $\theta$ , there is a significant decrease of both prices of call and put options. We also note that the call prices are more sensitive to changes in  $\theta$  than the put prices. Moreover, the price with the stochastic illiquidity is a little lower than the price given by the constant illiquidity model.

To investigate the reason why differences of the option prices are obtained here, Fig 8.2 illustrates the distribution of (log) return  $\ln(S_T/S_0)$  when pricing a European option for  $\lambda = 1, 3$  and  $5$ . For a call option in the left side of Fig 8.2, we discover that the illiquid underlying more frequently hits the strike price and rarely reaches a high level price, so that its distribution has a higher peak and a thinner right tail than that of the liquid asset. Therefore, the price of call option for the illiquid asset is lower than the Black-Scholes price as the factor of the illiquidity reduces the volatility of the

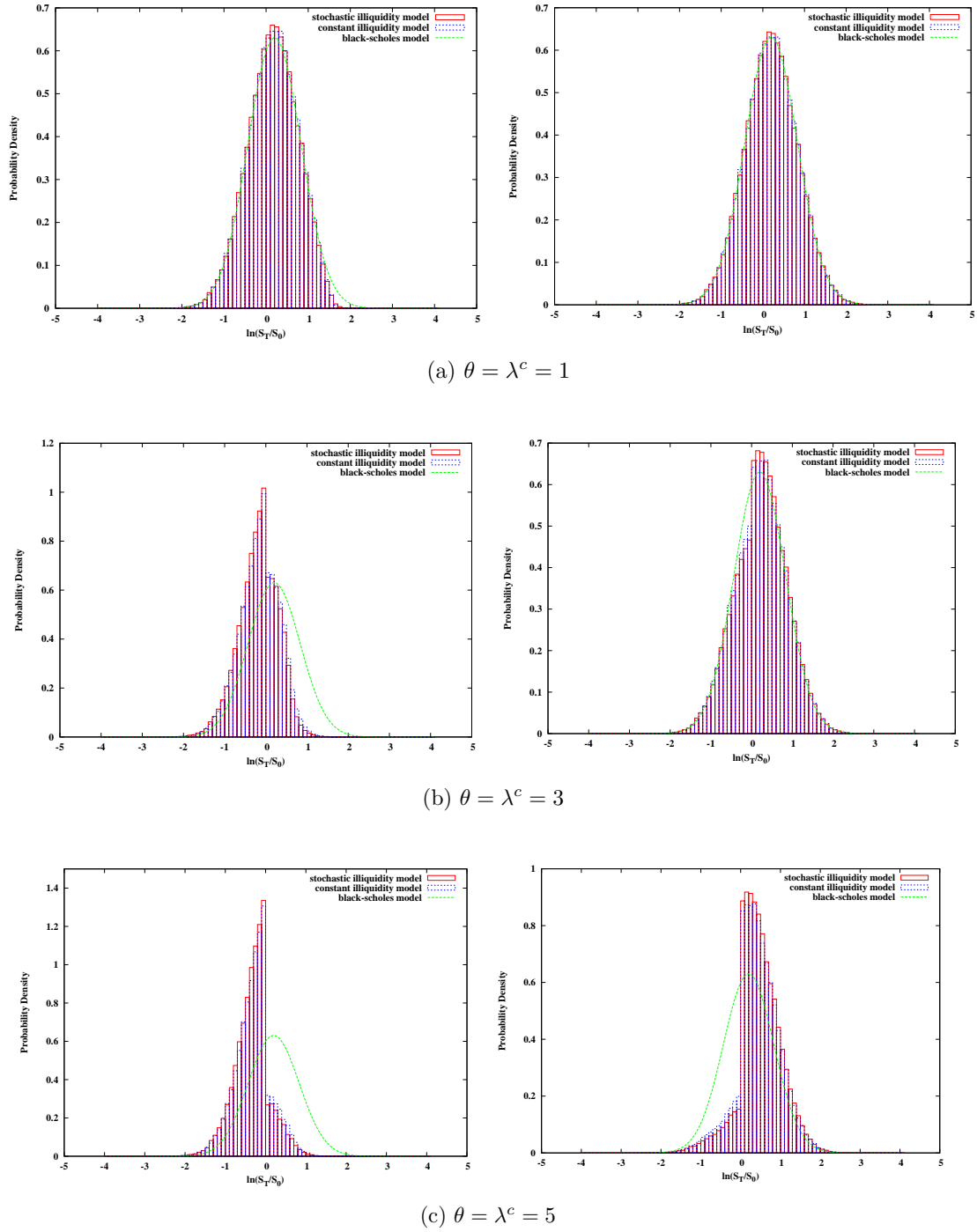


Figure 8.2: Probability density estimate of log return over ten-year horizon for pricing call options (left side) and put options (right side) under the stochastic (constant) illiquidity full feedback model with  $N((r - \frac{1}{2}\sigma^2)T, \sigma^2 T)$  density superimposed for Black-Scholes model.

underlying. As  $\theta$  increases, the histograms tend to move away from the Black-Scholes curve and shift to the left, where the call option will expire out-of-the-money. Both illiquidity models produce nearly the same distribution of log return, in particular when  $\theta = 3$  and  $5$ , the stochastic illiquidity model has a slightly higher peak which results in a lower call price than that for the constant illiquidity model. For a put option on the right side of Fig 8.2, there is a similar trend of underlying movements, which is that the underlying potentially moves to a price region where the put option will expire out-of-the-money. Nevertheless, the factor of illiquidity has less effect on pricing a put option than a call option with the same value of  $\theta$ , because the trend is not felt until  $\theta = 5$  for the put option. This result is consistent with the price reduction with respect to  $\theta$  found in Fig 8.1.

$\theta = \lambda_0$	Abandonment	Crossed	Unconvergent	Negative
0	0(0)	0(0)	0(0)	0(0)
0.05	0(0)	0(0)	0(0)	0(0)
0.1	2(0)	0(0)	2(0)	0(0)
0.3	150(0)	1(0)	50(0)	99(0)
0.5	1635(0)	10(0)	349(0)	1278(0)
0.7	6592(0)	67(0)	1377(0)	5151(0)
1	25318(5)	397(0)	6567(5)	18391(0)
3	420715(56222)	1.553e + 04 (1700)	2.266e + 05 (3.409e + 04)	179969 (20670)
5	558225(299950)	2.294e + 04 (2.299e + 04)	3.438e + 05 (1.562e + 05)	193334 (122174)

Table 8.2: The number of the abandoned paths in the full feedback model with stochastic  $\lambda$ . The data in parentheses stand for put options and others for call options.

We also give the corresponding data on the number of abandoned paths in Table 8.2. Compared with the data presented in Table 7.5 for the constant illiquidity model in Chapter 7, these suggest that the stochastic illiquidity leads to somewhat more abandoned paths in the simulation, but its maximum abandonment rate is around 55% when  $\theta = 5$ , which is still in an acceptable range so that the algorithm of option pricing is still useful. With regard to abandonment reasons, the main cause here is that simulated paths fail to obtain a convergent option price. This can help to explain why we obtain a thin right tail and normal left tail of histograms in Fig 8.2

when pricing a call option, because the computations for underlyings that expire DITM have to iterate to gain a convergent option price, but most of the time they will fail to produce a convergent price. The underlyings expiring OTM lead to zero Gammas, which reduces the illiquid asset to effectively a liquid asset and then in part generates a similar density as the Black-Scholes model. In general, both models produce more abandoned paths for valuing a call option than valuing a put option. This is because for these options, the Gammas  $V_{SS}$  estimated in our algorithm are usually much smaller than the corresponding Gammas of the call option, as a result, there is less effect of illiquidity on underlying price movement compared with pricing call options.

### 8.2.2 Maturity $T$ impact on option pricing

Another important factor impacting on the option price is maturity  $T$ , which can be used to distinguish clearly between stochastic and constant illiquidity models. In

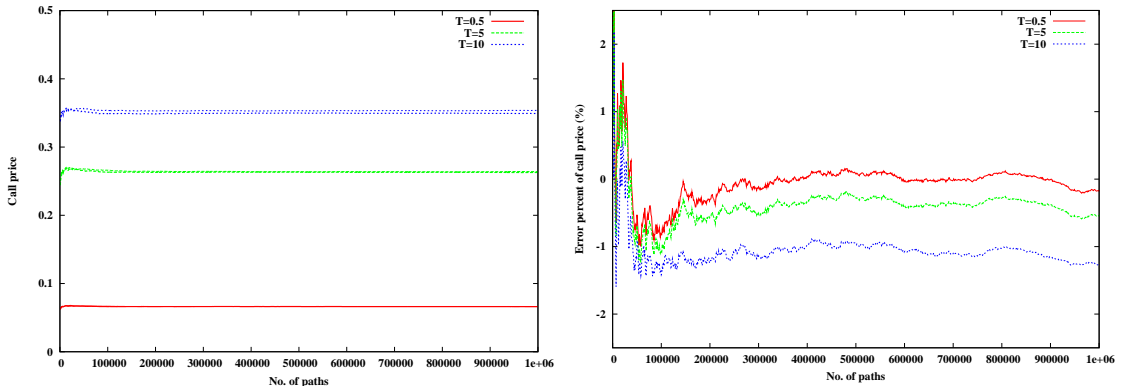


Figure 8.3: Call prices depends on maturity  $T$  in full feedback models with constant illiquidity (thinner lines) and stochastic illiquidity (thicker lines). The error percent is calculated by  $(C_{stoch} - C_{const})/C_{const}$ .

Fig 8.3, we examine the percent error of the call option in the illiquidity models with respect to different maturity  $T = 0.5, 5$  and  $10$ , which measured by  $(C_{stoch} - C_{const})/C_{const}$ . When  $T = 10$ , the call price given by the stochastic illiquidity model has been reduced by around 1% from the relative price in the constant illiquidity model, which is the maximum error among the three maturities  $T$ . This suggests that

increasing  $T$  can allow the stochastic illiquidity  $\lambda$  to affect option prices, otherwise for short-maturity options, there is no significant difference between the two illiquidity models. Fig 8.3 also indicates whether the illiquidity is stochastic or constant, the option price is increasing as  $T$  increases.

### 8.2.3 A comparison of full feedback model and first-order feedback model with constant and stochastic illiquidity

We further study two kinds of feedback models described in this thesis, which are first-order feedback model in Chapter 5 and 6 and full feedback models in Chapter 7 and 8. Under the same standard payments of options, we estimated call and put prices in different models with the default parameters in Table 8.1 (see Fig 8.4). Note that the call prices are estimated by put-call parity for the first-order feedback models. A

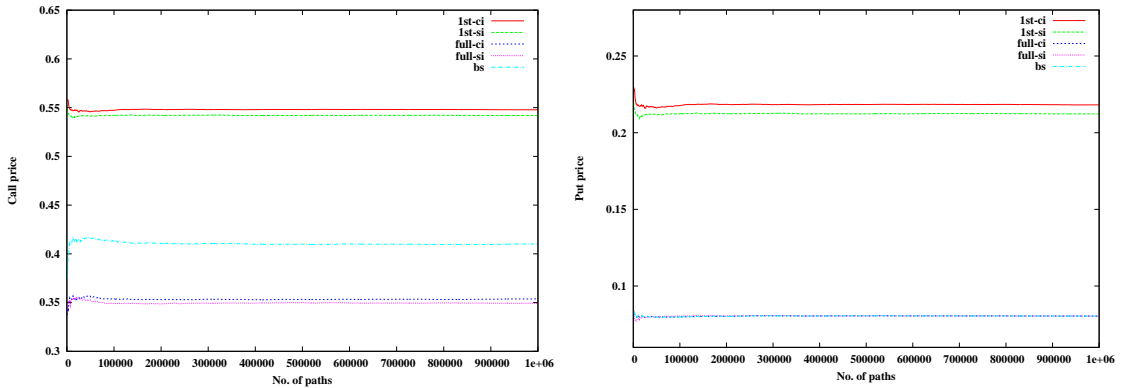


Figure 8.4: Option pricing in different feedback models: first-order feedback model with constant illiquidity (1st-ci) and with stochastic illiquidity (1st-si), full feedback model with constant illiquidity (full-ci) and with stochastic illiquidity (full-si), compared with Black-Scholes prices (bs).

common feature of both feedback models in Fig 8.4 is that the stochastic illiquidity  $\lambda$  leads to a lower option price than the fixed illiquidity  $\lambda^c$ . However, there is also a clear difference between option prices in the two models; that is, the option prices given by the first-order feedback models are greater than the Black-Scholes prices while the prices given by the full feedback models are less than or equal to the Black-Scholes prices under the parameter setting in Table 8.1. Recall the relationship

between option prices and illiquidity  $\lambda$  in Fig 6.9 for the first-order feedback model, i.e. the option price should increase beyond the Black-Scholes prices with  $\lambda$  first, then afterwards it decreases with  $\lambda$  and might be lower than the Black-Scholes price. This implies a problem with the application of the standard payoffs in the full feedback model. With standard payment functions we cannot see such a increase with  $\lambda$  in Fig 8.1, where the option prices estimated are shown to be close to the Black-Scholes prices and lower than the Black-Scholes prices when illiquidity parameters chosen are big enough, such as  $\theta = \lambda^c > 1$ . Therefore, a smoothed payoff will be introduced and discussed in the next section to complete our study of the full feedback problem.

## 8.3 Smoothing payoffs $\omega \neq 0$

In this section, we focus on the smoothing function introduced in Section 7.2 where  $\omega = 0.1$  and  $\omega = 1$ , which represent a slightly smoothed payoff and a much smoothed payoff, respectively. The impact of  $\lambda$  along nonzero  $\omega$  on pricing European options is illustrated and explored to investigate put-call parity. Moreover, we also analyze implied volatilities calculated by Black-Scholes option pricing formula (see reference in Wilmott, 2006) in the illiquidity models.

### 8.3.1 Illiquidity $\lambda$ impact on pricing option

Fig 8.5 provides the results of option prices and the corresponding deviations from put-call parity. It is clear that the option price estimated by the smoothed payoff is more sensitive to small values of  $\theta$  or  $\lambda^c$  than that of the price using a standard payoff, which is similar to the Black-Scholes price in Fig 8.1. For both options, there is a slight increase of option prices in  $\theta$ , with a significant decline thereafter in the stochastic illiquidity model, except for certain  $\theta$  such as  $\theta = 5$  for pricing a call option. Fig 8.5 also presents the corresponding option prices in the constant illiquidity model, and shows that both illiquidity models produce similar values of option price and deviation from put-call parity. We find that the full feedback model with the smoothed payoff differs from that of the standard payoffs with large values

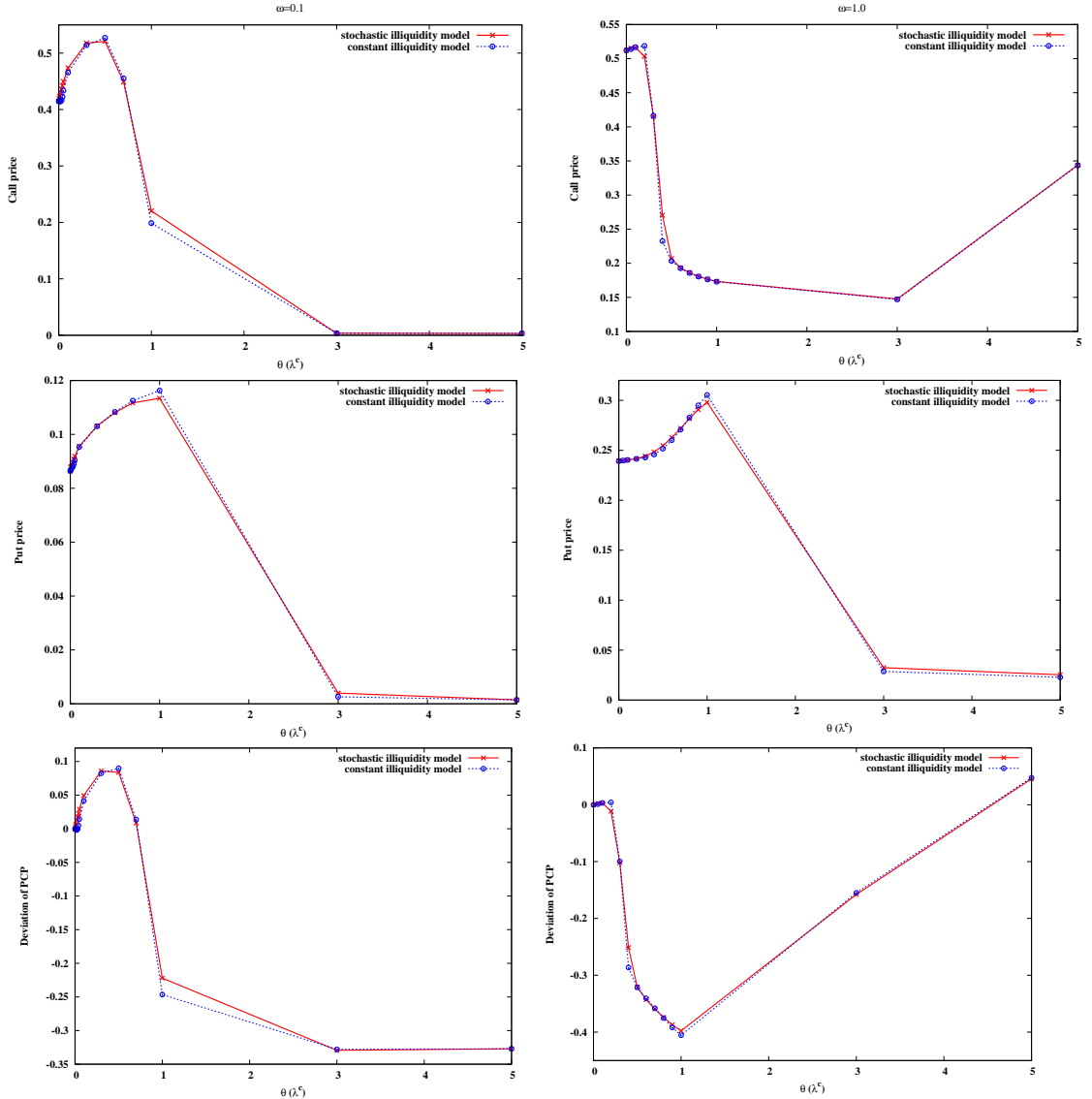


Figure 8.5: Option price depends on illiquidity in the stochastic (constant) illiquidity full feedback model under smoothing payoffs. We also give the corresponding error from put call parity assuming  $\theta = \lambda_0 = \lambda^c$ . The left panel is for  $\omega = 0.1$  and the right panel for  $\omega = 1.0$ .

of  $\theta$  as there is no sign to conclude that the stochastic illiquidity leads to lower option prices than the constant illiquidity. In particular, we find that larger values of  $\theta$  would cause abnormal behaviour of option prices, such as near zero prices or suddenly rising prices. To investigate the behaviour, we provide the number of abandoned paths from the relative simulations in Table 8.3. From Table 8.3, there are a significant number of abandoned paths occurring in the simulation when  $\theta$  is large, such as the abandonment rate is around 99% at  $\theta = 5$ . Therefore, a result from the simulations cannot be used as a fair price of the option. This implies that when using a smoothed payoff, we should take care to choose the values of  $\theta$  and  $\omega$ . In this example, it suggests that to avoid high rates of abandonment in the simulation, we require that  $\theta < 1$  for  $\omega = 0.1$  and  $\theta < 0.5$  for  $\omega = 1$ . Fig 8.6 illustrate how the smoothing parameter  $\omega$  impacts on the distributions of log return  $\ln(S_T/S_0)$  assuming  $\theta = 1$ . Compared with the case of  $\omega = 0$ , there exist few paths with  $\ln(S_T/S_0) \approx 0$  in the case of  $\omega = 0.1$ , i.e. the underlying rarely hits the strike price  $K = S_0$ . This is also found in the case of  $\omega = 1$ . In particular, for pricing the call option, most of the simulated paths expire out-of the money, i.e.  $S_T < K$ , then the call price is estimated be extremely small.

### 8.3.2 Implied volatility in illiquidity models

As stated in Liu and Yong (2005), price impact leads to an endogenous stochastic volatility, which is able to describe the ‘smile-pattern’ of the implied volatility obtained in the real market. We illustrate the Black-Scholes implied volatility arising from full feedback illiquidity models as well as the first-order feedback models shown in Chapter 5. The illustration in Fig 8.7 takes a trial value of  $\omega = 0.1$ , because a slightly smoothed function close to the standard payoff should not vanish the comparability between the full feedback effect and the first-order feedback. Similarly, we choose  $\lambda^c = 0.5$  to ensure that the algorithm would not create a high percentage of abandoned paths in the simulation. Also, the example is based on pricing a put option rather than a call option, because without capping the estimated price of the put option is more accurate than that for the call option as mentioned in

$\theta$		Abandoned	Crossed	Unconvergent	Negative	$\theta$	Abandoned	Crossed	Unconvergent	Negative
$\omega = 0.1$										
0	0	0	0	0	(0)	0	0	0	0	0
0.005	15635 (12764)	(0) 22 (16)	(0) 6234 (5830)	(0) 9384 (6921)	(0) 0.05 (49)	(0) 5389 (49)	(0) 98 (2)	(0) 98 (2)	(0) 3 (0)	(0) 5313 (47)
0.01	21247 (17451)	35 (29)	8607 (7740)	12608 (9683)	0.1 (359)	29421 (12)	649 (12)	649 (12)	5 (6)	28899 (342)
0.02	35998 (29589)	60 (61)	1.492e+04 (1.297e+04)	21023 (16571)	0.2 (4610)	173798 (191)	5400 (191)	5400 (191)	52 (55)	169358 (4389)
0.03	52104 (42961)	119 (115)	2.219e+04 (1.832e+04)	29819 (24544)	0.3 (21592)	402905 (1368)	1.762e+04 (1368)	1.762e+04 (1368)	151 (190)	388210 (20222)
0.04	68319 (56715)	186 (187)	2.917e+04 (2.308e+04)	38987 (33473)	0.4 (60079)	590624 (5180)	3.681e+04 (406)	3.681e+04 (406)	297 (406)	559385 (55157)
0.05	83334 (69168)	314 (341)	3.638e+04 (2.672e+04)	46702 (42167)	0.5 (120972)	681578 (1.446e+04)	6.101e+04 (1.446e+04)	6.101e+04 (1.446e+04)	499 (591)	628545 (107612)
0.1	138074 (112747)	1330 (1452)	5.964e+04 (3.054e+04)	77301 (80972)	0.6 (198322)	730891 (198322)	8.8e+04 (3.07e+04)	8.8e+04 (3.07e+04)	948 (646)	653229 (170389)
0.3	235937 (162112)	1.503e+04 (1.674e+04)	5.577e+04 (8143)	166831 (139313)	0.7 (285370)	765846 (285370)	1.122e+05 (5.245e+04)	1.122e+05 (5.245e+04)	1522 (676)	665871 (237416)
0.5	328740 (198744)	3.812e+04 (4.355e+04)	5.438e+04 (1.531e+04)	240059 (144548)	0.8 (375293)	793913 (8.141e+04)	1.281e+05 (8.141e+04)	1.281e+05 (8.141e+04)	2323 (585)	678729 (300482)
0.7	458295 (236266)	6.397e+04 (6.8e+04)	5.508e+04 (3.373e+04)	345702 (140928)	0.9 (461838)	816912 (461838)	1.366e+05 (1.194e+05)	1.366e+05 (1.194e+05)	2976 (623)	693544 (351053)
1.0	662058 (298953)	1.044e+05 (9.954e+04)	5.748e+04 (6.14e+04)	510484 (145548)	1.0 (540519)	836251 (540519)	1.39e+05 (1.688e+05)	1.39e+05 (1.688e+05)	3491 (592)	710105 (382751)
3.0	815877 (600430)	1.841e+05 (2.498e+05)	7.598e+04 (1.365e+05)	569625 (222848)	3.0 (967806)	970848 (4.144e+05)	1.161e+05 (4.144e+05)	1.161e+05 (4.144e+05)	1729 (865765)	847145 (560194)
5.0	844754 (636092)	2.033e+05 (2.771e+05)	7.095e+04 (1.356e+05)	583214 (232017)	5.0 (989322)	953035 (4.298e+05)	3.128e+04 (1.935e+04)	3.128e+04 (1.935e+04)	847145 (557518)	

Table 8.3: The number of the abandoned paths for European options in  $10^6$  sample paths. The data in parentheses stand for put options and others for call options.

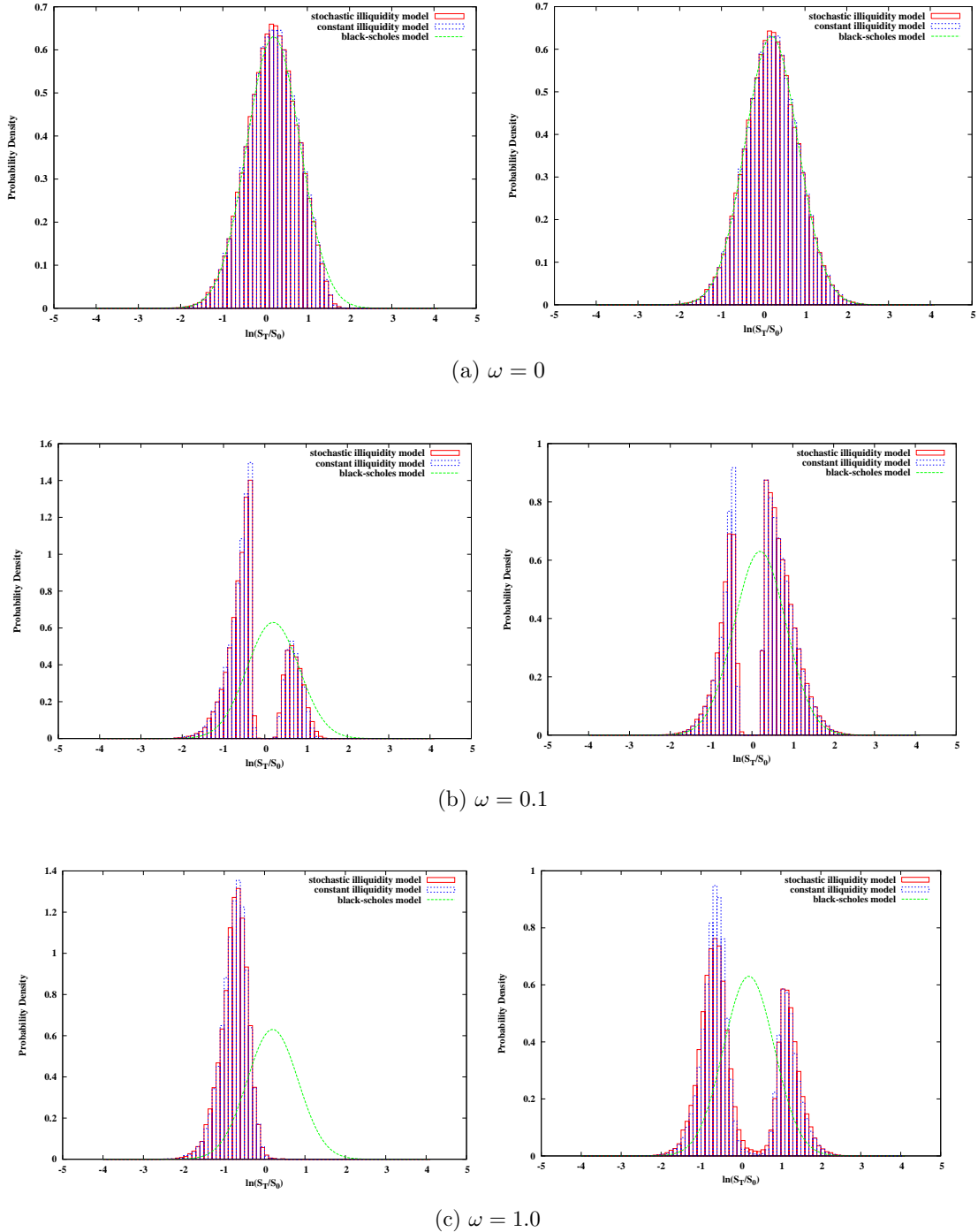


Figure 8.6: Probability density estimate of log return over a ten-year horizon for pricing call options (left side) and put options (right side) under the stochastic (constant) illiquidity full feedback model for  $\lambda^c = 1$  with  $N((r - \frac{1}{2}\sigma^2)T, \sigma^2 T)$  density superimposed for Black-Scholes model. Top:  $\omega = 0$ , middle:  $\omega = 0.1$  and bottom:  $\omega = 1$ .

Chapter 5. Fig 8.7 provides the changes of the put option price and the implied

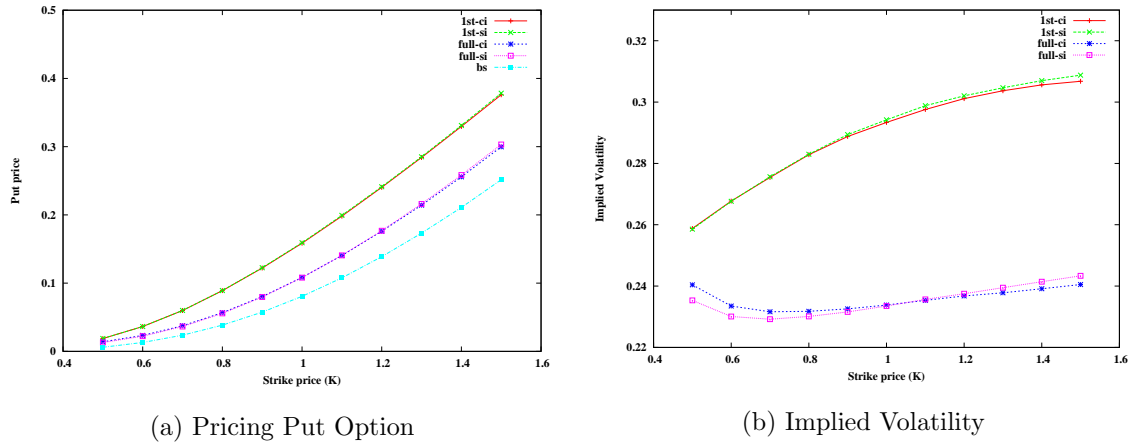


Figure 8.7: Pricing European put options (left) and the Black-Scholes implied volatilities (right) with respect to varying strike prices in different feedback models: first-order feedback model with constant illiquidity (1st-ci) and with stochastic illiquidity (1st-si), full feedback model with constant illiquidity (full-ci) and with stochastic illiquidity (full-si), compared with Black-Scholes prices (bs).

volatility with respect to different strike prices,  $K$ , when the spot price  $S_0 = 1$ . In Fig 8.7(a), with the same strike  $K$ , the highest option prices are given by both first-order feedback models (with constant or stochastic illiquidity), followed by both full feedback models, and the cheapest put option is produced by the standard Black-Scholes model. Moreover the feedback effect on the option price has been enhanced for the deep in-the-money option, i.e.  $K \gg S_0$ . Compared with the results given by the standard payoffs in Fig 8.4, the full feedback prices are clearly higher than the Black-Scholes prices when we use the smoothed payoffs. For two kinds of illiquidity, the price under the stochastic illiquidity process becomes higher than that of the constant illiquidity, but the difference seems to be small in Fig 8.4. Correspondingly, the implied volatility estimated by the standard Black-Scholes formula for pricing option is shown in Eq 8.7(b). We find that the implied volatility of the first-order feedback model is greater than that of the full feedback model, and both feedback models have a rather high implied volatility which is larger than the constant volatility in the Black-Scholes model, i.e.  $\sigma = 0.2$ . This is an explanation for the difference of option prices in Fig 8.7(a), since the higher the risk for underlying asset, the higher

the option price. The implied volatility in the first-order feedback models increases when the option tends to be in-the-money, while the implied volatility given by the full feedback models looks more like a skewed smile, which means a relatively high volatility is also obtained for deep out-of-the-money options. In addition, stochastic illiquidity is shown to have more impact on the implied volatility in the full feedback models than the first-order feedback models. That is, the model with the stochastic illiquidity provides a more skewed smile, where the increase of the volatility for deep in-the-money options is found to be more pronounced than the increase for the deep out-of-the-money. Therefore, the full feedback model with a stochastic illiquidity is to be considered a more accurate model to capture the famous important feature of the smile and skew volatility.

In summary, the numerical pricing option in the full feedback model is much more complicated than in the first-order feedback model. Following our analysis above, it turns out that the smoothed payoff is able to value the option price for small values of the illiquidity  $\theta$  or  $\lambda^c$ . However, there exists the difficulty of evaluating the price when  $\theta$  is relatively large because in such cases, the smoothing parameter,  $\omega$ , accompanied with the illiquidity,  $\theta$ , could cause a number of abandoned paths and eventually damage the simulation. Therefore, instead of the smoothed payoffs, for a severe illiquidity situation, such as  $\theta > 1$ , we recommend the use of a standard payoff to price options, which is shown to have a better performance in the option valuation. Besides the option pricing, we also explore that the Black-Scholes implied volatility in the feedback models. With a proper setting of parameters  $\theta$  and  $\omega$ , the results support that proposition that the full feedback model with stochastic illiquidity can be regarded as better than other models in capturing the smile pattern of implied volatility.

# Chapter 9

## Conclusions

*... derivatives are financial weapons of mass destruction, carrying dangers that, while now latent, are potentially lethal.*

– Warren Buffett, Chairman of Berkshire Hathaway,  
in the 2002 “Chairman’s Letter” to shareholders

### 9.1 Summaries

In this thesis, we have investigated applications of Monte Carlo methods to price financial derivatives under practical models: jump diffusion models and illiquid asset models with a feedback effect from large trades in markets.

For the jump diffusion processes introduced by Merton (1973), we develop a simulation-based algorithm for pricing European options and Bermudan options. There have been three modified jump diffusion models proposed in Chapter 3: multi-dimensional jump models, one-dimensional jump models with stochastic volatility and multi-dimensional jump models with stochastic volatility. To extend solution to multi-dimensional option pricing problems, there is a difficulty in calculating the correlation matrix for different underlying assets. The correlation in jump diffusion models is shown be more complicated than in standard Black-Scholes models, because we have to consider correlations not only for diffusion terms but also for jump terms with regard to jump size and jump frequency. Following Clift (2007), we assume that

the number of jumps is the sum of two independent Poisson random numbers, where one is individual to the specific asset and the other is common, shared by all assets. The jump size is determined by a multinormal distribution. Furthermore, we explore the two factor jump diffusion asset model with correlated stochastic volatility that follows a mean reverting jump diffusion process. Correlation is considered for different assets and the different volatilities of the relative assets on two aspects: diffusion term and jump term. The two-factor model requires roughly a doubling of computation cost to simulate the asset process compared with the one-factor model. The rate of increase in costs is linearly with the number of dimensions, which is slower than the rate of other numerical methods for high dimensional pricing problems (see Hull, 2009).

In Chapter 3 we focus on the analysis of pricing Bermudan options using the least-squares Monte-Carlo method proposed by Longstaff and Schwartz (2001). The method has been improved to achieve enhanced accurate results with an extrapolation process (see Duck et al., 2005). Through the results presented in Chapter 3, we conclude that a proper set of the number of sample paths is particularly important to correctly calculate Bermudan option prices when the extrapolation technique is employed. The convenient choice as suggested by Duck et al. (2005) is to set the number of sample paths as  $M = 2000, 4000$  and  $8000$  respectively for the least-squares regression, which implies that the option prices calculated by these three samples are accurate. Furthermore, our results show that the extrapolation method should be recommended to deal with pricing Bermudan option with a number of exercise opportunities, which produces a more correct option price.

From Chapter 4 to Chapter 8, another kind of practical model is studied here to realize the feedback trading which has a price impact on underlying assets. Our feedback models are derived mainly from Glover (2008) and we also provide an extended version of feedback model with undetermined volatility. For first-order feedback model in Chapter 5 and Chapter 6, the implementation of Monte Carlo is quite straightforward using the exact value of the second derivative of options with respect to stock prices from the Black-Scholes formula. There exists a potential problem

underlying asset price simulation for this model, which is production of (financially unreal) negative prices of the asset. We analyze the cause of the occurrence of negative prices and find the ‘dangerous’ area with respect to stock prices  $S$  and time to maturity  $\tau$ , where the following price  $S(\tau - \Delta t)$  simulated by  $S(\tau)$  is usually negative, assuming  $\Delta t$  is the size of timesteps used in the simulation. Our suggestion for these negative prices is to interrupt the particular path and to start simulating the next sample path. When the volatility follows a stochastic process, the asset price tends to be more volatile, leading to more negative prices occurring the simulation. It is important to subtract the number of negative paths from the total sample paths when calculating the expected value of option price.

For full feedback models in Chapter 7 and Chapter 8, we suggest estimating the second derivative (i.e. Gamma) using a three-point difference method. In order to apply this method, three sample paths are required, starting with a slightly different stock price, but simulating with the same set of random numbers for each timestep. We also need some additional conditions on the numerical method: the three sample paths cannot cross at each time point, otherwise the method fails; the resulting option price from the iteration process is shown to be convergent; the estimate of asset prices is strictly positive. We have to abandon sample paths that violate these necessary conditions. Assuming the law of large number still holds here, then the option price can be computed from the live simulated paths. However, the total number of abandoned paths should be noted and high levels of abandonment rate avoided via a proper set of parameters. A smoothed payoff function for European options has an advantage over the standard payoffs because it can realize more non-zero values of Gammas to reflect the price impact. We present the results of the standard payoffs and smoothing payoffs in the case of full feedback models. When considering a stochastic volatility process, the option price is shown to be slightly different from the price with the constant volatility.

There is another finding in these feedback models, which is the use of put-call parity. Our results show that the model is more suitable to price put options than call options, because some simulated asset prices can be extremely large when evaluating

a convergent price for call options.

## 9.2 Further research

Further research could study the illiquid asset model with jumps. The basic illiquidity model is able to capture price changes according to trading volume in the market, while the jump diffusion model is used to explain price movements as partly responsible for unexpected market crashes (irrelevant to the trading itself). Combining these two kinds of models, one might obtain a more reasonable model to capture realistic price movement in a stock market. Incorporating a stochastic volatility and/or a stochastic interest rate is another possible direction to complete our model. It is important to investigate the correlations between these state variables in the extended model, meanwhile the extended model may involve more computational difficulties in multi-dimensional framework.

Monte Carlo has been shown to be a feasible tool for pricing complex options in the more complex (and, we trust, more realistic) environment beyond Black-Scholes-Merton described in this thesis, such as Bermudan options, exotic options and multi-asset options. The Bermudan options priced using a LSM algorithm can still be evaluated in the illiquid model with jumps. Monte Carlo valuation for exotic options: barrier options, Asian options and Parisian/ParAsian option (see Xiao, 2007), has a significant advantage in terms of ease of implementation over most other numerical methods; the extension to options with other more exotic boundary conditions should follow naturally. One could then use the Monte Carlo method to mimic the behaviour of these exotic options in the feedback model with jumps. These options can be straightforwardly extended to multi-asset options, whose valuation is generally required less computational cost using the Monte Carlo methods as its  $O(1/\sqrt{n})$  convergence rate holds for all dimensions.

Alternatively, we can also pay attention to the efficiency of Monte Carlo estimators, in particular, for pricing complex options. Several basic and popular variance reduction techniques and discretization have been introduced in Chapter 2. We can

adopt these technologies to improve the Monte Carlo simulation for more sensible feedback models.

We have neglected calibration of the asset models presented in this thesis, which is an interesting area to investigate how to estimate these models using market data. The importance of different variables (e.g. illiquidity lambda, jump size, jump frequency, etc.) will be explored through these empirical test.

# Appendix A

## Basic Notation and Abbreviation

We adopt the following notation and abbreviations throughout the thesis.

Symbol	Description
$\mathbb{P}$	(real-world) probability measure
$\mathbb{Q}$	(risk-neutral) probability measure
$:=$	defined as or denoted by
$x^\top$	transpose of the vector $x$
$\sim$	with distribution
$\mathbb{E}$	expectation operator
$Var$	variance operator
$Cov$	covariance operator
$\log$	natural logarithm
$N(\mu, \sigma^2)$	Normal distribution with mean $\mu$ and variance $\sigma^2$
$Poisson(\lambda)$	Poisson distribution with mean $\lambda$
$Gamma(k, \lambda)$	Gamma distribution with mean $k\lambda$ and variance $k\lambda^2$
$(a, b)$	the open interval $a < x < b$
$[a, b]$	the closed interval $a \leq x \leq b$
$f'$	the first derivative of a function $f$
$f''$	the second derivative of a function $f$
$f^{(i)}$	the $i$ th derivative of a function $f$
$\frac{\partial^i f}{\partial x^i}$	the $i$ th order partial derivative of a function $f$ with respect to $x$
$O(n^{-m})$	the approximation error is of order less than $n^{-m}$ (the order of magnitude of $n^{-m}$ )

Table A.1: Mathematical Symbols

Symbol	Description
$r$	riskless interest rate
$\sigma$	volatility parameter of the stock
$W$	Wiener process (Brownian motion)
$\tau$	time to maturity
$t$	current time
$T$	maturity time
$S_t$	underlying price at time $t$
$K$	strike price

Table A.2: Elements of options

Abbreviations	Description
$a.s.$	almost surely
$i.i.d.$	independent and identical distributed
$w.r.t.$	with respect to
$r.v.$	random variable
CIR	Cox Ingersoll Ross model
MC	Monte Carlo
PDE	Partial Differential Equation
QMC	Quasi Monte Carlo
SDE	Stochastic Differential Equation

Table A.3: Abbreviations

## Appendix B

# Computational Time for 1D-MJD Models

Number of sample paths	Number of runs	$N = 5$	$N = 50$	$N = 100$	$N = 300$
1000	5000	27.57	61.63	103.45	314.62
	10000	62.87	131.45	216.42	640.32
2000	5000	63.10	133.92	219.28	654.60
	10000	125.63	273.67	446.65	1312.33
4000	5000	134.27	275.78	467.68	1366.67
	10000	275.95	557.68	937.18	2703.33
6000	5000	206.82	425.22	719.78	2068.35
	10000	420.17	856.37	1425.00	4146.62

Table B.1: The total computational time (minutes) required for 1D-MJD models. The parameters employed are the same as those in Fig 3.5

# References

- Abramowitz, M. and Stegun, I. (1972), *Handbook of mathematical functions with formulas, graphs, and mathematical tables*, Courier Dover Publications.
- Amin, K. and Ng, V. (1993), ‘Option valuation with systematic stochastic volatility’, *The Journal of Finance* **48**(3), 881–910.
- Andersen, L. (2000), ‘A simple approach to the pricing of Bermudan swaptions in the multi-factor LIBOR market model’, *Journal of Computational Finance* **3**(2), 5–32.
- Andersen, L. and Andreasen, J. (2000), ‘Jump-diffusion processes: volatility smile fitting and numerical methods for option pricing’, *Review of Derivatives Research* **4**, 231–262.
- Andersen, L. and Broadie, M. (2004), ‘Primal-dual simulation algorithm for pricing multidimensional American options’, *Management Science* **50**(9), 1222–1234.
- Andersen, T., Bollerslev, T., Diebold, F. and Labys, P. (2001), ‘The distribution of realized exchange rate volatility’, *Journal of the American Statistical Association* **96**(453), 42–55.
- Bakshi, G., Cao, C. and Chen, Z. (1997), ‘Empirical performance of alternative option pricing models’, *The Journal of Finance* **53**(5), 2003–2049.
- Bakstein, D. and Howison, S. (2003), ‘A non-arbitrage liquidity model with observable parameters’, *Mathematical Finance* .

## REFERENCES

---

- Ball, C. and Torous, W. (1985), ‘On jumps in common stock prices and their impact on call option pricing’, *The Journal of Finance* **40**(1), 155–173.
- Bally, V., Pages, G. and Printems, J. (2002), ‘First-order schemes in the numerical quantization method’, *Mathematical Finance* **13**(1), 1–16.
- Bally, V., Pages, G. and Printems, J. (2005), ‘A quantization method for pricing and hedging multi-dimensional American style options’, *Mathematical Finance* **15**(1), 119–168.
- Bank, P. and Baum, D. (2004), ‘Hedging and portfolio optimization in financial markets with a large trader’, *Mathematical Finance* **14**(1), 1–18.
- Barraquand, J. and Martineau, D. (1995), ‘Numerical valuation of high dimensional multivariate American securities’, *The Journal of Financial and Quantitative Analysis* **30**(3), 383–405.
- Bates, D. (1996), ‘Jumps and stochastic volatility: exchange rate processes implicit in deutsche mark options’, *The Review of Financial Studies* **9**(1), 69–107.
- Benhamou, E. (2002), ‘Smart Monte Carlo: various tricks using Malliavin calculus’, *Quantitative Finance* **2**(5), 329–336.
- Birge, J. (1995), Quasi-Monte Carlo approaches to option pricing, Technical report 94-19, Department of Industrial and Operations Engineering, University of Michigan, Ann Arbor, MI 48109.
- Black, F. and Scholes, M. (1973), ‘The pricing of options and corporate liabilities’, *The Journal of Political Economy* **81**(3), 637–654.
- Bolia, N. and Juneja, S. (2005), ‘Monte Carlo methods for pricing financial options’, *Sadhana* **30**(2&3), 347–385.
- Bossaerts, P. (1989), ‘Simulation estimators of optimal early exercise’, *working paper, Carnegie Mellon University, Pittsburgh, PA*.

## REFERENCES

---

- Box, G. and Muller, M. (1958), ‘A note on the generation of random normal deviates’, *The Annals of Mathematical Statistics* **29**(2), 610–611.
- Boyle, P. (1977), ‘Options: a Monte Carlo approach’, *Journal of Financial Economics* **4**(3), 323–338.
- Boyle, P., Broadie, M. and Glasserman, P. (1997), ‘Monte Carlo methods for security pricing’, *Journal of Economic Dynamics and Control* **21**, 1267–1321.
- Bratley, P., Fox, B. and Schrage, L. (1987), *A guide to simulation*, 2nd edn, Springer-Verlag, New York.
- Broadie, M. and Glasserman, P. (1996), ‘Estimating security price derivatives using simulation’, *Management Science* **42**(2), 269–285.
- Broadie, M. and Glasserman, P. (1997), ‘Pricing American-style securities using simulation’, *Journal of Economic Dynamics and Control* **21**(8-9), 1323–1352.
- Broadie, M. and Glasserman, P. (2004), ‘A stochastic mesh method for pricing high-dimensional American options’, *Journal of Computational Finance* **7**(4), 35–72.
- Carr, P. and Yang, G. (2001), Simulating Bermudan interest rate derivatives, in M. Avellaneda, ed., ‘Quantitative Analysis in Financial Markets: collected papers of the New York University Mathematical Finance Seminar’, Vol. 2, World Scientific, pp. 295–316.
- Carriere, J. (1996), ‘Valuation of the early-exercise price for options using simulations and nonparametric regression’, *Insurance: Mathematics and Economics* **19**(1), 19–30.
- Cerrato, M. and Cheung, K. (2007), Valuing American style options by least squares method, Money Macro and Finance (MMF) Research Group Conference 2006 49, Money Macro and Finance Research Group.
- Cetin, U., Jarrow, R. and Protter, P. (2004), ‘Liquidity risk and arbitrage pricing theory’, *Finance and Stochastics* **8**(3), 311–342.

## REFERENCES

---

- Cetin, U., Jarrow, R., Protter, P. and Warachka, M. (2006), ‘Pricing options in an extended Black Scholes economy with illiquidity: theory and empirical evidence’, *The Review of Financial Studies* **19**(2), 493–529.
- Cetin, U. and Rogers, L. (2006), ‘Modeling liquidity effects in discrete time’, *Mathematical Finance* **17**(1), 15–29.
- Chan, W. (2003), ‘A correlated bivariate Poisson jump model for foreign exchange’, *Empirical Economics* **28**(4), 669–686.
- Clement, E., Lamberton, D. and Protter, P. (2002), ‘An analysis of a least squares regression method for American option pricing’, *Finance and Stochastics* **6**(4), 449–472.
- Clewlow, L. and Strickland, C. (1998), Pricing interest rate exotics by Monte Carlo simulation, in B. Dupire, ed., ‘Monte Carlo: Methodologies and Applications for Pricing and Risk Management’, Risk Publications, London, chapter 17.
- Clift, S. (2007), Linear and non-linear monotone methods for valuing financial options under two-factor, jump-diffusion models, PhD thesis, University of Waterloo.
- Cox, J., Ingersoll, J. and Ross, S. (1985), ‘A theory of the term structure of interest rates’, *Econometrica* **53**(2), 385–407.
- Cox, J. and Ross, S. (1976), ‘The valuation of options for alternative stochastic processes’, *Journal of Financial Economics* **3**(1-2), 145–166.
- Cuoco, D. and Cvitanic, J. (1998), ‘Optimal consumption choices for a ‘large’ investor’, *Journal of Economic Dynamics and Control* **22**(3), 401–436.
- Cvitanic, J. and Ma, J. (1996), ‘Hedging options for a large investor and forward-backward SDEs’, *The Annals of Applied Probability* **6**, 370–398.
- Duck, P., Newton, D., Widdicks, M. and Leung, Y. (2005), ‘Enhancing the accuracy of pricing American and Bermudan options’, *Journal of Derivatives* **12**(4), 34–44.

## REFERENCES

---

- Duffie, D. and Glynn, P. (1995), ‘Efficient Monte Carlo simulation of security prices’, *The Annals of Applied Probability* **5**(4), 897–905.
- Duffie, D., Pan, J. and Singleton, K. (2000), ‘Transform analysis and asset pricing for affine jump-diffusions’, *Econometrica* **68**(6), 1343–1376.
- Duffy, D. (2008), ‘Numerical analysis of jump diffusion models: a partial differential equation approach’, *Datasim Financial Website* .  
\*<http://www.datasimfinancial.com/UserFiles/articles/PIDE.pdf>
- El-Borai, M., El-Nadi, K., Mostafa, O. and Ahmed, H. (2005), ‘Numerical methods for some nonlinear stochastic differential equations’, *Applied Mathematics and Computation* **168**(1), 65–75.
- Eraker, B., Johannes, M. and Polson, N. (2003), ‘The impact of jumps in volatility and returns’, *The Journal of Finance* **58**(3), 1269–1300.
- Esser, A. and Monch, B. (2002), ‘Modeling feedback effects with stochastic liquidity’, *SSRN eLibrary* .
- Feller, W. (1951), ‘Two singular diffusion problems’, *The Annals of Mathematics* **54**(1), 173–182.
- Fournie, E., Lasry, J., Lebuchoux, J. and Lions, P. (2001), ‘Applications of Malliavin calculus to Monte-Carlo methods in Finance II’, *Finance and Stochastics* **5**(2), 201–236.
- Fournie, E., Lasry, J., Lebuchoux, J., Lions, P. and Touzi, N. (1999), ‘Applications of Malliavin calculus to Monte Carlo methods in finance’, *Finance and Stochastics* **3**, 391–412.
- Frey, R. (1996), ‘The pricing and hedging of options in finitely elastic markets’, *SSRN eLibrary* .

## REFERENCES

---

- Frey, R. (2000), Market illiquidity as a source of model risk in dynamic hedging, *in* R. Gibson, ed., ‘Model risk: concepts, calibration and pricing’, Risk Publication, London, pp. 125–136.
- Frey, R. and Patie, P. (2002), Risk management for derivatives in illiquid markets: a simulation study, *in* K. Sandmann, P. Schonbucher and D. Sondermann, eds, ‘Advances in finance and stochastics: essays in honour of Dieter Sondermann’, Springer, pp. 137–159.
- Frey, R. and Stremme, A. (1997), ‘Market volatility and feedback effects from dynamic hedging’, *Mathematical Finance* **7**(4), 351–374.
- Garcia, D. (2003), ‘Convergence and biases of Monte Carlo estimates of American option prices using a parametric exercise rule’, *Journal of Economic Dynamics and Control* **27**(10), 1855–1879.
- Glasserman, P. (2003), *Monte Carlo Methods in Financial Engineering*, Springer.
- Glasserman, P., Heidelberger, P. and Shahabuddin, P. (1999), ‘Asymptotically optimal importance sampling and stratification for pricing path-dependent options’, *Mathematical Finance* **9**(2), 117–152.
- Glasserman, P. and Yu, B. (2004), ‘Number of paths versus number of basis functions in American option pricing’, *The Annals of Applied Probability* **14**(4), 2090–2119.
- Glover, K. (2008), The analysis of PDEs arising in nonlinear and non-standard option pricing, PhD thesis, University of Manchester.
- Guasoni, P. and Robertson, S. (2008), ‘Optimal importance sampling with explicit formulas in continuous time’, *Finance and Stochastics* **12**(1), 1–19.
- Halton, J. (1960), ‘On the efficiency of certain quasi-random sequences of points in evaluating multi-dimensional integrals’, *Numerische Mathematik* **2**(1), 84–90.
- Haugh, M. and Kogan, L. (2004), ‘Pricing American options: a duality approach’, *Operations Research* **52**(2), 258–270.

## REFERENCES

---

- Heston, S. (1993), ‘A closed-form solution for options with stochastic volatility with applications to bond and currency options’, *The Review of Financial Studies* **6**(2), 327–343.
- Higham, D. (2001), ‘An algorithmic introduction to numerical simulation of stochastic differential equations’, *SIAM Review* **43**(3), 525–546.
- Higham, D. (2004), *An introduction to financial option valuation: mathematics, stochastics and computation*, Cambridge University Press.
- Higham, D. and Mao, X. (2005), ‘Convergence of Monte Carlo simulations involving the mean-reverting square root process’, *Journal of Computational Finance* **8**(3), 35–62.
- Huang, X. and Tauchen, G. (2005), ‘The relative contribution of jumps to total price variance’, *Journal of Financial Econometrics* **3**(4), 456–499.
- Hull, J. (2009), *Options, futures, and other derivatives*, 7th edn, Pearson Prentice Hall.
- Hull, J. and White, A. (1987), ‘The pricing of options on assets with stochastic volatilities’, *The Journal of Finance* **42**(2), 281–300.
- Itô, K. (1951), ‘On stochastic differential equations’, *Memoirs of the American Mathematical Society* **4**.
- Jarrow, R. (1992), ‘Market manipulation, bubbles, corners and short squeezes’, *The Journal of Financial and Quantitative Analysis* **27**(3), 311–336.
- Jarrow, R. (1994), ‘Derivative securities markets, market manipulation and option pricing theory’, *The Journal of Financial and Quantitative Analysis* **29**(2), 241–261.
- Jarrow, R. and Rosenfeld, E. (1984), ‘Jump risks and the intertemporal capital asset pricing model’, *The Journal of Business* **57**(3), 337–351.

## REFERENCES

---

- Jensen, M. and Svenstrup, M. (2005), ‘Efficient control variates and strategies for Bermudan swaptions in a Libor market model’, *Journal of Derivatives* **12**(4), 20–33.
- Jorion, P. (1988), ‘On jump processes in the foreign exchange and stock markets’, *The Review of Financial Studies* **1**(4), 427–445.
- Joy, C., Boyle, P. and Tan, K. (1996), ‘Quasi-Monte Carlo methods in numerical finance’, *Management Science* **42**(6), 926–938.
- Kloeden, P. and Platen, E. (1999), *Numerical solution of stochastic differential equation*, Springer.
- Kou, S. (2002), ‘A jump-diffusion model for option pricing’, *Management Science* **48**(8).
- Kwok, Y. (2008), *Mathematical models of financial derivatives*, Springer.
- Law, A. and Kelton, W. (1991), *Simulation modeling and analysis*, 2nd edn, McGraw-Hill, New York.
- Lehmer, D. (1951), Mathematical methods in large-scale computing units, in ‘Proceedings of the 2nd Symposium on Large-Scale Digital Calculating Machinery’, Cambridge, MA: Harvard University Press, pp. 141–146.
- Lewis, A. (2001), ‘A simple option formula for general jump-diffusion and other exponential Levy processes’, *SSRN eLibrary*.
- Liao, H., Chen, T. and Chou, T. (2005), ‘Multi-period corporate short-term credit risk assessment— a state-dependent stochastic liquidity balance model’, *SSRN eLibrary*.
- Liu, B. (2009), Extensions on defaultable bond valuation with Parasian and nonlinearity features, PhD thesis, University of Manchester.
- Liu, H. and Yong, J. (2005), ‘Option pricing with an illiquid underlying asset market’, *Journal of Economic Dynamics and Control* **29**(12), 2125–2156.

## REFERENCES

---

- London, J. (2004), *Modeling derivatives in C++*, John Wiley and Sons.
- Longstaff, F. and Schwartz, E. (2001), ‘Valuing American options by simulation: a simple least-squares approach’, *The Review of Financial Studies* **14**(1), 113–147.
- Martzoukos, S. (2003), ‘Contingent claims on foreign assets following jump-diffusion processes’, *Review of Derivatives Research* **6**(1), 27–45.
- Matei, S. (2005), A multivariate jump-diffusion model and pricing of multi-currency options, Master’s thesis, University of Zurich.
- Matsuda, K. (2004), ‘Introduction to Merton jump diffusion model’, *working paper*.
- Merton, R. (1973), ‘The theory of rational option pricing’, *The Bell Journal of Economics and Management Science* **4**(1), 141–183.
- Merton, R. (1976), ‘Option pricing when underlying stock returns are discontinuous’, *Journal of Financial Economics* **3**(1-2), 125–144.
- Miller, I. and Miller, M. (2004), *John E. Freund’s mathematical statistics with applications*, 7th edn, Pearson Prentice Hall.
- Milstein, G. (1975), ‘Approximate integration of stochastic differential equations’, *Theory of Probability and its Applications* **19**(3).
- Milstein, G. (1979), ‘A method of second-order accuracy integration of stochastic differential equations’, *Theory of Probability and its Applications* **23**, 396–401.
- Moreno, M. and Navas, J. (2003), ‘On the robustness of least-squares Monte Carlo (LSM) for pricing American derivatives’, *Review of Derivatives Research* **6**(2), 107–128.
- Niederreiter, H. (1992), *Random number generation and quasi-Monte Carlo methods*, Society for Industrial and Applied Mathematics (SIAM), Philadelphia, PA.
- Owen, A. (1997), ‘Scrambled net variance for integrals of smooth functions’, *The Annals of Statistics* **25**(4), 1541–1562.

## REFERENCES

---

- Paskov, S. and Traub, J. (1995), ‘Faster valuation of financial derivatives’, *The Journal of Portfolio Management* **22**(1), 113–123.
- Platen, E. and Schweizer, M. (1998), ‘On feedback effects from hedging derivatives’, *Mathematical Finance* **8**(1), 67–84.
- Rasmussen, N. (2005), ‘Control variates for Monte Carlo valuation of American options’, *Journal of Computational Finance* **9**(1), 83–118.
- Raymar, S. and Zwecher, M. (1997), ‘Monte Carlo estimation of American call options on the maximum of several stocks’, *Journal of Derivatives* **5**(1), 7–24.
- Rogers, L. (2002), ‘Monte Carlo valuation of American options’, *Mathematical Finance* **12**(2), 271–286.
- Rogers, L. and Singh, S. (2006), ‘Modeling liquidity and its effects on price’, *working paper*.
- Schonbucher, P. and Wilmott, P. (2000), ‘The feedback effect of hedging in illiquid markets’, *SIAM Journal on Applied Mathematics* **61**(1), 232–272.
- Scott, L. (2002), ‘Pricing stock options in a jump-diffusion model with stochastic volatility and interest rates: applications of Fourier inversion methods’, *Mathematical Finance* **7**(4), 413–426.
- Seydel, R. (2009), *Tools for computational finance*, 4th edn, Springer.
- Sircar, K. and Papanicolaou, G. (1998), ‘General Black-Scholes models accounting for increased market volatility from hedging strategies’, *Applied Mathematical Finance* **5**(1), 45–82.
- Sobol, I. (1967), ‘On the distribution of points in a cube and the approximate evaluation of integrals’, *USSR Computational Mathematics and Mathematical Physics* **7**(4).
- Stein, E. and Stein, J. (1991), ‘Stock price distributions with stochastic volatility: an analytic approach’, *The Review of Financial Studies* **4**(4), 727–752.

## REFERENCES

---

- Stoll, H. (1969), ‘The relationship between put and call option prices’, *The Journal of Finance* **24**(5), 801–824.
- Talay, D. (1984), Efficient numerical schemes for the approximation of expectations of functionals of the solution of a S.D.E. and applications, in ‘Lecture Notes in Control and Information Sciences’, Vol. 61, Springer, pp. 294–313.
- Talay, D. and Tubaro, L. (1990), ‘Expansion of the global error for numerical schemes solving stochastic differential equations’, *Stochastic Analysis and Applications* **8**(4), 483–509.
- Tilley, J. (1993), ‘Valuing American options in a path simulation model’, *Transactions of the Society of Actuaries* **45**, 83–104.
- Tsitsiklis, J. and Van Roy, B. (2001), ‘Regression methods for pricing complex American-style options’, *IEE Transaction on Neural Networks* **12**(4), 694–703.
- Van Der Corput, J. (1935), ‘Verteilungsfunktionen’, *Nederl. Akad. Wetensch. Proc.* **38**, 813–820.
- Wilmott, P. (2006), *Paul Wilmott on quantitative finance*, 2nd edn, John Wiley and Sons.
- Wilmott, P. (2007), *Paul Wilmott introduces quantitative finance*, 2nd edn, John Wiley and Sons.
- Wilmott, P., Howison, S. and Dewynne, J. (1995), *The mathematics of financial derivatives: a student introduction*, Cambridge University Press.
- Xiao, X. (2007), Advanced Monte Carlo techniques: an approach for foreign exchange derivative pricing, PhD thesis, University of Manchester.
- Yan, G. and Hanson, F. (2006), ‘Option pricing for a stochastic-volatility jump-diffusion model with log-uniform jump-amplitudes’, *Proceedings of 2006 American Control Conference* pp. 2989–2994.

## REFERENCES

- Zhu, Z. and Hanson, F. (2005), A Monte-Carlo option-pricing algorithm for log-uniform jump-diffusion model, *in* ‘Proceedings of the 44th IEEE Conference on Decision and Control and European Control Conference’, pp. 5221–5226.